

UC Irvine

UC Irvine Electronic Theses and Dissertations

Title

Small Molecules for Peptides: A Photoaffinity Label for Trimers Derived from A β and Noncanonical Amino Acids for the Peptide Antibiotic Novo29 (Clovibactin)

Permalink

<https://escholarship.org/uc/item/4f423199>

Author

Krumberger, Maj

Publication Date

2023

Peer reviewed|Thesis/dissertation

UNIVERSITY OF CALIFORNIA,
IRVINE

Small Molecules for Peptides: A Photoaffinity Label for Trimers Derived from A β and
Noncanonical Amino Acids for the Peptide Antibiotic Novo29 (Clovibactin)

DISSERTATION

submitted in partial satisfaction of the requirements
for the degree of

DOCTOR OF PHILOSOPHY

in Chemistry

by

Maj Krumberger

Dissertation Committee:
Distinguished Professor James S. Nowick, Chair
Professor Vy M. Dong
Professor Christopher D. Vanderwal

2023

DEDICATION

To

mami and tati

my family

my friends

Hvala vam za vse, vse vas imam neizmerno rad in moj doktorat posvečam vam.

Thank you for everything, I love all of you and I dedicate this thesis to you.

•

“Don't ever let somebody tell you, you can't do something. Not even me. Alright?! You got a dream, you got to protect it. People can't do something themselves; they want to tell you you can't do it. You want something, go get it. Period.”

Will Smith as Chris Gardner to his son Jaden Smith as Christopher Jarrett Gardner Jr. in the 2006 movie “The Pursuit of Happyness” – one of the constant reminders on my immigrant journey to continue pursuing my dreams and to not be afraid of failure.

•

“Tinin dur!” (Eng. Keep going!)

“Ne obupaj, zaupaj!” (Eng. Never give up, always believe!)

“Kar je treba ni težko!” (Eng. What has to be done isn't hard!)

Quotes from my grandfather or nono (Stanislav) Stanko Uršič that have helped me get through moving to the other side of the world, living away from my family, building my life, and pursuing my dreams in America.

TABLE OF CONTENTS

	Page
LIST OF FIGURES	iv
LIST OF TABLES	vi
ACKNOWLEDGEMENTS	vii
VITA	viii
ABSTRACT OF THE DISSERTATION	xiv
CHAPTER I: A Photoaffinity Label to Target Trimers Derived from A β	1
Abstract	1
Introduction	2
Results and Discussion	4
Conclusion	10
References and Notes	10
Supporting Information for Chapter I	14
CHAPTER II: Capturing Higher Order Assemblies with Carbene-Mediated Crosslinking	58
Abstract	58
Introduction	58
Results and Discussion	60
Conclusion	67
References and Notes	68
Supporting Information for Chapter I	71
CHAPTER III: Expanded Studies on the Synthesis and Stereochemical Determination of the Peptide Antibiotic Novo29 (Clovibactin)	84
Abstract	84
Introduction	85
Results and Discussion	86
Conclusion	101
References and Notes	102
Supporting Information for Chapter I	106
CHAPTER IV: Efforts Toward the Synthesis of aza-Novo29 (aza-Clovibactin), a Macrolactam Analogue of Novo29 (Clovibactin) with an Improved Hydrolytic Stability	171
Abstract	171
Introduction	172
Results and Discussion	173
Conclusion	178
References and Notes	178
Supporting Information for Chapter I	180

LIST OF FIGURES

	Page	
Figure 1.1	Structures of CrV and CrVD	3
Figure 1.2	Structures of trimer 1 and 2	5
Figure 1.3	Synthesis of CrVD	6
Figure 1.4	Labeling experiments of trimer 1	8
Figure S1.1	Conditions for condensation to 8	16
Figure S1.2	Labeling of A β ₄₂	18
Figure S1.3	Enrichment of labeled trimer 1	18
Figure 2.1	Structures of peptides 10 and 11	59
Figure 2.2	X-Ray crystallographic structure of peptide 10	60
Figure 2.3	X-Ray crystallographic structure of peptide 11	62
Figure 2.4	SDS–PAGE of peptide 11	64
Figure 2.5	Photolysis of peptide 11	66
Figure S2.1	Crystals of peptide 11	73
Figure S2.2	Structures of potential oligomers	74
Figure S2.3	Mass spectra of captured oligomers	75
Figure S2.4	Competition experiment	76
Figure 3.1	Structures of Novo29 and teixobactin	86
Figure 3.2	Structures of amino acid building blocks	87
Figure 3.3	Synthesis of Fmoc-(2 <i>R</i> ,3 <i>R</i>)-hydroxyasparagine-OH	88
Figure 3.4	Synthesis of Fmoc-(2 <i>R</i> ,3 <i>S</i>)-hydroxyasparagine-OH	89
Figure 3.5	Synthesis of Novo29 and <i>epi</i> -Novo29	91
Figure 3.6	Spectral comparison of natural products	92
Figure 3.7	X-Ray Crystallography of <i>epi</i> -Novo29	96
Figure 3.8	Molecular model of Novo29	98
Figure 3.9	Assembly comparison in NMR samples	100

Figure S3.1	Establishment of (2 <i>R</i> ,3 <i>R</i>) stereochemistry in building block	108
Figure S3.2	LC-MS of natural, synthetic, and <i>epi</i> -Novo29	109
Figure S3.3	Mass spectra of hydrolyzed Novo29 crystal	110
Figure 4.1	Hydrolysis of Novo29	172
Figure 4.2	Structure of aza-Novo29	173
Figure 4.3	Different synthetic approaches toward aza-Novo29	175
Figure 4.4	Attempted synthetic route toward amino acid building blocks	176
Figure 4.5	Azidation reaction conditions	177
Figure S4.1	Mass spectrometric studies of hydrolysis of Novo29	182

LIST OF TABLES

	Page	
Table S1.1	Conditions for condensation to 8	16
Table S1.2	Concentrations for UV-Vis spectroscopy	20
Table S2.1	Crystallographic properties of peptide 11	72
Table 3.1	MIC values of natural, synthetic, and <i>epi</i> -Novo29	93
Table 3.2	Chemical shifts of the amide NH resonances of sample of Novo29	101
Table S3.1	Crystallographic properties of PDB ID 8CUG	111
Table S3.2	Crystallographic properties of PDB ID 8CUF	112
Table S3.3	Chemical shift assignments for natural Novo29	167
Table S3.4	Chemical shift comparison between natural and synthetic Novo29	169
Table 4.1	Hydrolysis of Novo29	174
Table 4.2	Azidation reaction conditions	177

ACKNOWLEDGEMENTS

Thank you, James, for being the mentor that you are. I will never forget the first time we met in your office, and you made me feel so welcome and made me feel like I belonged. I have often struggled with fitting in to places, in Slovenia I never felt like I belonged with the rest of the people, in America I always felt lonely in navigating my immigration problems, and even in my Ph.D. journey I felt as an outcast as I did not graduate with a Bachelor's degree in chemistry. But you made me feel like I belonged, you made me feel like I was in the right place, and that here I can pursue my dreams as an organic chemist. You have helped me grow into the scientist that I am today, for that I will be eternally grateful.

To the Nowick group alumni and current members, thank you! You have stood by me through these past five years when I needed comfort, offered advice whether I asked for it or not (something that I always appreciate) and have helped me decide on my future. There have been so many of you that I cannot list everyone, but I need to thank some of you who I have spent the most time with. Drs. Michael Morris, Sheng Zhang, Tuan Samdin, Xingyue Li, and Gretchen Guaglianone, you all have become more than lab mates, you all become dear friends. I have come to you in times of trouble, and in times of joy. When I needed to complain you always listened, when I was happy to share good news, you always cheered me on. You have helped me become the man that I am today, and you continue to inspire me both as scientists and as people, I can only aspire that I do such great things as you all have done. Thank you for being there for me, and I cannot wait to see what the future holds for all of us. And to some of my closest lab mates that are still in the Nowick Group with me – Chelsea Parrocha, Chelsea Jones, and Chris Dickson – we have shared many lunches on the NSI patio filled with joy, laughter, and fun, but also with outrage and sadness. Thank you for sharing everything with me, and I cannot wait to see what we all do in the future.

Thank you, (Yang) Lily Bi and Andrew Cunningham. My two undergraduate students who have taught me far more than I was able to teach you. I am so immensely proud of both of you and of the people that you are becoming. You brought so much joy into my life, and have taught me so much, let it be about the Chinese alphabet, the current trends that Gen-Z is following, or about chemistry. I want you to know that the work in this thesis would never have been completed if it was not for the two of you. Lily was heavily involved with the work in Chapter I, and Andrew with the work in Chapter III. You both should consider yourselves as co-authors of this thesis and the work that I present here. Life will take you your own ways, but I will always and forever be grateful for the time that we had together, and I cannot wait to see what you both accomplish.

Last, but certainly not least, to my family and friends. A Ph.D. is an intrinsically lonely journey, but all of you have made it so much better. I would like to thank every single one of you if I could, but let me just say - mami, tati, Mila, Stanko, An, Maja, Cayla, Alex, Jonah, Rushabh, Aleš, and so many more who I cannot name here due to length restrictions – from the bottom of my heart hvala and thank you for everything that you are, and everything that you continue to be. I love you all.

VITA
MAJ KRUMBERGER

EDUCATION

University of California, Irvine *July 2018 – present*
Ph.D. candidate, Chemistry, Nowick Group, GPA: 3.770
Advisor: Distinguished Professor James S. Nowick

University of California, Irvine *December 2022*
M.S., Chemistry, Nowick Group, GPA: 3.762
MS degree title: “Synthesis and Stereochemical Determination of the Peptide Antibiotic Novo29”
Advisor: Distinguished Professor James S. Nowick

The University of Arizona *December 2012 – December 2016*
B. S., Neuroscience & Cognitive Science, Neurobiology Emphasis, *Magna Cum Laude*, GPA: 3.875
Advisor: Professor Emeritus Victor J. Hruby

SKILLS

- **Organic Chemistry:** small molecule synthesis, solid-phase peptide synthesis, molecular design, flash- column purification (hand column and automated), preparative RP-HPLC, modeling protein interactions and docking in Schrödinger MacroModel and AutoDock Vina.
- **Chemical Biology:** photoaffinity probe design, synthesis, and analysis; peptide and small molecule analysis (LCMS, NMR, SDS-PAGE), bacterial culture, minimum inhibitory concentration (MIC) assays.
- **Analytical Chemistry:** 1D (¹H, ¹³C, ¹⁹F, ³¹P) and 2D (COSY, TOCSY, NOESY, DOSY) NMR spectroscopy, mass spectrometry (LC-MS, MALDI, QDa, ESI), analytical HPLC, IR, UV-Vis, polarimetry.
- **Computational Chemistry:** molecular modeling and docking in MacroModel and AutoDock Vina.

PROFESSIONAL EXPERIENCE

Graduate Research Assistant – University of California, Irvine *July 2018 – present*
Advisor: Distinguished Professor Dr. James S. Nowick

- **Synthesis**
- First to synthesize and determine the stereochemistry of a new peptide antibiotic Novo29 (clovibactin) that is currently in pre-clinical development by NovoBiotic, LLC. Obtained the product in >95 % purity.

- Developed a synthetic route for two noncanonical amino acids up to 500 mg in >90 % purity. Utilized the products to synthesize Novo29 and an epimer to establish the unknown stereochemistry and perform *in vitro* testing of Novo29.
 - Developed a novel approach to performing a critical condensation reaction for an unstable photoaffinity label (diazirine), and synthesized up to 10 mg of the desired product photoaffinity probe.
 - Spearheaded the design, synthesis, and evaluation of a small molecule photoaffinity probe for the detection of toxic amyloid- β oligomers.
 - Executed the solid-phase synthesis, HPLC purification, and chemical analysis of numerous macrocyclic peptides as models of toxic amyloid- β oligomers, and synthetic analogues of novel peptide antibiotics.
- **Molecular Design**
 - Designed and executed *in silico* testing for a small molecule photoaffinity probe in AutoDock Vina which inspired the design of a small molecule photoaffinity probe that I synthesized.
 - Pioneered the use of molecular modeling (MacroModel and AutoDock Vina) for the design of peptide-based SARS-CoV-2 M_{pro} inhibitor. This finding led to the screening of numerous *in silico* analogues and identification of a lead candidate with good binding activity as an inhibitor for SARS-CoV-2 M_{pro}.
 - Orchestrated and co-developed a guide for students to conduct docking in a free and accessible modeling software.
- **Analytical Techniques**
 - Utilized ¹H, ¹³C, ¹⁹F, and numerous 2D NMR techniques, mass spectrometry, IR, and polarimetry for the analysis of intermediates and final products.
 - Determined the stereochemistry of two unknown stereocenters in a peptide antibiotic by NMR.
 - Developed absorbance and analytical mass spectrometric experiments for the determination of photoaffinity probe activity.
 - Analyzed novel peptide antibiotic by a Minimum Inhibitory Concentration assay for the determination of activity with the hypothesized stereochemistry as a comparison to the isolated natural product.
- **Science Communication and Funding**
 - Communicated scientific results in three published publications, one submitted publication, one publication in preparation, and at 11 regional, national, and international scientific conferences, with two more upcoming presentations (work presented in these publications and at the scientific meetings was financially supported by the National Science Foundation (NSF), and the National Institutes of Health (NIH)).
 - Co-authored two R21 grants submitted to the NIH, one of which was selected for funding (~\$220,000/year). First grant focusing on synthesizing noncanonical amino acids for a natural product peptide antibiotic to establish the stereochemistry, and to modify the antibiotic to improve its hydrolytic stability (Grant number: AI168966). Second grant focusing on the synthesis of a noncanonical amino acid for the synthesis of teixobactin, a peptide antibiotic, as a prodrug.

- Selected as the *Department of Chemistry Science Communications Fellow* for two years. Represented the UCI Department of Chemistry on social media, wrote articles about ongoing research, and helped increase awareness and knowledge about chemical research.

Research Assistant – The University of Arizona

April 2016 – May 2018

Advisor: Regents Professor Emeritus Dr. Victor J. Hruby

- Synthesized novel cyclic peptides through solid phase peptide synthesis as selective agonists for the Melanocortin 4 Receptor and evaluated their activity through cAMP assays.
- Presented results as an undergraduate student at two poster presentations and obtained a travel award for attending the Peptide Therapeutics Symposium in 2017.

Undergraduate Research Assistant – The University of Arizona

May 2015 – December 2015

Advisor: Associate Professor Dr. Kristian P. Doyle

- Performed immunohistochemistry, microscopy, and animal studies to determine the neurotoxic effects of white blood cells following ischemia.
- Communicated my scientific results through one publication, and three poster presentations. Received a travel grant and presented my results at the American Society for Neurochemistry Meeting in 2016.

PUBLICATIONS, GRANTS, AND REVIEWS

- **Krumberger, M.***; Li, X.*; Kreutzer, A. G.; Peoples, A. J.; Nitti, A. G.; Cunningham, A.M.; Jones, C. R.; Achorn, C.; Ling, L. L.; Hughes, D. E.; Nowick, J. S. Synthesis and Stereochemical Determination of the Peptide Antibiotic Novo29. *J. Org. Chem.* **2023**, *88*, 2214. (Project financially supported by NovoBiotic Pharmaceuticals LLC, and the National Institutes of Health (NIH) through an R21 grant - AI168966).
- **Krumberger, M.**; Li, X.; Griffin, J. H.; Jones, C. R.; Nowick, J. S. Synthesis and Evaluation of aza-Novo29 as an Antibiotic Candidate. NIH R21 grant funded in 2022 (funding of \$217,095 for 2022 fiscal year). Project Number: 1R21AI168966-01A1.
- **Krumberger, M.**; Bi, Y.; Salveson, P. J.; Nowick, J. S. Design, Synthesis, and Study of a Photoaffinity Label to Target Trimers Derived from Amyloid- β . *Manuscript in preparation for submission*. (Project financially supported by the National Science Foundation (NSF) – CHE-1808096).
- Zhang, S.; **Krumberger, M.***; Morris, M. A.*; Parrocha, C. M. T.; Kreutzer, A. G.; Nowick, J. S. Structure-based drug design of an inhibitor of the SARS-CoV-2 (COVID-19) Main Protease Using Free Software: A Tutorial for Students and Scientists *Eur. J. Med. Chem.* **2021**, *218*, 11390.
- Kreutzer, A. G.; **Krumberger, M.**; Diessner, E. M. Parrocha, C. M. T.; Morris, M. A.; Guaglianone, G.; Butts, C. T.; Nowick, J. S. A cyclic peptide inhibitor of the SARS-CoV-2 Main Protease *Eur. J. Med. Chem.* **2021**, *221*, 113530.
- Zbesko, J. C.; Nguyen, T. V.; Frye, J. B.; Hussain, O.; Hayes, M.; Chung, A.; Day, W. A.; Stepanovic, K.; **Krumberger, M.**; Mona, J.; Longo, F. M.; Doyle, K. P. Glial scars are permeable to the neurotoxic environment of chronic stroke infarcts *Neurobiol. Dis.* **2018**, *112*, 63-78.

- Invited as a reviewer for the *European Journal of Medicinal Chemistry* for three articles (two published, in *Eur. J. Med. Chem.* **2022**, one article was rejected).
*These authors contributed equally.

TEACHING, MENTORSHIP, AND LEADERSHIP EXPERIENCE

Mentor to undergraduate research associates

August 2019 – present

- Mentored two undergraduate students in the Nowick group working on two different projects. Supervised and taught small molecule synthesis, chromatographic purification, and analytical chemistry methods such as thin-layer chromatography (TLC), liquid chromatography mass spectrometry (LC-MS), nuclear magnetic resonance (NMR) spectroscopy.
- Fostered an active learning environment and encouraged students to think critically about each step of the synthesis. Current undergraduate mentee is applying to graduate programs and is a co-author on a submitted manuscript. The already graduated mentee is pursuing higher education in the organic chemistry Ph.D. program in the group of Professor Charles E. McKenna at the University of Southern California.

Graduate Safety Team

March 2020 – present

- Worked with a group of chemistry graduate students to promote safe chemistry practices in the department.
- Invited and coordinated with industry speakers from Amgen and Vertex to promote the safety culture amongst graduate students, faculty, and personnel.
- Led the efforts to curb the COVID-19 spread on campus as a lead from the group and a graduate student representative to the School of Physical Sciences COVID-19 Safety Committee.
- Co-authored work guidelines and requirements that were eventually adopted campus-wide for safe work in research laboratories during the pandemic.
- Acted as the safety representative for the Nowick Group for over 4 years. Helped organize annual cleanups, promote the safety culture, train new members of the group on safety.

UC Irvine Chemistry Outreach Program

October 2018 – March 2020

- Coordinated the chemistry outreach program, reaching over 2000 school-aged children annually across numerous public schools in Orange County, CA. Designed, performed, and explained chemistry experiments to children aged 5 – 18 to promote scientific and chemical literacy, and to showcase chemistry as a potential career path.
- Program funded through an R21 grant by the National Science Foundation (NSF).

Teaching Assistant – University of California, Irvine

October 2018 – present

- Taught two undergraduate organic chemistry courses, an undergraduate medicinal chemistry course, and a medicinal chemistry laboratory: CHEM 51C (twice), CHEM 177C, CHEM 177L.
- Led discussions with up to 40 enrolled students, facilitated discussions, and encouraged an environment of learning.

Senior Instructional Specialist – University of Arizona

August 2014 – May 2018

- Taught general and organic chemistry laboratory courses with a total enrollment of over 400 students (with up to 24 students per section).
- Developed new laboratory teaching techniques that were adapted by the Department of Chemistry and Biochemistry as exemplary teaching techniques. Effort was recognized by being awarded the highest attainable evaluation for teaching, based on students' course evaluations and reports submitted by supervisors.
- Managed and coordinated monthly review session with attendance of over 2000 students.

Alpha Epsilon Delta – Pre-health Honors Society

August 2013 – December 2016

- Functioned as the Vice President for the society during 2016, and improved outreach, increased membership and promoted health-related professions.
- Functioned as the Philanthropy Chair for the Society during 2015, organized over 1000 hours of volunteering opportunities for our members in the greater Tucson community.
- Deployed an original restructuring to the society that led to an increased member retention rate, and a vast increase in applications.
- Improved organizational and leadership skills with the emphasis on health-related careers, spiked interest in the medical field through interaction with different professional.

Professional Membership

2021 – present

- Member of the *American Chemical Society (ACS)*
- Member of the *ACS Organic Chemistry Division*
- Member of the *ACS Medicinal Chemistry Division*
- Member of the *ACS Biological Chemistry Division*
- Member of the *American Peptide Society (APS)*

PRESENTATIONS

- Pfizer Chemistry Connect Organic Symposium, *Oral Presentation*, **November 2022.**
- Boulder Peptide Symposium, *Poster Session*, **November 2022.**
- Peptide Therapeutics Symposium, *Poster Session*, **October 2022.**
- ACS Division of Organic Chemistry Graduate Research Symposium, *Poster Presentation*, **July 2022.**
- 47th National Organic Chemistry Symposium, *Poster Presentation*, **July 2022.**
- University of California Chemical Symposium, *Oral Presentation*, **March 2022.**
- ACS Spring 2022 Meeting, *Oral Presentation*, **March 2022.**
- Synthetic and Chemical Biology Club, *Oral Presentation*, **November 2021.**
- Peptide Therapeutics Symposium, *Poster Presentation*, **October 2021.**
- Peptide Therapeutics Symposium, *Poster Presentation*, **October 2017.**
- 28th Annual Undergraduate Biology Research Program Conference, *Poster Presentation*, **January 2017.**
- American Society for Neurochemistry Meeting, *Poster Presentation*, **March 2016.**
- 27th Annual Undergraduate Biology Research Program Conference, *Poster Presentation*, **January 2016.**

- Neuroscience and Cognitive Science Summer Research Program, *Poster Presentation*, August 2016.

AWARDS AND HONORS

- Chosen as the *Department of Chemistry Science Communications Fellow* for 2020/21 and 2021/22. Awarded to one graduate student annually and provided half of annual stipend funding and all tuition expenses (~\$66,000).
- Obtained travel award for the *Boulder Peptide Therapeutics Symposium* in 2022.
- Obtained one of five awarded *Travel Grant Awards* to present my research at the Peptide Therapeutics Symposium in 2021 and 2022.
- Conducted research for the development of a photoaffinity probe for detecting toxic oligomers derived from amyloid- β , funded by an R21 grant from the National Science Foundation (NSF).
- Awarded a \$1300 travel grant by the Neuroscience and Cognitive Science department for presenting research at the *American Society for Neurochemistry Meeting* in Denver, CO in 2016.
- Awarded the *Neuroscience and Cognitive Science Outstanding Senior Award* at The University of Arizona in 2016, an honor that is awarded to one graduating student from the department per term. Was nominated by faculty to receive this award.
- Received the *Vivian Pham Leadership Scholarship* awarded to dedicated members of the Alpha Epsilon Delta Pre-health Honors Society for going above and beyond in their leadership roles.
- Received the *University of Arizona International Tuition Award* of \$6,000/year (highest attainable scholarship) for 4 years for high academic achievement.
- Placed on the *Academic Distinction List* for 2 years for obtaining a 3.5 – 3.9 GPA and on the *Dean's List with Distinction* for 2 semesters, for obtaining a 4.0 GPA.
- Obtained a tuition and expenses scholarship by the *Public Scholarship, Development, Disability, and Maintenance Fund of the Republic of Slovenia* to finance my undergraduate degree (2012 – 2016). \$40,000/year awarded to ~90 Slovenian students.

ABSTRACT OF THE DISSERTATION

Small Molecules for Peptides: A Photoaffinity Label for Trimers Derived from A β and Noncanonical Amino Acids for the Peptide Antibiotic Novo29 (Clovibactin)

by

Maj Krumberger

Doctor of Philosophy in Chemistry

University of California, Irvine, 2023

Professor James S. Nowick, Chair

In my thesis I aim to explore the use of small molecules in studying peptides. All chapters utilize small molecules as either probes for peptide assembly, or as building blocks for synthesizing biologically relevant peptides.

In Chapter I, I discuss the design, synthesis, and studies of – crystal violet diazirine (CrVD) – a photoaffinity probe for A β -derived peptides — crystal violet diazirine (CrVD). A β oligomers are central to the pathogenesis of Alzheimer’s disease, however they are difficult to study due to their solubility, metastability, and heterogeneity. The development of probes that can covalently label and capture these elusive species are paramount to our understanding of them. Previously, crystal violet (CrV) was shown to interact with trimer peptides derived from A β . Here, I describe the design of CrVD which is isosteric to CrV but contains a photoaffinity labeling group — trifluoromethyl diazirine in lieu of one of the *N,N*-dimethylamino groups. In this chapter I describe the computational studies that aided in the CrVD, the synthesis of CrVD in seven steps, and show that CrVD labels trimers derived from A β , and it also labels full-length A β monomers and oligomers.

In Chapter II, I build upon the utility of photoaffinity labeling groups by designing and synthesizing a peptide that contains a noncanonical amino acid – photomethionine in lieu of the native methionine residue. Peptide **10** was previously shown to form toxic oligomers but none of these oligomers have ever been captured to be studied by LC-MS. I designed peptide **11** which is an isostere of peptide **10** that contains photomethionine (an alkyl diazirine containing methionine analogue). I discuss the design and synthesis of peptide **11**, as well as explore new interesting assemblies that were observed. Peptide **11** forms non-covalent hexamers and covalent dimers by SDS-PAGE and assembles into a hexamer by X-ray crystallography. LC-MS studies of photolyzed peptide **11** reveal that different assemblies formed in solution as opposed to in the crystal form. Solution-based photolysis almost exclusively contains dimers of peptide **11**, but the photolyzed crystals contain dimers as well as trimers that were not previously observed.

In Chapter III, I discuss and expand on the studies of Novo29 (Clovibactin), a new antibiotic peptide natural product that is active against Gram positive bacteria without inducing antibiotic resistance. Until the publication of the corresponding article that this chapter builds upon the stereochemistry of a noncanonical amino acid in Novo29 (hydroxyasparagine) was unknown. In this chapter I describe the synthesis of two building blocks Fmoc-(2*R*,3*R*)-hydroxyasparagine-OH and Fmoc-(2*R*,3*S*)-hydroxyasparagine-OH that were then used in solid-phase peptide synthesis to prepare Novo29 and *epi*-Novo29. Correlation with an authentic sample of Novo29 through ¹H NMR spectroscopy, LC-MS, and in vitro antibiotic activity established that Novo29 contains (2*R*,3*R*)-hydroxyasparagine. X-ray crystallography reveals that *epi*-Novo29 adopts an amphiphilic conformation, with a hydrophobic surface and a hydrophilic surface. Four sets of *epi*-Novo29 molecules pack in the crystal lattice to form a hydrophobic core. I then used the crystal structure of *epi*-Novo29 to create a computational model of Novo29. I conclude the chapter by

exploring the interesting properties of assembly of Novo29 observed in the NMR and LC-MS studies. Assembly is crucial to the activity of the related antibiotic teixobactin and could hence play an important role in the mechanism of action of Novo29.

In Chapter IV, I try to address the finding that Novo29 hydrolyzes in neutral or basic pH. This issue is currently preventing Novo29 from being further pursued as a preclinical candidate as hydrolysis leads to an inactive linear version of Novo29. To try and prevent this hydrolysis I propose the synthesis of aza-Novo29 (aza-Clovibactin) which contains an amide bond in the place of a hydrolytically labile ester bond. I explore numerous approaches toward the synthesis of aza-Novo29, however unfortunately none of the approaches thus far have been successful. This chapter serves as the groundwork for future graduate students working on the synthesis and studies of aza-Novo29.

Chapter I

A Photoaffinity Label to Target Trimers Derived from A β

ABSTRACT

Photoreactive chemical probes that can tag and allow the identification of metastable A β oligomers may further the understanding of Alzheimer's disease by identifying these elusive and heterogeneous species involved in neurodegeneration. Chemical models of A β oligomers are useful tools to study their structures and assemblies. Crystal violet interacts with toxic peptide models of trimers derived from full-length A β and allows their identification but lacks the ability to serve as a probe that captures these oligomeric species through covalent bond formation. We designed crystal violet diazirine (CrVD) as an isosteric analogue of crystal violet containing a photoaffinity labeling probe. CrVD was synthesized from α,α,α -trifluoroacetophenone by forming the diazirine, introducing an aldehyde group by Rieche formylation, and condensation with *N,N*-dimethylaniline. Mass spectrometric analysis established that crystal violet diazirine selectively labels a synthetic trimer previously developed in our laboratory. CrVD also labels full-length A β and it differentiates between monomeric or oligomeric A β and fibrillar A β .

INTRODUCTION

Molecular probes are valuable tools for identifying and studying aggregates of amyloid beta ($A\beta$), which are one of the hallmarks of pathophysiology of Alzheimer's disease. $A\beta$ forms insoluble fibrils, as well as soluble, neurotoxic, heterogenous oligomeric assemblies. For almost a century, the azo dye Congo red has enabled $A\beta$ containing plaques in the brains of people who lived with Alzheimer's disease through optical microscopy.¹ The thiazole-containing molecules thioflavin T (ThT) and thioflavin S (ThS) are routinely used to detect $A\beta$ fibrils in vitro and in post-mortem brain tissue.²⁻⁵ A variety of molecular probes have enabled studies of $A\beta$ fibrils and plaques. Probes for positron emission tomography (PET) — florbetaben (^{18}F), florbetapir (^{18}F), and flumetamol (^{18}F) — have enabled clinicians to detect the presence of amyloid plaques in the brains of living patients and thus allow diagnosis and monitoring of Alzheimer's disease.⁶ The latter, flumetamol (^{18}F), as well as a related ^{11}C -containing compound, Pittsburg compound B, are closely related in structure to ThT.⁷ As a result of recent advances in CryoEM, NMR spectroscopy, and other high-resolution techniques, the structures of many $A\beta$ fibrils have now been determined.^{8,9}

The structures of $A\beta$ oligomers remain elusive due to their heterogeneity and metastability. The development of molecular probes to identify $A\beta$ oligomers has lagged behind the development of molecular probes to identify $A\beta$ fibrils. Most techniques used to detect $A\beta$ oligomers rely on the use of antibodies. A variety of antibodies against $A\beta$ oligomers have been developed that target different epitopes. Oligomer-specific antibodies such as A11 and OMAB do not recognize $A\beta$ fibrils and have been shown to detect oligomers in human brain tissue.^{10,11} Various antibodies have been developed against truncated versions of the $A\beta$ peptide sequence, such as the 6E10 antibody

and 4G8.¹² While these antibody-based approaches can be used in detecting various oligomeric species, they do not offer insight into the structural features of these oligomers.

While antibodies can detect A β oligomers, they cannot reveal the structural details of the assemblies that cause toxicity. Chemical probes are needed as alternatives to antibodies that can tag and identify structural features of A β oligomers. I envision the creation of small-molecule probes like ThT and Congo Red, but specific for A β oligomers. Such probes could enable imaging of A β oligomers in the brain, monitoring of oligomers in vitro, and even PET imaging in patients. These developments could provide new tools for the quantification of A β and contribute to a better understanding of their role in the development of Alzheimer's disease.

To better understand these elusive oligomers, our laboratory has been developing chemical models of A β oligomers that consist of conformationally constrained β -hairpins derived from A β .^{13,25} In 2014, Spencer et al. reported that conformationally constrained β -hairpins derived from A β_{17-36} assemble to form triangular trimers.¹⁴ Crosslinking of the vertices of the trimers with disulfide linkages by Kreutzer et al. allowed the creation of stable trimers that are cytotoxic toward SH-SY5Y cells and react with the amyloid-oligomer specific antibody A11.¹⁵ In 2018, Salveson et al. discovered that the triphenylmethane dye crystal violet (CrV) can act as a probe by exhibiting enhanced fluorescence upon binding one of the trimers, trimer **1** (Figure 1.1A, B).¹⁶ In the current study I set out to introduce a photolabile functional group — trifluoromethyl diazine — on CrV and use the resulting molecule as a photoaffinity probe to label trimers derived from A β .

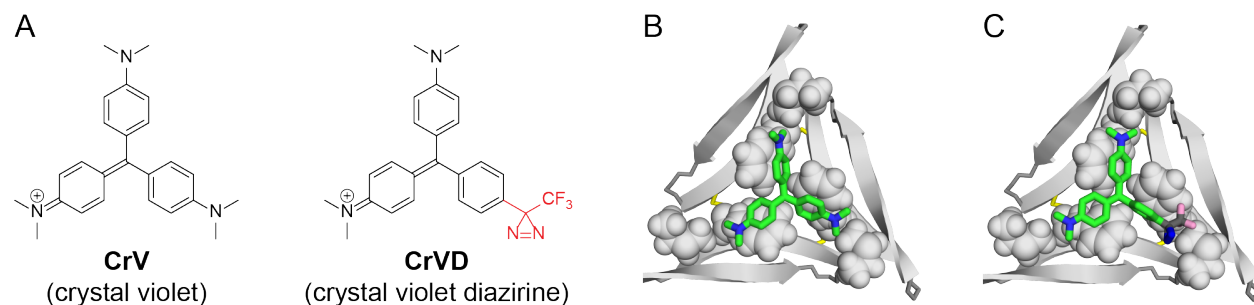


Figure 1.1. (A) Structures of crystal violet (CrV) and the photoaffinity labeling homologue crystal violet diazirine (CrVD). (B) Structure of the lowest energy structure of CrV docked to the X-ray crystallographic structure of trimer **1** (PDB ID: 5SUR). (C) Structure of the lowest energy structure of CrVD docked to the X-ray crystallographic structure of trimer **1** (PDB ID: 5SUR).

RESULTS AND DISCUSSION

I designed CrVD as a diazirine analogue of CrV by replacing one of the dimethylamino groups of crystal violet with a trifluoromethyl diazirine photoaffinity label, and I envisioned that CrVD would bind to the trimer in a fashion similar to that of CrV (Figure 1.1) Trifluoromethyl diazirines form carbenes upon irradiation with UV light, which form covalent bonds with proteins through insertion into carbon-hydrogen or heteroatom-hydrogen bonds of nearby residues.^{17,18} Because the carbene is highly reactive, the irradiated photoaffinity label reacts only with proximal residues of the protein, or is quenched by solvent, and does not diffuse or react with unbound protein.¹⁸ Comparison of a molecular model of CrVD to a molecular model of CrV, illustrates that the trifluoromethyl diazirine group is almost isosteric with the *N,N*-dimethylamino group (Figure 1.1B, C).

Docking studies using AutoDock Vina indicate that CrV should bind to the trimer **1** through interactions with one its hydrophobic surfaces. X-ray crystallographic studies had previously shown that trimer **1** (PDB ID 5SUR) contains two hydrophobic surfaces, the “Phe₁₉ surface” and the “Phe₂₀ surface”. The Phe₁₉ surface contains the side chains of Phe₁₉, Ile₃₂, Leu₃₄,

and Val₃₆; the Phe₂₀ surface contains the side chains of Val₁₈, Phe₂₀, and Ile₃₁ (Figure 1.2). Docking studies had shown that CrV binds exclusively to the Phe₂₀ surface. In the lowest energy docked structure, the three-fold symmetrical CrV rests on the three Phe₂₀ residues, and the *N,N*-dimethylamino groups lie near Ile₃₁ and Phe₂₀ (Figure 1.1B). CrVD docks in a similar fashion, with the triphenylmethyl group resting on the aromatic rings of the three Phe₂₀ residues and the diazirine group lies near Ile₃₁ and Phe₂₀ (Figure 1.1C). The carbon atom of the diazirine group is about 5 Å from the nearest hydrogen atoms of Phe₂₀ and Ile₃₁ and is thus poised for C–H insertion into these residues upon carbene formation through photolysis. These docking studies encouraged me to pursue the synthesis of CrVD and attempt photoaffinity labeling of the trimer.

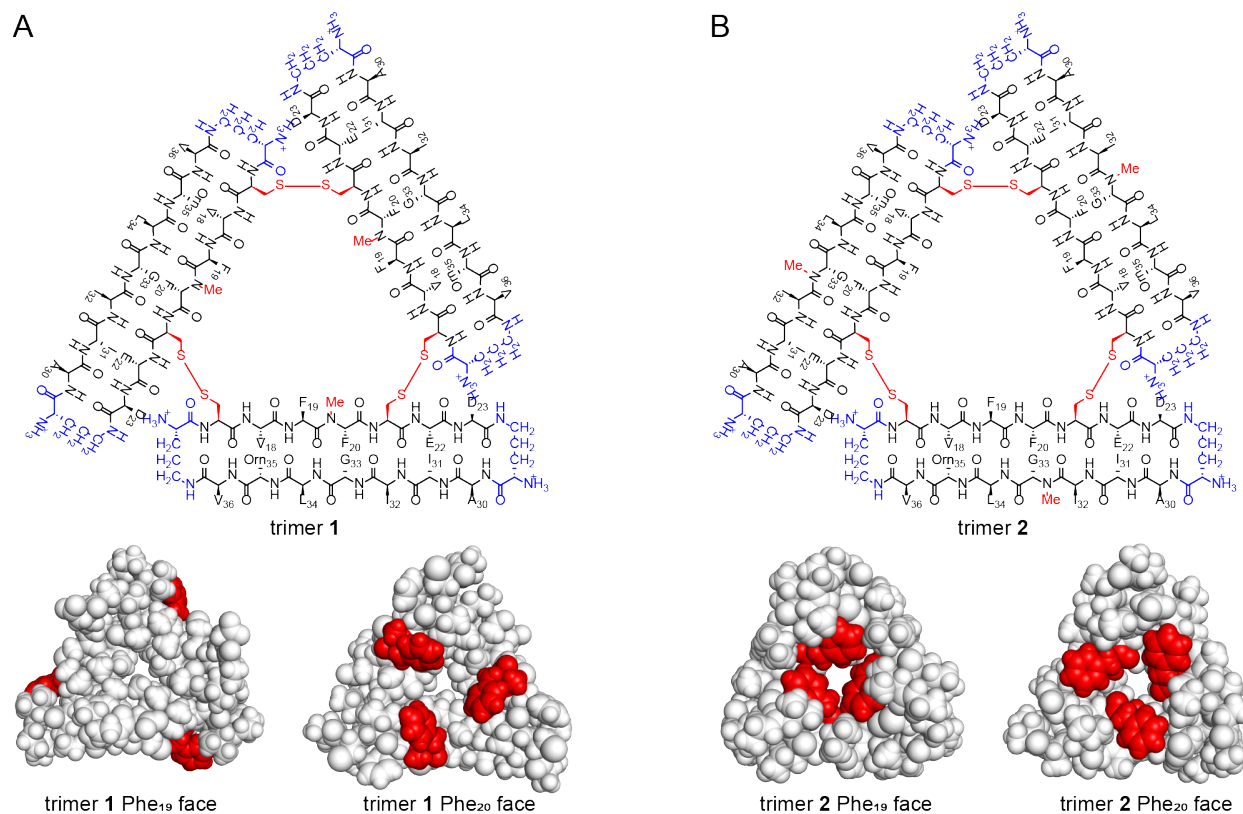


Figure 1.2. Structures of trimers 1 and 2. (A) Chemical structure of trimer 1 and X-ray crystallographic structures the Phe₁₉ and the Phe₂₀ faces of trimer 1 (PDB ID 5SUR). Phe₁₉ and

Phe₂₀ are shown in red. (B) Chemical structure of trimer **2** and X-ray crystallographic structures of the Phe₁₉ and the Phe₂₀ faces of trimer **2** (PDB ID 5SUT). Phe₁₉ and Phe₂₀ are shown in red.

I synthesized CrVD from α,α,α -trifluoroacetophenone by forming the diazirine ring, introducing an aldehyde group by Rieche formylation, and condensing the aldehyde with *N,N*-dimethylaniline. α,α,α -Trifluoroacetophenone was converted to oxime **3** by treatment with hydroxylamine hydrochloride in pyridine, according to published procedures (Figure 1.3).¹⁹ Oxime **3** was then converted to the corresponding tosylate, tosylate **4**, by treatment with tosyl chloride and triethylamine. Both oxime **3** and tosylate **4** were generated as mixtures of stereoisomers. Displacement of the tosylate group with ammonia led to the formation of diaziridine **5**, which was then oxidized with iodine in methanol to form diazirine **6**.²⁰

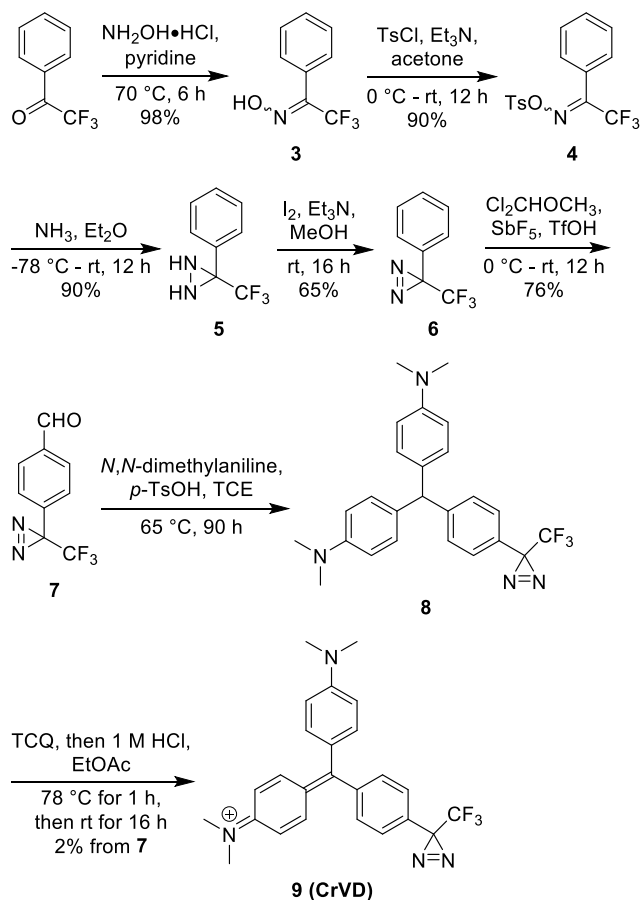


Figure 1.3. Synthesis of crystal violet diazirine (CrVD).

Rieche formylation of diazirine **6** with 1,1-dichloromethylmethyl ether and SbF₅ in trifluoromethanesulfonic acid afforded aldehyde **7**. Hatanaka et al. previously reported screening conditions and optimized this reaction with a variety of different Lewis acids, with TiCl₄ yielding the best results.²¹ In my hands, however, TiCl₄ gave poor yields, and the yield for this reaction was substantially improved by using SbF₅ as the Lewis acid.

Acid-catalyzed condensation of aldehyde **7** with *N,N*-dimethylaniline in 1,1,2,2-tetrachloroethane (TCE) over 90 hours at 65 °C gave the penultimate product **8**, the reduced form of CrVD. I found the choice of solvent and temperature to be critical in this reaction. When I ran this reaction in toluene at 111 °C, decomposition of the diazirine occurred rapidly. At 65 or 80 °C in toluene, the reaction did not proceed. The aldehyde was sufficiently activated and the diazirine thermally stable in TCE at 65 °C (Figure S1.1 and Table S1.1). In the final step the reduced CrVD was oxidized with tetrachloroquinone, which has previously been shown as a good oxidizing agent for crystal violet.²² Followed by a reverse phase purification I obtained the final product — crystal violet diazirine (CrVD) in up to 10 mg.

I previously observed that CrV forms a complex with trimer **1**.¹⁶ Complexation results in a change in color of CrV and a shift in λ_{max} to longer wavelength. Titrating CrVD with trimer **1** also resulted in a shift of wavelength from 628 nm to 636 nm at a 1:1 ratio of trimer **1** and CrVD, suggesting that CrVD also forms a complex with trimer **1** (Figure 1.4B). Upon photolysis of this mixture at 365 nm for 10 minutes, a further shift in the λ_{max} occurred to 642 nm (Figure 1.4B). The further shift in λ_{max} following photolysis indicates that a further change to the chromophore has occurred, associated with the photolytic decomposition of the diazirine group.

Mass spectrometric analysis establishes that CrVD covalently labels trimer **1**. To assess the labeling of the trimer **1**, I first incubated CrVD with trimer **1** and photolyzed it at 365 nm. Labeling

by diazirines is generally low yielding (e.g. ~1–2%); the main product of photolysis typically involves reaction of the carbene intermediate with water. For this reason, I next enriched the sample in labeled trimer by HPLC, selecting the peak with an absorbance at 620 nm. Enriched samples were collected in five fractions with fraction four containing the largest amount of labeled trimer **1** (Figure S1.3). Complete separation of unlabeled trimer **1** from the labeled species was not possible. Figure 1.4A illustrates the complexation and labelling process schematically.

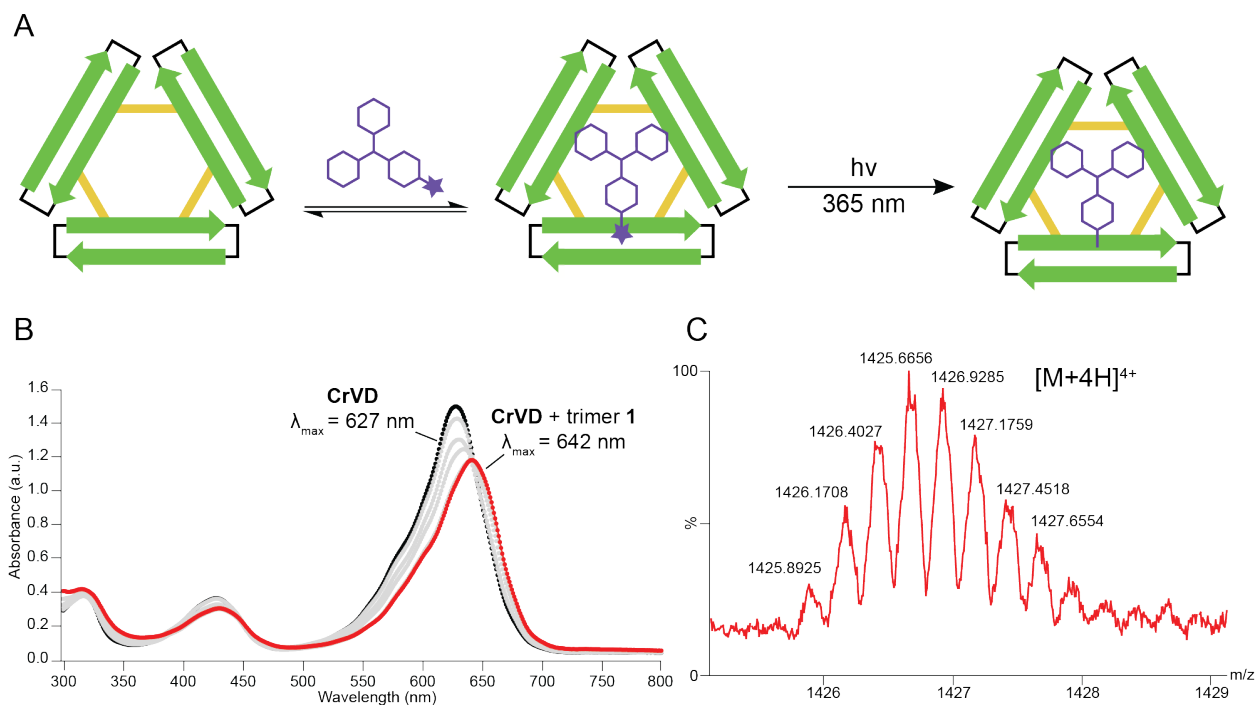


Figure 1.4. Labeling of trimer **1** with CrVD. (A) Typical procedure for labeling trimer **1** with CrVD. Trimer **1** is depicted a green cartoon, CrVD is depicted as a purple cartoon. Trimer **1** is incubated with CrVD for ten minutes and then photolyzed at 365 nm for ten minutes. (B) Absorbance spectrum of free CrVD in ammonium acetate buffer (black dotted line), increasing concentration of trimer **1** added to CrVD (grey dotted lines), and of CrVD with an equimolar amount of trimer **1** added and photolyzed (red dotted line). (C) Representative mass spectrometric peak that corresponds to the mass of labeled trimer **1** with CrVD. Ions ranging from $[M+3H]^{3+}$ to $[M+8H]^{8+}$ were observed in the ESI mass spectrum.

I further analyzed the enriched HPLC fraction by mass spectrometry to try and identify which specific residues are being labeled. MS/MS analysis of macrocyclic peptides is difficult and

hence we attempted to first reduce the disulfide bonds with TCEP that covalently stabilize the trimer, followed by enzymatic digestion with pepsin. Reduction of the disulfide bonds resulted in a sufficient amount of CrVD labeled disulfide reduced peptide, but I was unable to detect sufficient quantities of peptide fragments following pepsin digestion to be able to identify the labeling sites.

To evaluate the specificity of the labeling, I studied the labeling of an isomeric trimer that adopts a different conformation. Trimer **2** is identical in sequence and composition to trimer **1**, but bears an *N*-methyl group on Gly₃₃, instead of Phe₂₀. X-ray crystallography shows substantial differences in the conformations of the Phe₁₉ and Phe₂₀ residues between the two trimers (Figure 2). Molecular docking studies between CrVD and trimer **2** suggested that CrVD should not bind to trimer **2**. In the docking of analysis of CrVD to an equilibrated model of the X-ray crystallographic structure of trimer 2 (PDB ID 5SUT) I observed no binding of CrVD to the Phe₂₀ residues and only non-specific interactions between the two molecules. When I treated trimer **2** with CrVD, photolyzed the mixture, and analyzed by mass spectrometry, we observed no labeling of trimer **2**. The difference in labeling the two trimers by CrVD shows that shape complementarity is critical in the recognition of A β oligomer models.

To determine if CrVD also labels full-length A β oligomers, I incubated CrVD with oligomeric A β ₄₂ photolyzed the mixture, and then analyzed for adducts by LC-MS. I prepared oligomeric A β ₄₂ following published procedures, by incubating a DMSO stock of A β ₄₂ at 4 °C in F-12 cell culture media for 24 hours.²⁷ After incubation and photolysis, LC-MS revealed covalent adducts between CrVD and A β ₄₂. Analysis of the [M+5H]⁵⁺ and an [M+6H]⁶⁺ species in the mass spectra revealed CrVD adducts, in addition to unlabeled A β ₄₂. To further explore the labeling preferences of CrVD we also explored the labeling of monomeric and fibrillar preparations of A β ₄₂. Monomers and fibrils of A β ₄₂ were also prepared following related published procedures.²⁴

Photolysis, followed by LC-MS revealed that CrVD labels the monomeric, but not the fibrillar preparation of A β ₄₂ (Figure S1.2). This result suggests that CrVD exhibits some selectivity in binding to different types of assemblies that A β ₄₂ forms.

CONCLUSION

The photoaffinity probe crystal violet diazirine (CrVD) labels trimer **1**, a synthetic trimer derived from A β while it does not label isomeric trimer **2**, and labels full-length A β ₄₂. CrVD is an isostere of the threefold symmetrical dye crystal violet (CrV) and can be prepared in seven steps from α,α,α -trifluoroacetophenone. To my knowledge, CrVD represents the first photoaffinity probe tailored to react with oligomeric species derived from A β . Molecular modeling and docking studies suggest that CrVD may target certain three-fold symmetrical arrangements of the central hydrophobic region of A β but not others and may thus exhibit shape selectivity. Although there is still no chemical probe that could detect and isolate toxic oligomeric species of A β in biological samples, CrVD represents a step toward the design of photo-reactive chemical probes for biologically relevant amyloid oligomers.

REFERENCES AND NOTES

1. Divry P. Étude histo-chimique des plaques séniles. *J. Belge de Neurol. et de Psychiat.* **1927**, *27*, 643–657.
2. Vassar, P. S.; Culling, C. F. Fluorescent Stains, with Special Reference to Amyloid and Connective Tissues. *Arch. Pathol.* **1959**, *68*, 487–498.
3. Kelenyi, G. On the Histochemistry of Azo Group-Free Thiazole Dyes. *J. Histochem. Cytochem.* **1967**, *15*, 172–180.

4. LeVine III, H. Thioflavine T Interaction with Synthetic Alzheimer's Disease β -Amyloid Peptides: Detection of Amyloid Aggregation in Solution. *Protein Sci.* **1993**, *2*, 404–410.
5. LeVine, H. Quantification of β -Sheet Amyloid Fibril Structures with Thioflavin T. *Methods in Enzymo. Amyloid, Prions, and Other Protein Aggregates*; **1999**, *309*, 274–284.
6. Yeo, J. M.; Waddell, B.; Khan, Z.; Pal, S. A Systematic Review and Meta-Analysis of ¹⁸F-Labeled Amyloid Imaging in Alzheimer's Disease. *Alzheimers Dement. Diagn. Assess. Dis. Monit.* **2015**, *1*, 5–13.
7. Klunk, W. E.; Engler, H.; Nordberg, A.; Wang, Y.; Blomqvist, G.; Holt, D. P.; Bergström, M.; Savitcheva, I.; Huang, G.-F.; Estrada, S.; Ausén, B.; Debnath, M. L.; Barletta, J.; Price, J. C.; Sandell, J.; Lopresti, B. J.; Wall, A.; Koivisto, P.; Antoni, G.; Mathis, C. A.; Långström, B. Imaging Brain Amyloid in Alzheimer's Disease with Pittsburgh Compound-B. *Ann. Neurol.* **2004**, *55*, 306–319.
8. Tycko, R. Solid-State NMR Studies of Amyloid Fibril Structure. *Annu. Rev. Phys. Chem.* **2011**, *62*, 279–299.
9. Kollmer, M.; Close, W.; Funk, L.; Rasmussen, J.; Bsoul, A.; Schierhorn, A.; Schmidt, M.; Sigurdson, C. J.; Jucker, M.; Fändrich, M. Cryo-EM Structure and Polymorphism of A β Amyloid Fibrils Purified from Alzheimer's Brain Tissue. *Nat. Commun.* **2019**, *10*, 4760.
10. Kaye, R.; Head, E.; Thompson, J. L.; McIntire, T. M.; Milton, S. C.; Cotman, C. W.; Glabe, C. G. Common Structure of Soluble Amyloid Oligomers Implies Common Mechanism of Pathogenesis. *Science* **2003**, *300*, 486–489.
11. Lindhagen-Persson, M.; Brännström, K.; Vestling, M.; Steinitz, M.; Olofsson, A. Amyloid- β Oligomer Specificity Mediated by the IgM Isotype – Implications for a Specific Protective Mechanism Exerted by Endogenous Auto-Antibodies. *PLOS ONE* **2010**, *5*, e13928.

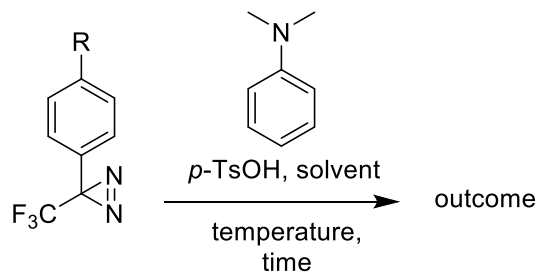
12. Baghallab, I.; Reyes-Ruiz, J. M.; Abulnaja, K.; Huwait, E.; Glabe, C. Epitomic Characterization of the Specificity of the Anti-Amyloid A β Monoclonal Antibodies 6E10 and 4G8. *J. Alzheimers Dis.* **66**, 1235–1244.
13. Samdin, T. D.; Kreutzer, A. G.; Nowick, J. S. Exploring Amyloid Oligomers with Peptide Model Systems. *Curr. Opin. Chem. Biol.* **2021**, *64*, 106–115.
14. Spencer, R. K.; Li, H.; Nowick, J. S. X-Ray Crystallographic Structures of Trimers and Higher-Order Oligomeric Assemblies of a Peptide Derived from A β _{17–36}. *J. Am. Chem. Soc.* **2014**, *136*, 5595–5598.
15. Kreutzer, A. G.; Yoo, S.; Spencer, R. K.; Nowick, J. S. Stabilization, Assembly, and Toxicity of Trimers Derived from A β . *J. Am. Chem. Soc.* **2017**, *139*, 966–975.
16. Salveson, P. J.; Haerianardakani, S.; Thuy-Boun, A.; Yoo, S.; Kreutzer, A. G.; Demeler, B.; Nowick, J. S. Repurposing Triphenylmethane Dyes to Bind to Trimers Derived from A β . *J. Am. Chem. Soc.* **2018**, *140*, 11745–11754.
17. Dubinsky, L.; Krom, B. P.; Meijler, M. M. Diazirine Based Photoaffinity Labeling. *Bioorg. Med. Chem.* **2012**, *20*, 554–570.
18. Halloran, M. W.; Lumb, J.-P. Recent Applications of Diazirines in Chemical Proteomics. *Chem. Eur. J.* **2019**, *25*, 4885–4898.
19. Wang, L.; Murai, Y.; Yoshida, T.; Ishida, A.; Masuda, K.; Sakihama, Y.; Hashidoko, Y.; Hatanaka, Y.; Hashimoto, M. Alternative One-Pot Synthesis of (Trifluoromethyl)Phenyldiazirines from Tosyloxime Derivatives: Application for New Synthesis of Optically Pure Diazirinyphenylalanines for Photoaffinity Labeling. *Org. Lett.* **2015**, *17*, 616–619.

20. Nakamoto, K.; Ueno, Y. Diazirine-Containing RNA Photo-Cross-Linking Probes for Capturing MicroRNA Targets. *J. Org. Chem.* **2014**, *79*, 2463–2472.
21. Nakashima, H.; Hashimoto, M.; Sadakane, Y.; Tomohiro, T.; Hatanaka, Y. Simple and Versatile Method for Tagging Phenyldiazirine Photophores. *J. Am. Chem. Soc.* **2006**, *128*, 15092–15093.
22. Budin, G.; Chung, H. J.; Lee, H.; Weissleder, R. A Magnetic Gram Stain for Bacterial Detection. *Angew. Chem. Int. Ed.* **2012**, *51*, 7752–7755.
23. Yamasaki, S.; Nikaido, E.; Nakashima, R.; Sakurai, K.; Fujiwara, D.; Fujii, I.; Nishino, K. The Crystal Structure of Multidrug-Resistance Regulator RamR with Multiple Drugs. *Nat. Commun.* **2013**, *4*, 2078.
24. Stine, W. B.; Jungbauer, L.; Yu, C.; LaDu, M. J. Preparing Synthetic A β in Different Aggregation States. *Methods Mol. Biol.* **2011**, *670*, 13–32.
25. Kreutzer, A. G.; Nowick, J. S. Elucidating the Structures of Amyloid Oligomers with Macrocyclic β -Hairpin Peptides: Insights into Alzheimer's Disease and Other Amyloid Diseases. *Acc. Chem. Res.* **2018**, *51*, 706–718.

A Photoaffinity Label to Target Trimers Derived from A β **Table of Contents**

Figure S1.1	16
Table S1.1	16
Figure S1.2	18
Figure S1.3	18
Materials and Methods	19
UV-Vis Spectroscopy	20
Table S1.2	20
Chemical synthesis of trimers 1 and 2	20
Chemical synthesis of CrVD	20
Intermediates 3–8 and CrVD (9)	20
Docking with AutoDock Vina	27
References	32
Characterization Data	34
Characterization of trimer 1	34
Analytical HPLC trace of trimer 1	34
Mass spectrum of trimer 1	35
Characterization of trimer 2	35
Analytical HPLC trace of trimer 2	35
Mass spectrum of trimer 2	37
NMR spectra of intermediates	38
¹ H NMR spectrum of 3	38
¹³ C NMR spectrum of 3	39
¹⁹ F NMR spectrum of 3	40
¹ H NMR spectrum of 4	41
¹³ C NMR spectrum of 4	42
¹⁹ F NMR spectrum of 4	43
¹ H NMR spectrum of 5	44
¹³ C NMR spectrum of 5	45

¹⁹ F NMR spectrum of 5	46
¹ H NMR spectrum of 6	47
¹³ C NMR spectrum of 6	48
¹⁹ F NMR spectrum of 6	49
¹ H NMR spectrum of 7	50
¹³ C NMR spectrum of 7	51
¹⁹ F NMR spectrum of 7	52
¹ H NMR spectrum of CrVD (9)	53
¹³ C NMR spectrum of CrVD (9)	54
¹⁹ F NMR spectrum of CrVD (9)	55
Analytical HPLC trace of CrVD (9)	56



entry	R	solvent	temperature (°C)	time (h)	outcome
1	-CHO	toluene	111	12	decomposition
2	-H	toluene- <i>d</i> ₈	111	1	decomposition
3	-H	toluene- <i>d</i> ₈	82	1	decomposition
4	-H	acetonitrile- <i>d</i> ₃	82	24	decomposition
5	-CHO	neat	25	90	no reaction
6	-CHO	methanol- <i>d</i> ₄	65	24	acetal*
7	-CHO	toluene- <i>d</i> ₈	65	48	no reaction
8	-CHO	TCE- <i>d</i> ₂	111	1	decomposition
9	-CHO	TCE- <i>d</i> ₂	82	1	decomposition
10	-CHO	TCE- <i>d</i> ₂	65	90	CrVD

Figure S1.1 and **Table S1.1**. Conditions for condensation of formylated diazirine **7** and *N,N*-dimethylaniline to obtain leuco-CrVD **8**. *The acetal that formed is 3-(4-(dimethoxymethyl)phenyl)-3-(trifluoromethyl)-3*H*-diazirine.

Initially, formylated diazirine **5** was subjected to conditions previously described by Parvin et al. for the synthesis of various triarylmethane dyes, none of which contained a diazirine group.¹ Following the 12 hour heating at 111 °C, it became apparent that the diazirine decomposed due to thermal instability, as observed by the presence of numerous peaks in the ¹⁹F NMR spectrum, and the presence of numerous masses in the ESI-MS spectrum corresponding to adducts of **7** to other molecules in the reaction mixture through the formation of the carbene (entry 1). Diazirine **7** was tested for its thermal stability in toluene-*d*₈ and acetonitrile-*d*₃ at 111 and 82 °C (entries 2 – 4). This sequence of experiments revealed that solvents play an important role in the stability of the diazirine as it decomposed much slower in acetonitrile-*d*₃ than in toluene-*d*₈. An attempt was made to perform the condensation reaction at high concentration without heating (entry 5), but this did not result in the formation of any product and only starting materials were observed after 90 hours.

Treatment of **5** in methanol- d_4 with *p*-TsOH and *N,N*-dimethylaniline at 65 °C for 24 hours led to the formation of 3-(4-(dimethoxymethyl)phenyl)-3-(trifluoromethyl)-3*H*-diazirine, indicating that methanol was reacting with the aldehyde group to form the acetal. While this was not the desired product it showed that the diazirine was stable at 65 °C for at least 24 hours, and that the aldehyde was sufficiently activated (entry 6). Running the same conditions in toluene- d_8 did not result in the formation of any product (entry 7). I attempted to run this reaction in a polarizable solvent (1,1,2,2-tetrachloroethane- d_2 or TCE- d_2) that I hypothesized would have a similar protecting effect on the diazirine at elevated temperatures as the other polar solvents have had (entries 4 and 6) while also not containing any nucleophilic moieties to react with the aldehyde group. Running this reaction in TCE- d_2 at 111 and 85 °C resulted in rapid decomposition of the diazirine (entries 8 and 9) but running it at 65 °C yielded the desired product — CrVD.

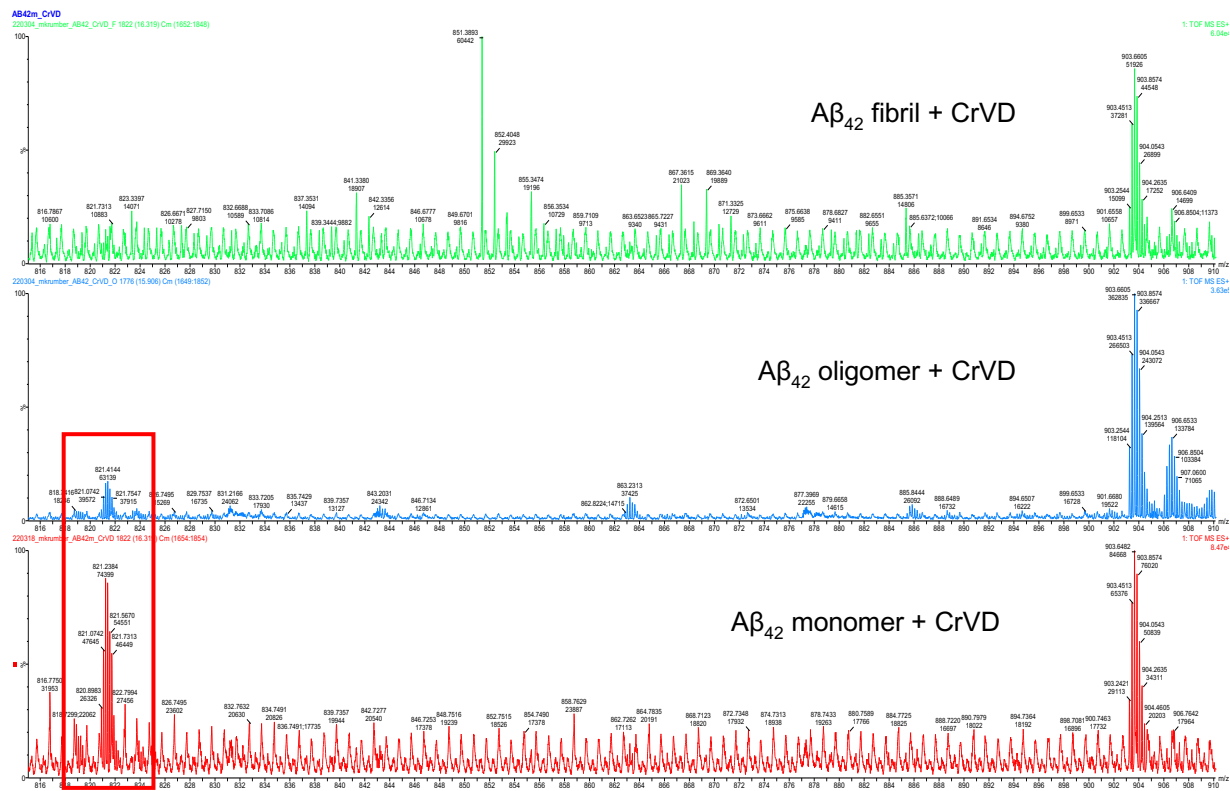


Figure S1.2. ESI-MS trace of the labeling of A β ₄₂ monomers, oligomers, and fibrils. Representative mass spectrometric peak that corresponds to the mass of labeled A β ₄₂ monomer and oligomer with CrVD is shown, the peak corresponds to and [M+6H]⁶⁺ charge.

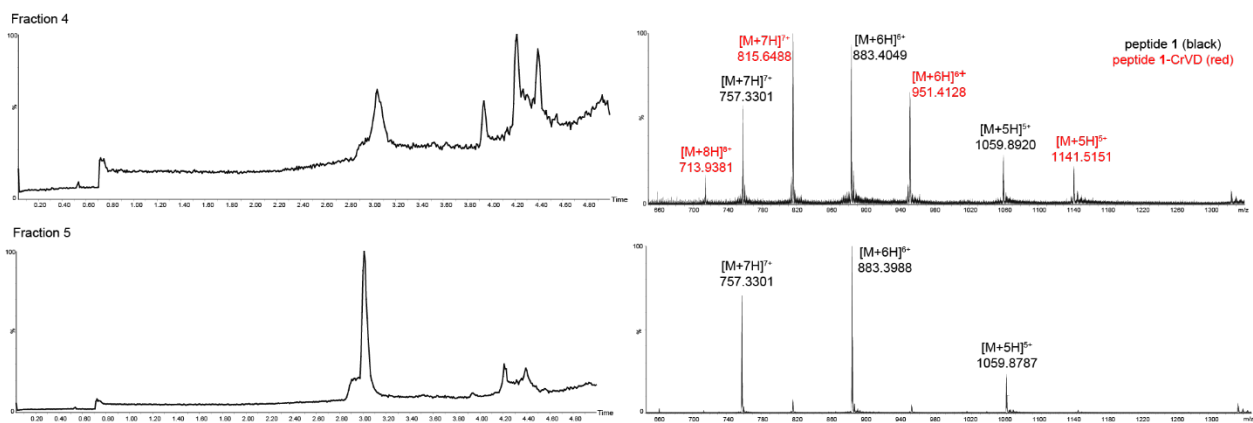


Figure S3. LC-MS traces of fractions four and five following a RP-HPLC enrichment. Fraction four (top) contains unlabeled peptide 1 (black) and CrVD labeled peptide 1 (red). Fraction five contains mostly unlabeled peptide 1.

General Materials and Methods:

All chemicals were used as received unless otherwise noted. Dry diethyl ether (Et₂O), methanol (MeOH), triethylamine (Et₃N), methylene chloride (CH₂Cl₂), and toluene were obtained by passing drying columns in a solvent system. Water that was used in work-up steps was reverse osmosis water (RO H₂O). Yields refer to isolated and chromatographically purified compounds, unless otherwise stated. Commercial reagents were used without purification, unless otherwise stated. Reactions were monitored by thin layer chromatography (TLC) using heat and UV for visualization. Thermo Fisher Scientific silica gel (60, particle size 0.040 – 0.063 mm) was used for column chromatography. ESI data was collected on an ESI LC-TOF Microass LCT 3 instrument or on a Waters CRS-173 QDA. Infrared (IR) spectra were obtained on a Thermo Scientific Nicolet iS5 spectrometer with iD5 ATR tip. NMR spectra were recorded on a Bruker DRX 400 and DRX600 spectrometer with either a BBO probe or TCI cryoprobe as standard and calibrated using residual solvent (CDCl₃: δ_H = 7.26 ppm, δ_C = 77.16 ppm; TCE-*d*₂: δ_H = 6.00 ppm, δ_C = 78.78 ppm). ¹⁹F NMR spectra were calibrated to their corresponding ¹H NMR spectra. Abbreviations used to designate multiplicities include: s = singlet, d = doublet, t = triplet, q = quartet, m = multiplet, dd = doublet of doublets, dt = doublet of triplets, td = triplet of doublets, ddd = doublets of doublets of doublets.

UV-Vis spectroscopy

UV-Vis spectroscopy experiments were based on those previously published by our laboratory, using the same concentrations of peptide and dye, as well as the same instrumentation.² Visible absorbance spectra were recorded on a Thermo Scientific MULTISKAN GO instrument equipped with a cuvette reader. Data were acquired from samples in a quartz cuvette with a 1 cm path length.

Table S1.2. Representative sample preparation for UV-Vis spectroscopy experiments.

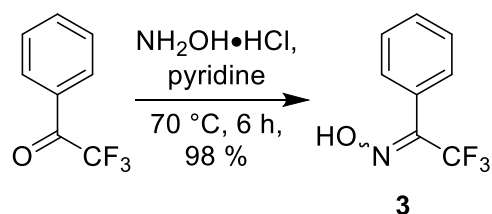
conc. (μM) trimer 1	conc. (μM) CrVD	~ratio trimer 1 : CrVD	vol. (μL) stock trimer 1	vol. (μL) stock CrVD	vol. (μL) ammonium acetate buffer
0	37.5	0.0 : 1.0	0	30.0	370.0
9.4	37.5	0.25 : 1.0	2.4	30.0	367.6
18.8	37.5	0.5 : 1.0	4.8	30.0	365.2
28.1	37.5	0.75 : 1.0	7.2	30.0	362.8
37.5	37.5	1.0 : 1.0	9.0	30.0	361.0

Synthetic Procedures:

Synthesis of trimers 1 and 2³

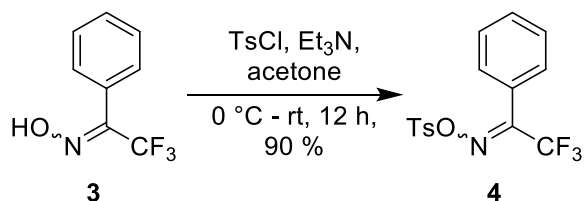
Trimers 1 and 2 were synthesized following our previously published procedures.³

Chemical synthesis of CrVD



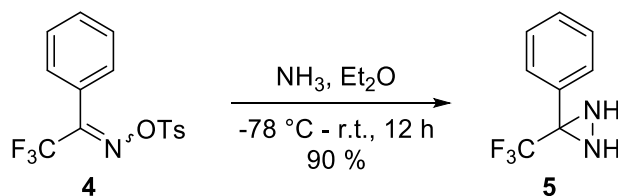
α,α,α -Trifluoro-1-phenylethan-1-one oxime 3.⁴ A 500-mL, single-necked round-bottom flask, equipped with a magnetic stirring rod, and a nitrogen inlet adaptor was charged with 150 mL pyridine and α,α,α -trifluoroacetophenone (8 mL, 57 mmol, 1.0 equiv.), followed by the

addition of hydroxylamine hydrochloride (4.75 g, 68 mmol, 1.2 equiv.). The reaction mixture was heated to 70 °C and stirred for 6 hours. Then, the solution was allowed to cool to room temperature, and concentrated to dryness by rotary evaporation. The resulting colorless oil was dissolved in 100 mL ethyl acetate and washed with 120 mL 1 M HCl. The organic layer was extracted with 120 mL water, 120 mL of saturated aqueous NaCl, dried over MgSO₄, filtered, and concentrated to afford a white solid (98 % yield, 10.6 g). Oxime **3** was used without further purification. ¹H NMR (600 MHz, CDCl₃) (two diastereomers): δ 9.56 (s, 1H), 9.43 (s, 1H), 7.60 – 7.43 (m, 8 H). ¹³C{¹H} NMR (150 MHz, CDCl₃) (two diastereomers): δ 148.5, 148.3, 148.1, 148.0, 147.9, 147.8, 147.7, 147.5, 130.8, 130.6, 129.9, 128.69, 128.68, 128.4, 125.9, 120.4 (q, *J*_{C-F} = 282.2 Hz) 118.4 (q, *J*_{C-F} = 276.9 Hz). ¹⁹F NMR (564 MHz, CDCl₃) (two diastereomers): δ -62.53, -66.77. HRMS (ESI-TOF) *m/z*: [M - H]⁻ calcd for C₈H₆F₃NO⁻ 188.0323, observed 188.0318.



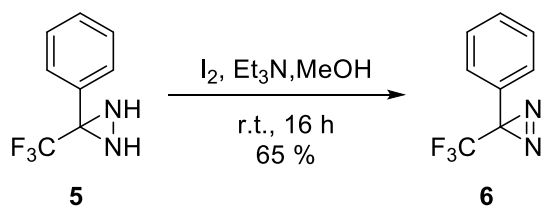
***α,α,α*-Trifluoro-1-phenylethan-1-one *O*-tosyl oxime **4**.**⁴ A 500-mL, single-necked round-bottom flask, equipped with a magnetic stirring bar, and a nitrogen inlet adaptor containing oxime **3** (7.56 g, 40.0 mmol, 1 equiv.) was charged with 250 mL of acetone and cooled to 0 °C in an ice bath. Triethylamine (16.7 mL, 119.9 mmol, 3.0 equiv.) was added, followed by the addition of *p*-toluenesulfonyl chloride (9.1 g, 47.9 mmol, 1.2 equiv.). The ice bath was removed, and the reaction mixture was stirred at room temperature for 12 hours. An insoluble salt byproduct (triethylammonium chloride) was removed by gravity filtration, and the remaining mixture was concentrated to dryness by rotary evaporation. The resulting pale-yellow oil was dissolved in 100

mL EtOAc. The mixture was washed with 120 mL 1 M HCl, and the organic layer was washed with 120 mL H₂O followed by 120 mL saturated aqueous NaCl. The organic layer was dried with MgSO₄ and the solution was concentrated to dryness by rotary evaporation to afford oxime **4** as a beige solid (90 % yield, 12.3 g). Tosyl oxime **4** was used without further purification. ¹H NMR (600 MHz, CDCl₃) (two diastereomers): δ 7.89 (t, *J* = 8.6 Hz, 4H), 7.53 (t, *J* = 7.4 Hz, 2H), 7.48 (t, *J* = 7.9 Hz, 2H), 7.35–7.46 (m, 10H), 2.48 (s, 3H), 2.46 (s, 3H). ¹³C{¹H} NMR (150 MHz, CDCl₃) (two diastereomers): δ 154.4, 154.3, 154.2, 153.9, 153.8, 153.7, 146.2, 146.0, 131.8, 131.7, 131.5, 131.3, 129.9, 129.2, 128.9, 128.8, 128.7, 128.5, 127.8, 125.7, 117.9 (q, *J*_{C-F} = 284.7 Hz), 21.84, 21.83. ¹⁹F NMR (564 MHz, CDCl₃) (two diastereomers): δ -61.46, -66.74. HRMS (ESI-TOF) *m/z*: [M + Na]⁺ calcd for C₈H₆F₃NOHNa⁺ 366.0388, observed 366.0384.



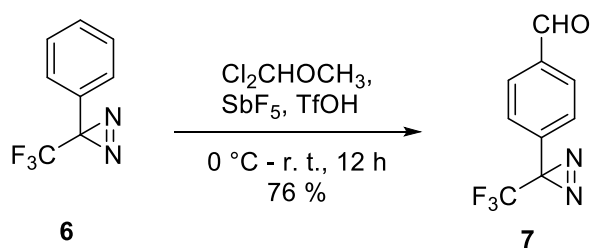
3-Phenyl-3-(trifluoromethyl)diaziridine 5.⁴ An oven-dried 120 mL Ace pressure tube, equipped with a magnetic stirring rod was capped with a rubber septum that was pierced with an 18g needle. The Ace pressure tube was evacuated with vacuum, filled with N₂, and placed in an acetone/dry-ice bath at -78 °C. The Ace pressure tube was then slowly charged with 30 mL (excess) ammonia from an ammonia tank while being connected to an outlet bubbler to remove any excess nitrogen as it gets displaced by NH₃. Tosyl **4** (5.2 g, 15.0 mmol, 1 equiv.) was dissolved in a minimal amount of Et₂O (30 mL) and slowly added to the Ace pressure tube through the septum via a 30 mL syringe. The Ace pressure tube was capped and allowed to warm to room temperature. The reaction mixture was stirred for 12 hours at room temperature behind a blast shield. Then, the reaction mixture was cooled to -78 °C and fitted with a rubber septum pierced

with an 18-gauge needle, and 30 mL of Et₂O was slowly added. The mixture was allowed to warm to 0 °C in an ice-bath, for 1 hour, and then to room temperature, for 2 hours, to allow for the NH₃ to evaporate. The reaction mixture was diluted in 20 mL water, and the organic layer was washed with 100 mL of water followed by 100 mL of saturated aqueous NaCl, dried over MgSO₄. The solution was concentrated to dryness by rotary evaporation at 0 °C to prevent evaporation of the product. The product was purified via flash column chromatography in 9:1 dichloromethane/hexanes and concentrated by rotary evaporation at 0 °C to afford diaziridine **5** as a yellow oil (2.54 g, 90 % yield). ¹H NMR (600 MHz, CDCl₃): δ 7.66 (d, *J* = 7.4 Hz, 2H), 7.39–7.48 (m, 3H), 2.79 (br d, *J* = 8.9 Hz, 1H), 2.24 (br d, *J* = 7.9 Hz, 1H). ¹³C {¹H} NMR (150 MHz, CDCl₃): δ 131.8, 130.2, 129.6, 128.7, 128.2, 127.1, 126.5, 123.6 (q, *J*_{C-F} = 276.5 Hz). ¹⁹F NMR (564 MHz, CDCl₃): δ -75.54.



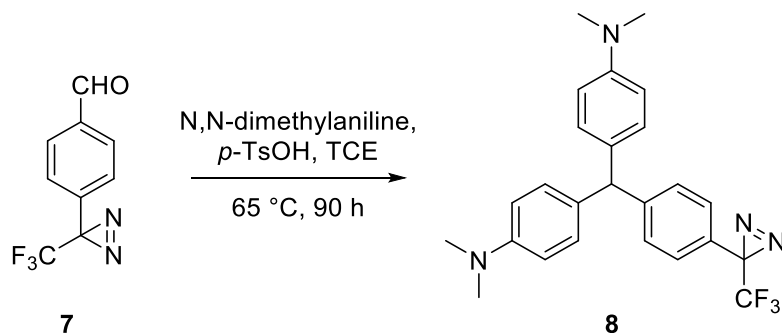
3-Phenyl-3-(trifluoromethyl)-3H-diaziridine 6.⁵ The diaziridine **5** (1.12 g, 6.0 mmol, 1 equiv.) was dissolved in minimal amount of dry MeOH (10 mL) and transferred to a 100-mL oven-dried round-bottom flask equipped with a magnetic stirring rod. Et₃N (1.9 mL, 15.0 mmol, 2.5 equiv.) was added. In a separate vial, I₂ (3.04 g, 12.0 mmol, 2 equiv.) was dissolved in MeOH (40 mL) and added to the reaction mixture until the reaction mixture was completely dark purple in color. The reaction mixture was stirred for 16 hours at room temperature. The reaction mixture was partitioned between 50 mL Na₂S₂O₃ and 50 mL pentane. The organic layer was washed with 50 mL saturated aqueous NaCl and dried over Na₂SO₄. The solution was concentrated to dryness by rotary evaporation. The product was purified using a Kugelrohr distillation apparatus at 50 °C

and under reduced pressure to obtain pure diazirine **6** as a yellow oil (0.73 g, 65 % yield). ^1H NMR (600 MHz, CDCl_3): δ 7.37–7.46 (m, 3H), 7.18–7.24 (d, $J = 7.3$ Hz, 2H). $^{13}\text{C}\{^1\text{H}\}$ NMR (150 MHz, CDCl_3): δ 129.7, 129.2, 128.87, 128.86, 126.50, 126.49, 122.2 (q, $J_{\text{C-F}} = 272.2$ Hz), 103.7. ^{19}F NMR (564 MHz, CDCl_3): δ -65.21.

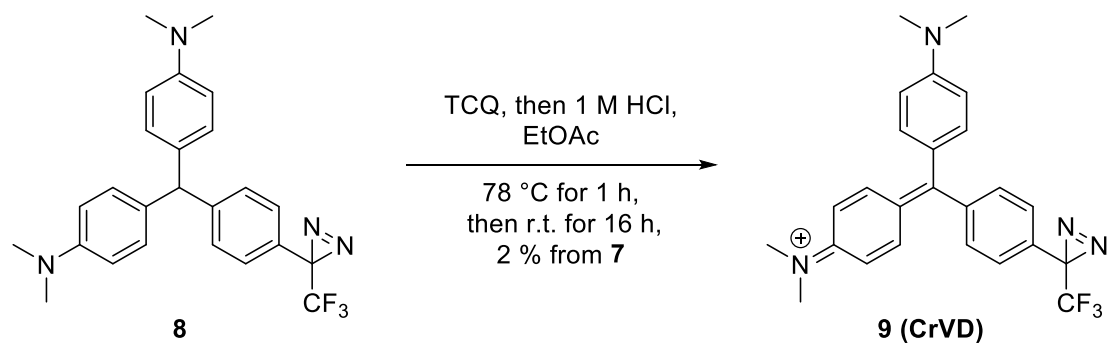


4-(3-(Trifluoromethyl)-3H-diazirin-3-yl)benzaldehyde 7.⁶ Antimony pentafluoride, SbF_5 , (0.19 ml, 2.6 mmol, 1.3 equiv.) and trifluoromethanesulfonic acid, TfOH , (0.46 mL, 5.2 mmol, 2.6 equiv.) were added to a flame-dried 1-dram vial. Meanwhile, the diazirine **6** (0.37 g, 2.0 mmol, 1.0 equiv.) was added to a two-neck 25 mL flame-dried round bottom flask, under N_2 ; followed by 1,1-dichloromethyl methyl ether (2.17 mL, 24.0 mmol, 12.0 equiv.). The two-neck round bottom flask was cooled to $0\text{ }^\circ\text{C}$ in an ice bath. The SbF_5 and TfOH mixture was added in drops over 10 minutes to the chilled two-neck round bottom flask, under N_2 . Once the mixture became a homogenous solution, it was slowly allowed to warm to room-temperature and then stirred for 12 hours at room temperature. The reaction mixture was then cooled to $0\text{ }^\circ\text{C}$ and quenched with 10 mL water. Next, the reaction mixture was neutralized with ~20 mL saturated sodium carbonate (Na_2CO_3) and extracted with ~20 mL hexanes. The organic layer was washed twice with 30 mL saturated aqueous NaCl and dried over Na_2SO_4 . The solution was concentrated to dryness by rotary evaporation. The product was purified via flash column chromatography in 4:1 hexane/diethyl ether and concentrated to dryness at $0\text{ }^\circ\text{C}$ by rotary evaporation to afford formylated diazirine **7** as a yellow oil (0.33 g, 76 % yield). ^1H NMR (600 MHz, CD_3SOCD_3): δ

10.08 (s, 1H), 8.05 (d, $J = 9.2$ Hz, 2H), 7.53 (d, $J = 8.1$ Hz, 2H). $^{13}\text{C}\{^1\text{H}\}$ NMR (150 MHz, CD_3SOCD_3): δ 193.0, 137.5, 133.7, 132.5, 131.5, 130.9, 127.62, 127.61, 122.2 (q, $J_{\text{C-F}} = 270.0$ Hz). ^{19}F NMR (564 MHz, CD_3SOCD_3): δ -64.29.



4,4'-((4-(3-(Trifluoromethyl)-3H-diazirin-3-yl)phenyl)methylene)bis(N,N-dimethylaniline) 8. Aldehyde **7** (0.25 g, 1.17 mmol, 1 equiv.) was placed in an oven-dried 25-mL round bottom flask, equipped with a magnetic stirring bar. 1,1,2,2-Tetrachloroethane, TCE, (4 mL) was added, followed by *N,N*-dimethylaniline (0.593 mL, 4.68 mmol, 4 equiv.) and *p*-toluenesulfonic acid, TsOH, (0.223 g, 1.17 mmol, 1 equiv.). The reaction mixture was stirred for 90 hours at 65 °C and was then allowed to cool to room temperature, diluted in 10 mL benzene, washed twice with 20 mL saturated Na_2CO_3 , and dried over Na_2SO_4 . The solution was concentrated to dryness by rotary evaporation to afford a dark-green oil. Crude product **8** (0.491 g) was used without further purification and was not isolated for analysis.



CrVD (9).⁷ Compound **8** (0.491 g, 1.12 mmol, 1 equiv.) was dissolved in EtOAc (6 mL), transferred to a 2-neck round bottom flask equipped with a magnetic stirring rod and a condenser fitted with a nitrogen inlet adapter. Tetrachloroquinone (0.413 g, 1.68 mmol, 1.5 equiv.) was added to the reaction mixture which was then stirred at 78 °C for 1 hour under a constant flow of N₂. The reaction mixture was cooled to room temperature and 1 M HCl (6 mL, 0.1 M final concentration of **8**) was added and the reaction mixture was stirred at room temperature for 16 hours. The reaction mixture was then diluted with 10 mL H₂O and the aqueous layer was washed four times with 10 mL EtOAc. The aqueous layer which was an intense green color was concentrated *in vacuo* at 45 ° to a volume of ~5 mL. The mixture was purified on a reverse-phase HPLC (gradient elution 10–45 % CH₃CN/H₂O (+ 0.1% TFA) over 45 minutes). The fractions that contained the correct mass of CrVD by ESI-MS were combined and lyophilized to obtain a green TFA salt of CrVD (0.09 g, 2 % yield from **7**). ¹H NMR (600 MHz, CDCl₃): δ 7.30–7.39 (m, 8H), 9.43 (br d, *J* = 7.1 Hz, 4H), 3.34 (br s, 12H). ¹³C{¹H} NMR (150 MHz, CDCl₃) (partial data): δ 174.9, 157.1, 140.8, 140.7, 134.6, 133.8, 127.3, 126.3, 114.03, 41.0. ¹⁹F NMR (564 MHz, CDCl₃): δ -64.62. HRMS (ESI-TOF) *m/z*: [M]⁺ calcd for C₂₅H₂₄F₃N₄⁺ 437.1953, observed 437.1971.

Docking with AutoDock Vina^{8,9}

While learning how to perform docking with the AutoDock Vina software I wrote instructions on how to do that for ease of future use. These instructions are specifically written for Windows computers:

To run AutoDock Vina you will need to download AutoDockTools (<http://mgltools.scripps.edu/downloads>) and AutoDock Vina (<http://vina.scripps.edu/download.html>).

Setting up the directories

It is important to keep all your files (PDBQT files as well as the vina.exe application in the same directory). I suggest creating a new folder on the Local Disk :C called “ADTworkspace”. To do this (on Windows) go to: This PC > Local Disc (:C) > Right click > New > Folder. Then, rename the New Folder to “ADTworkspace”.

In this directory you will be creating different folders to run different dockings. For now, create a new folder titled “ligand1”.

Go to your Program Files where you installed AutoDock Vina. If you had not moved it, it should be in :C\Program Files (x86)\The Scripps Research Institute\Vina and copy the vina application (vina.exe). Next, paste this in the directory that you previously created “ligand1”.

You will need the PDBs of your receptor or protein that you are docking to and the ligand that you are docking. Obtain or create those PDB files and copy them into “ligand1”. Rename the protein

PDB file to “protein.pdb” and the ligand PDB to “ligand1.pdb”. Note that the ligand should be previously minimized in Maestro/MacroModel or a similar software.

Preparing the protein for docking

Open AutoDockTools (ADT) and do the following:

File > Preferences > Set... under the “General” tab in the “Startup Directory” paste the path to the “ligand1” folder. If you have followed these instructions exactly it should be :C\ADTworkspace\ligand1 and then press “Make Default” and “Set” buttons consecutively. You can now exit out of this window.

File > Read Molecule and select the protein.pdb file

Edit > Delete Water

Edit > Hydrogens > Add... select the “Polar Only” option and click OK

Grid > Macromolecule > Choose and select the “protein_model1” and click “Select Molecule” then click “OK”. A window will pop up and prompt you to save the file as a PDBQT (this is the file type that we need to run AutoDock Vina). Name the file as “protein.pdbqt”. The protein backbone should turn grey.

Setting up the Grid Box

Grid > Grid Box -> a new window will pop up titled “Grid Options”. In this window we will set up where exactly we want our ligand to dock. We will do the following:

Right click on “Spacing (angstrom)” and in the new window that popped up change the “Value” to 1. Click “Apply” and then “OK”. The box in your protein should enlarge.

Maneuver both the “Center Grid Box” and the “number of points” in each dimension to fully cover the site that you want to be docked. Leave this window open while you do the next step.

Setting up the configurations file

When you have the area that you want covered go to your “ligand1” folder and Right click > New > Text document. Rename it to “config” (NOTE: do NOT write an extension in the name, so only name it config, NOT config.txt). This is the file where all the commands for running Vina will be saved. In this document write the following:

```
receptor = protein.pdbqt
```

```
ligand = ligand1.pdbqt
```

```
out = out.pdbqt
```

```
center_x = (type in the number from the “Grid Options” window under x center)
```

```
center_y = (type in the number from the “Grid Options” window under y center)
```

```
center_z = (type in the number from the “Grid Options” window under z center)
```

```
size_x = (type in the number from the “Grid Options” window under number of points in x-  
dimensions)
```

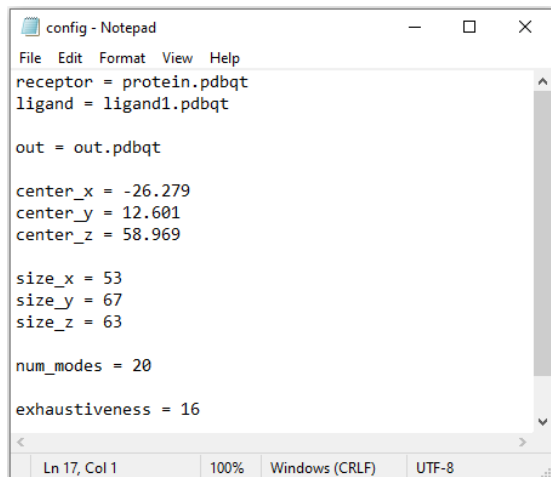
```
size_y = (type in the number from the “Grid Options” window under number of points in y-  
dimensions)
```

```
size_z = (type in the number from the “Grid Options” window under number of points in z-  
dimensions)
```

```
num_modes = 20 (# of configurations that it will compute, 20 seems to be the max)
```

```
exhaustiveness = 16 (how exhaustive the search is, default for this is 8)
```

Your text file should look something like this:



```
config - Notepad
File Edit Format View Help
receptor = protein.pdbqt
ligand = ligand1.pdbqt

out = out.pdbqt

center_x = -26.279
center_y = 12.601
center_z = 58.969

size_x = 53
size_y = 67
size_z = 63

num_modes = 20

exhaustiveness = 16

Ln 17, Col 1    100%    Windows (CRLF)    UTF-8
```

Preparing the ligand for docking

It is now okay to close the “Grid Options” window.

Ligand > Input > Open... next to “File name” there is a drop-down menu that is set to PDBQT files: (*.pdbqt). Change this to PDB files: (*.pdb) and choose the “ligand1” PDB file. Click “Open”. A message will pop up, click OK.

Rotate the view in ADT using your mouse (rotate with left mouse button, zoom-in with the scroll wheel, move with right mouse button) to see the ligand. Hide the protein by deselecting the red circle in the “DashBoard” on the left-hand side of ADT, to the right of “protein_model1”

Ligand > Output > Save as PDBQT... save it as “ligand1.pdbqt”

It is now okay to close out of ADT.

Running AutoDock Vina

Open Command Prompt and type in the following commands:

```
cd C:\ADTworkspace\ligand1 [Press enter]
```


vina.exe --config config.txt --log log.txt [Press enter]

AutoDock Vina should now run, you can follow the progress by the movement of **** under the %.

Interpreting results

AutoDock Vina will generate two files out.pdbqt and log.txt in the “ligand1” folder. You can open the out.pdbqt in PyMol or ADT. Open this alongside the protein file in Pymol and observe the docked structures. To maneuver between the different outputs use the left and right arrows. The first structure is the lowest energy one and the last one is the highest energy structure.

The log file contains the affinity data for all the outputs.

Docking of CrV and CrVD to trimer 1

The crystal structure of trimer **1** was used by downloading the previously deposited crystal structure (PDB ID 5SUR). The crystal structure of CrV was used by extracting it from a deposited structure containing CrV (PDB ID 3VW1) and minimizing the structure in PyMol. To generate a model of CrVD the extracted and minimized structure of CrV was used and one of the *N,N*-dimethylamino groups was changed into a trifluoromethyldiazirine group in PyMol, followed by an energy minimization.

Docking was performed using AutoDock Tools and AutoDock Vina. In AutoDock Tools, a grid was chosen to encompass the entirety of trimer **1** in the size of 30x30x30 Å. Trimer **1** was treated as a rigid receptor in these calculations. The lowest energy cluster, as determined by AutoDock Vina, was chosen to represent the docking model shown in Figure 1.1 in the main text.

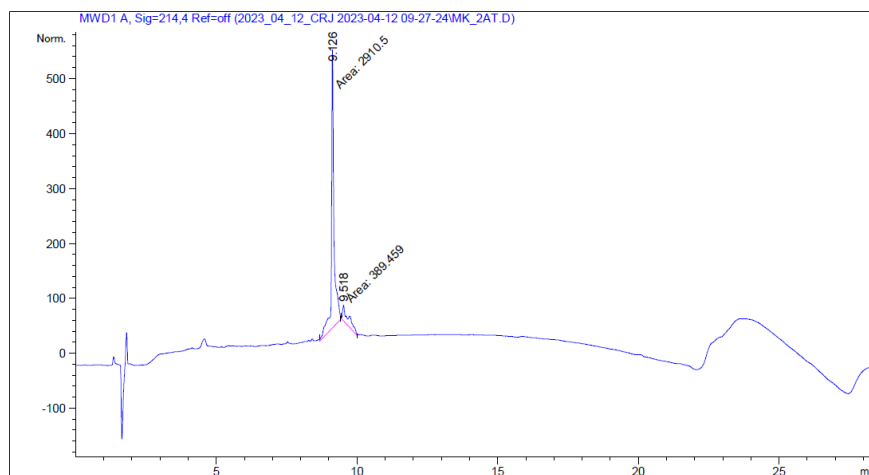
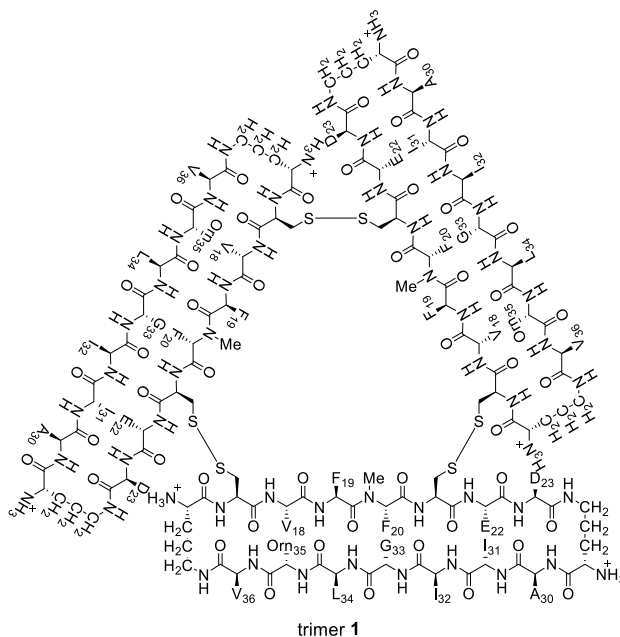
References

1. Kraus, G. A.; Jeon, I.; Nilsen-Hamilton, M.; Awad, A. M.; Banerjee, J.; Parvin, B. Fluorinated Analogs of Malachite Green: Synthesis and Toxicity. *Molecules* **2008**, *13*, 986–994.
2. Salveson, P. J.; Haerianardakani, S.; Thuy-Boun, A.; Yoo, S.; Kreutzer, A. G.; Demeler, B.; Nowick, J. S. Repurposing Triphenylmethane Dyes to Bind to Trimers Derived from A β . *J. Am. Chem. Soc.* **2018**, *140*, 11745–11754.
3. The procedure for peptide synthesis follow closely to those that our laboratory has previously published. The procedures in this section were either adapted from or taken verbatim from: Kreutzer, A. G.; Yoo, S.; Spencer, R. K.; Nowick, J. S. Stabilization, Assembly, and Toxicity of Trimers Derived from A β . *J. Am. Chem. Soc.* **2017**, *139*, 966–975.
4. Wang, L.; Murai, Y.; Yoshida, T.; Ishida, A.; Masuda, K.; Sakihama, Y.; Hashidoko, Y.; Hatanaka, Y.; Hashimoto, M. Alternative One-Pot Synthesis of (Trifluoromethyl)Phenyldiazirines from Tosyloxime Derivatives: Application for New Synthesis of Optically Pure Diazirinyphenylalanines for Photoaffinity Labeling. *Org. Lett.* **2015**, *17*, 616–619.
5. Nakamoto, K.; Ueno, Y. Diazirine-Containing RNA Photo-Cross-Linking Probes for Capturing MicroRNA Targets. *J. Org. Chem.* **2014**, *79*, 2463–2472.
6. Nakashima, H.; Hashimoto, M.; Sadakane, Y.; Tomohiro, T.; Hatanaka, Y. Simple and Versatile Method for Tagging Phenyldiazirine Photophores. *J. Am. Chem. Soc.* **2006**, *128*, 15092–15093.
7. Budin, G.; Chung, H. J.; Lee, H.; Weissleder, R. A Magnetic Gram Stain for Bacterial Detection. *Angew. Chem. Int. Ed.* **2012**, *51*, 7752–7755.

8. Trott, O.; Olson, A. J. AutoDock Vina: Improving the Speed and Accuracy of Docking with a New Scoring Function, Efficient Optimization, and Multithreading. *J. Comput. Chem.* **2010**, *31*, 455–461.
9. Eberhardt, J.; Santos-Martins, D.; Tillack, A. F.; Forli, S. AutoDock Vina 1.2.0: New Docking Methods, Expanded Force Field, and Python Bindings. *J. Chem. Inf. Model.* **2021**, *61*, 3891–3898.

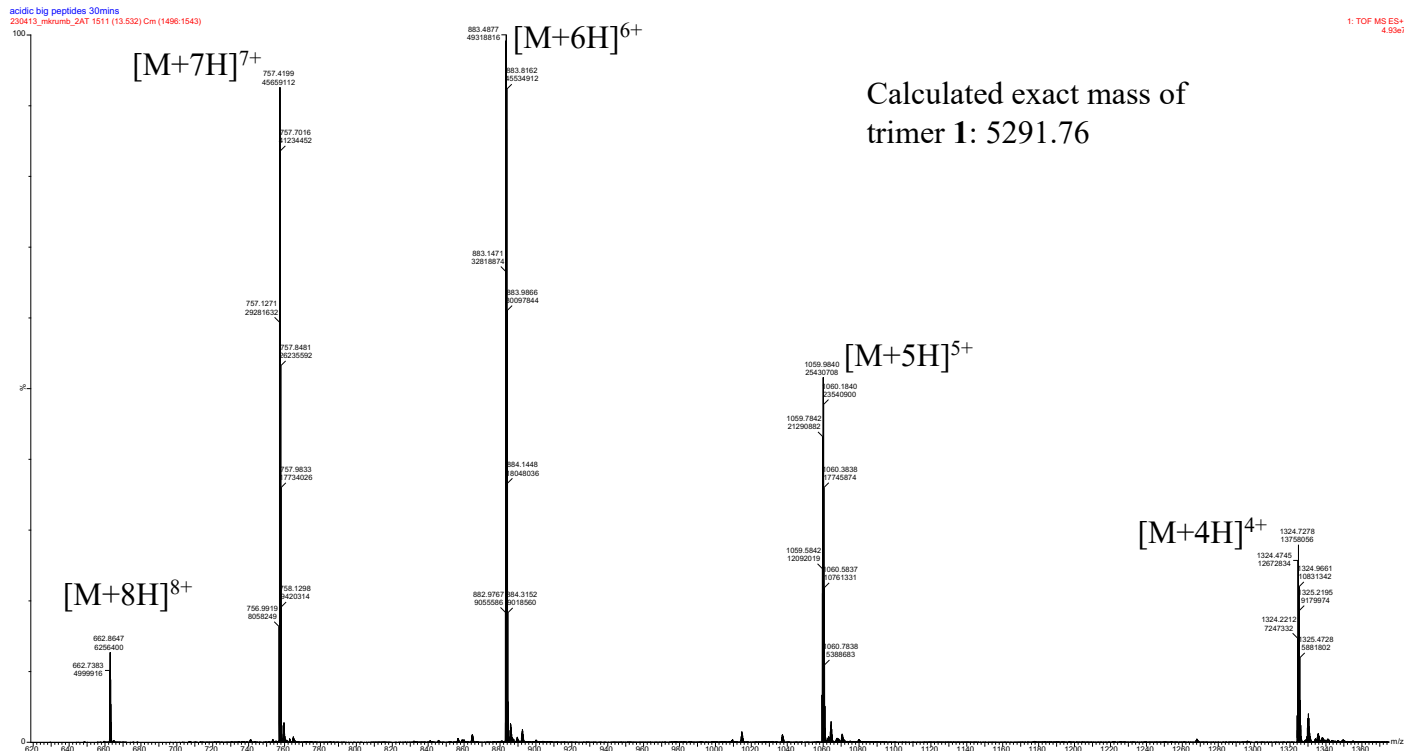
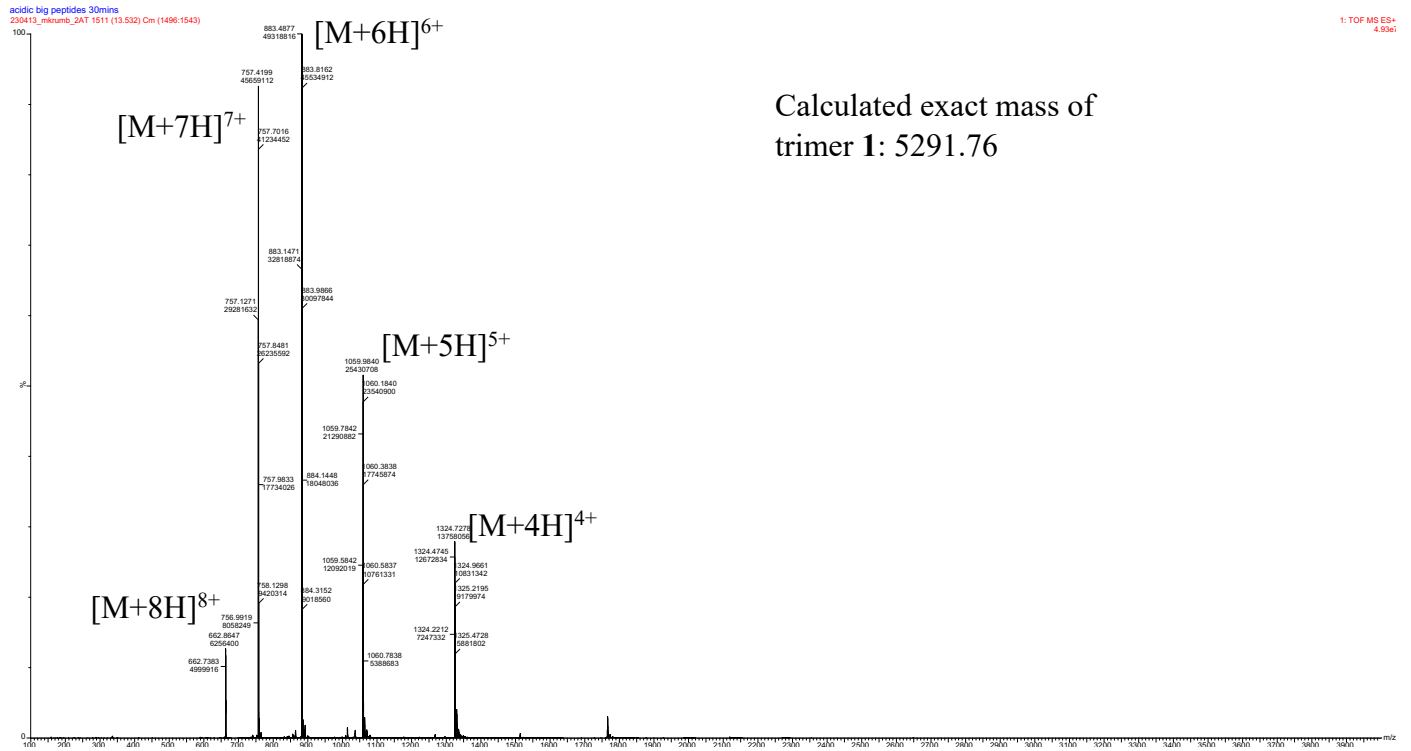
Characterization data

Characterization of trimer 1

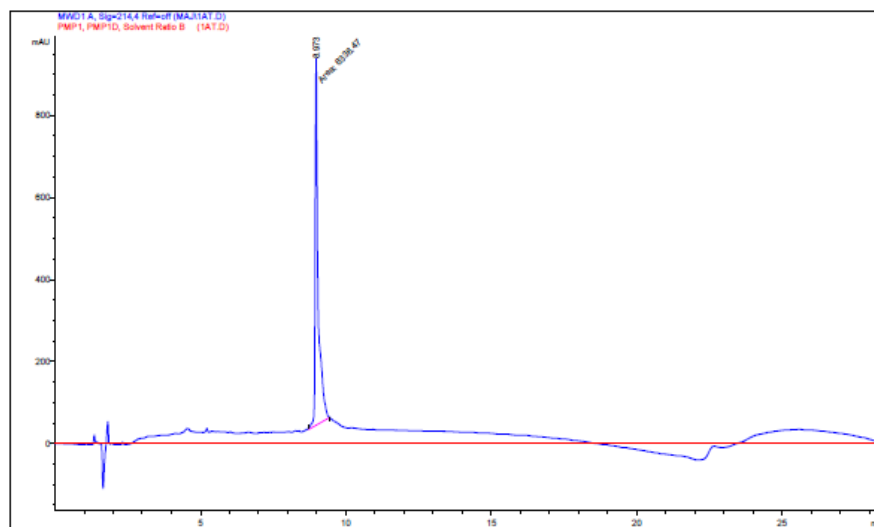
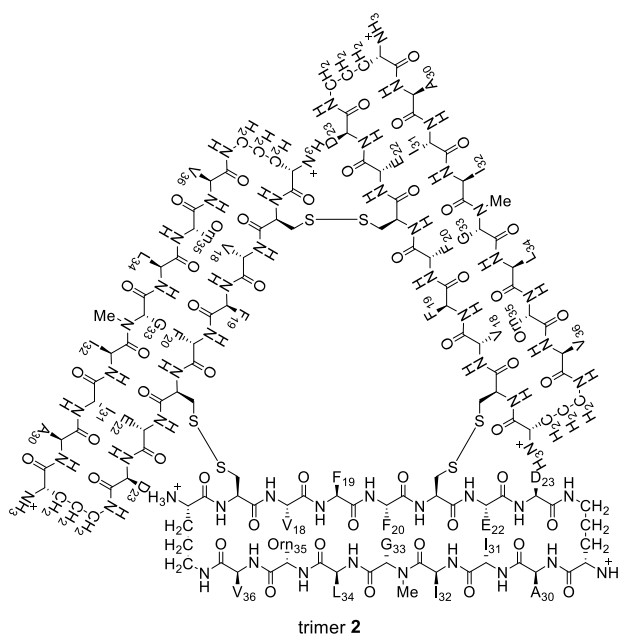


Peak #	RetTime [min]	Type	Width [min]	Area [mAU*s]	Height [mAU]	Area %
1	9.126	MM	0.1057	2910.50464	458.99066	88.1981
2	9.518	MM	0.2550	389.45923	25.45078	11.8019

Mass spectrum and expansions of trimer 1

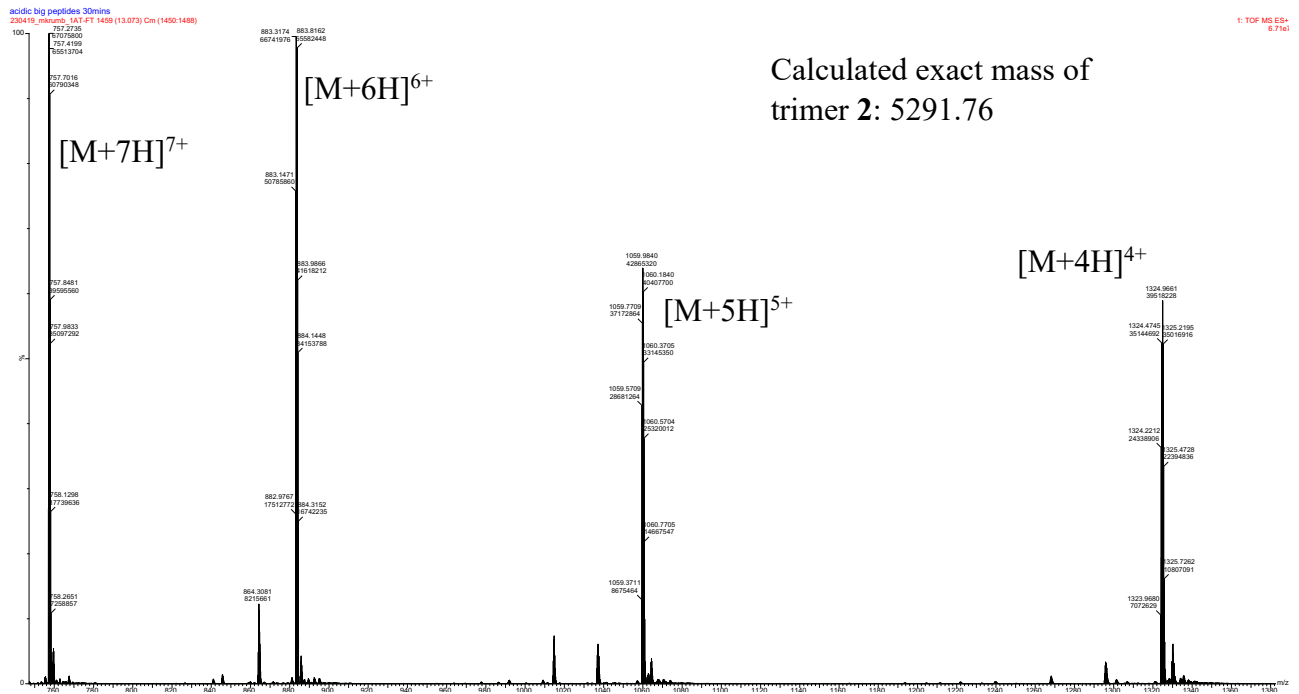
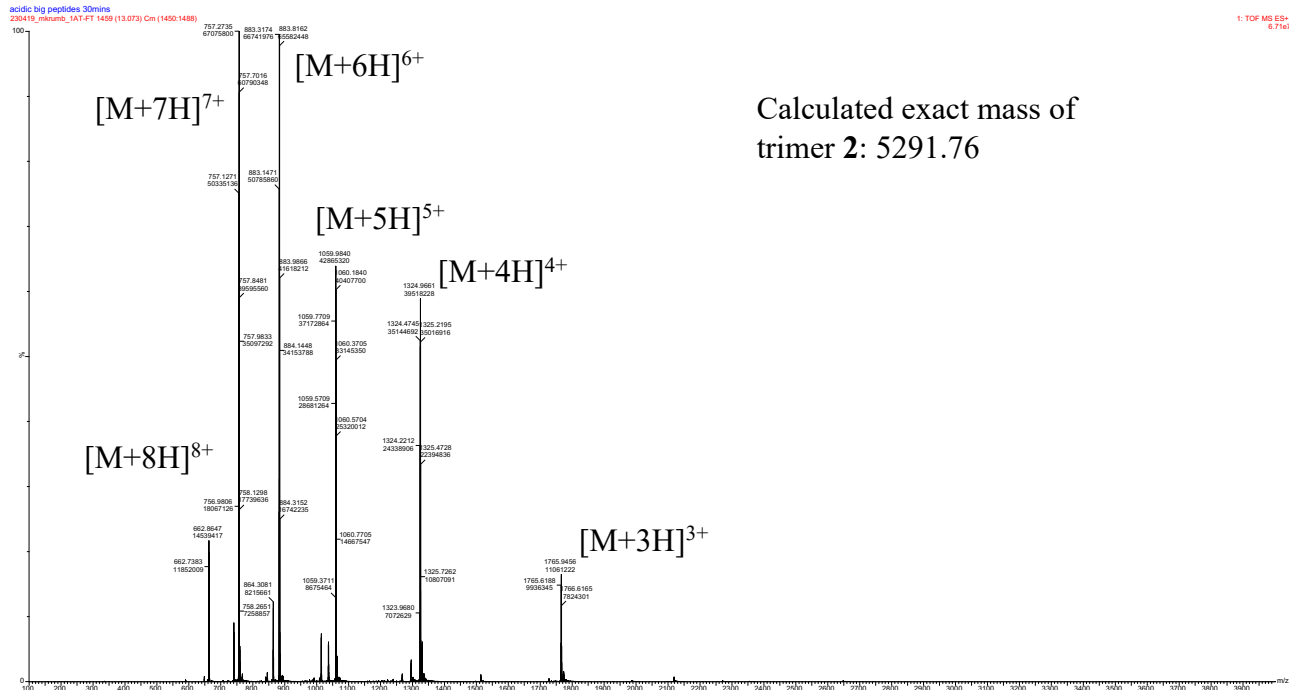


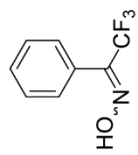
Characterization of trimer 2



Peak #	RetTime [min]	Type	Width [min]	Area [mAU*s]	Height [mAU]	Area %
1	8.973	MM	0.1177	6338.47070	897.29651	100.0000

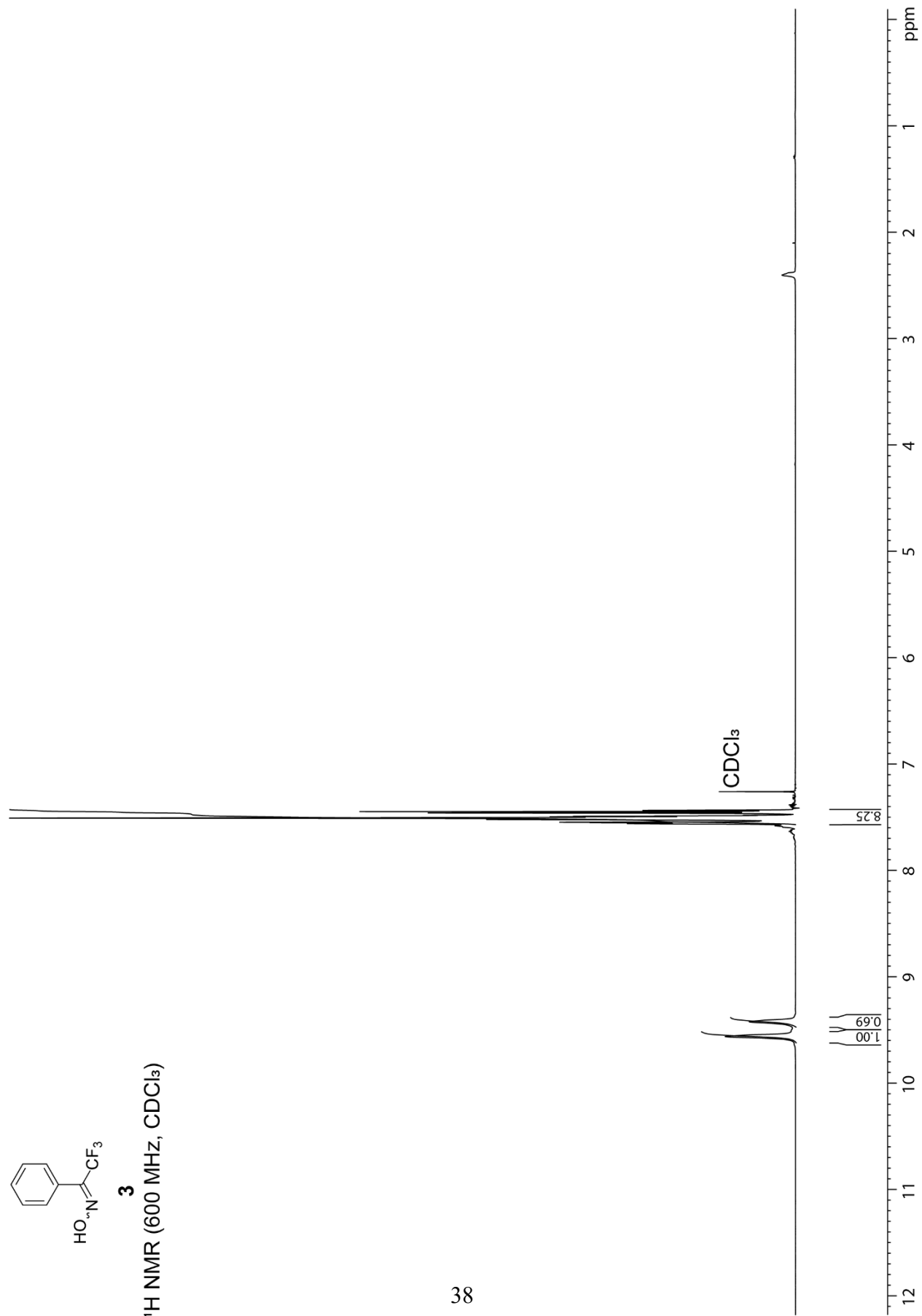
Mass spectrum and expansions of trimer 1

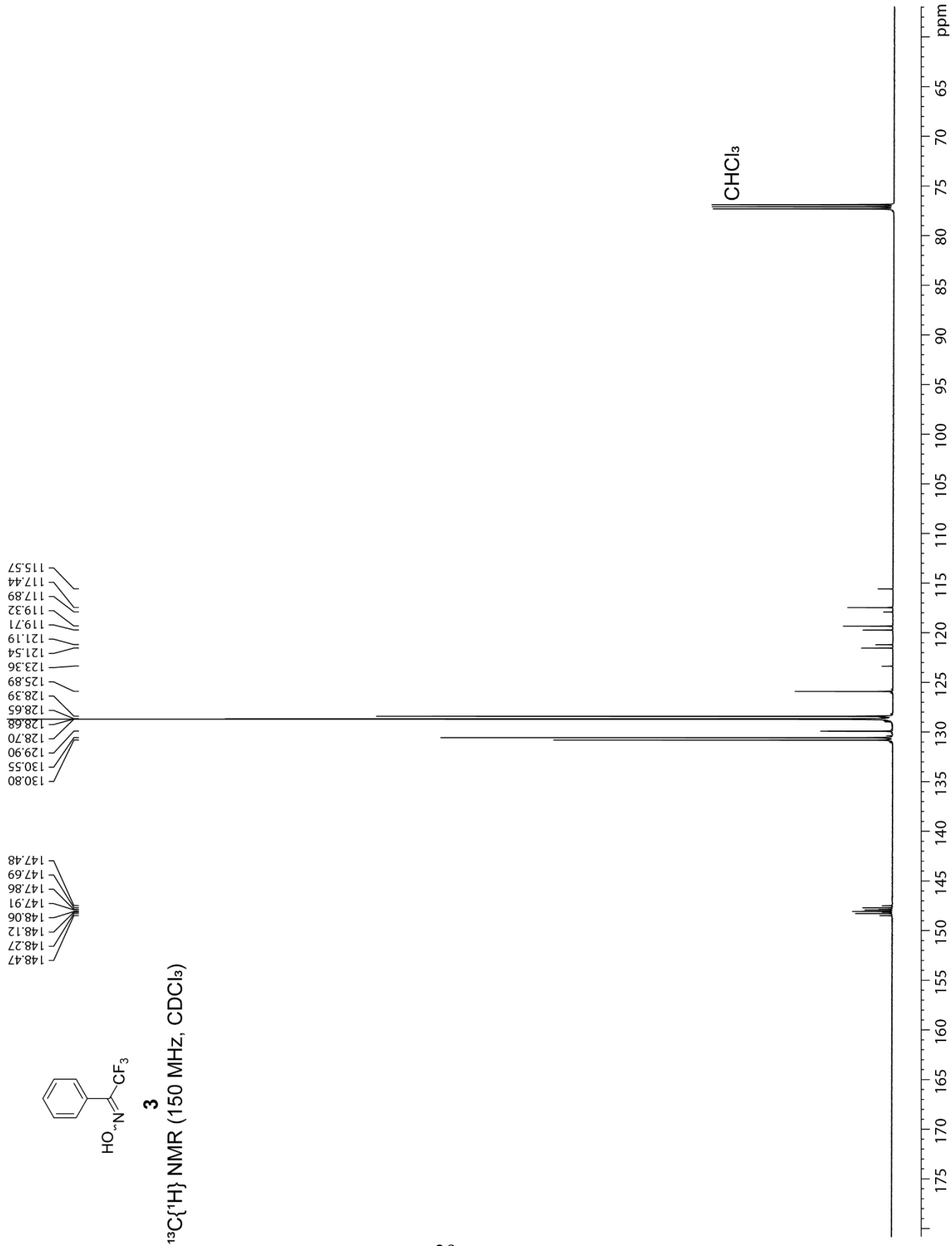


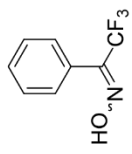


3

¹H NMR (600 MHz, CDCl₃)

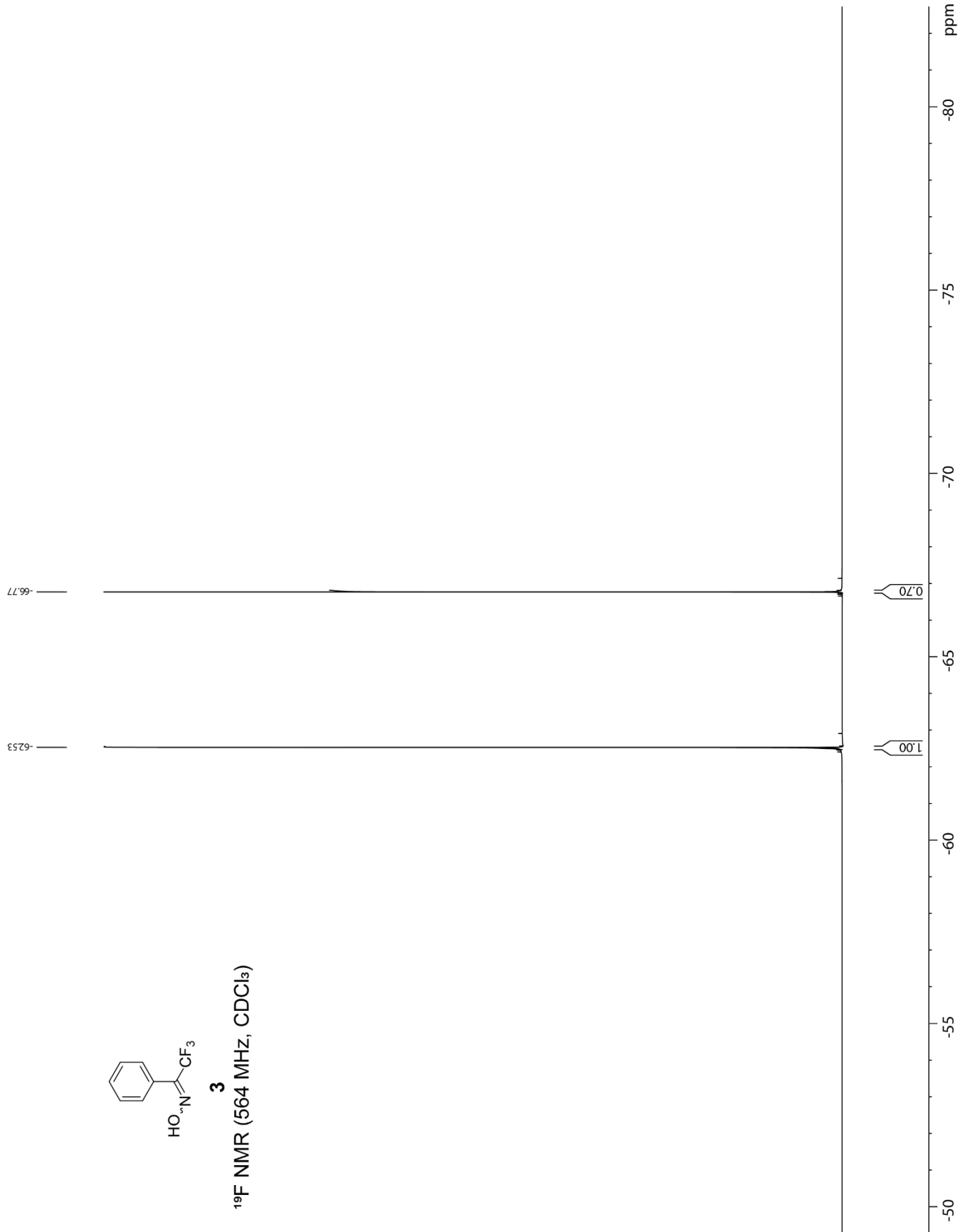


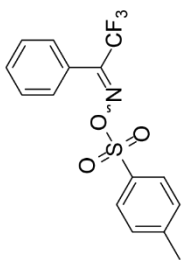




3

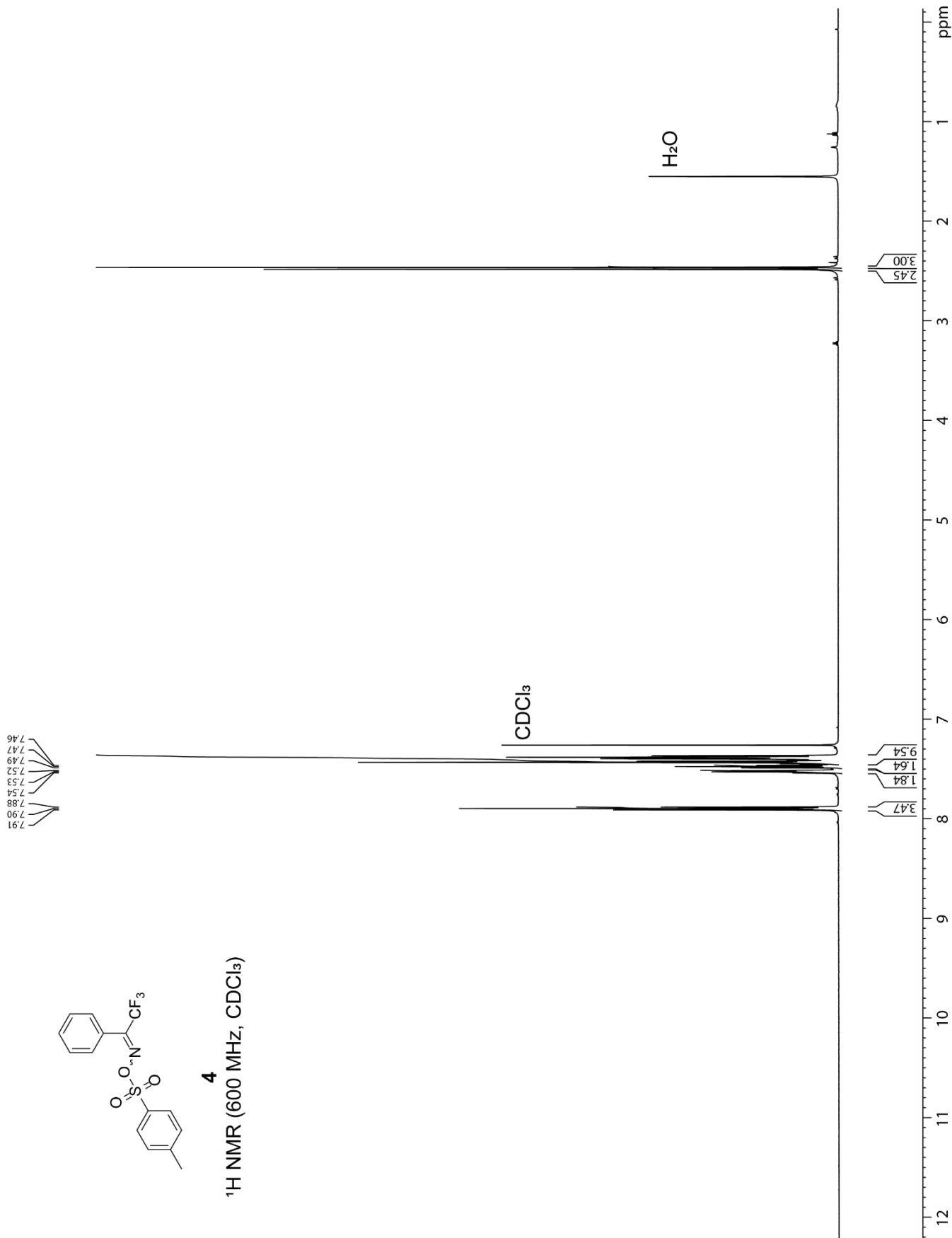
¹⁹F NMR (564 MHz, CDCl₃)



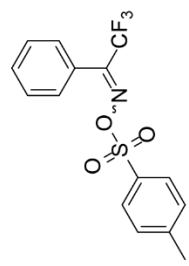


4

¹H NMR (600 MHz, CDCl₃)



154.44
154.38
154.21
154.16
153.99
153.95
153.77
153.74
146.03
146.18
131.80
131.68
131.52
131.26
129.94
129.33
129.19
128.90
128.87
128.76
128.43
127.83
124.68
120.57
120.18
118.73
118.30
116.42

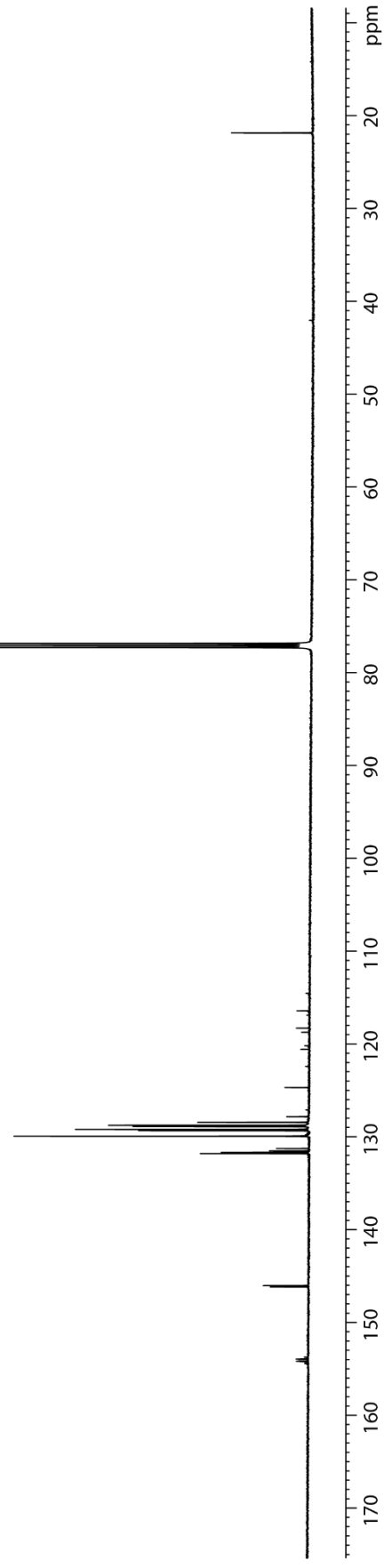


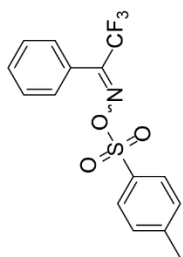
4

$^{13}\text{C}\{^1\text{H}\}$ NMR (150 MHz, CDCl_3)

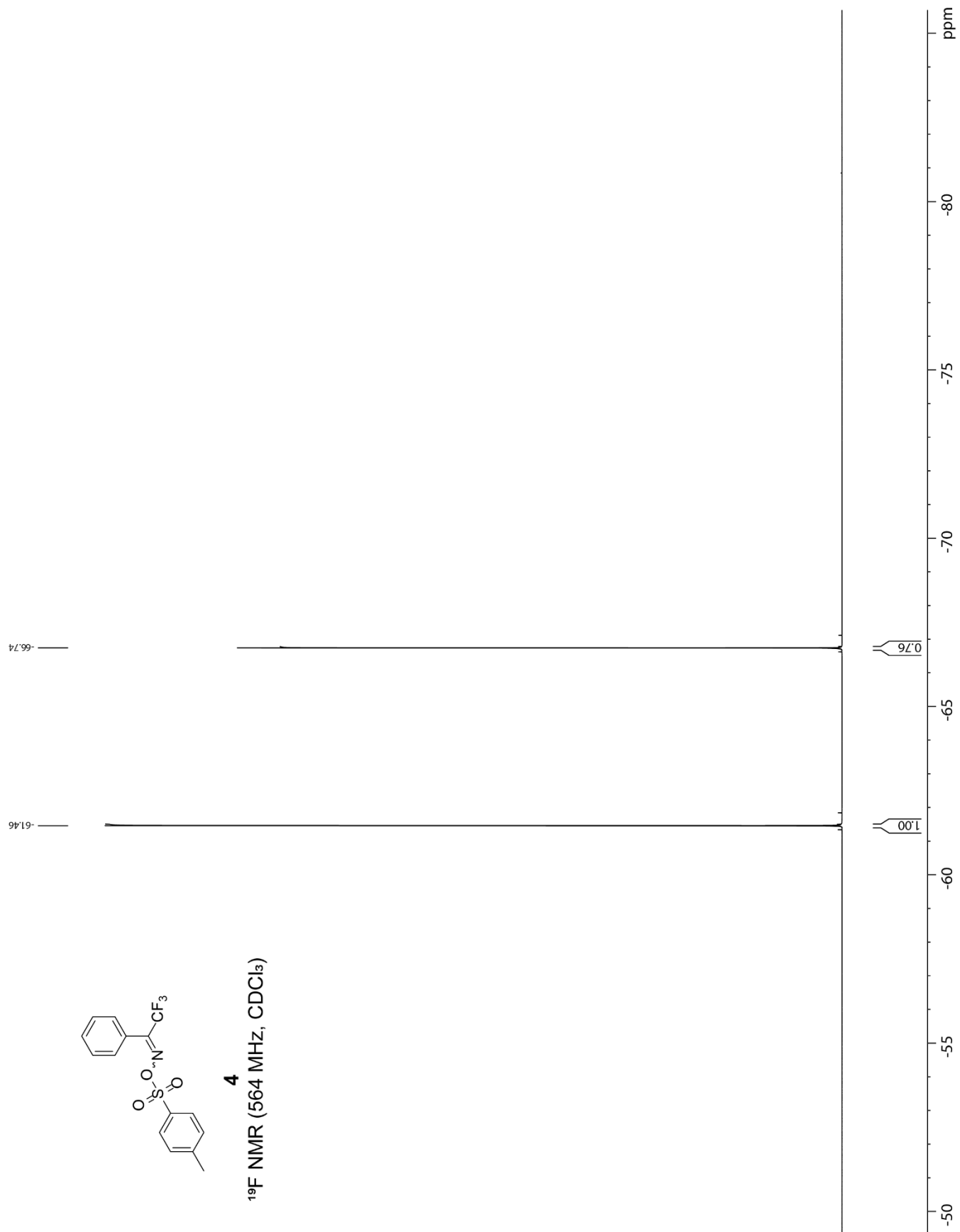
CHCl_3

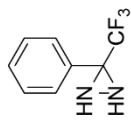
21.85
21.83





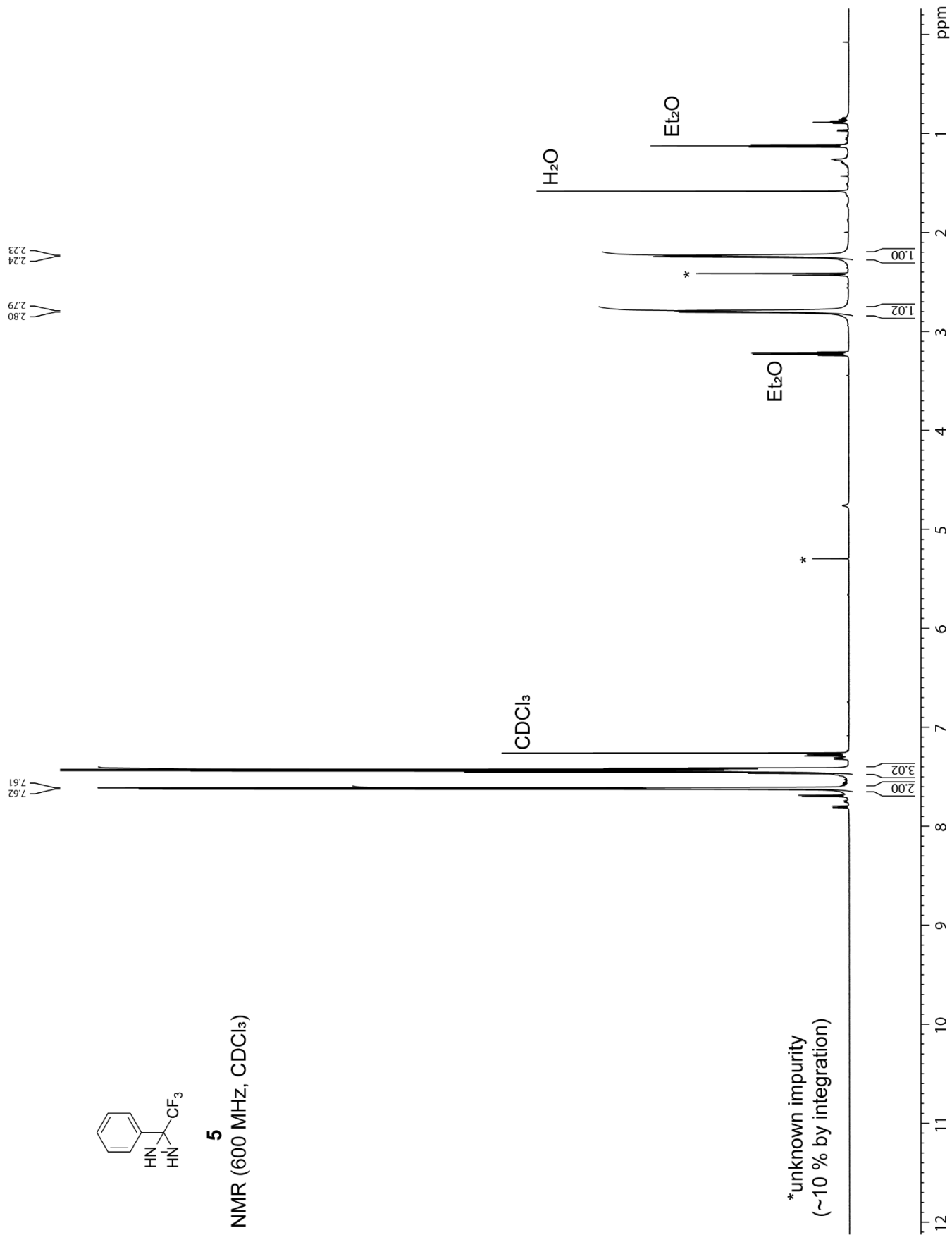
4
¹⁹F NMR (564 MHz, CDCl₃)





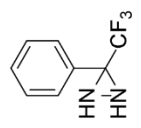
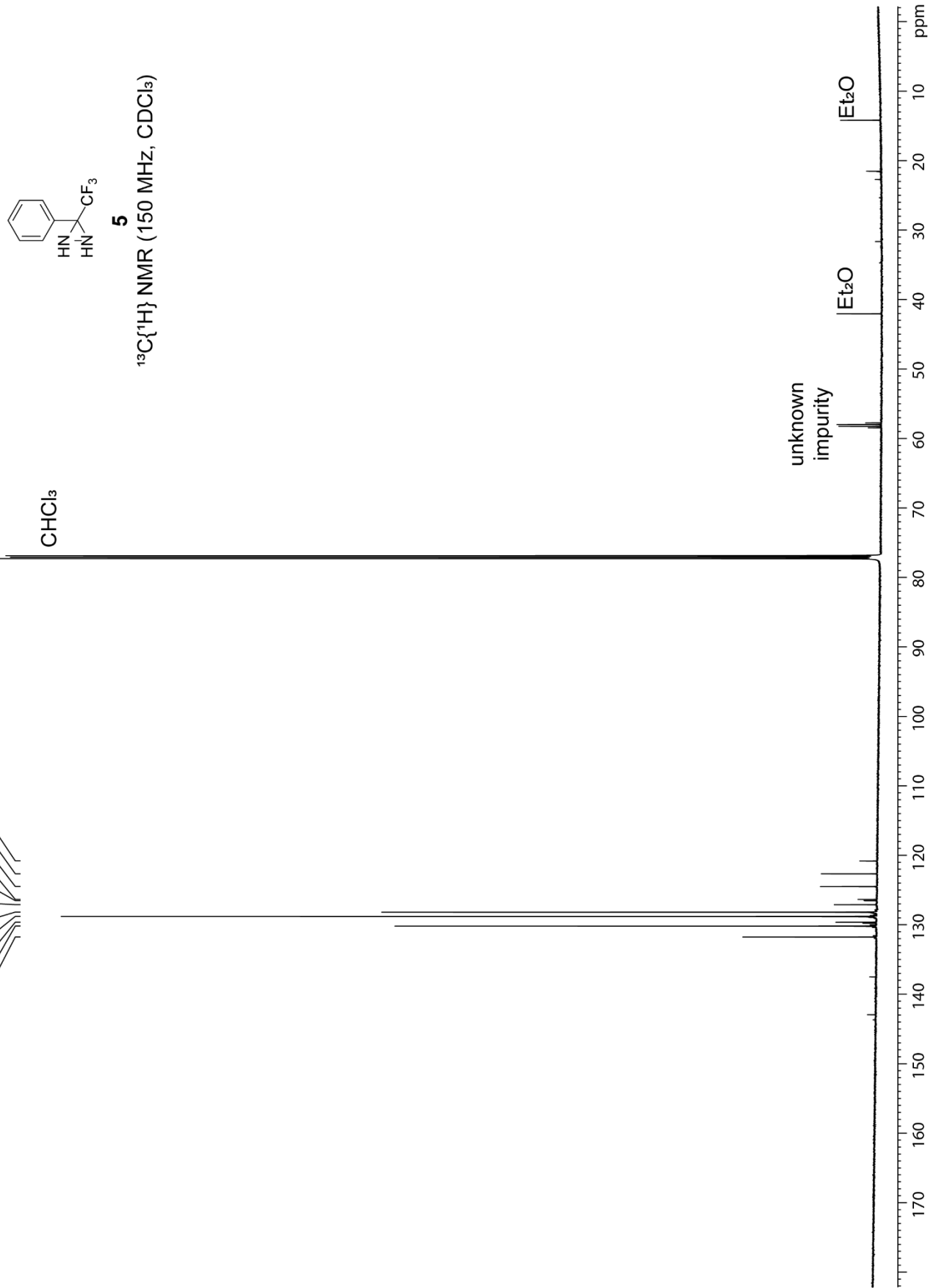
5

¹H NMR (600 MHz, CDCl₃)



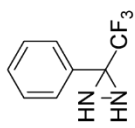
*unknown impurity
(~10 % by integration)

131.76
130.20
129.62
128.80
128.18
127.09
126.53
126.34
124.50
122.65
120.81



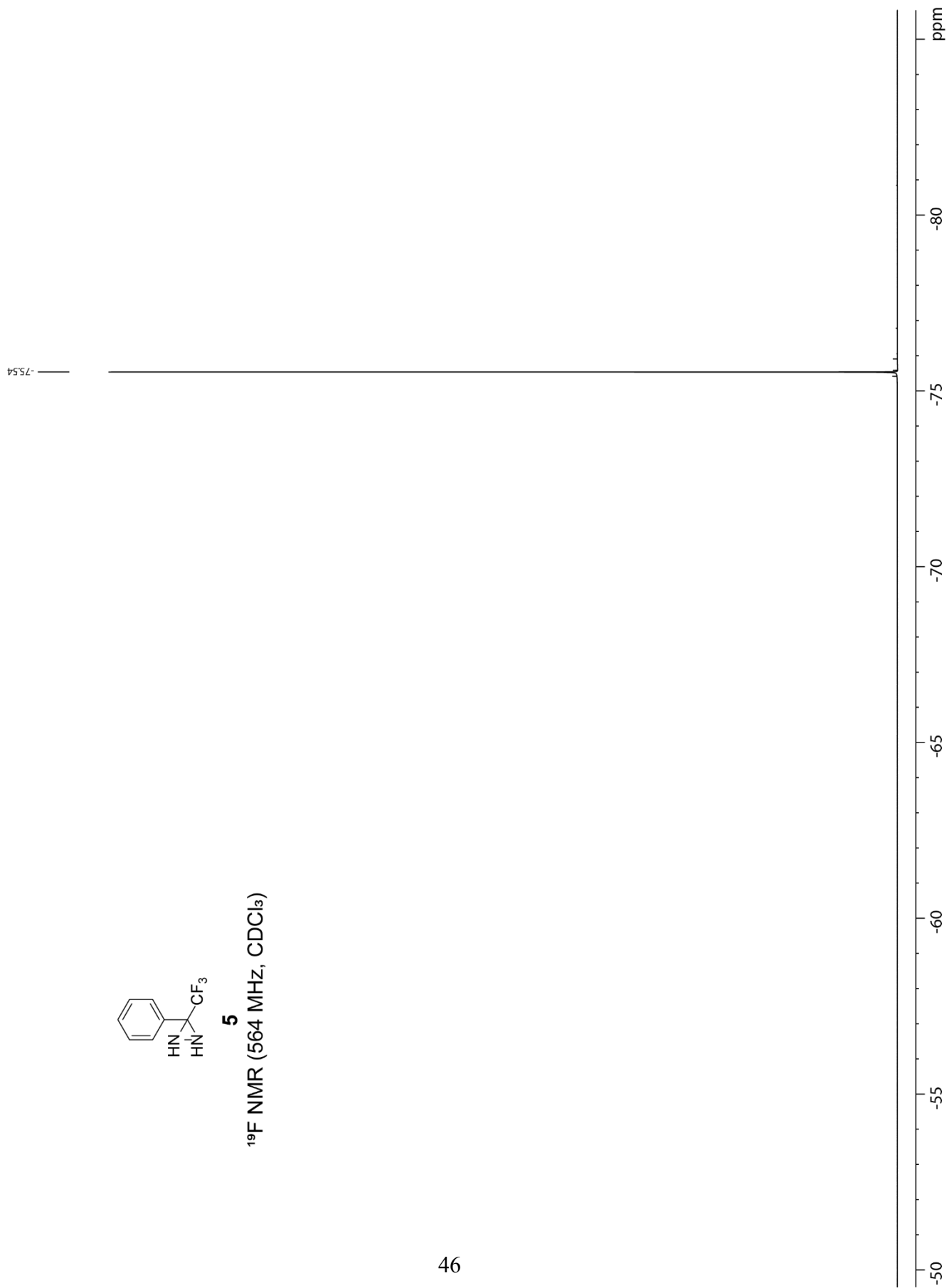
5

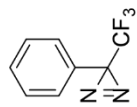
¹³C{¹H} NMR (150 MHz, CDCl₃)



5

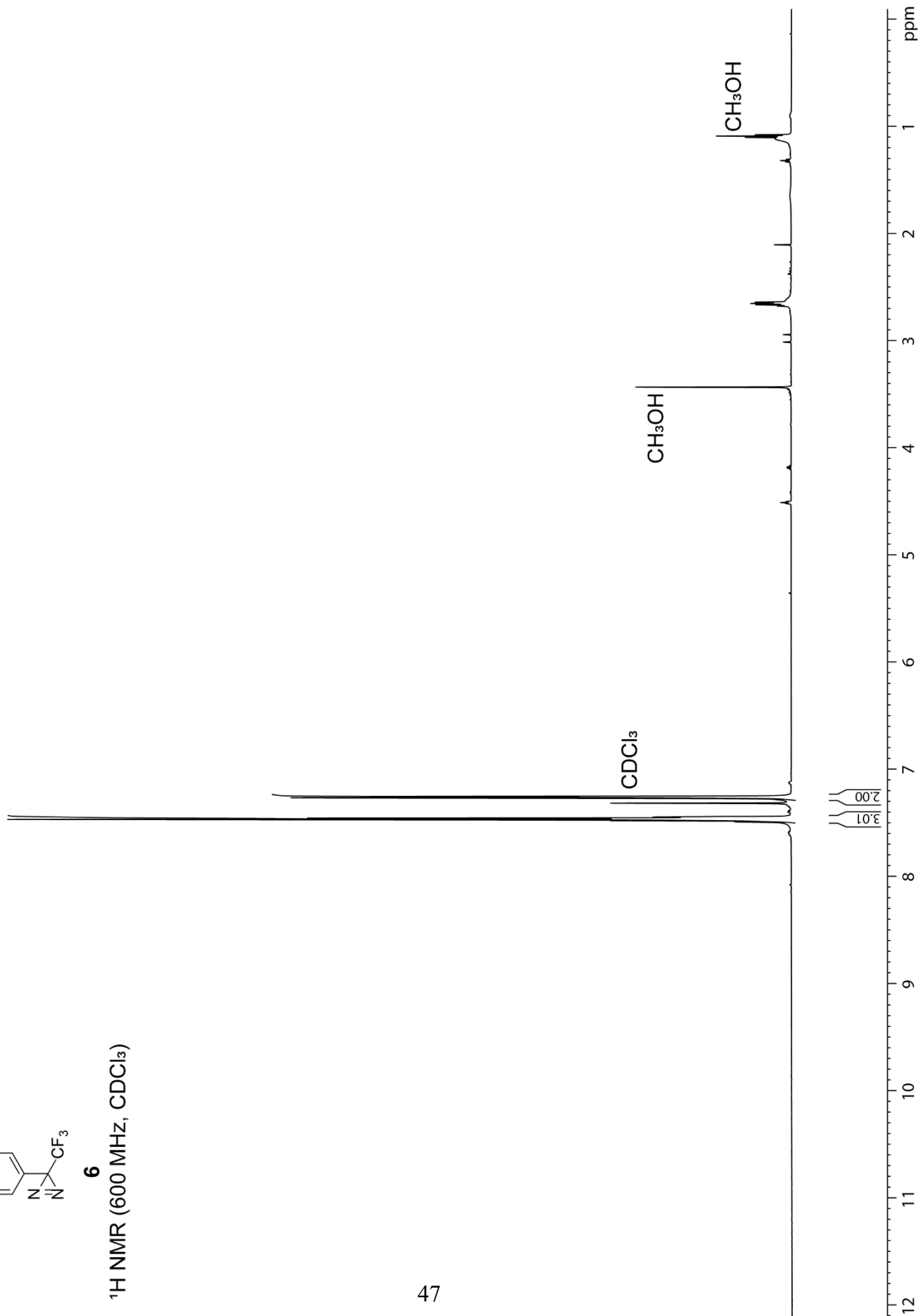
¹⁹F NMR (564 MHz, CDCl₃)

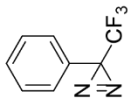




6

¹H NMR (600 MHz, CDCl₃)



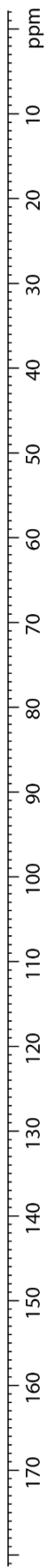


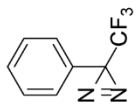
6

$^{13}\text{C}\{^1\text{H}\}$ NMR (150 MHz, CDCl_3)

129.66
129.16
128.87
128.87
126.50
126.50
124.92
123.10
121.28
119.46

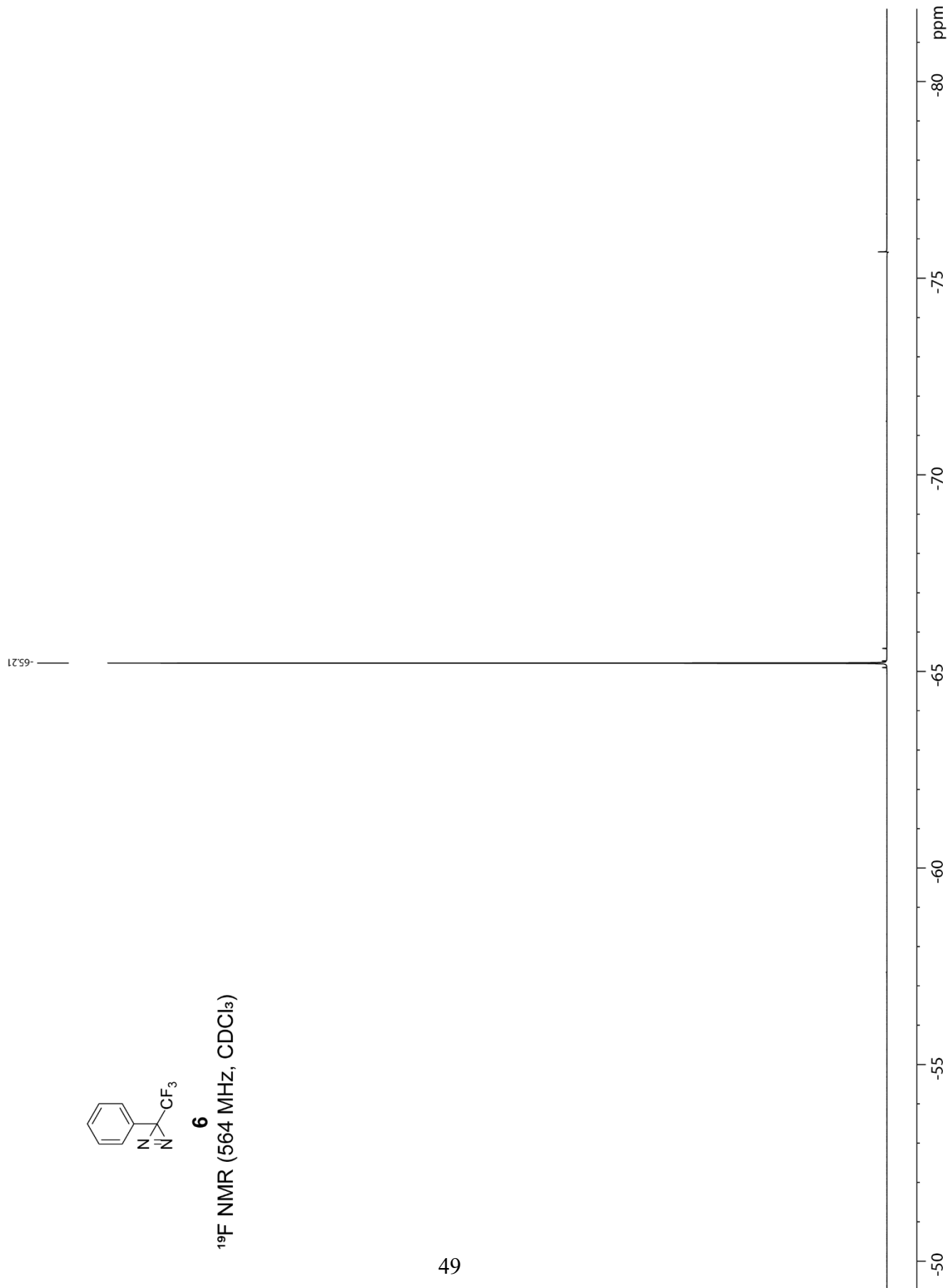
CHCl_3

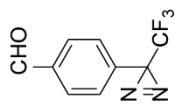




6

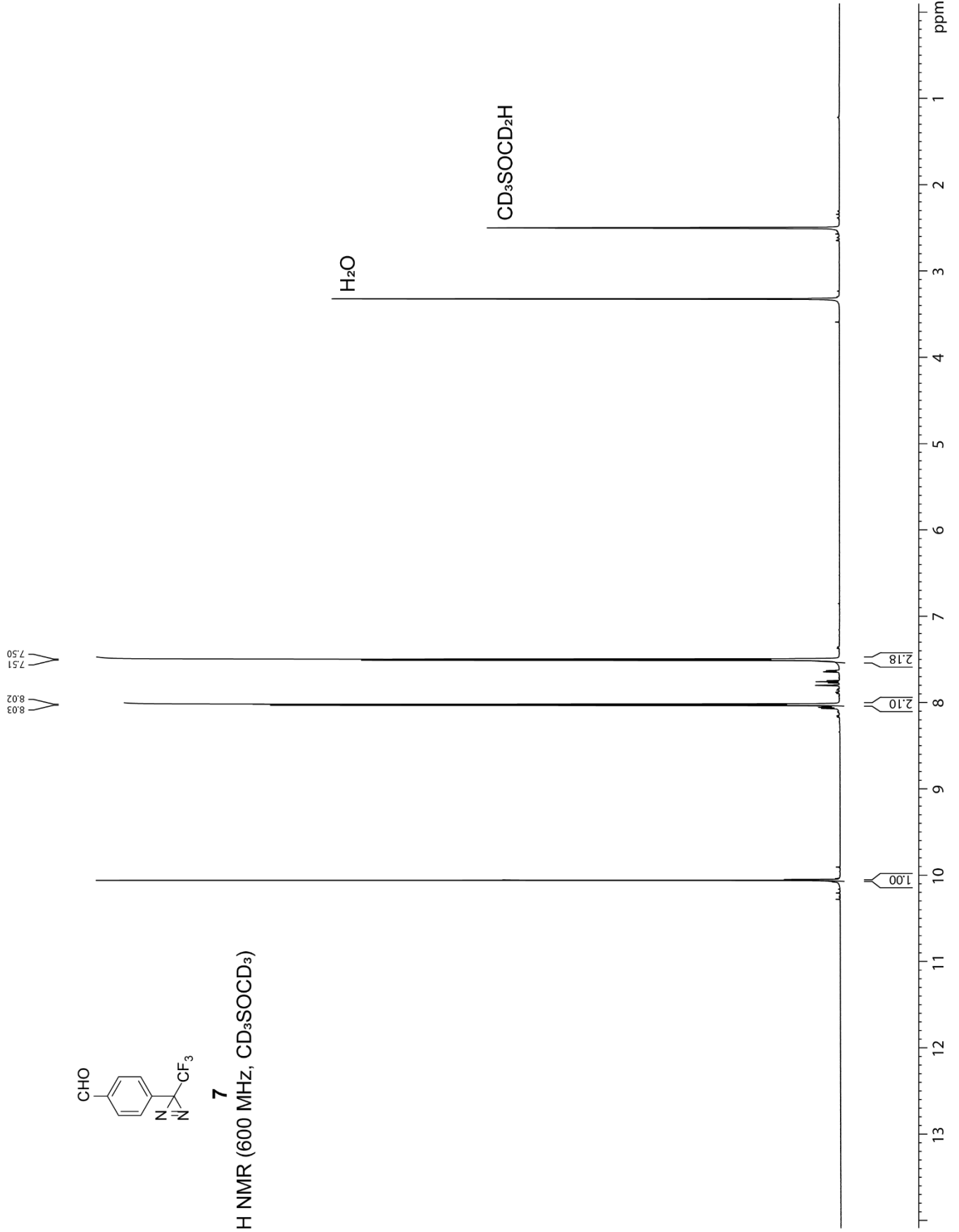
¹⁹F NMR (564 MHz, CDCl₃)



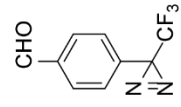


7

¹H NMR (600 MHz, CD₃SOCD₃)



137.46
133.73
132.54
131.45
130.99
127.62
127.62
124.86
123.03
121.21
121.21
119.40



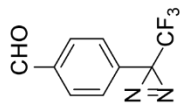
7

$^{13}\text{C}\{^1\text{H}\}$ NMR (150 MHz, CD_3SOCD_3)

CD_3SOCD_3

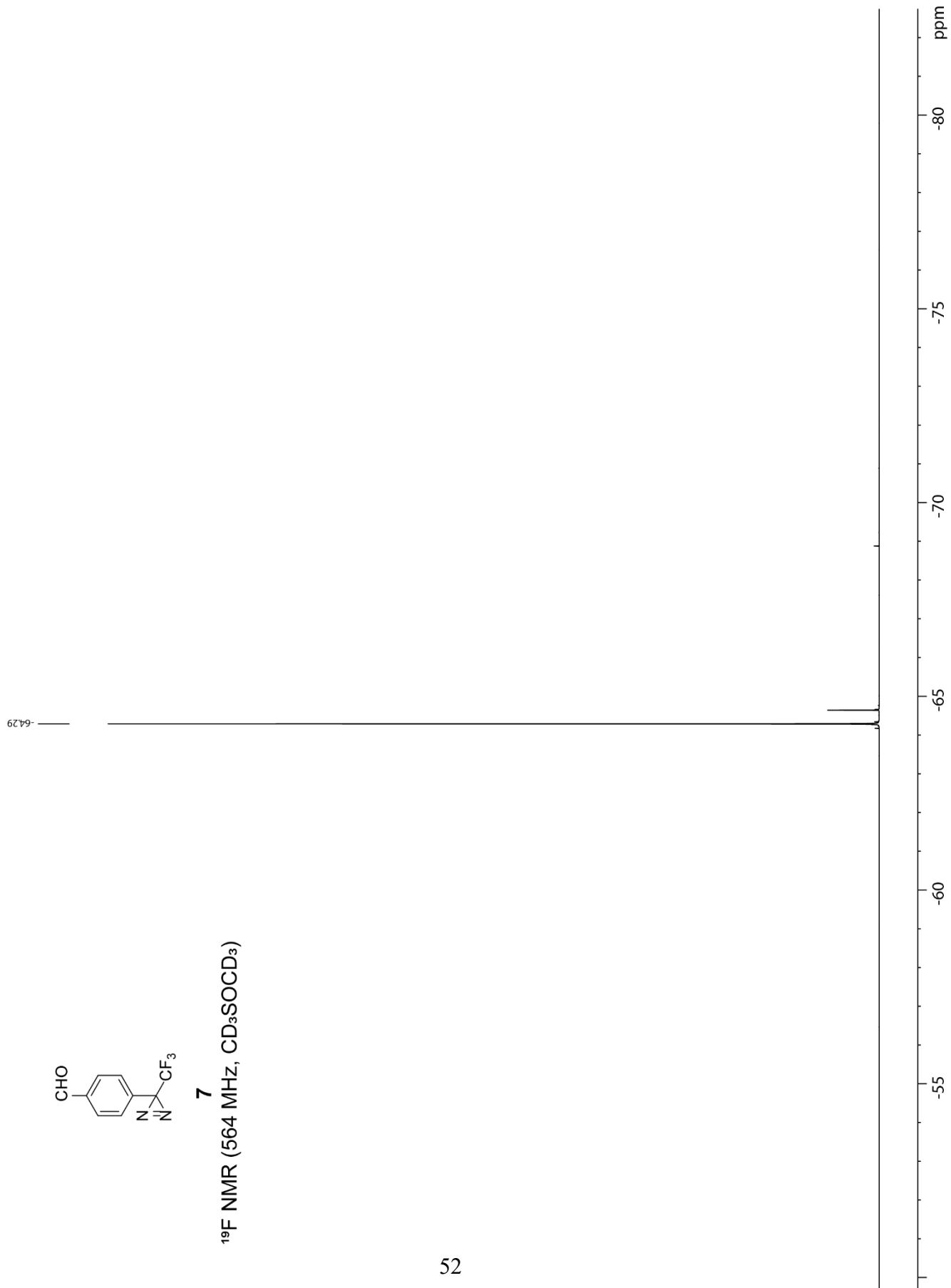
193.04

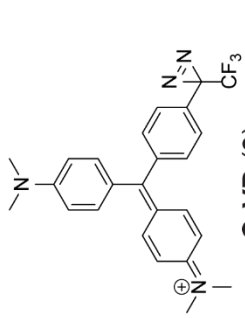




7

¹⁹F NMR (564 MHz, CD₃SOCD₃)



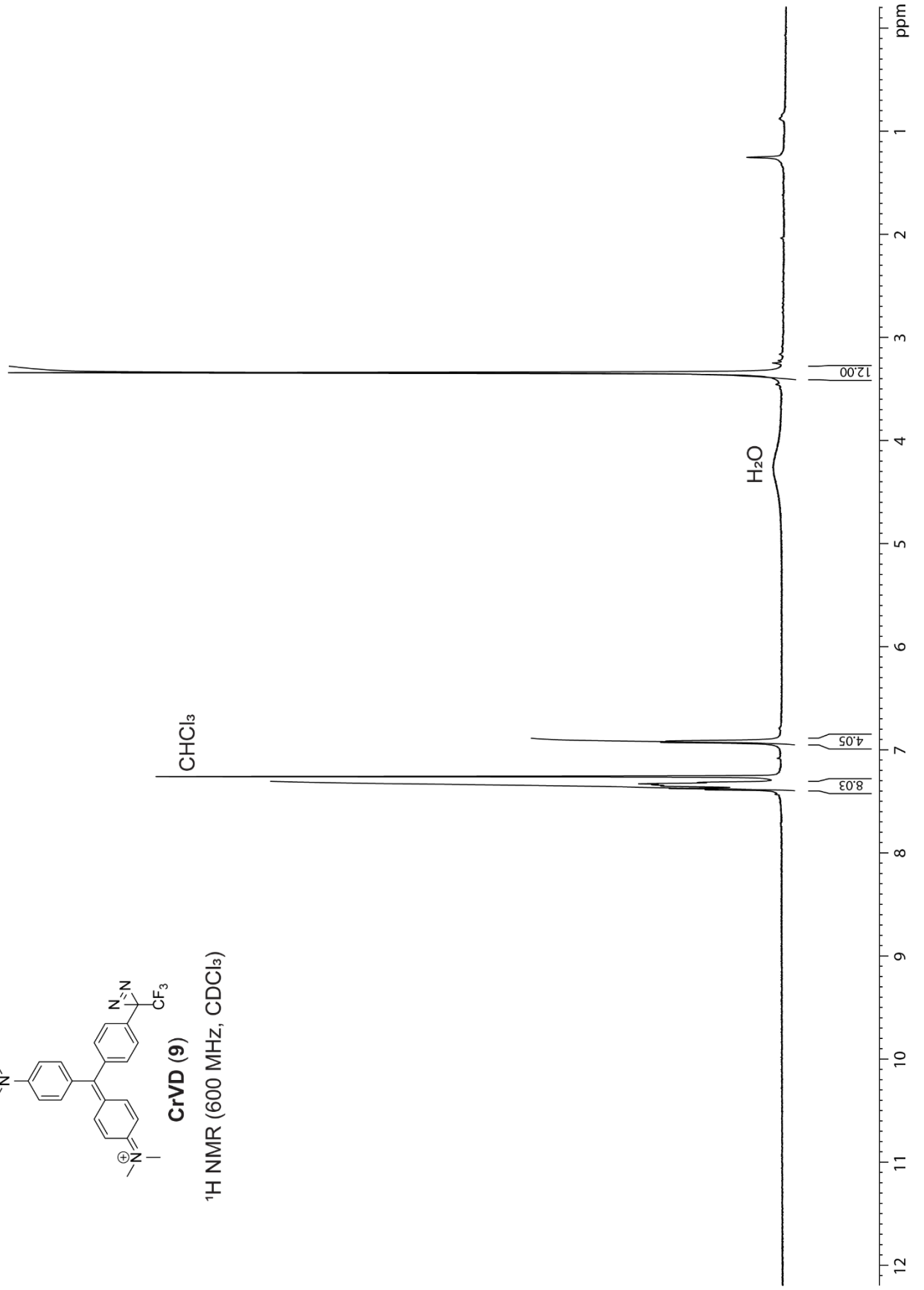


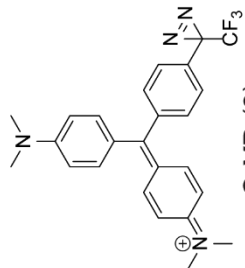
CrVD (9)

¹H NMR (600 MHz, CDCl₃)

6.93
6.92

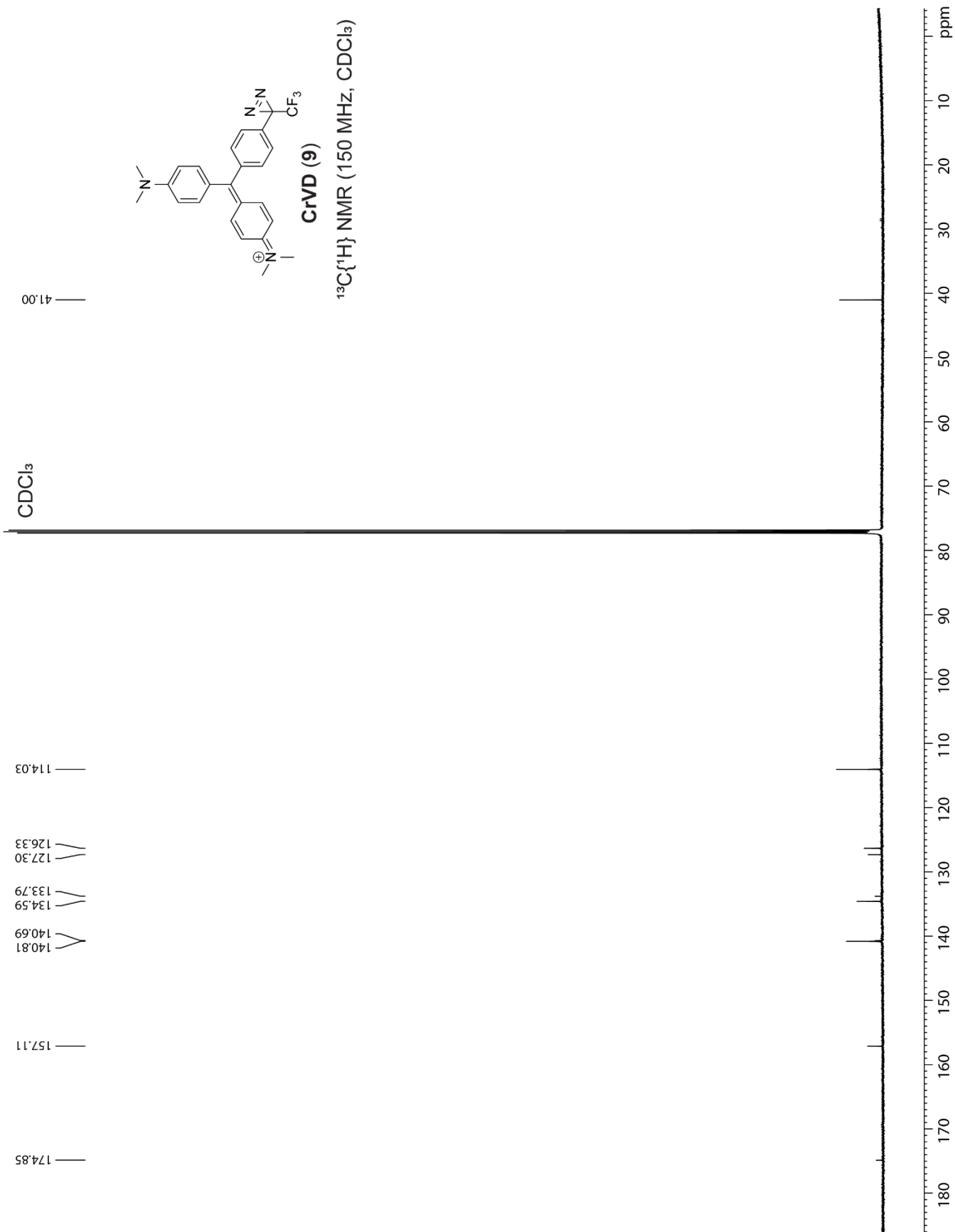
CHCl₃

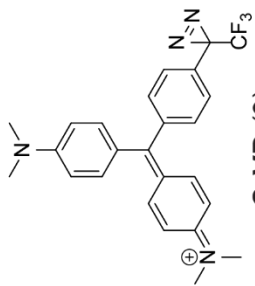




CrVD (9)

$^{13}\text{C}\{^1\text{H}\}$ NMR (150 MHz, CDCl_3)





CrVD (9)

¹⁹F NMR (564 MHz, CDCl₃)

-75.62

-64.62

CF₃COO⁻

-85 ppm

-80

-75

-70

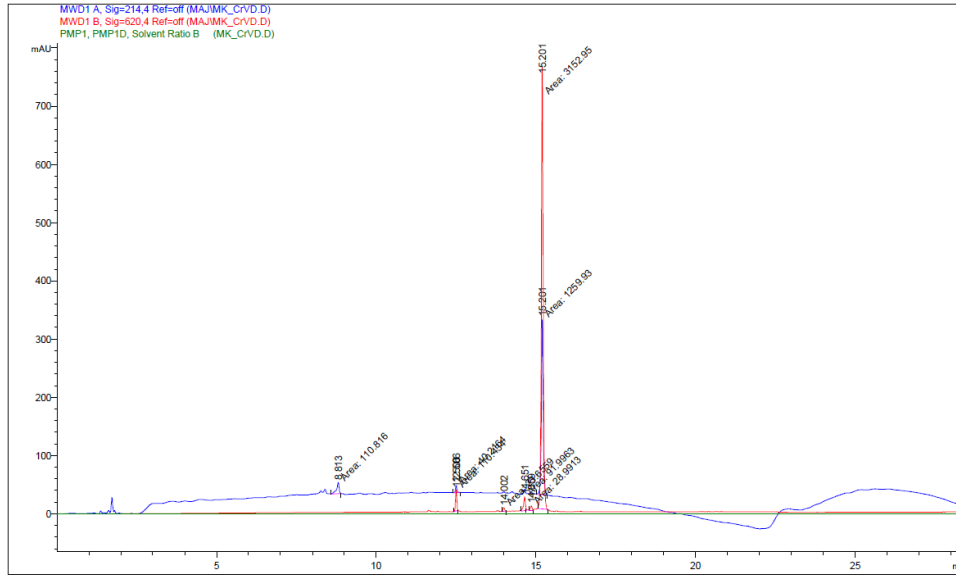
-65

-60

-55

-50

CrVD (9) analytical RP-HPLC trace at 214 nm (blue) and 620 nm (red)



Signal 1: MWD1 A, Sig=214,4 Ref=off

Peak #	RetTime [min]	Type	Width [min]	Area [mAU*s]	Height [mAU]	Area %
1	8.813	MM	0.0964	110.81645	19.15050	7.8539
2	12.506	MM	0.0539	40.21640	12.43984	2.8503
3	15.201	MM	0.0695	1259.93433	302.14481	89.2958

Signal 2: MWD1 B, Sig=620,4 Ref=off

Peak #	RetTime [min]	Type	Width [min]	Area [mAU*s]	Height [mAU]	Area %
1	12.506	MM	0.0497	110.43396	37.00518	3.2404
2	14.002	MM	0.0603	23.65589	6.54333	0.6941
3	14.651	MM	0.0647	91.99634	23.70169	2.6994
4	14.859	MM	0.0642	28.99134	7.52945	0.8507
5	15.201	MM	0.0689	3152.95215	762.18719	92.5154

Chapter II

Capturing Higher Order Assemblies with Carbene-Mediated Crosslinking

ABSTRACT

Oligomeric assemblies are central to the pathogenesis of amyloid β in Alzheimer's disease. However, amyloid β oligomers are difficult to study due to their solubility, heterogeneity, and metastability. To try and understand the possible oligomeric structures that contribute to the toxicity of amyloid β we have designed, synthesized, and studied numerous peptide models that form higher order assemblies. This chapter describes the design, synthesis, and characterization of peptide **11**, a photolabile A β -derived peptide model developed to study these assemblies by capturing them with covalent bond formation through photolysis. Peptide **11** is designed to mimic the A β_{16-36} β -hairpin and contains a photolabile moiety — diazirine at the 35 position through a mutation of the native methionine to a noncanonical amino acid — photomethionine. Peptide **11** runs as a dimer and hexamer on SDS-PAGE after UV irradiation; the dimer is only observed following UV irradiation, indicating the ability of photomethionine to form covalent bonds between oligomeric assemblies. Studies by X-ray crystallography, SDS-PAGE, and LC-MS offer an insight into the types of dimeric assemblies that peptide **11** forms. Peptide **11** serves a tool for better understanding the structural motifs that lead to the toxicity of amyloid β oligomers.

INTRODUCTION

Oligomers of the amyloid β (A β) peptide are central to the pathogenesis of Alzheimer's disease, yet we lack an understanding of their assembly and structures. A β oligomers are soluble, they are heterogeneous, and they are metastable with the thermodynamically stable assembly of

A β being insoluble fibrils that develop into plaques. These three issues hinder the ability to isolate and study oligomeric assemblies for their structural elucidation by nuclear magnetic spectroscopy (NMR), cryo-EM, X-ray crystallography, or through mass spectrometric techniques.

X-ray crystallographic elucidation of A β oligomers has been widely used to elucidate structures.¹⁻⁴ Our laboratory has published numerous X-ray crystallographic structures of A β -derived peptide models to try and elucidate the structural motifs that are responsible for the toxicity of A β .⁴⁻¹⁶ To further study these assemblies our lab has previously turned to the use of sodium dodecyl sulfate (SDS) migrating as discrete assemblies in SDS–polyacrylamide gel electrophoresis (PAGE) experiments. These toxic oligomers tend to contain antiparallel β -sheets, while non-toxic fibrils contain parallel β -sheets.^{1,2,4}

Our laboratory has developed peptide models that mimic the formation of antiparallel β -sheets and form the simplest arrangement of antiparallel β -sheets, a β -hairpin. These β -hairpin peptides contain two β -strand fragments locked in an antiparallel β -sheet by two δ -linked ornithine (δ Orn) turn linkers, and also contain an *N*-methylated residue to prevent uncontrolled aggregation. These studies have to date shown the propensity of many of these A β peptides to form oligomers in the crystal state, including dimers, trimers, hexamers, octamers, nonamers, and dodecamers.^{12,16}

In 2017, our laboratory reported X-ray crystallographic studies of peptide **10**, a peptide that is designed to mimic the A β_{16-36} β -hairpin (Figure 2.1).¹² The two strands in this peptide A β_{16-22} and A β_{30-36} are linked by two δ Orn turn linkers, the Phe₁₉ position is *N*-methylated to prevent uncontrolled aggregation, and the peptide contains a native methionine residue at position 35. Peptide **10** was toxic toward human neuroblastoma cell line SH-SY5Y, it formed a hexamer by X-ray crystallography and ran as a hexamer by SDS–PAGE, by size exclusion chromatography (SEC) peptide **10** appeared to form dimers and trimers. To attempt to capture these oligomeric

assemblies by creating a covalent linkage between them, so that they can be studied by LC-MS, I set out to create peptide **11**, a homologue to peptide **10** where the methionine residue at the 35 position is mutated to a noncanonical, commercially available amino acid photomethionine (Figure 2.1).

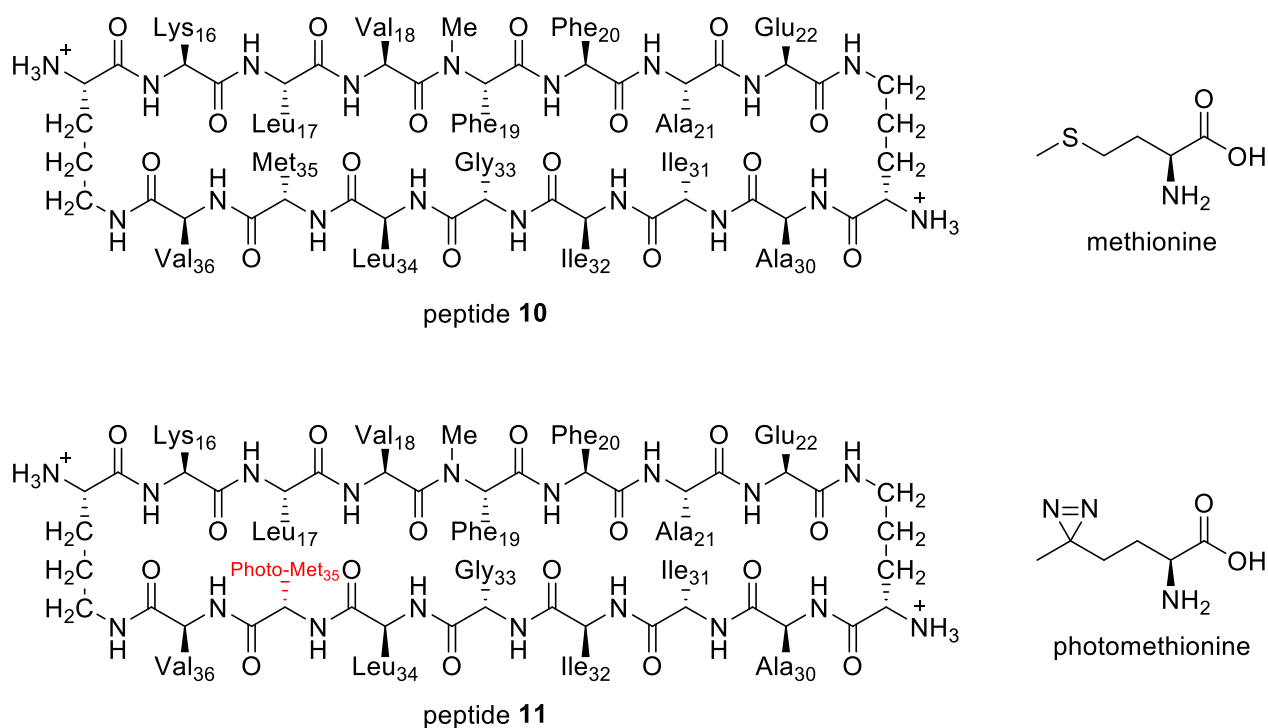


Figure 2.1. Chemical structures of peptide **10** and methionine (top), and peptide **11** and the photolabile isostere of methionine – photomethionine (bottom).

RESULTS AND DISCUSSION

Design and synthesis of peptide 11

Peptide **11** is designed to mimic the previously reported peptide **10** but contains a photolabile moiety – an alkyl diazirine as a methionine homologue in the 35 position. Upon UV irradiation the diazirine can form a highly reactive carbene species that reacts with nearby residues either through a C-H or a heteroatom-H insertion. Position 35 is amenable to this mutation due to two reasons, photomethionine is a well-established photoaffinity labeling isostere of the native

methionine residing at the 35 position, and residues Leu₁₇, Phe₁₉, Ala₂₁, Ile₃₁, and Met₃₅ all form a hydrophobic core in the hexamer formed by X-ray crystallography. In the X-ray crystallographic structure of peptide **10** the sulfur of Met₃₅ is between 3.7 – 5.1 Å from its nearby residues (Figure 2.2), which positions it well for carbene-mediated covalent bond formation when mutated to photomethionine.

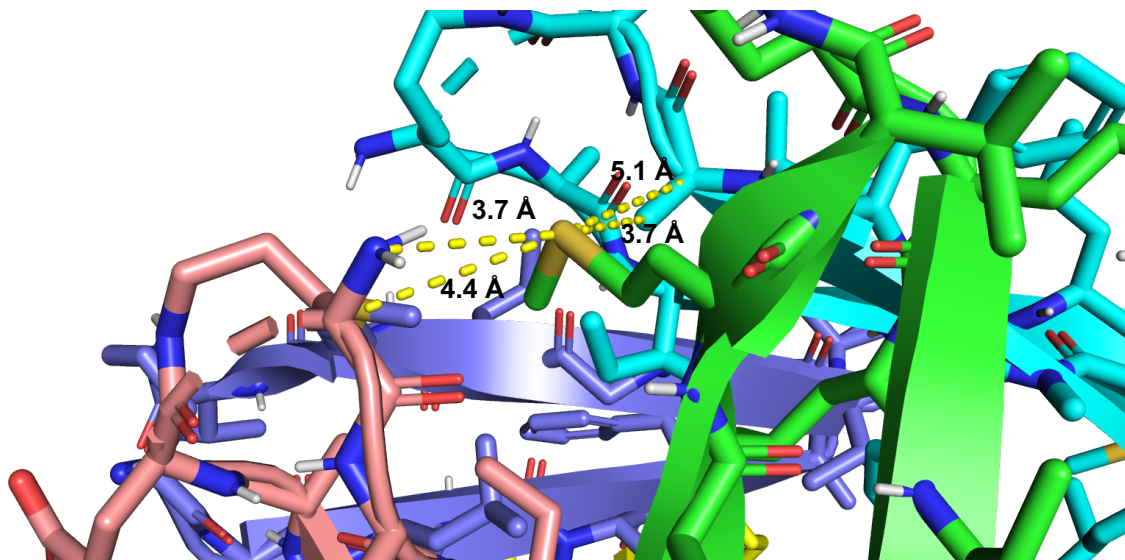


Figure 2.2. X-Ray crystallographic structure of peptide **10** (PDB ID 4NW9) depicting the position of residue Met₃₅ and showing the distance measurements to nearby residues that depict the potential for photocrosslinking when Met₃₅ is mutated to a photomethionine residue.

I synthesized peptide **11** by similar procedures to those our laboratory has previously developed for other macrocyclic β -sheet peptides: Fmoc-based synthesis of the linear peptide on 2-chlorotrityl resin, followed by cleavage of the protected linear peptide from the resin with HFIP, solution-phase macrocyclization and global deprotection of the resulting macrocyclic peptide by TFA. I purified peptide **11** by reverse phase HPLC (RP-HPLC) followed by lyophilization of pure fractions. This synthesis on a 0.1 mmol scale afforded 40 mg of peptide **11** in $\geq 95\%$ purity.¹⁷

Crystallographic studies of peptide 11

Peptide **11** afforded crystals suitable for X-ray diffraction from aqueous HEPES buffer with magnesium chloride and isopropanol. These conditions have previously afforded structures that are isosteric to peptide **11**.^{12,16} To solve the X-ray crystallographic structure of peptide **11** molecular replacement with a previously solved crystal structure (PDB ID 7JQS) was used as a search model. The X-ray crystallographic structure diffracted to the resolution of 1.23 Å with $R_{\text{work}} = 0.19$, and $R_{\text{free}} = 0.21$ (Table S2.1).

The X-ray crystallographic structure of peptide **11** reveals that the peptide folds to form a twisted β -hairpin (Figure 2.3A). Six β -hairpin monomers of peptide **11** assemble to form a hexamer (Figure 2.3B), almost identical to the hexamer that is formed in the X-ray crystallographic structure of peptide **10**. These findings are also important, because they further confirm that photomethionine can be substituted for methionine at the 35 position without disrupting hexamer formation. The crystal structure can be interpreted as a dimer of trimers where the orange, yellow, and green monomers form one trimer, and the cyan, purple, and violet monomers form the other trimer. To try and test whether peptide **11** in crystal form could form dimers or other higher order oligomers covalently the crystals were subjected to UV irradiation at 365 nm for two hours at 25 °C, 4 °C and under a steady stream of liquid nitrogen. While the crystals appeared to be morphologically identical the irradiated crystals did not diffract (Figure S2.1). I hypothesized that is due to the formation of new covalent species, and hence a disruption in the crystal assembly that does not allow for the crystals to diffract.

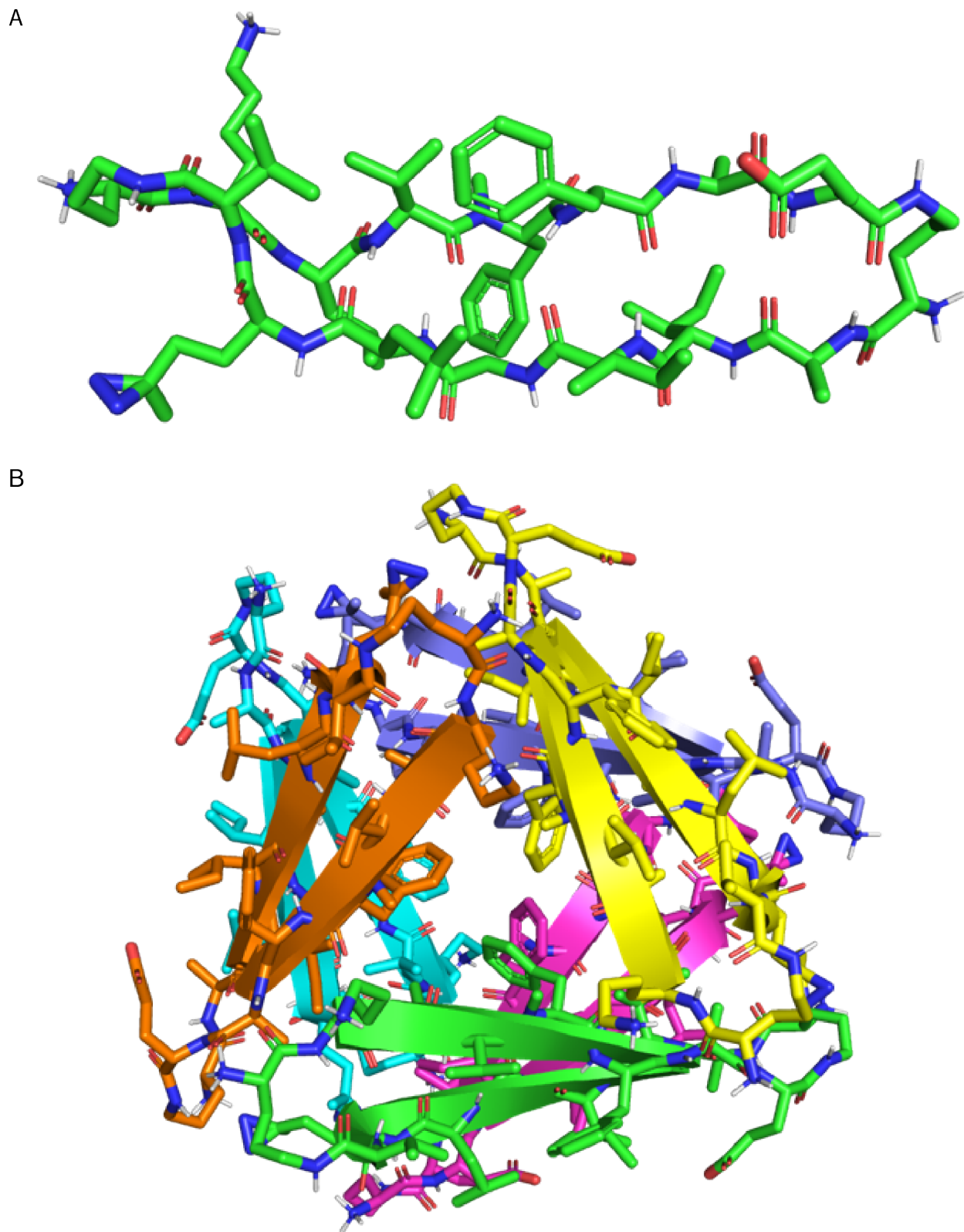


Figure 2.3. X-ray crystallography of peptide **11**. (A) Stick model of peptide **11** X-ray crystallographic structure. (B) Cartoon and stick model of the hexamer that peptide **11** forms in a

crystal structure. The hexamer appears to form as a dimer of trimers, one trimer is represented by the monomers shown in orange, yellow, and green and the cyan, purple, and violet monomers form the other trimer.

SDS-PAGE studies of peptide 11

Peptide **11** runs as a hexamer on SDS-PAGE without irradiation with UV at 365 nm, but runs as both a hexamer and a dimer when irradiated. The previously reported peptide **10** ran as a hexamer in SDS-PAGE, consistent with its assembly in the crystal lattice. To test if peptide **11** will also run as the hexamer that was observed by X-ray crystallography, I ran it on SDS-PAGE with and without UV irradiation at 365 nm. Peptide **11** ran as a hexamer without UV irradiation, however running peptide **11** following UV irradiation reveals a new assembly — a putative dimer (Figure 2.4). This interesting finding reveals that new potential oligomeric formations can be observed following photolysis that were not previously observed by X-ray crystallography or SDS-PAGE. The formation of the dimer seems to be neither solvent nor concentration dependent with the dimer forming when peptide **11** was irradiated at concentrations ranging between 0.25 mg/mL and 1 mg/mL in water, and between 0.5 mg/mL and 1 mg/mL in PBS. The formation of the dimer appears to be covalent by SDS-PAGE as the dimer is absent when no UV treatment of the samples was performed. There appears to be a higher concentration of the dimer formed when the UV irradiation was performed in water, as opposed to in PBS. This could be because assembly in PBS is weaker, or because the carbene is more readily quenched in PBS than water.

Assembly and the formation of higher order oligomers, notably dimers increase with elongated irradiation time. Peptide **11** was dissolved at 2.5 mg/mL, 5 mg/mL, and 10 mg/mL in PBS buffer and irradiated for either 1, 6, or 12 hours, and a control was not irradiated (Figure 2.4). Peptide **11** assembles into a dimer at all concentrations and with varying times of irradiation. Interestingly, the relationship between length of irradiation and amount of dimer by SDS-PAGE

appears directly correlated, while the relationship between the concentration of sample and amount of dimer by SDS-PAGE appears inversely correlated. The longer the peptide was irradiated for, the more dimer seemed to form, but the higher the concentration of the peptide in solution, the less dimer seemed to form (Figure 2.4). This inverse relationship could be the result of precipitation forming at higher concentrations and due to the poor solubility of peptide **11**.

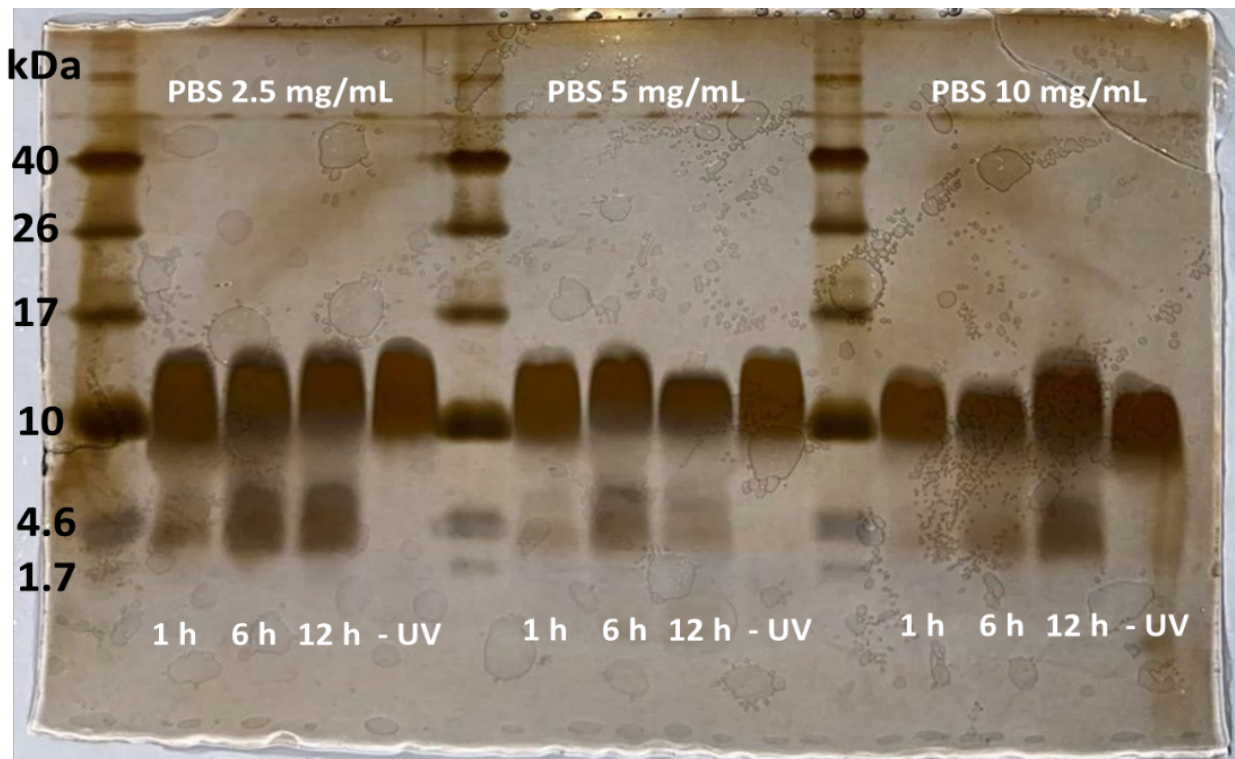


Figure 2.4. Silver-stained SDS-PAGE gel of peptide **11** performed on 0.05 mg/mL diluted from 2.5 mg/mL, 5 mg/mL, and 10 mg/mL. Samples were irradiated at 365 nm at the three different concentrations in PBS buffer for 1, 6, or 12 hours, and a control was not irradiated. Hexamer (~10.6 kDa) can be observed at all concentration and regardless of irradiation, the formation of dimer (~3.5 kDa) can only be observed in irradiated samples but is absent in the samples that were not irradiated.

Mass spectrometric studies of peptide 11

LC-MS analysis indicates that peptide **11** forms a covalent dimer upon irradiation. When peptide **11** was subjected to UV irradiation for over 48 hours the formation of a covalent dimer can be observed (Figure 2.5). This new species elutes as a new peak on LC-MS and is identified as a mass of monomer of peptide **11** minus the mass of N₂ and a mass of an intact monomer. However, numerous other species can also be observed (Figure S2.2 and Figure S2.3).

The diazirine at the 35 positions seems to be preferentially capturing oligomeric assemblies rather than random interactions. To study whether the rapid interaction in the photolysis reaction in peptide **11** is specific to capturing different oligomeric assemblies of this peptide I performed a competition experiment with two other β -sheet forming peptides – peptide **10** and glucagon. When peptide **11** is irradiated by itself approximately 0.16 % of the resulting mixture forms peptide **11** dimers, when peptide **11** is mixed with peptide **10** approximately 0.75 % of the resulting mixture forms peptide **10**–peptide **11** dimers, but when peptide **11** is mixed with glucagon only approximately 0.05 % of the resulting mixture forms glucagon–peptide **11** dimers by LC-MS (Figure S2.4). The percentages represent the area under the curve in the TIC trace, corresponding to their distinct masses.

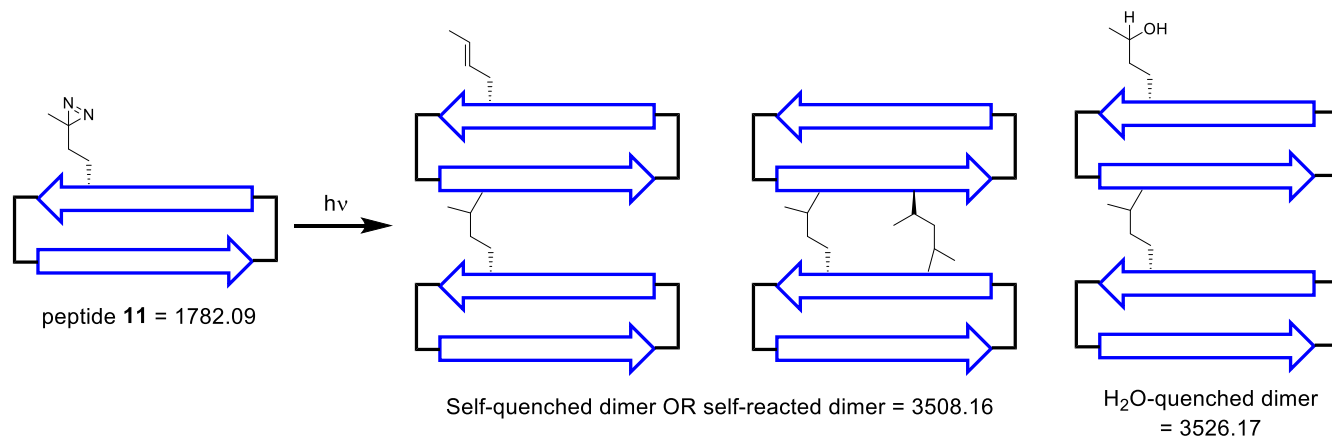


Figure 2.5. Cartoon representation of different types of dimers that can form following the irradiation of peptide **11**. Masses corresponding to the self-quench dimer or homodimer and H₂O-quenched dimer were both observed by LC-MS analysis. Masses corresponding to the self-quenched or self-reacted dimer, as well as the H₂O-quenched dimer were observed by LC-MS.

Peptide **11** formed a hexamer in the X-ray crystallographic structure, both a hexamer and dimer by SDS-PAGE following irradiation, and a covalent dimer by LC-MS. To probe the different assemblies observed by solution-phase irradiation and those observed by X-ray crystallography, I irradiated the crystals at 365 nm and conduct LC-MS analysis of these irradiated crystals. The irradiated crystals reveal the formation of a dimeric species by LC-MS, as well as the formation of a new species that was previously not observed – a trimer (Figure S2.2 and Figure S2.3). Following irradiation at 365 nm peptide **11** forms a dimer by SDS-PAGE and LC-MS when irradiated in solution, but when peptide **11** is irradiated in crystal form it also forms trimers.

CONCLUSION

Peptide **11** assembles to form dimers in solution that can be captured by photolyzing the diazirine in photomethionine at the 35 position through SDS-PAGE and LC-MS studies. Peptide **11** also forms hexamers by X-ray crystallography, similarly to the previously published peptide **10**. A competition experiment with peptide **11** and glucagon reveals that the structures that are

captured by the photolysis of photomethionine are specific to the oligomers that are formed by A β -derived peptides, and are not random interactions as the amount of dimers formed by peptide **11** and glucagon are significantly smaller compared to those only coming from peptide **11** by LC-MS. This study offers a tool that allows for capturing oligomeric assemblies in solution, and crystal form and can serve as a good starting point for understanding the importance of oligomers that are critical in the formation of toxic species by A β in Alzheimer's disease.

REFERENCES AND NOTES

1. Laganowsky, A.; Liu, C.; Sawaya, M. R.; Whitelegge, J. P.; Park, J.; Zhao, M.; Pensalfini, A.; Soriaga, A. B.; Landau, M.; Teng, P. K.; Cascio, D.; Glabe, C.; Eisenberg, D. Atomic View of a Toxic Amyloid Small Oligomer. *Science* **2012**, *335*, 1228–1231.
2. Apostol, M. I.; Perry, K.; Surewicz, W. K. Crystal Structure of a Human Prion Protein Fragment Reveals a Motif for Oligomer Formation. *J. Am. Chem. Soc.* **2013**, *135*, 10202–10205.
3. Liu, C.; Zhao, M.; Jiang, L.; Cheng, P.-N.; Park, J.; Sawaya, M. R.; Pensalfini, A.; Gou, D.; Berk, A. J.; Glabe, C. G.; Nowick, J.; Eisenberg, D. Out-of-Register β -Sheets Suggest a Pathway to Toxic Amyloid Aggregates. *Proc. Natl. Acad. Sci.* **2012**, *109*, 20913–20918.
4. Pham, J. D.; Chim, N.; Goulding, C. W.; Nowick, J. S. Structures of Oligomers of a Peptide from β -Amyloid. *J. Am. Chem. Soc.* **2013**, *135*, 12460–12467.
5. Spencer, R. K.; Li, H.; Nowick, J. S. X-Ray Crystallographic Structures of Trimers and Higher-Order Oligomeric Assemblies of a Peptide Derived from A β_{17-36} . *J. Am. Chem. Soc.* **2014**, *136*, 5595–5598.
6. Pham, J. D.; Spencer, R. K.; Chen, K. H.; Nowick, J. S. A Fibril-Like Assembly of Oligomers of a Peptide Derived from β -Amyloid. *J. Am. Chem. Soc.* **2014**, *136*, 12682–12690.
7. Kreutzer, A. G.; Hamza, I. L.; Spencer, R. K.; Nowick, J. S. X-Ray Crystallographic Structures of a Trimer, Dodecamer, and Annular Pore Formed by an A β_{17-36} β -Hairpin. *J. Am. Chem. Soc.* **2016**, *138*, 4634–4642.
8. Kreutzer, A. G.; Yoo, S.; Spencer, R. K.; Nowick, J. S. Stabilization, Assembly, and Toxicity of Trimers Derived from A β . *J. Am. Chem. Soc.* **2017**, *139*, 966–975.

9. Chen, K. H.; Corro, K. A.; Le, S. P.; Nowick, J. S. X-Ray Crystallographic Structure of a Giant Double-Walled Peptide Nanotube Formed by a Macrocyclic β -Sheet Containing A β _{16–22}. *J. Am. Chem. Soc.* **2017**, *139*, 8102–8105.
10. Salveson, P. J.; Spencer, R. K.; Kreutzer, A. G.; Nowick, J. S. X-Ray Crystallographic Structure of a Compact Dodecamer from a Peptide Derived from A β _{16–36}. *Org. Lett.* **2017**, *19*, 3462–3465.
11. Samdin, T. D.; Wierzbicki, M.; Kreutzer, A. G.; Howitz, W. J.; Valenzuela, M.; Smith, A.; Sahrai, V.; Truex, N. L.; Klun, M.; Nowick, J. S. Effects of N-Terminal Residues on the Assembly of Constrained β -Hairpin Peptides Derived from A β . *J. Am. Chem. Soc.* **2020**, *142*, 11593–11601.
12. Kreutzer, A. G.; Spencer, R. K.; McKnelly, K. J.; Yoo, S.; Hamza, I. L.; Salveson, P. J.; Nowick, J. S. A Hexamer of a Peptide Derived from A β _{16–36}. *Biochemistry* **2017**, *56*, 6061–6071.
13. Kreutzer, A. G.; Samdin, T. D.; Guaglianone, G.; Spencer, R. K.; Nowick, J. S. X-Ray Crystallography Reveals Parallel and Antiparallel β -Sheet Dimers of a β -Hairpin Derived from A β _{16–36} That Assemble to Form Different Tetramers. *ACS Chem. Neurosci.* **2020**, *11*, 2340–2347.
14. Haerianardakani, S.; Kreutzer, A. G.; Salveson, P. J.; Samdin, T. D.; Guaglianone, G. E.; Nowick, J. S. Phenylalanine Mutation to Cyclohexylalanine Facilitates Triangular Trimer Formation by β -Hairpins Derived from A β . *J. Am. Chem. Soc.* **2020**, *142*, 20708–20716.
15. Howitz, W. J.; Guaglianone, G.; McKnelly, K. J.; Haduong, K.; Ashby, S. N.; Laayouni, M.; Nowick, J. S. Macrocyclic Peptides Derived from Familial Alzheimer's Disease Mutants

- Show Charge-Dependent Oligomeric Assembly and Toxicity. *ACS Chem. Neurosci.* **2022**, *13*, 714–720.
16. McKnelly, K. J.; Kreutzer, A. G.; Howitz, W. J.; Haduong, K.; Yoo, S.; Hart, C.; Nowick, J. S. Effects of Familial Alzheimer's Disease Mutations on the Assembly of a β -Hairpin Peptide Derived from A β_{16-36} . *Biochemistry* **2022**, *61*, 446–454.
17. Guaglianone, G.; Kreutzer, A. G.; Nowick, J. S. Chapter Five - Synthesis and Study of Macrocyclic β -Hairpin Peptides for Investigating Amyloid Oligomers. *Methods in Enzymol.* **2021**, *656*, 123–168.

Capturing Higher Order Assemblies with Carbene-Mediated Crosslinking

Table of Contents

Table S2.1 – Crystallographic properties of peptide 11	72
Figure S2.1	73
Figure S2.2	74
Figure S2.3	75
Figure S2.4	76
Materials and Methods	77
Synthesis of peptide 11	77
X-Ray crystallography of peptide 11	80
References	81
Characterization Data	82
Characterization of peptide 11	82
Analytical HPLC trace of peptide 11	82
Mass spectrum of peptide 11	83

Table S2.1. Crystallographic properties, crystallization conditions, and data collection and model refinement statistics for peptide **11**.

peptide	peptide 11
PDB ID	N/A
space group	<i>P4₁32</i>
<i>a, b, c</i> (Å)	47.5867, 47.5867, 47.5867
α, β, λ (°)	90, 90, 90
peptides per asymmetric unit	1
crystallization conditions	0.1 M pH 7 HEPES, 0.25 M MgCl ₂ , 28 % iPrOH
wavelength (Å)	1.23
resolution (Å)	33.65–1.23 (1.274–1.23)
total reflections	11518 (1116)
unique reflections	5759 (557)
multiplicity	2.0 (2.0)
completeness (%)	99.86 (100.00)
mean <i>I</i> / σ	56.31 (2.89)
Wilson B factor	20.29
<i>R</i> _{merge}	0.002106 (0.1666)
<i>R</i> _{measure}	0.002979 (0.2356)
CC _{1/2}	1 (0.944)
CC*	1 (0.985)
<i>R</i> _{work}	0.1919 (0.2714)
<i>R</i> _{free}	0.2104 (0.2799)
number of non-hydrogen atoms	145
RMS _{bonds}	0.019
RMS _{angles}	1.52
Ramachandran favored (%)	100
outliers (%)	0
clashscore	16.53
average B-factor	33.41
ligands/ions	1
water molecules	17

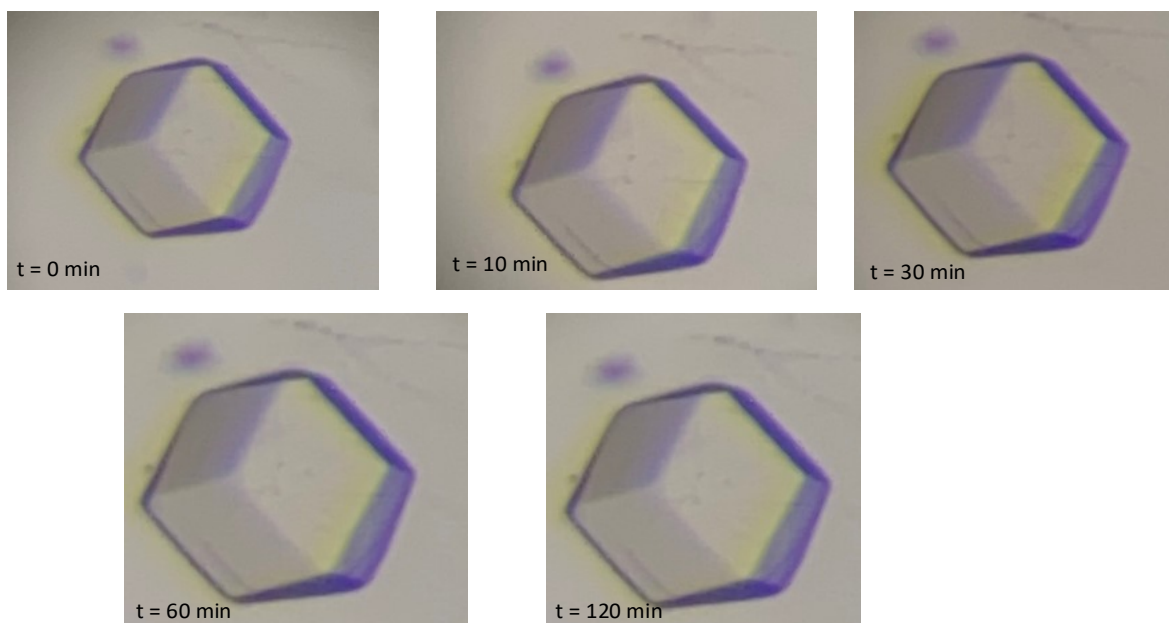


Figure S2.1. Photos of crystal of peptide **11** following irradiation with UV light at 365 nm after 0, 20, 30, 60, and 120 minutes. The crystal remains the same morphologically, but it no longer diffracts even after only the 10-minute irradiation timepoint. LC-MS analysis reveals that the diazirine on the photomethionine residue is activated and dimers of peptide **11** are detected by LC-MS.

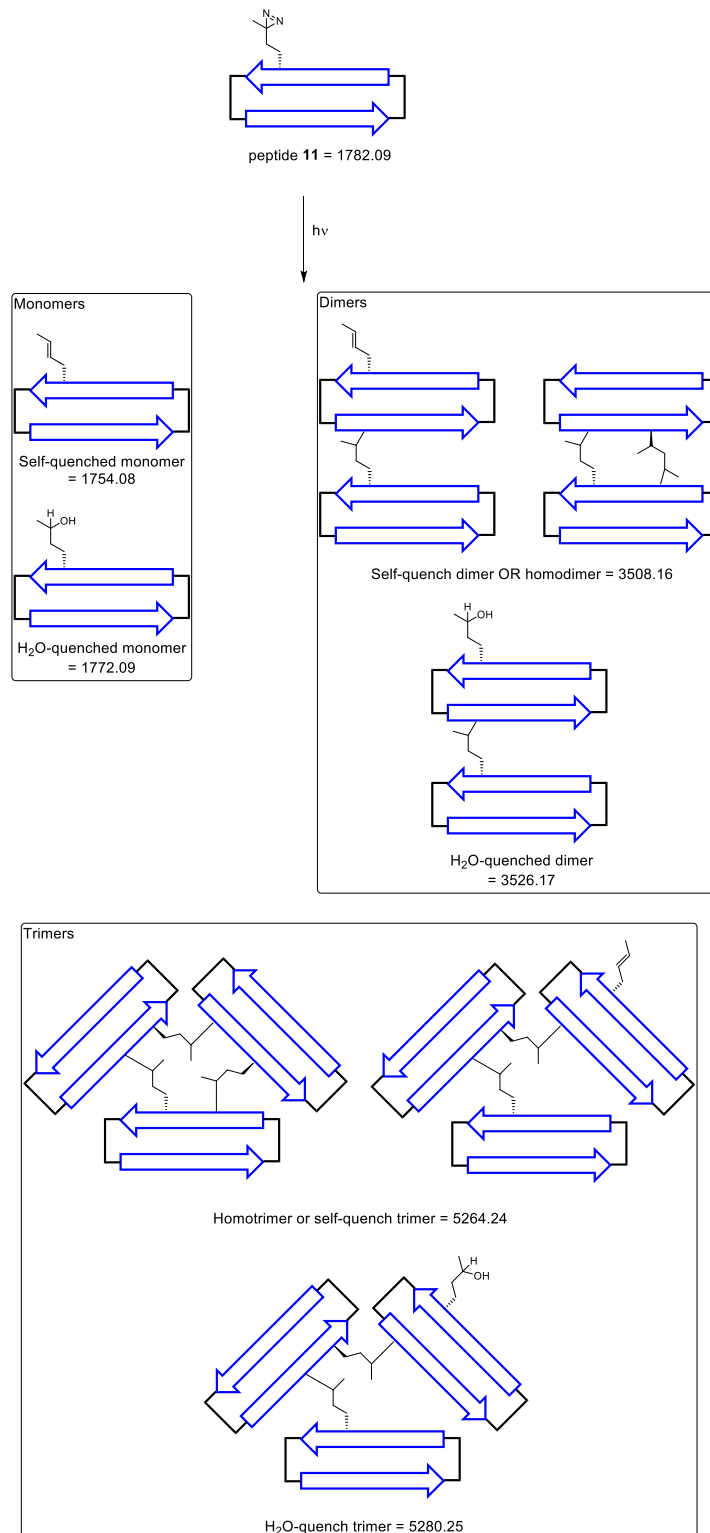
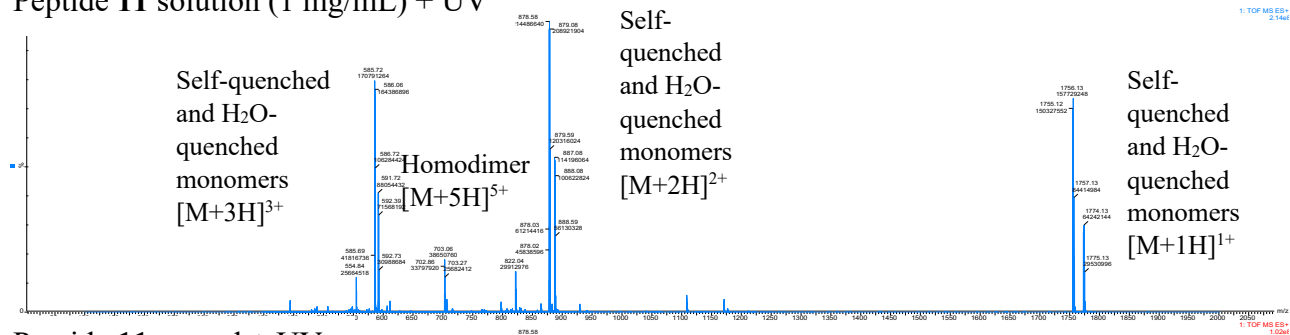
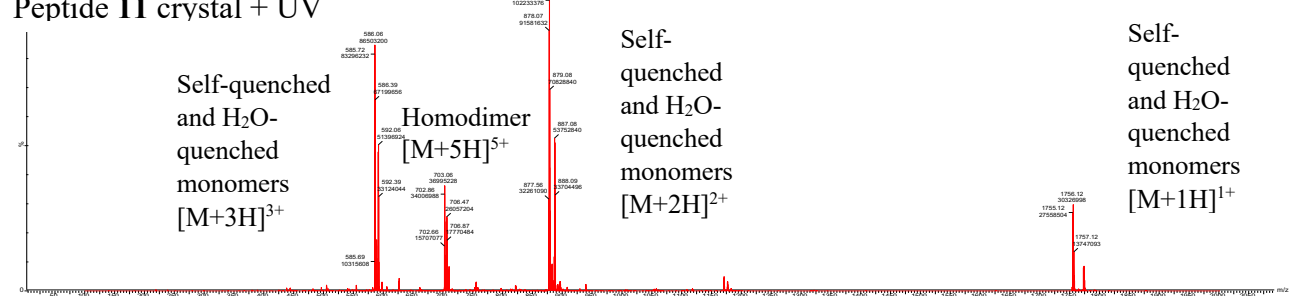


Figure S2.2. Structures and masses of potential oligomers formed following UV irradiation.

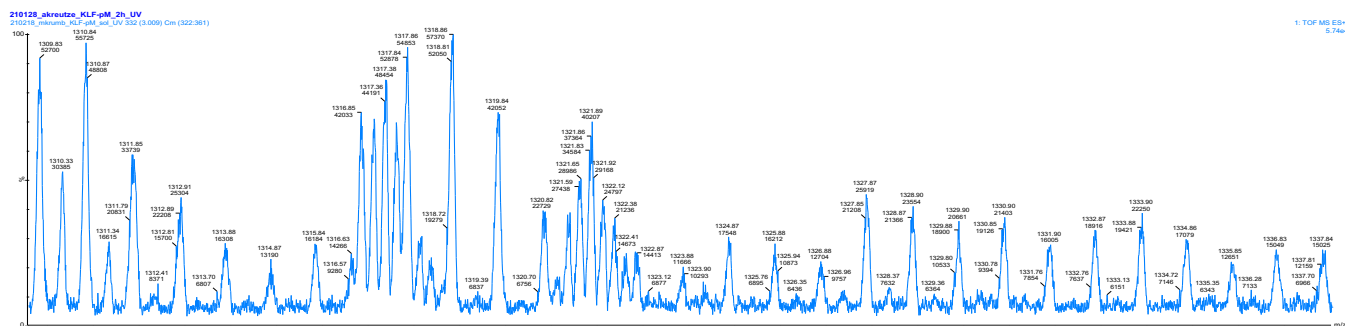
Peptide 11 solution (1 mg/mL) + UV



Peptide 11 crystal + UV



Peptide 11 solution (1 mg/mL) + UV



Peptide 11 crystal + UV

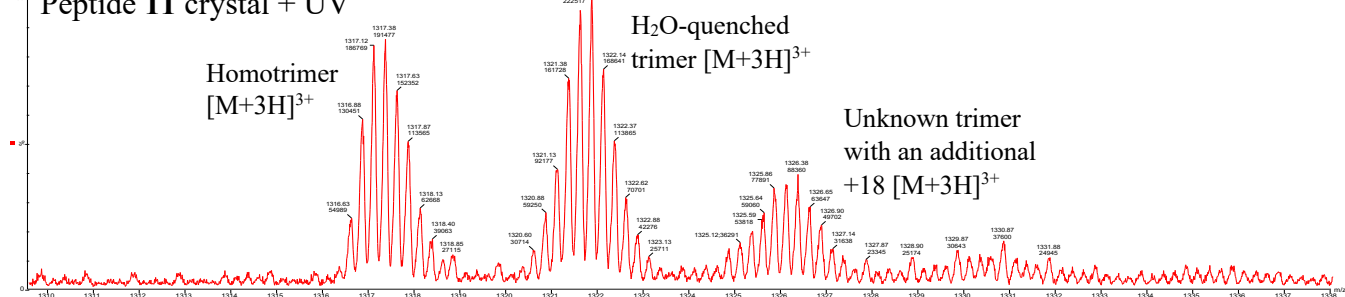


Figure S2.3. Representative mass spectra of peptide 11 following UV irradiation either in solution (blue traces) or as a crystal (red traces). Different oligomers such as various dimers and trimers can be observed.

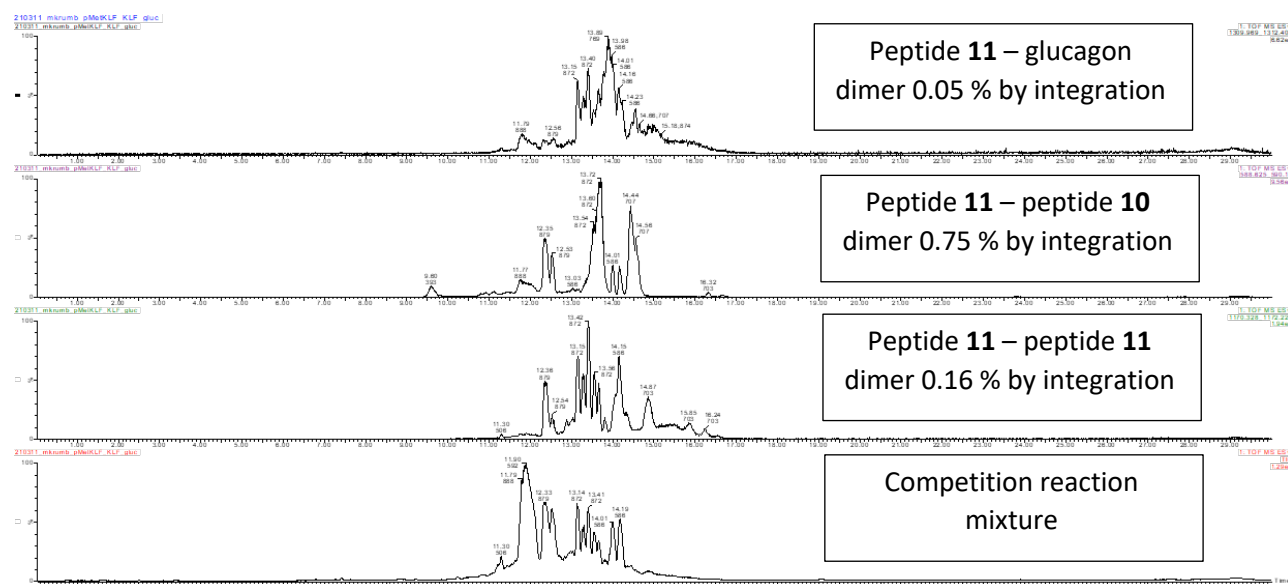


Figure S2.4. A competition reaction of equal concentrations (1 mg/mL) of peptide 10, peptide 11, and an unrelated peptide glucagon were mixed and irradiated. The LC-MS trace was then filtered for the masses corresponding to dimers of all three species and the area under the curve was integrated. Peptide 11 and glucagon dimer forms about 0.05 % of total area, peptide 11 and peptide 10 dimer forms 0.75 % of total area, and peptide 11 and peptide 11 dimer forms about 0.16 %.

Materials and Methods

General information

Chemicals and Supplies. All chemicals were used as received unless otherwise noted. Dry methylene chloride (CH_2Cl_2), and *N,N*-dimethylformamide (DMF) were obtained by passing through alumina under argon prior to use. Anhydrous, amine-free *N,N*-dimethylformamide (DMF), DIPEA, 2,4,6-collidine, and piperidine were purchased Alfa Aesar. HPLC grade acetonitrile and deionized water (18 M Ω), each containing 0.1% trifluoroacetic acid (TFA), were used for analytical and preparative reverse-phase HPLC, as well as reverse-phase chromatography using a Biotage® Isolera One flash column chromatography instrument. Commercial agents were used without purification, unless otherwise stated. Amino acids, coupling agents, 2-chlorotriyl chloride resin, DIC, and triisopropylsilane were purchased from Chem-Impex.

Instrumentation. Analytical reverse-phase HPLC was performed on Agilent 1260 Infinity II instrument equipped with a Phenomenex bioZen PEPTIDE 2.6 μm XB-C18 column (150x4.6 mm), eluting with a gradient of acetonitrile and water (each containing 0.1% TFA) from 5-100% over 20 minutes. Peptides were purified on a Biotage Isolera One flash column chromatography instrument with a Biotage® SfarBio C18 D – Duo 300 Å 20 μm 10 g column. Peptides were then further purified by preparative reverse-phase HPLC on a Rainin Dynamax equipped with an Agilent Zorbax 250x 21.2 mm SB-C18 column. Peptides were prepared and used as the trifluoroacetate (TFA) salts and were assumed to have one trifluoroacetic acid molecule per amine group on each peptide (two TFA molecules per peptide). LC/MS analysis was performed of the intact peptide sample (ACQUITY UPLC H-class system, Xevo G2-XS QToF, Waters corporation). The C4 column that was used was ACQUITY UPLC Protein BEH C4, 300 Å, 1.7 μm , 2.1 mm x 50 mm, Waters corporation. The Xevo Z-spray source was operated in positive MS resolution mode, 400-4000da, with a capillary voltage of 3000V and a cone voltage of 40V (NaCsI calibration, Leu-enkephalin lock-mass). Nitrogen was used as the desolvation gas at 350C and a total flow of 800 L h⁻¹. Retention times are given in minutes (min).

Synthetic Procedures:

Synthesis of peptide 11¹

a. *Loading of the resin.* 2-Chlorotriethyl chloride resin (300 mg, 1.2 mmol/g) was added to a Bio-Rad Poly-Prep chromatography column (10 mL). The resin was suspended in dry CH₂Cl₂ (10 mL) and allowed to swell for 30 min. The solution was drained from the resin and a solution of Boc-Orn(Fmoc)-OH (0.50 equiv, 82 mg, 0.18 mmol) in 6% (v/v) 2,4,6-collidine in dry CH₂Cl₂ (8 mL) was added immediately and the suspension was gently agitated

for 12 h. The solution was then drained and a mixture of $\text{CH}_2\text{Cl}_2/\text{MeOH}/N,N$ -diisopropylethylamine (DIPEA) (17:2:1, 10 mL) was added immediately. The mixture was gently agitated for 1 h to cap the unreacted 2-chlorotrityl chloride resin sites. The resin was then washed with dry CH_2Cl_2 (2x) and dried by passing nitrogen through the vessel. This procedure typically yields 0.12–0.15 mmol of loaded resin (0.4–0.5 mmol/g loading).

b. *Manual peptide coupling.* The Boc-Orn(Fmoc)-2-chlorotrityl resin generated from the previous step was suspended in dry DMF and then transferred to a solid-phase peptide synthesis vessel. Each residue was manually coupled using Fmoc-protected amino acid building blocks. The coupling cycle consisted of *i.* Fmoc-deprotection with 20% (v/v) piperidine in DMF (5 mL) for 5 min at room temperature, *ii.* Washing with dry DMF (6 x 5 mL) *iii.* Coupling of the amino acid (4 equiv.) with HCTU (4 equiv.) in 20% (v/v) 2,4,6-collidine in dry DMF (5 mL) for 30 min at room temperature, and *iv.* Washing with dry DMF (6 x 5 mL). [NOTE: The unnatural amino acid Fmoc-photomethionine-OH was coupled for 1 hour.] *v.* After the last amino acid was coupled, and its Fmoc protecting group deprotected, the resin was transferred to a new BioRad Poly-Prep chromatography column. The resin was washed with CH_2Cl_2 (6 x 5 mL) and dried by passing nitrogen through the column.

c. *Cleavage of the peptide from the resin.* The linear peptide was cleaved from the resin by agitating the resin for 1 h with a solution of 1,1,1,3,3,3-hexafluoroisopropanol (HFIP) in CH_2Cl_2 . (1:4, 7 mL).² The suspension was filtered and the filtrate was collected in a 250 mL round-bottomed flask. The resin was washed with additional HFIP in CH_2Cl_2 (1:4, 7 mL) and then with CH_2Cl_2 (2x10 mL). The combined filtrates were concentrated by rotary evaporation to give a white solid. The white solid was further dried by vacuum pump to afford the crude protected linear peptide, which was cyclized without further purification.

- d. *Cyclization of the linear peptide.* The crude protected linear peptide was dissolved in dry DMF (150 mL). HOBt (114 mg, 0.75 mmol, 5 equiv) and HBTU (317 mg, 0.75 mmol, 5 equiv) were added to the solution. DIPEA (0.33 mL, 1.8 mmol, 12 equiv) was added to the solution and the mixture was stirred under nitrogen for 24 h. The mixture was concentrated under reduced pressure to afford the crude protected cyclic peptide.
- e. *Global deprotection of the cyclic peptide.* The protected cyclic peptide was dissolved in TFA/triisopropylsilane (TIPS)/H₂O (18:1:1, 20 mL) in a 250 mL round-bottomed flask equipped with a nitrogen-inlet adaptor. The solution was stirred for 1.5 h. The reaction mixture was then concentrated by rotary evaporation under reduced pressure to afford the crude cyclic peptide as a thin yellow film on the side of the round-bottomed flask. The crude cyclic peptide was immediately subjected to purification by reverse-phase HPLC (RP-HPLC), as described below.
- f. *Reverse-phase HPLC purification.* The peptide was dissolved in H₂O and acetonitrile (7:3, 10 mL), and the solution was filtered through a 0.2 μm syringe filter and purified by RP-HPLC (gradient elution with 20–50% CH₃CN over 50 min). Pure fractions were concentrated by rotary evaporation and lyophilized. Synthesis yielded ~50 mg of the peptide as the TFA salt.

X-ray crystallography of peptide 11²

Crystallization of peptide 11. The hanging-drop vapor-diffusion method was used to determine initial crystallization conditions for peptide **11**. Each peptide was screened in 96-well plate format using three crystallization kits (Crystal Screen, Index, and PEG/ION) from Hampton Research. A TTP LabTech Mosquito nanodisperse was used to make three 150 nL hanging drops for each well condition. The three hanging drops differed in the ratio of peptide to well solution for each condition in the 96-well plate. A 10 mg/mL solution of peptide **11** in deionized water was combined with a well solution in ratios of 1:1, 1:2, and 2:1 peptide:well solution at appropriate volumes to create the three 150 nL hanging drops. Crystals of peptide **11** grew in well conditions of 2.8 M sodium acetate at pH 7.0.

Data collection, data processing, and structure determination. X-ray diffraction data from a single peptide **11** crystal soaked in a mixture of well solution and potassium iodide were collected using a Rigaku Micromax-007HF X-ray diffractometer with a rotating copper anode and a HyPix-6000HE Hybrid Photon Counting (HPC) X-ray detector. X-ray diffraction data were also collected from a single peptide **11** crystal using a synchrotron X-ray source (Advanced Light Source beamline 5.0.2) and a Pilatus3 6M 25 Hz detector. The dataset was indexed and integrated with XDS and scaled and merged with pointless and aimless. The crystallographic phase determination was done with Phaser. The structure was refined using phenix.refine, with manipulation of the model performed using Coot. Data collection and refinement statistics are shown Tables S2.1

References

1. The procedure for peptide synthesis follows closely to those that our laboratory has previously published. The procedures in this section were either adapted from or taken verbatim from:

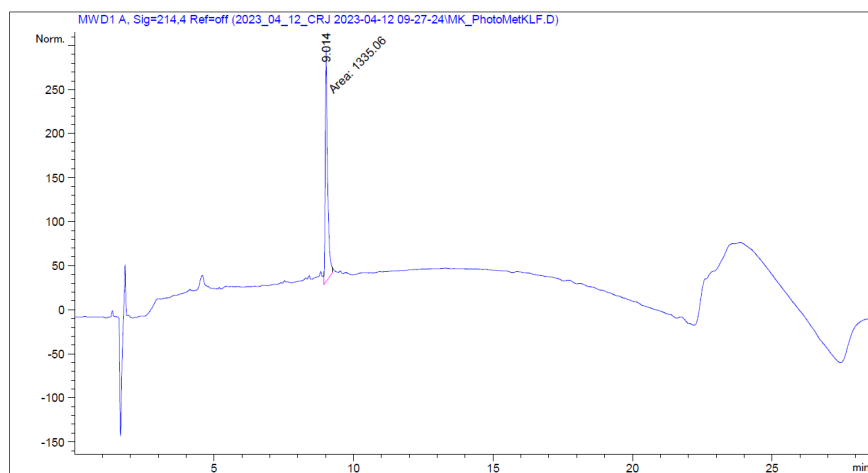
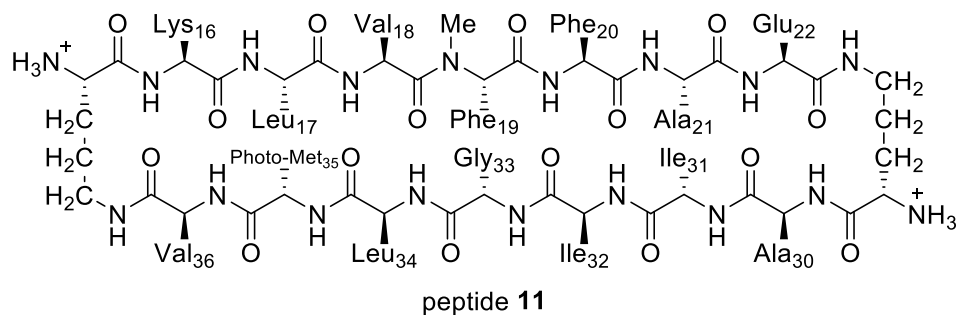
Kreutzer, A. G.; Spencer, R. K.; McKnelly, K. J.; Yoo, S.; Hamza, I. L.; Salveson, P. J.; Nowick, J. S. A Hexamer of a Peptide Derived from A β _{16–36}. *Biochemistry* **2017**, *56*, 6061–6071.

2. General procedures for X-ray crystallography were either adapted from or taken verbatim from: McKnelly, K. J.; Kreutzer, A. G.; Howitz, W. J.; Haduong, K.; Yoo, S.; Hart, C.; Nowick, J. S. Effects of Familial Alzheimer’s Disease Mutations on the Assembly of a β -Hairpin Peptide Derived from A β _{16–36}. *Biochemistry* **2022**, *61*, 446–454.

Characterization data

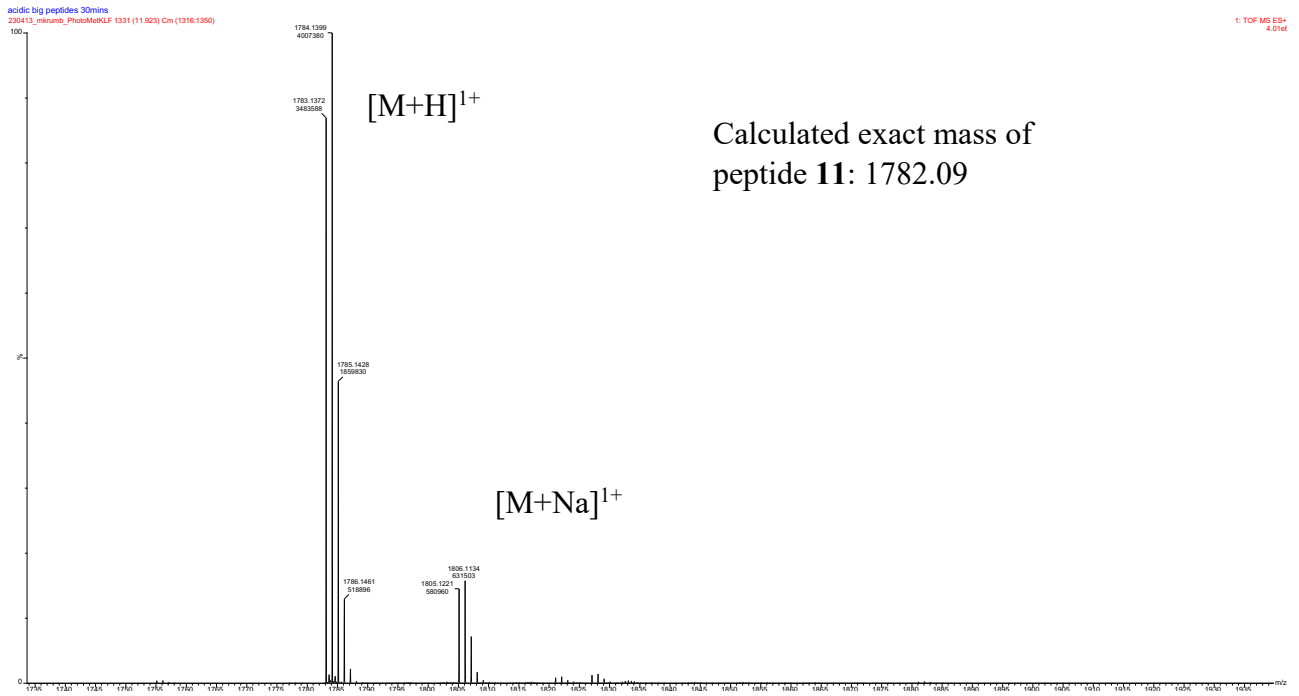
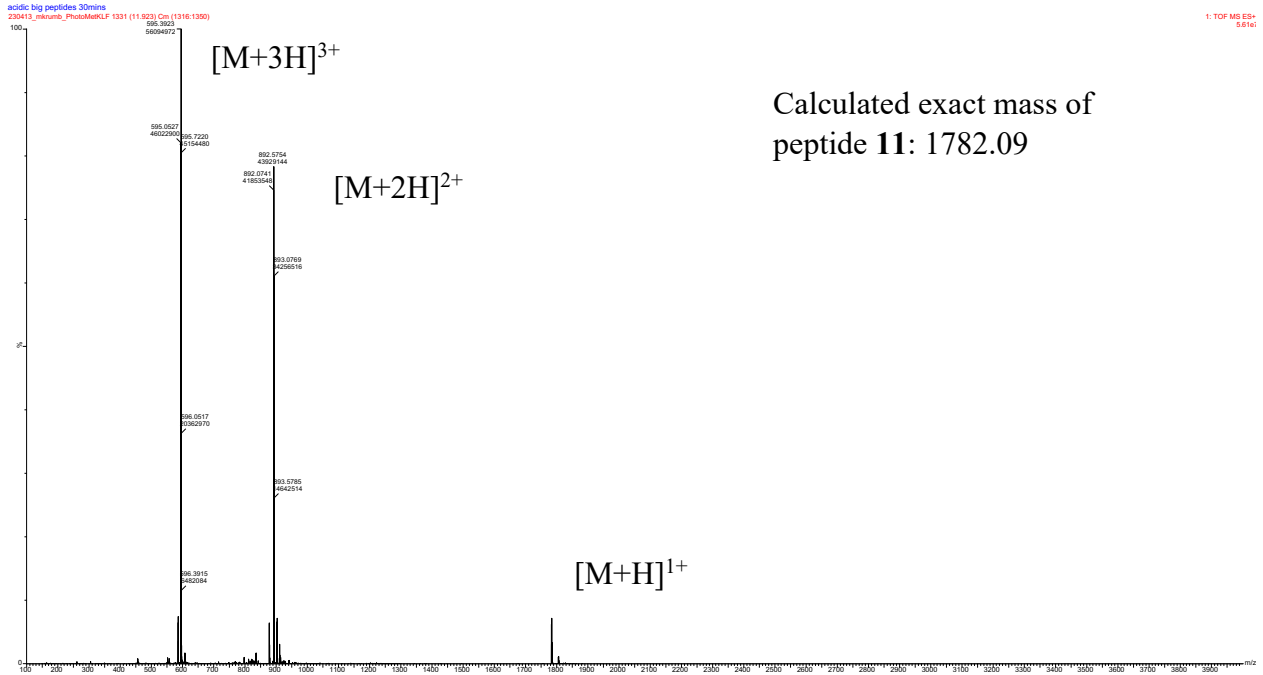
Peptide **10** was not synthesized for this work and an older sample prepared by a former graduate student from the Nowick Group – Dr. Adam Kreutzer was used.

Characterization of peptide **11**



Peak #	RetTime [min]	Type	Width [min]	Area [mAU*s]	Height [mAU]	Area %
1	9.014	MM	0.0933	1335.05835	238.59657	100.0000

Mass spectrum and expansions of peptide 11



Chapter III

Expanded Studies on the Synthesis and Stereochemical Determination of the Peptide Antibiotic Novo29 (Clovibactin)

This chapter was either adapted or taken verbatim from studies recently published by myself and a past Nowick Group member Dr. Xingyue Li as co-first authors in *J. Org. Chem.* **2023**, *88*, 2214–2220, as well as in my Master's Thesis, but it also expands on those studies through additional work never previously published.

ABSTRACT

This chapter describes the synthesis and stereochemical determination of Novo29 (clovibactin), a new peptide antibiotic that is related to teixobactin and is active against Gram-positive bacteria. Novo29 is an eight-residue depsipeptide that contains the noncanonical amino acid hydroxyasparagine of hitherto undetermined stereochemistry in a macrolactone ring. The amino acid building blocks Fmoc-(2*R*,3*R*)-hydroxyasparagine-OH and Fmoc-(2*R*,3*S*)-hydroxyasparagine-OH were synthesized from (*R,R*)- and (*S,S*)-diethyl tartrate. Novo29 and *epi*-Novo29 were then prepared by solid-phase peptide synthesis using these building blocks. Correlation with an authentic sample of Novo29 through ¹H NMR spectroscopy, LC-MS, and *in vitro* antibiotic activity established that Novo29 contains (2*R*,3*R*)-hydroxyasparagine. X-ray crystallography reveals that *epi*-Novo29 adopts an amphiphilic conformation, with a hydrophobic surface and a hydrophilic surface. Four sets of *epi*-Novo29 molecules pack in the crystal lattice to

form a hydrophobic core. The macrolactone ring adopts a conformation in which the main-chain amide NH groups converge to create a cavity, which binds ordered water and acetate anion. The amphiphilic conformation of *epi*-Novo29 is reminiscent of the amphiphilic conformation adopted by the related antibiotic teixobactin and its derivatives, which contains a hydrophobic surface that interacts with the lipids of the bacterial cell membrane and a hydrophilic surface that interacts with the aqueous environment. Molecular modeling suggests that Novo29 can adopt an amphiphilic conformation similar to teixobactin, suggesting that Novo29 may interact with bacteria in a similar fashion to teixobactin. Novo29 exhibits signs of hydrolytic instability which can be observed in a hydrolyzed crystal, additionally Novo29 seems to be assembling even at low concentrations and in solvents such as DMSO-*d*₆, assembly is critical to the activity of teixobactin and could be an important aspect of the mechanism of action in Novo29.

INTRODUCTION

Novo29, a new antibiotic from a soil bacterium closely related to *Eleftheria terrae*, was recently reported.¹ Novo29 is an eight-residue depsipeptide comprising a macrolactone ring and a linear tail. It is active against Gram-positive bacteria, including drug-resistant human pathogens, such as MRSA and VRE. Novo29 kills bacteria by inhibiting bacterial cell-wall synthesis, with no detectable resistance occurring upon serial passaging.^{2,3} Although the amino acid sequence of Novo29 was determined, the stereochemistry of the rare noncanonical amino acid hydroxyasparagine at position 5 was not able to be determined. Neither NMR spectroscopic analysis nor correlation with authentic hydroxyasparagine of known stereochemistry has thus far been feasible, leaving open the question of which hydroxyasparagine stereoisomer constituted the natural product.

Novo29 is related in structure to teixobactin, which is produced by *E. terrae*, but it is smaller, containing eight residues instead of eleven (Figure 3.1).^{2,3} Like teixobactin, Novo29 exhibits good activity against Gram-positive bacteria and targets cell-wall precursors. Novo29 is a promising antibiotic drug candidate, because it kills drug-resistant pathogens without detectable resistance and exhibits reduced propensity to form gels upon intravenous dosing.⁴ In the current study, we establish the stereochemistry of the hydroxyasparagine (hydroxyAsn) residue at position 5 and confirm the structure of Novo29 through chemical synthesis and spectroscopic and functional correlation. We also report the X-ray crystallographic structure of a hydroxyAsn epimer of Novo29 (*epi*-Novo29), which may provide insights into how Novo29 binds bacterial cell-wall precursors.

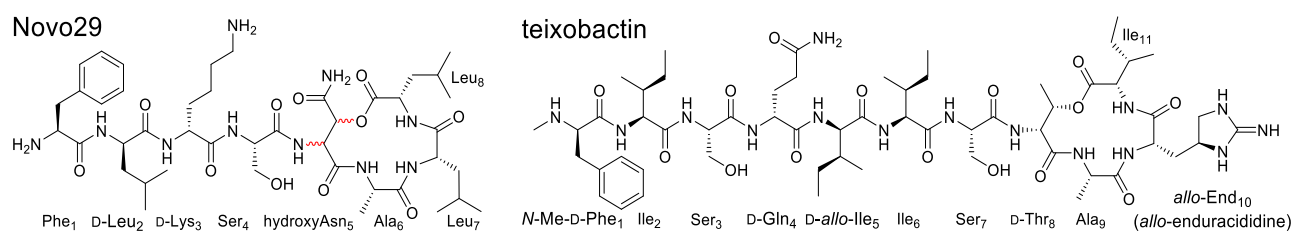


Figure 3.1. Structures of Novo29 and teixobactin. The unassigned stereochemistry of hydroxyAsn at position 5 of Novo29 is highlighted in red.

RESULTS AND DISCUSSION

Synthesis of Novo29 and epi-Novo29

We hypothesized the stereochemistry at position 5 to be (2*R*,3*R*)-hydroxyAsn, based on the similarity in structure and connectivity of D-Thr₈ of teixobactin, as well as the related depsipeptide antibiotic hyeptin.⁵ We developed and carried out the synthesis of a suitably protected (2*R*,3*R*)-hydroxyAsn as a building block that could be readily incorporated into solid-phase peptide synthesis (SPPS). This building block is Fmoc-protected at the α -amino

position; the hydroxyl and primary amide groups can tolerate SPPS without protection.^{6,7} For comparison, we also synthesized the Fmoc-protected (2*R*,3*S*)-hydroxyAsn diastereomer (Figure 3.2).

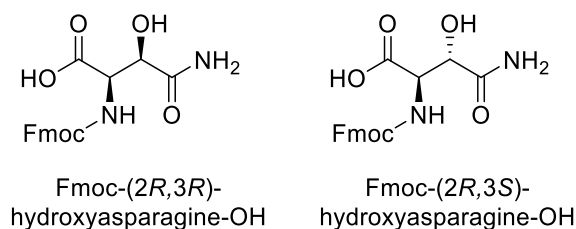


Figure 3.2. Structures of Fmoc-(2*R*,3*R*)-hydroxyasparagine-OH and Fmoc-(2*R*,3*S*)-hydroxyasparagine-OH.

We synthesized Fmoc-(2*R*,3*R*)-hydroxyasparagine-OH from (+)-diethyl L-tartrate as outlined in Figure 3. (2*R*,3*R*)-(+)-Diethyl L-tartrate was converted to bromo alcohol **12** by conversion to the cyclic sulfite and oxidation to the cyclic sulfate followed by ring opening with LiBr.⁸ This sequence was previously established for diisopropyl and dimethyl tartrates and resulted in the formation of 80:20 and 85:15 mixtures of diastereomers.^{9,10} In our hands the LiBr reaction proceeded with the formation of the two diastereomers of bromo alcohol **12** in a 70:30 ratio favoring the desired diastereomer (Figure S3.1). Treatment of the mixture of diastereomers with sodium azide, to give the corresponding azido alcohols with inversion of stereochemistry, followed by reduction with H₂ and Pd/C and chromatographic separation of diastereomers afforded amino alcohol **13**.

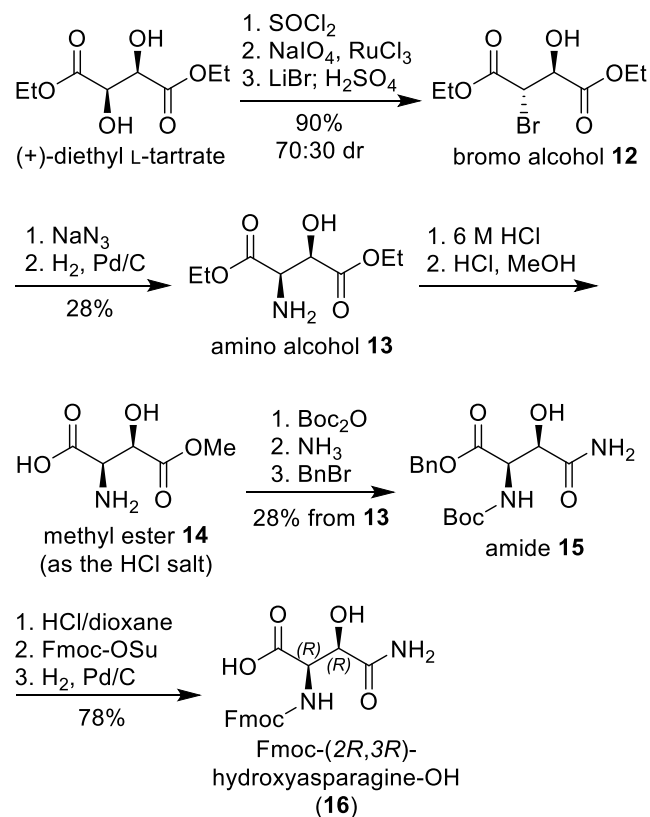


Figure 3.3. Synthesis of Fmoc-(2R,3R)-hydroxyasparagine-OH.

Amino alcohol **13** was converted to methyl ester **14** by hydrolysis of the ethyl ester groups in 6 M HCl followed by regioselective differentiation of the two carboxylic acid groups by Fischer esterification with HCl in CH₃OH.¹¹ The methyl esterification proceeds regioselectively, possibly because the ammonium group at the 2-position deactivates the carboxylic acid group at the 1-position.¹² Methyl ester **14** was then converted to amide **15** by Boc protection of amino group at the 2-position, ammonolysis to the amide at the 4-position, and benzyl ester protection of the carboxylic acid at the 1-position. Amide **15** was subsequently converted to Fmoc-(2R,3R)-hydroxyasparagine-OH by removal of the Boc group with 4 M HCl in dioxane, Fmoc protection of the amino group with Fmoc-OSu, and hydrogenolysis of the benzyl ester group with H₂ and Pd/C.

We synthesized the Fmoc-(2*R*,3*S*)-hydroxyasparagine-OH diastereomer from (-)-diethyl D-tartrate in a related fashion, as outlined in Figure 3.4. (2*S*,3*S*)-(-)-Diethyl D-tartrate was converted to amino alcohol **17** by conversion to the cyclic sulfite with thionyl chloride, followed by ring opening with sodium azide and reduction of the azido group with H₂ and Pd/C.¹³ Amino alcohol **17** was then converted to Fmoc-(2*R*,3*S*)-hydroxyasparagine-OH in a similar fashion to that described above for amino alcohol **13**.

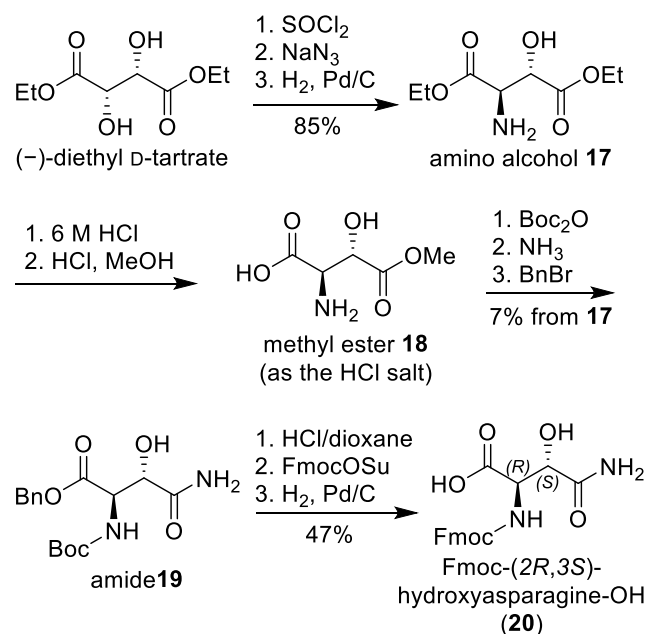


Figure 3.4. Synthesis of Fmoc-(2*R*,3*S*)-hydroxyasparagine-OH.

We determined the stereochemistry of Novo29 by synthesizing (2*R*,3*R*)-hydroxyAsn-Novo29 and (2*R*,3*S*)-hydroxyAsn-Novo29 and then correlating these synthetic peptides with natural Novo29 by ¹H NMR spectroscopy, LC-MS analysis, and MIC assays. (2*R*,3*R*)-hydroxyAsn-Novo29 and (2*R*,3*S*)-hydroxyAsn-Novo29 were synthesized by solid-phase peptide synthesis of a protected acyclic precursor followed by solution-phase cyclization, in a fashion similar to that which we have developed for the synthesis of teixobactin analogues

(Figure 3.5).^{6,14-18} The synthesis begins with loading Fmoc-Leu-OH (position 7) onto 2-chlorotrityl resin, followed by incorporation of residues 6 through 1. Leu₈ was esterified onto the β -hydroxy group of the (2*R*,3*R*)-hydroxyAsn or (2*R*,3*S*)-hydroxyAsn residue at position 5 by treatment with Fmoc-Leu-OH, DIC, and DMAP.¹⁹ Fmoc deprotection of Leu₈ and cleavage of the peptide from the resin with 20% hexafluoroisopropanol (HFIP) in CH₂Cl₂ afforded the protected peptide with a free carboxylic acid group on Leu₇ and a free amino group on Leu₈. Cyclization between Leu₈ and Leu₇ was achieved with HBTU and HOBt.²⁰ Global deprotection with trifluoroacetic acid (TFA) and reverse-phase HPLC purification yielded (2*R*,3*R*)-hydroxyAsn-Novo29 and (2*R*,3*S*)-hydroxyAsn-Novo29 as the trifluoroacetate salts.

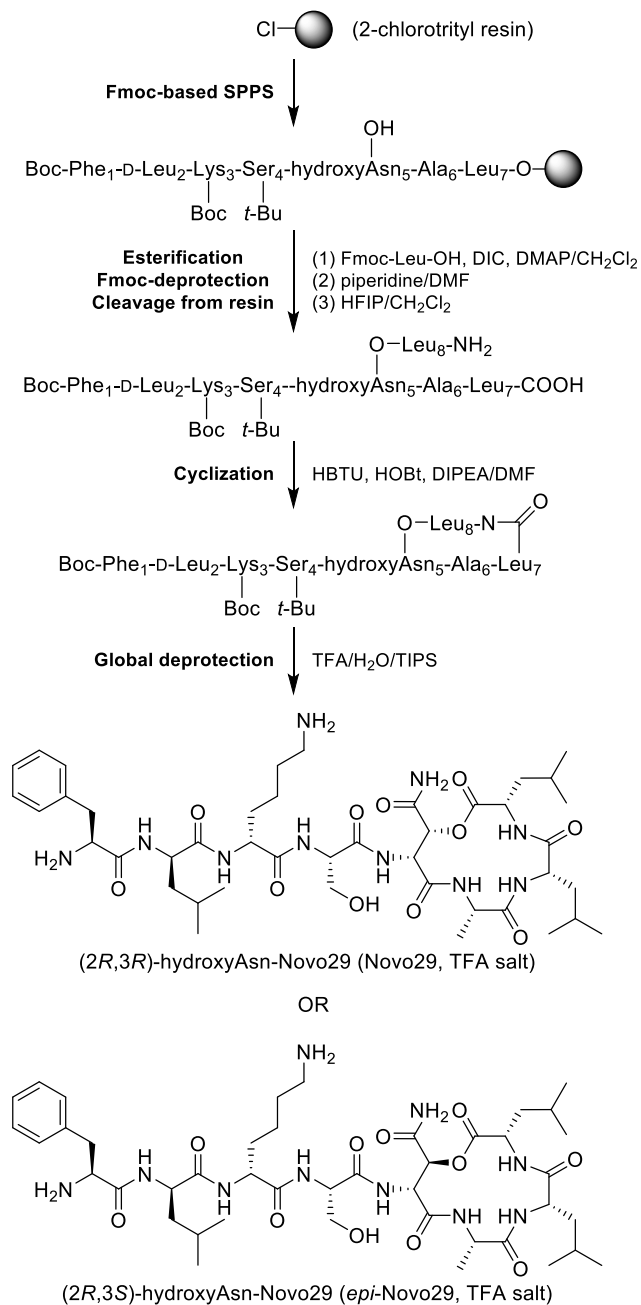


Figure 3.5. Synthesis of Novo29 and *epi*-Novo29.

Stereochemical determination of Novo29

The ¹H NMR spectrum of natural Novo29 in DMSO-*d*₆ matches that of (2*R*,3*R*)-hydroxyAsn-Novo29 and differs significantly from that of synthetic (2*R*,3*S*)-hydroxyAsn-Novo29 (Figure 3.6). Notably, the α - and β -proton resonances of the hydroxyAsn residue in natural and (2*R*,3*R*)-hydroxyAsn-Novo29 both appear at 5.04 and 5.29 ppm, respectively,

while those of (2*R*,3*S*)-hydroxyAsn-Novo29 appear at 5.14 and 5.00 ppm. From here on (2*R*,3*R*)-hydroxyAsn-Novo29 will be referred to as Novo29, and (2*R*,3*S*)-hydroxyAsn-Novo29 will be referred to as *epi*-Novo29. The amide NH region of both natural and synthetic Novo29 also match reasonably well and differ substantially from that of *epi*-Novo29. Surprisingly, the chemical shifts of the NH groups of Novo29 proved sensitive to concentration, varying by as much as 0.1 ppm over concentrations from 1–3 mM. This observation suggests that even in DMSO, Novo29 undergoes relatively strong self-association (Figure 3.9 and Table 3.2).

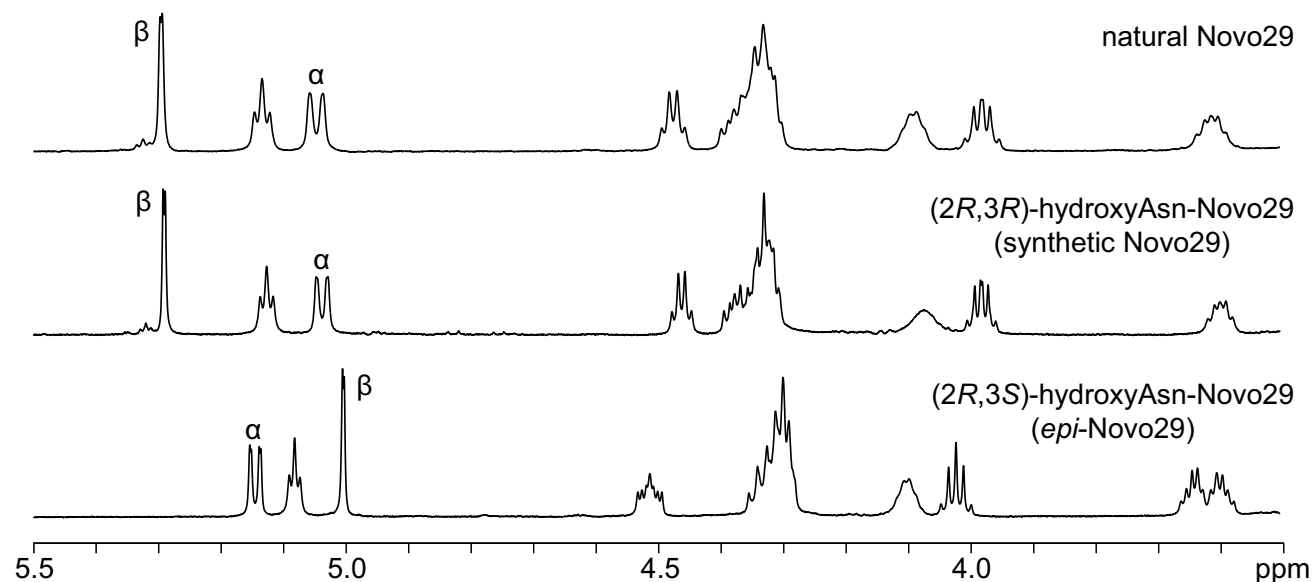


Figure 3.6. ^1H NMR spectra of natural Novo29, synthetic Novo29, and *epi*-Novo29 (3.5–5.5 ppm expansion, 500 MHz, 2 mM in $\text{DMSO-}d_6$). The α - and β -protons of hydroxyAsn are labeled.

To corroborate the stereochemical identity of Novo29 we compared natural Novo29 to synthetic Novo29 and *epi*-Novo29 by LC-MS. With a gradient of 3–27 % CH_3CN over 25 minutes on a C4 column, natural and synthetic Novo29 elute comparably (15.81 and 15.88 minutes, respectively), whereas *epi*-Novo29 elutes substantially later (16.57 minutes). The

retention time and peak shape of Novo29 proved highly concentration dependent, with broad peaks and shorter elution times resulting at higher concentrations, again suggesting strong self-association (Figure S3.2).

To further corroborate the stereochemical identity of Novo29, and to evaluate the importance of the stereochemistry of the hydroxyAsn residue, we tested the antibiotic activity of natural Novo29, synthetic Novo29, and *epi*-Novo29 using minimum inhibitory concentration (MIC) assays against two Gram-positive bacteria, *B. subtilis*, and *S. epidermidis*. We used the Gram-negative bacterium *E. coli* as a negative control. Natural Novo29 and synthetic Novo29 exhibit comparable antibiotic activity against the Gram-positive bacteria, with MIC values of 0.125 µg/mL for *B. subtilis* and 0.25 µg/mL for *S. epidermidis* (Table 3.1). To our surprise, both synthetic Novo29 and natural Novo29 also exhibited modest activity against *E. coli*, with MIC values of 8 µg/mL.²¹ In contrast, *epi*-Novo29 exhibited no MIC activity (>32 µg/mL) against any of the bacteria, thus indicating that the 2*R*,3*R* stereochemistry of the hydroxyAsn residue is critical to the antibiotic activity of Novo29.

Table 3.1. MIC values of natural Novo29, synthetic Novo29, and *epi*-Novo29 in µg/mL.

	<i>Bacillus subtilis</i> ATCC 6051	<i>Staphylococcus epidermidis</i> ATCC 14990	<i>Escherichia coli</i> ATCC 10798
natural Novo29	0.125	0.25	8
synthetic Novo29	0.125	0.25	8
<i>epi</i> -Novo29	>32	>32	>32

Crystallographic studies of Novo29, epi-Novo29, a molecular model of Novo29, and studies of assembly of Novo29 and epi-Novo29

X-ray crystallography permitted the structural elucidation of *epi*-Novo29 and may provide insights into the conformation and mechanism of action of Novo29. Both *epi*-Novo29 and Novo29 were screened for crystallization in a 96-well plate format using crystallization kits from Hampton Research (PEG/Ion, Index, and Crystal Screen). Novo29 did not form crystals from any of the conditions tested. *epi*-Novo29 formed rod-shaped crystals from 2.8 M sodium acetate at pH 7.0. Further optimization in a 24-well plate format afforded long rectangular crystals suitable for X-ray diffraction from 2.8 M sodium acetate at pH 6.6. Novo29 hydrolyzed in the conditions that afforded crystals of *epi*-Novo29, which is likely the reason why no crystals were formed (Figure S3.3). The hydrolysis of Novo29 is explored in more detail in Chapter IV. Diffraction data were initially collected using an X-ray diffractometer on an *epi*-Novo29 crystal that was soaked in KI to incorporate iodide ions into the lattice (PDB 8CUF). The crystallographic phases were determined using single-wavelength anomalous diffraction (SAD) phasing from the incorporated iodide ions. Higher-resolution diffraction data were subsequently collected out to 1.13 Å resolution on an unsoaked *epi*-Novo29 crystal using a synchrotron (PDB 8CUG). The crystallographic phases of the higher-resolution data were determined by molecular replacement using the KI-soaked structure as a search model. The asymmetric unit contains two molecules of *epi*-Novo29, which exhibit only minor differences in conformation.

In the X-ray crystallographic structure, *epi*-Novo29 adopts an amphiphilic conformation, with the side chains of Phe₁, D-Leu₂, Leu₇, and Leu₈ creating a hydrophobic surface and the side chains of D-Lys₃, Ser₄, and (2*R*,3*S*)-hydroxyAsn₅, as well as the *N*-terminal

ammonium group, creating a hydrophilic surface (Figure 3.7A). An intramolecular hydrogen bond between the main-chain NH group of Ala₆ and the side chain OH group of Ser₄ helps enforce this conformation. In the lattice, *epi*-Novo29 packs so that the hydrophobic surfaces come together, with four sets of *epi*-Novo29 molecules forming a hydrophobic core (Figure 3.7C). The macrolactone ring of *epi*-Novo29 adopts a conformation in which the main-chain NH groups of (2*R*,3*S*)-hydroxyAsn₅, Ala₆, Leu₇, and Leu₈ converge to create a cavity, which binds ordered water and acetate anion.

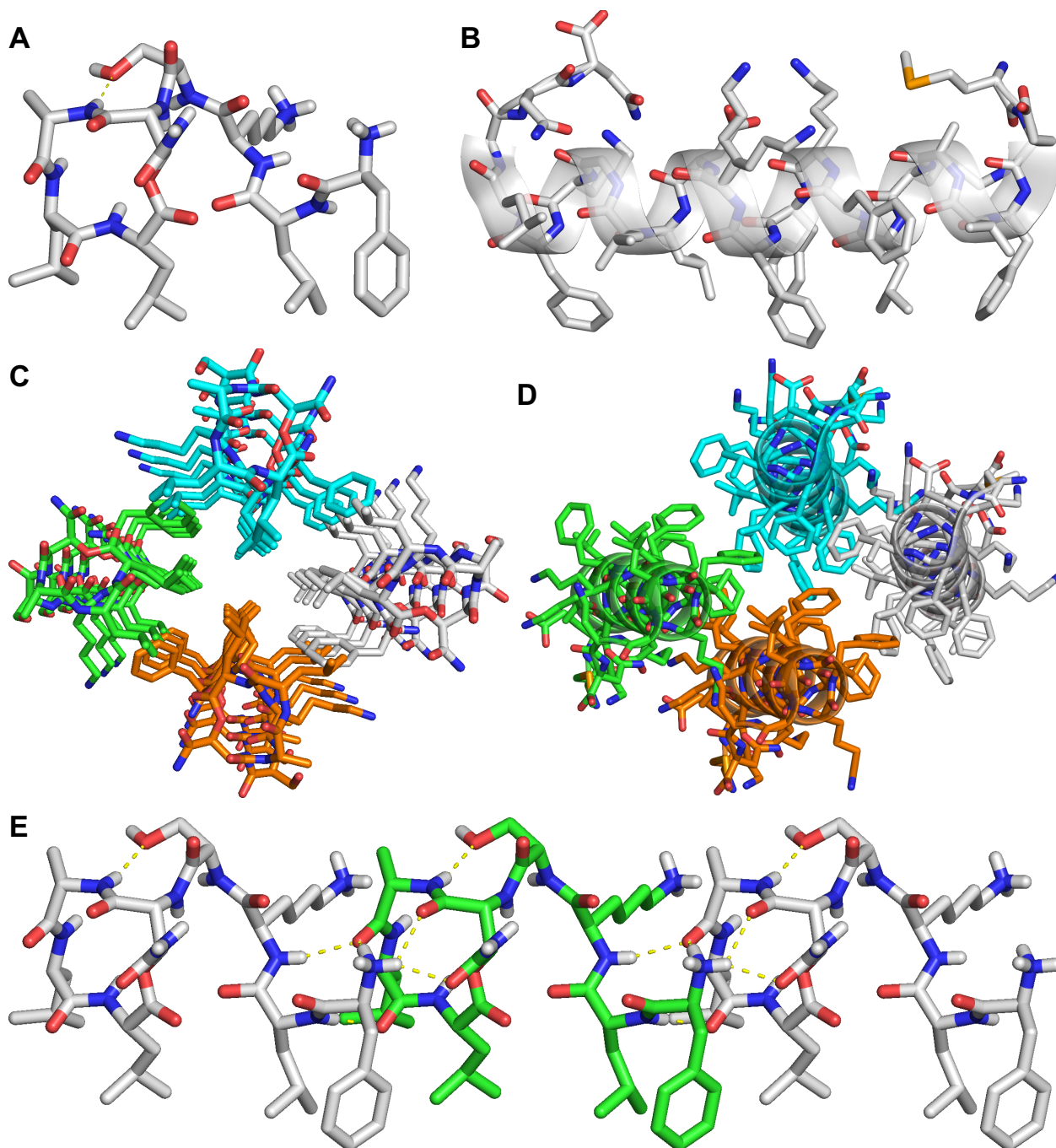


Figure 3.7. (A) X-ray crystallographic structure of *epi*-Novo29 (PDB 8CUG). (B) X-ray crystallographic structure of PSMa3 (PDB 5I55), illustrating the relationship of this amphiphilic 22-residue α -helical peptide to *epi*-Novo29. (C) Crystal packing of *epi*-Novo29. Molecules assemble in columns in the crystal lattice, with four columns of molecules arranged in a hydrophobic cluster through packing of Phe₁, D-Leu₂, Leu₇, and Leu₈. (D) Crystal packing of PSMa3, illustrating the relationship to the crystal packing of *epi*-Novo29. (E) Assembly of *epi*-Novo29 in the crystal lattice, illustrating the intermolecular hydrogen-bonding between molecules comprising the columns. Three molecules are shown.

The amphiphilic structure of *epi*-Novo29 is reminiscent of the amphiphilic structure our laboratory has previously observed for teixobactin derivatives, in which the side chains of *N*-methyl-D-Phe₁, Ile₂, D-*allo*-Ile₅, and Ile₆ create a hydrophobic surface and the side chains of Ser₃, D-Gln₄, and Ser₇ create a hydrophilic surface.^{6,18} In teixobactin, this conformation is biologically significant, providing a hydrophobic surface that interacts with the lipids of the bacterial cell membrane and a hydrophilic surface to interact with the aqueous environment.^{18,22–24} In Novo29, the amphiphilic structure likely provides similar opportunity for interaction with the bacterial cell membrane. In teixobactin, the cavity created by the macrolactone ring binds the pyrophosphate groups of lipid II and related bacterial cell-wall precursors. The macrolactone ring of Novo29 has the potential to bind the pyrophosphate groups of lipid II in a similar fashion.

The amphiphilic structure of *epi*-Novo29 is similar to that of the α -helices of phenol-soluble modulin $\alpha 3$ (PSM $\alpha 3$), a cytotoxic 22-residue peptide secreted by *S. aureus* which aggregates to form novel “cross- α ” amyloid fibrils.²⁵ The α -helices formed by PSM $\alpha 3$ present phenylalanine and leucine residues on one surface, and polar residues on the other surface (Figure 3.7B). PSM $\alpha 3$ packs so that the hydrophobic surfaces come together in extended layers, in which the packing of four PSM $\alpha 3$ molecules resembles that of four *epi*-Novo29 molecules (Figure 3.7D). Although *epi*-Novo29 is much smaller than PSM $\alpha 3$ — 8 residues instead of 22 residues — the *epi*-Novo29 molecules daisy-chain through intermolecular hydrogen bonding to form extended structures that resemble the larger α -helices of PSM $\alpha 3$ (Figure 3.7E).

To gain additional insights into the mechanism of action of Novo29, we used the X-ray crystallographic structure of *epi*-Novo29 to create a molecular model of Novo29. Inversion of the 3*S*-stereocenter of the (2*R*,3*S*)-hydroxyAsn residue of the crystal structure, followed by geometry optimization of only the side chain of the resulting (2*R*,3*R*)-hydroxyAsn residue, afforded a crystallographically based molecular model of Novo29 (Figure 8). In this model, the molecule still adopts an amphiphilic conformation. The only difference in structure is that the side-chain amide NH group of the (2*R*,3*R*)-hydroxyAsn residue hydrogen bonds to the carbonyl group of Phe₁. This intramolecular hydrogen bond, in addition to the intramolecular hydrogen bond between the main-chain NH group of Ala₆ and the side chain OH group of Ser₄ helps enforce the amphiphilic conformation.

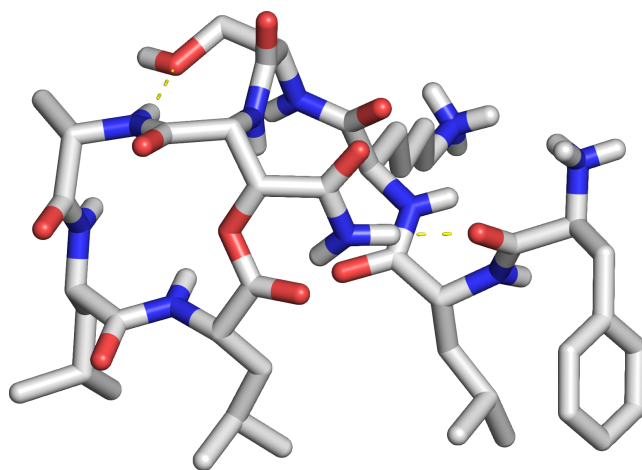


Figure 3.8. Molecular model of Novo29, based on the X-ray crystallographic structure of *epi*-Novo29. Intramolecular hydrogen bonds (yellow dashed lines) help enforce a preorganized conformation, in which the side chains of Phe₁, D-Leu₂, Leu₇, and Leu₈ align and can interact with the cell membrane of Gram-positive bacteria, and the macrolactone ring adopts a conformation that can bind the pyrophosphate groups of lipid II and related cell-wall precursors.

The X-ray crystallographic structure of *epi*-Novo29 and the crystallographically based molecular model of Novo29 suggest that Novo29 might be able to act upon Gram-positive

bacteria in a fashion similar to teixobactin. Teixobactin adopts an amphiphilic conformation on bacteria, in which the side chains of *N*-methyl-D-Phe₁, Ile₂, *D*-allo-Ile₅, and Ile₆ insert into the cell membrane and the macrolactone ring binds the pyrophosphate groups of lipid II and related cell-wall precursors.²² The teixobactin molecules form hydrogen-bonded dimers that further assemble on the cell membrane through β -sheet formation, causing lipid II and related cell-wall precursors to cluster and ultimately lyse the bacteria. We envision that Novo29 also adopts an amphiphilic conformation on Gram-positive bacteria, in which the side chains of Phe₁, *D*-Leu₂, Leu₇, and Leu₈ insert into the cell membrane and the macrolactone ring binds the pyrophosphate groups of lipid II and related cell-wall precursors. The Novo29 molecules may further assemble through side-to-side hydrophobic interactions and end-to-end hydrogen bonding, and thus cause lipid II and related cell-wall precursors to cluster. We anticipate that the studies described in this paper will help lay the groundwork for testing this hypothesis.

Novo29 shows signs of assembly by NMR and LC-MS. Despite running NMR experiments in DMSO-*d*₆ which should prevent hydrogen bonding occurring and tends to break up assembly most commonly observed in aqueous environments there are signs of assembly present in the NMR spectra (Figure 3.9 and Table 3.2). Natural Novo29 was dissolved in three nominal concentrations into DMSO-*d*₆ – 1, 2, and 3 mM. While the aliphatic proton signals in the NMR remain unshifted, notable shifts in the amide region (~ 7.35 – 8.60 ppm). can be observed between the different concentrations. Differences between the 1 mM and 3 mM sample range up to 0.11 ppm for amide 14 (Table 3.2). Interestingly, the amide region for synthetic Novo29 at the prepared 2 mM nominal concentration most closely resembles the 3 mM nominal concentration of natural Novo29. This difference can be ascribed to small errors occurring in weighing out milligram quantities of the lyophilized powder for

either sample. LC-MS analysis running *epi*-, natural, and synthetic Novo29 at either 0.002 mg/mL or at 0.02 mg/mL reveals potential assembly due to shark-fine appearance of the peaks at the higher concentration (Figure S3.2).

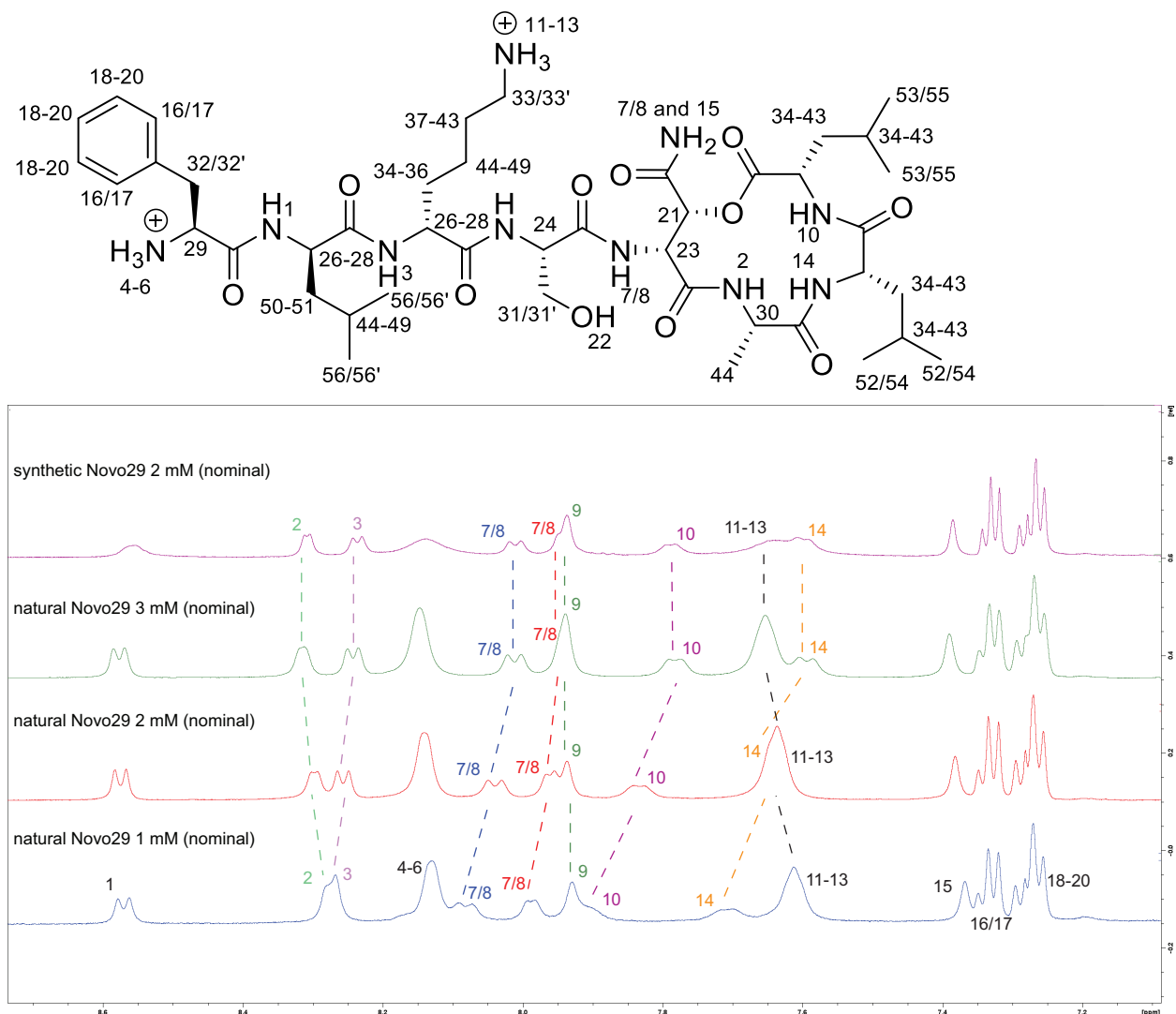


Figure 3.9. Comparison of the amide NH regions of the 500 MHz ^1H NMR spectra of samples of Novo29 in $\text{DMSO-}d_6$. Samples of natural Novo29 were prepared gravimetrically at nominal concentrations of 1, 2, and 3 mM. The chemical shifts of the NH resonances vary strongly with concentration. The ^1H NMR spectrum of a sample of synthetic Novo29 prepared gravimetrically at a nominal concentration of 2 mM matches that of the 3 mM nominal concentration sample of natural Novo29. All samples were prepared by dissolving 1–2 mg of peptide in $\text{DMSO-}d_6$. Discrepancies in concentration reflect errors associated with weighing out small quantities of peptide.

Table 3.2. Chemical shifts of the amide NH resonances of samples of Novo29.

#	natural 1 mM (nominal)	natural 2 mM (nominal)	natural 3 mM (nominal)	synthetic 2 mM (nominal)
1	8.57	8.57	8.57	8.56
2	8.28	8.29	8.31	8.30
3	8.27	8.26	8.24	8.24
4-6	8.13	8.14	8.15	8.14
7/8	8.08	8.04	8.01	8.01
	&	&	&	&
	7.98	7.96	7.95	7.94
9	7.99	7.96	7.94	7.94
10	7.90	7.83	7.78	7.78
11-13	7.61	7.64	7.65	7.65
14	7.71	7.65	7.60	7.60
15	7.37	7.38	7.39	7.39
16/17	7.33	7.33	7.33	7.33
18-20	7.27	7.27	7.27	7.27

CONCLUSION

The antibiotic Novo29 has *2R,3R* stereochemistry in the hydroxyAsn residue at position 5. Novo29 and diastereomer *epi*-Novo29 are prepared by Fmoc-based solid-phase peptide synthesis followed by solution-phase cyclization. The corresponding amino acid building blocks Fmoc-(*2R,3R*)-hydroxyasparagine-OH and Fmoc-(*2R,3S*)-hydroxyasparagine-OH are prepared from (*R,R*)- and (*S,S*)-diethyl tartrate. Correlation of synthetic Novo29 and *epi*-Novo29 with natural Novo29 through NMR spectroscopy, LC-MS, and MIC assays establishes the *2R,3R* stereochemistry of the hydroxyAsn residue and confirms that Novo29 is active against Gram-positive bacteria. X-ray crystallography of *epi*-Novo29 reveals an amphiphilic conformation and packing of the molecules through hydrophobic and hydrogen-bonding interactions. Molecular modeling suggests that Novo29 should be able to adopt a similar amphiphilic conformation that is further stabilized through an additional hydrogen bond between the primary amide group of the (*2R,3R*)-hydroxyAsn residue and the carbonyl group of the phenylalanine residue.

REFERENCES AND NOTES

1. "Depsipeptides and uses thereof", Peoples, A. J.; Hughes, D.; Ling, L. L.; Millett, W.; Nitti, A. G.; Spoering, A.; Steadman, V. A.; Chiva, J. C.; Lazarides, L.; Jones, M. K.; Poullennes, K. G.; Lewis, K.; Epstein, S. U.S. Patent 11,203,616.
2. Novobiotic Pharmaceuticals, <https://www.novobiotic.com/the-science>.
3. Ling, L. L.; Schneider, T.; Peoples, A. J.; Spoering, A. L.; Engels, I.; Conlon, B. P.; Mueller, A.; Schäberle, T. F.; Hughes, D. E.; Epstein, S.; Jones, M.; Lazarides, L.; Steadman, V. A.; Cohen, D. R.; Felix, C. R.; Fetterman, K. A.; Millett, W. P.; Nitti, A. G.; Zullo, A. M.; Chen, C.; Lewis, K. A new antibiotic kills pathogens without detectable resistance. *Nature* **2015**, *517*, 455–459.
4. Ling, L. L. Preclinical Development of Novo29, a New Antibiotic, *NIH RePORTER*, <https://reporter.nih.gov/project-details/10111451>.
5. Wirtz, D. A.; Ludwig, K. C.; Arts, M.; Marx, C. E.; Krannich, S.; Barac, P.; Kehraus, S.; Josten, M.; Henrichfreise, B.; Müller, A.; König, G. M.; Peoples, A. J.; Nitti, A. G.; Spoering, A. L.; Ling, L. L.; Lewis, K.; Crüsemann, M.; Schneider, T. Biosynthesis and Mechanism of Action of the Cell Wall Targeting Antibiotic Hypeptin. *Angew. Chem. Int. Ed.* **2021**, *60*, 13579–13586.
6. Yang, H.; Pishenko, A. V.; Li, X.; Nowick, J. S. Design, Synthesis, and Study of Lactam and Ring-Expanded Analogues of Teixobactin. *J. Org. Chem.* **2020**, *85*, 1331–1339.
7. Sieber, P.; Riniker, B. Protection of carboxamide functions by the trityl residue. Application to peptide synthesis. *Tetrahedron Lett.*, **1991**, *32*, 739–742.
8. Gao, B.; Sharpless, K. B. Vicinal diol cyclic sulfates. Like epoxides only more reactive. *J. Am. Chem. Soc.* **1988**, *110*, 7538–7539.

9. He, L.; Byun, H.S.; Bittman, R. Efficient synthesis of chiral α,β -epoxyesters via a cyclic sulfate intermediate. *Tetrahedron Lett.* **1998**, *39*, 2071–2074.
10. France, B.; Bruno, V.; Nicolas, I. Synthesis of a protected derivative of (2R,3R)- β -hydroxyaspartic acid suitable for Fmoc-based solid phase synthesis. *Tetrahedron Lett.* **2013**, *54*, 158–161.
11. Guzmán-Martinez; A.; Vannieuwenhze, M. S. An Operationally Simple and Efficient Synthesis of Orthogonally Protected L-threo-beta-Hydroxyasparagine. *Synlett* **2007**, *10*, 1513–1516.
12. An 83:12:5 mixture of methyl ester **3**, the corresponding diacid precursor, and the corresponding dimethyl ester was used in the next step without further purification.
13. Liu, L.; Wang, B.; Bi, C.; He, G.; Chen, G. Efficient preparation of β -hydroxy aspartic acid and its derivatives. *Chin. Chem. Lett.* **2018**, *29*, 1113–1115.
14. Chen, K. H.; Le, S. P.; Han, X.; Frias, J. M.; Nowick, J. S. Alanine scan reveals modifiable residues in teixobactin. *Chem. Commun.* **2017**, *53*, 11357–11359.
15. Yang, H.; Chen, K. H.; Nowick, J. S. Elucidation of the Teixobactin Pharmacophore, *ACS Chem. Biol.* **2016**, *11*, 1823–1826.
16. Yang, H.; Du Bois, D. R.; Ziller, J. W.; Nowick, J. S. X-ray crystallographic structure of a teixobactin analogue reveals key interactions of the teixobactin pharmacophore. *Chem. Commun.* **2017**, *53*, 2772–2775.
17. Morris, M. A.; Malek, M.; Hashemian, M. H.; Nguyen, B. T.; Manuse, S.; Lewis, K. L.; Nowick, J. S. A Fluorescent Teixobactin Analogue. *ACS Chem. Biol.* **2020**, *15*, 1222–1231.

18. Yang, H.; Wierzbicki, M.; Du Bois D. R.; Nowick, J. S. X-ray Crystallographic Structure of a Teixobactin Derivative Reveals Amyloid-like Assembly. *J. Am. Chem. Soc.* **2018**, *140*, 14028–14032.
19. Neises, B.; Steglich, W. Simple Method for the Esterification of Carboxylic Acids. *Angew. Chem. Int. Ed. Engl.* **1978**, *17*, 522–524.
20. The macrolactamization reaction proceeds without significant formation of epimers at position 7. The esterification at position 8, however, does result in epimer formation. The epimeric impurity is readily removed during the HPLC purification step.
21. Independent experiments at NovoBiotic Pharmaceuticals LLC under similar conditions gave MIC values of 16–32 µg/mL for *E. coli* ATCC 10798.
22. Shukla, R.; Lavore, F.; Maity, S.; Derks, M. G. N.; Jones, C. R.; Vermeulen, B. J. A.; Melcrová, A.; Morris, M. A.; Becker, L. M.; Wang, X.; Kumar, R.; Medeiros-Silva, J.; van Beekveld, R. A. M.; Bonvin, A. M. J. J.; Lorent, J. H.; Lelli, M.; Nowick, J. S.; MacGillavry, H. D.; Peoples, A. J.; Spoering, A. L.; Ling, L. L.; Hughes, D. E.; Roos, W. H.; Breukink, E.; Lewis, K. and Weingarh, M. Teixobactin kills bacteria by a two-pronged attack on the cell envelope. *Nature* **2022**, *608*, 390–396.
23. Shukla, R.; Medeiros-Silva, J.; Parmar, A.; Vermeulen, B. J. A.; Das, S.; Paioni, A. L.; Jekhmene, S.; Lorent, J.; Bonvin, A. M. J. J.; Baldus, M.; Lelli, M.; Veldhuizen, E. J. A.; Breukink, E.; Singh, I.; Weingarh, M. Mode of action of teixobactins in cellular membranes. *Nat. Commun.*, **2020**, *11*, 2848.
24. Öster, C.; Walkowiak, G. P.; Hughes, D. E.; Spoering, A. L.; Peoples, A. J.; Catherwood, A. C.; Tod, J. A.; Lloyd, A. J.; Herrmann, T.; Lewis, K.; Dowson, C. G.; Lewandowski, J. R.

Structural studies suggest aggregation as one of the modes of action for teixobactin. *Chem. Sci.* **2018**, *9*, 8850–8859.

25. Tayeb-Fligelman, E.; Tabachnikov, O.; Moshe, A.; Goldshmidt-Tran, O.; Sawaya, M. R.; Coquelle, N.; Colletier, J.; Landau, M. The cytotoxic *Staphylococcus aureus* PSM α 3 reveals a cross- α amyloid-like fibril. *Science* **2017**, *355*, 831–833.

Expanded Studies on the Synthesis and Stereochemical Determination of the Peptide Antibiotic Novo29 (Clovibactin)

Table of Contents

Figure S3.1	109
Figure S3.2	110
Figure S3.3	111
Table S3.1 – crystallographic properties of PDB 8CUG	112
Table S3.2 – crystallographic properties of PDB 8CUF	113
Materials and Methods	114
Chemical synthesis of Fmoc-(2<i>R</i>,3<i>R</i>)-hydroxyAsn-OH	112
Bromo alcohol 12	115
Amino alcohol 13	117
Methyl ester 14	119
Amide 15	120
Fmoc-(2 <i>R</i> ,3 <i>R</i>)-hydroxyAsn-OH	122
Chemical synthesis of Fmoc-(2<i>R</i>,3<i>S</i>)-hydroxyAsn-OH	124
Amino alcohol 17	124
Methyl ester 18	125
Amide 19	127
Fmoc-(2 <i>R</i> ,3 <i>S</i>)-hydroxyAsn-OH.....	129
Synthesis of Novo29 and <i>epi</i>-Novo29	130
NMR spectroscopic studies of Novo29 and <i>epi</i>-Novo29	133
MIC assays	134
X-ray crystallography of <i>epi</i>-Novo29	135
References	137
Characterization Data	139
Characterization of natural Novo29	139
Analytical HPLC trace of natural Novo29.....	139
Mass spectrum of natural Novo29	140
Characterization of synthetic Novo29	141
Analytical HPLC trace of synthetic Novo29	141
Mass spectrum of synthetic Novo29.....	142
Characterization of <i>epi</i>-Novo29	143

Analytical HPLC trace of <i>epi</i> -Novo29.....	143
Mass spectrum of <i>epi</i> -Novo29	144
NMR spectra of intermediates	145
¹ H NMR spectrum of bromo alcohol 12	145
¹³ C NMR spectrum of bromo alcohol 12	146
¹ H NMR spectrum of amino alcohol 13	147
¹³ C NMR spectrum of amino alcohol 13	148
¹ H NMR spectrum of methyl ester 14	149
¹³ C NMR spectrum of methyl ester 14	150
¹ H NMR spectrum of amide 15	151
¹³ C NMR spectrum of amide 15	152
¹ H NMR spectrum of Fmoc-(2 <i>R</i> ,3 <i>R</i>)-hydroxyAsn-OH	153
¹³ C NMR spectrum of Fmoc-(2 <i>R</i> ,3 <i>R</i>)-hydroxyAsn-OH	154
EXSY spectrum of Fmoc-(2 <i>R</i> ,3 <i>R</i>)-hydroxyAsn-OH	155
¹ H NMR spectrum of amino alcohol 17	156
¹³ C NMR spectrum of amino alcohol 17	157
¹ H NMR spectrum of methyl ester 18	158
¹³ C NMR spectrum of methyl ester 18	159
¹ H NMR spectrum of amide 19	160
¹³ C NMR spectrum of amide 19	161
¹ H NMR spectrum of Fmoc-(2 <i>R</i> ,3 <i>S</i>)-hydroxyAsn-OH.....	162
¹³ C NMR spectrum of Fmoc-(2 <i>R</i> ,3 <i>S</i>)-hydroxyAsn-OH	163
EXSY spectrum of Fmoc-(2 <i>R</i> ,3 <i>S</i>)-hydroxyAsn-OH	164
NMR spectra and chemical shift assignments of natural Novo29.....	165
¹ H NMR spectrum of natural Novo29	165
TOCSY NMR spectrum of natural Novo29	166
NOESY NMR spectrum of natural Novo29	167
Table S3.3 – chemical shift assignments of natural Novo29	168
¹H NMR spectrum of synthetic Novo29	169
Table S3.4 – chemical shift comparison between natural and synthetic Novo29.....	170
¹H NMR spectrum of <i>epi</i>-Novo29	171

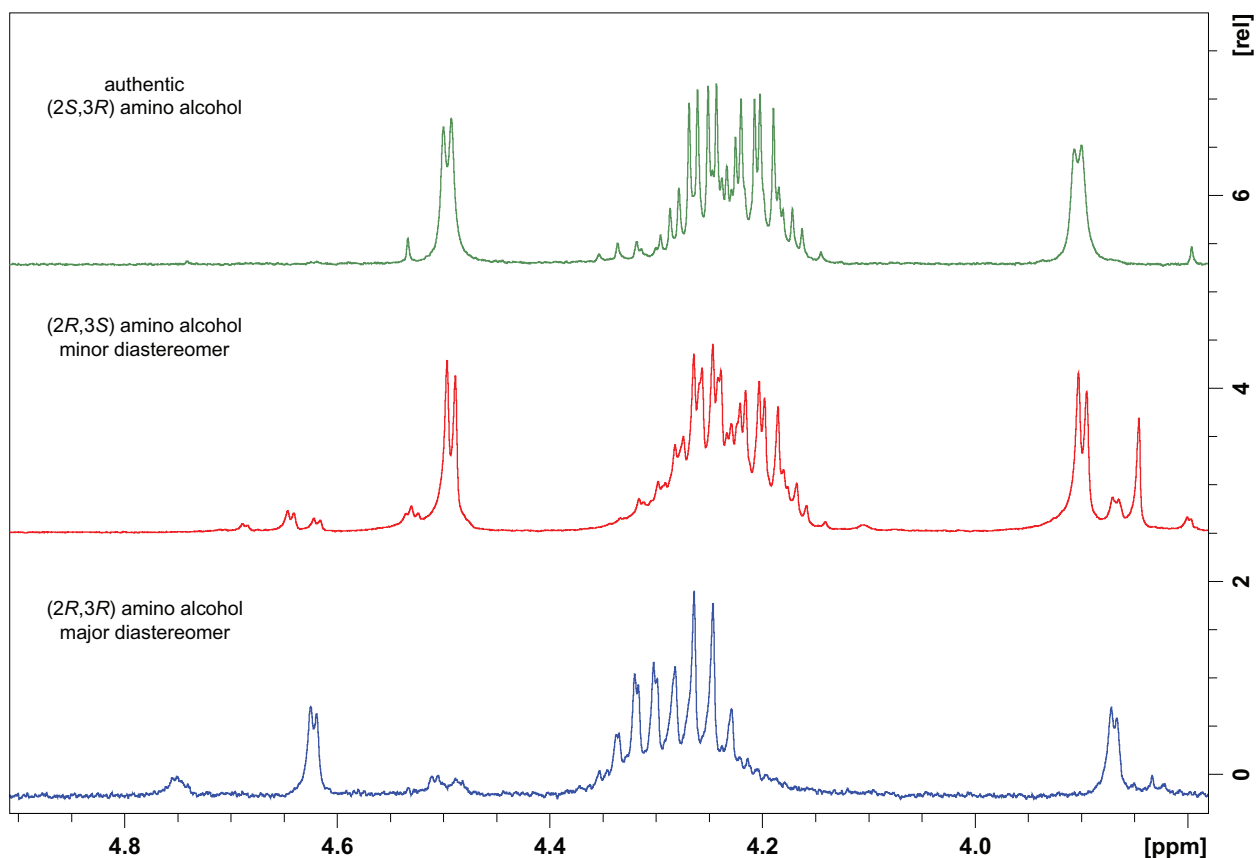


Figure S3.1. Establishment of $(2R,3R)$ stereochemistry of amino alcohol **2** and the $(2S,3R)$ stereoisomer by ^1H NMR spectroscopic correlation with an authentic sample of the $(2S,3R)$ stereoisomer (the enantiomer of amino alcohol **5**) that was synthesized from (+)-diethyl L-tartrate by the route shown in Figure 4 of the main manuscript. Amino alcohol **2** was synthesized as shown in Figure 3 as a 70:30 mixture of diastereomers, which was then separated by column chromatography. Expansions of the ^1H NMR spectra of the major diastereomer ($2R,3R$, blue) and minor diastereomer ($2S,3R$, red) are shown. Correlation with an authentic sample of the $(2S,3R)$ diastereomer (green) establishes that the minor diastereomer of amino alcohol **2** is $(2S,3R)$, and thus that the major diastereomer is $(2R,3R)$.

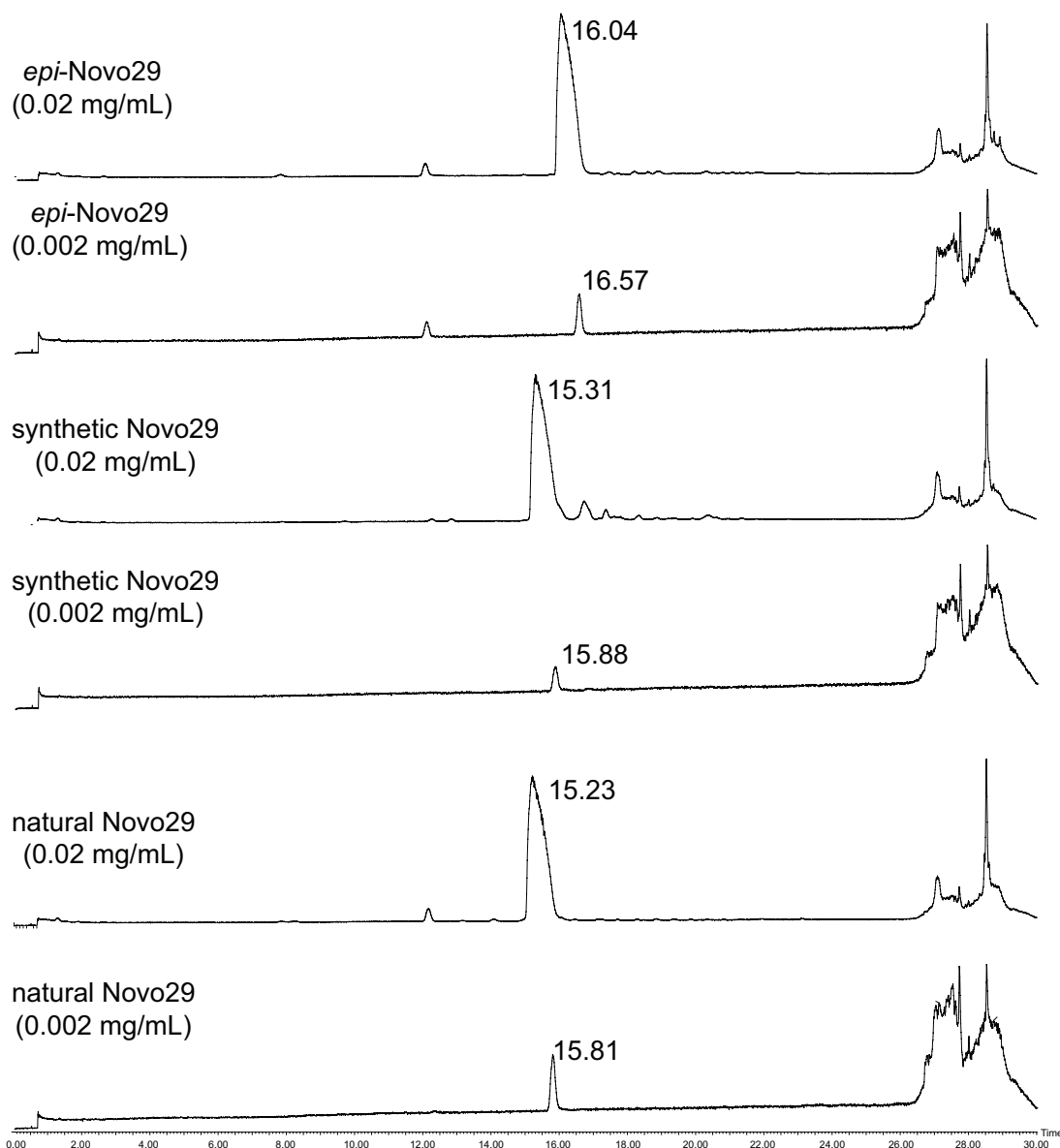


Figure S3.2. LC-MS of natural Novo29, synthetic Novo29, and *epi*-Novo29. Samples were run at (0.02 mg/mL) and (0.002 mg/mL). Traces are the total ion current (TIC) chromatograms of the samples run on a C4 column with a 3–27% CH₃CN over 25 minutes, followed by a 90% CH₃CN wash over two minutes, and a 3% CH₃CN 97% H₂O wash over one minute. The retention time and peak shape of Novo29 proved highly concentration dependent, with broad peaks and shorter elution times resulting at higher concentrations, again suggesting strong self-association.

LC/MS analysis was performed of the intact peptide sample (ACQUITY UPLC H-class system, Xevo G2-XS QToF, Waters corporation). The C4 column that was used was ACQUITY UPLC Protein BEH C4, 300 Å, 1.7 μm, 2.1 mm x 50 mm, Waters corp. The Xevo Z-spray source was operated in positive MS resolution mode, 400–4000da, with a capillary voltage of 3000V and a cone voltage of 40V (NaCsI calibration, Leu-enkephalin lock-mass). Nitrogen was used as the

desolvation gas at 350C and a total flow of 800 L h⁻¹. Retention times are given in minutes (min).

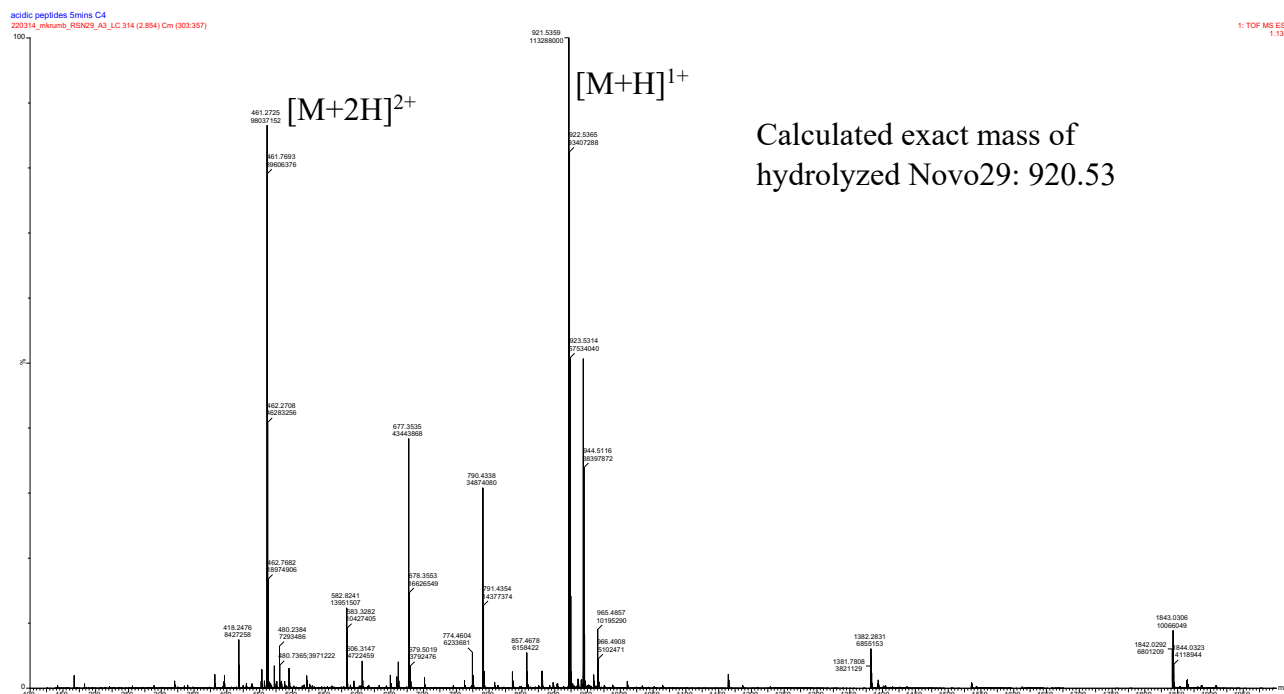


Figure S3.3. Mass spectrum of hydrolyzed crystal. After one week of setting up crystal screening conditions the liquid was tested on LC-MS and the only observed mass was that of the hydrolyzed peptide.

Table S3.1. Crystallographic properties, crystallization conditions, and data collection and model refinement statistics for *epi*-Novo29 (PDB ID 8CUG).

peptide	<i>epi</i> -Novo29 (synchrotron structure)
PDB ID	8CUG
space group	$P2_12_12_1$
a, b, c (Å)	12.105, 31.898, 37.101
α, β, λ (°)	90, 90, 90
peptides per asymmetric unit	2
crystallization conditions	2.8 M sodium acetate trihydrate pH 6.6
wavelength (Å)	1.00
resolution (Å)	24.19–1.13 (24.19–1.131)
total reflections	58890 (1401)
unique reflections	5590 (398)
multiplicity	10.5 (3.5)
completeness (%)	96.44 (69.54)
mean I/σ	22.28 (4.20)
Wilson B factor	8.32
R_{merge}	0.07324 (0.3204)
R_{measure}	0.07694 (0.3701)
$CC_{1/2}$	0.998 (0.938)
CC^*	0.999 (0.984)
R_{work}	0.1308 (0.2378)
R_{free}	0.1450 (0.2242)
number of non-hydrogen atoms	174
RMS_{bonds}	0.012
RMS_{angles}	1.63
Ramachandran favored (%)	100
outliers (%)	0
clashscore	3.77
average B-factor	13.49
ligands/ions	1
water molecules	42

Table S3.2. Crystallographic properties, crystallization conditions, and data collection and model refinement statistics for *epi*-Novo29 (PDB ID 8CUF).

peptide	<i>epi</i> -Novo29 (X-ray diffractometer structure with KI)
PDB ID	8CUF
space group	$P2_12_12_1$
a, b, c (Å)	12.1027, 31.5547, 36.9613
α, β, λ (°)	90, 90, 90
peptides per asymmetric unit	2
crystallization conditions	2.8 M sodium acetate trihydrate pH 6.6
wavelength (Å)	1.54
resolution (Å)	15.95–1.68 (1.74–1.68)
total reflections	22879 (199)
unique reflections	1741 (111)
multiplicity	13.1 (1.8)
completeness (%)	95.61 (63.07)
mean I/σ	36.10 (5.16)
Wilson B factor	8.93
R_{merge}	0.2386 (0.2593)
R_{measure}	0.2465 (0.3302)
$CC_{1/2}$	0.869 (0.822)
CC^*	0.964 (0.95)
R_{work}	0.1509 (0.2198)
R_{free}	0.1672 (0.0923)
number of non-hydrogen atoms	152
RMS_{bonds}	0.008
RMS_{angles}	1.08
Ramachandran favored (%)	100
outliers (%)	0
clashscore	3.75
average B-factor	9.85
ligands/ions	3
water molecules	18

Materials and Methods

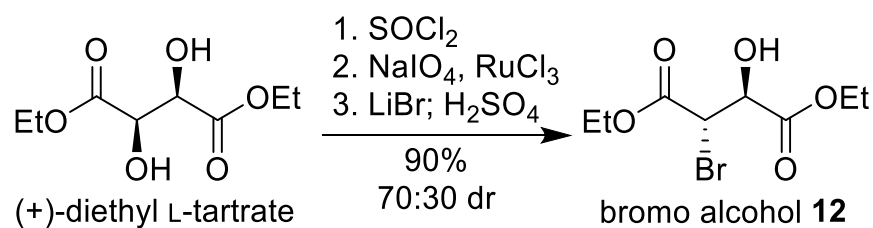
General information

Chemicals and Supplies. All chemicals were used as received unless otherwise noted. Dry methylene chloride (CH_2Cl_2), tetrahydrofuran (THF), methanol (MeOH), and *N,N*-dimethylformamide (DMF) were obtained by passing through alumina under argon prior to use. 1,4-Dioxane (dioxane) was used without added stabilizers. Anhydrous, amine-free *N,N*-dimethylformamide (DMF), DIPEA, 2,4,6-collidine, and piperidine were purchased Alfa Aesar. HPLC grade acetonitrile and deionized water (18 M Ω), each containing 0.1% trifluoroacetic acid (TFA), were used for analytical and preparative reverse-phase HPLC, as well as reverse-phase chromatography using a Biotage® Isolera One flash column chromatography instrument. Commercial agents were used without purification, unless otherwise stated. (-)-Diethyl-D-tartrate was purchased from Chem-Impex. (+)-Diethyl L-tartrate, thionyl chloride (SOCl_2), and palladium activated on carbon (Pd/C, 10% Pd, 50 % wet with water) were purchased from Sigma Aldrich. Sodium azide (NaN_3) and benzyl bromide (BnBr) were purchased from Alfa Aesar. Hydrogen (H_2) and ammonia (NH_3) were purchased from Praxair. Sodium periodate (NaIO_4) and hydrochloric acid (HCl) were purchased from Fisher Chemicals. Di-*tert*-butyl dicarbonate (Boc_2O) and Fmoc *N*-hydroxysuccinimide ester (Fmoc-OSu) were purchased from GL Biochem. Ruthenium (III) chloride trihydrate ($\text{RuCl}_3 \cdot 3\text{H}_2\text{O}$) was purchased from Chem Scene. Lithium bromide (LiBr) was purchased from TCI. Amino acids, coupling agents, 2-chlorotriyl chloride resin, DIC, and triisopropylsilane were purchased from Chem-Impex.

Instrumentation. Bacteria were incubated in a Thermo Fisher Scientific MaxQ Shaker 6000. NMR spectra were recorded on a Bruker AVANCE 500 or AVANCE 600 spectrometers equipped with cryoprobes and were calibrated using residual solvent peaks (CDCl_3 : $\delta_{\text{H}} = 7.26$ ppm, $\delta_{\text{C}} = 77.16$ ppm, $\text{DMSO-}d_6$: $\delta_{\text{H}} = 2.50$ ppm, $\delta_{\text{C}} = 39.51$ ppm, and CD_3OD : $\delta_{\text{H}} = 3.31$ ppm, $\delta_{\text{C}} =$

49.15 ppm). Structural assignments of major and minor rotamers were made with additional EXSY information from gNOESY experiments. Assignments for natural Novo29, synthetic Novo29, and *epi*-Novo29 were made with additional information from gTOCSY and gNOESY experiments. Analytical reverse-phase HPLC was performed on Agilent 1260 Infinity II instrument equipped with a Phenomenex bioZen PEPTIDE 2.6 μ m XB-C18 column (150x4.6 mm), eluting with a gradient of acetonitrile and water (each containing 0.1% TFA) from 5-100% over 20 minutes. Peptides were purified on a Biotage Isolera One flash column chromatography instrument with a Biotage® SfarBio C18 D – Duo 300 Å 20 μ m 10 g column. *epi*-Novo29 was then further purified by preparative reverse-phase HPLC on a Rainin Dynamax equipped with an Agilent Zorbax 250x 21.2 mm SB-C18 column. Both peptides were prepared and used as the trifluoroacetate (TFA) salts and were assumed to have one trifluoroacetic acid molecule per amine group on each peptide (two TFA molecules per peptide). Natural Novo29 was provided by NovoBiotic Pharmaceuticals LLC as the trifluoroacetate (TFA) salt. HRMS measurements were performed on a Waters LCT Premier with a TOF analyzer.

Chemical synthesis of Fmoc-(2*R*,3*R*)-hydroxyAsn-OH.¹⁻⁵



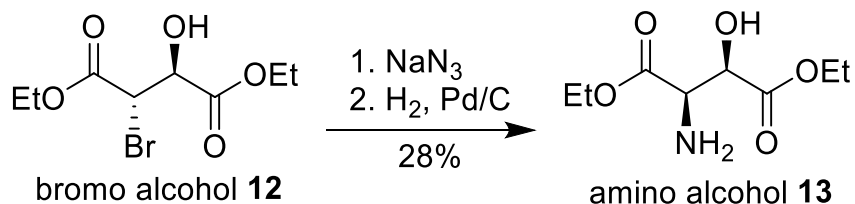
Bromo alcohol 12. A 500-mL, single-necked, round-bottom flask equipped with a magnetic stirring bar and a condenser fitted with a nitrogen inlet adapter was charged with a solution of (+)-diethyl L-tartrate (8.56 mL, 50.00 mmol, 1.0 equiv.) in 250 mL of CH_2Cl_2 . (The

reaction was run at ca. 0.2 M concentration of the diethyl L-tartrate.) To the solution, SOCl_2 (7.25 mL, 100.00 mmol, 2.0 equiv.) was added in drops over ca. 5 minutes, followed by anhydrous DMF as a catalyst (0.25 mL, 3.20 mmol, 6 mol %) The reaction mixture was heated to 35 °C and stirred for 2 hours. Then, the solution was allowed to cool to room temperature, and concentrated to dryness by rotary evaporation to afford a cyclic sulfite intermediate as a yellow oil (12.61 g, 99% yield of the unpurified product). The cyclic sulfite was used without further purification.

The cyclic sulfite intermediate (12.61 g, 50.00 mmol, 1.0 equiv.) was dissolved in 250 mL CH_2Cl_2 , 125 mL CH_3CN , and 62.5 mL H_2O , and the mixture was transferred to a 500-mL, single-necked, round-bottom flask equipped with a magnetic stirring bar and a nitrogen inlet adapter. $\text{RuCl}_3 \cdot 3\text{H}_2\text{O}$ (0.327 g, 1.25 mmol, 2.5 mol %) was dissolved in 62.5 mL H_2O and added, followed by NaIO_4 (21.39 g, 100 mmol, 2 equiv.). The reaction mixture was stirred at 25 °C for 16 hours under N_2 , and then diluted with 500 mL of Et_2O and 100 mL of H_2O . The organic layer was washed with 400 mL of saturated aqueous NaHCO_3 , followed by 400 mL of saturated aqueous NaCl . The organic layer was concentrated to dryness by rotary evaporation to afford a cyclic sulfate intermediate as a yellow oil (12.39 g, 92 % yield of the unpurified product). The cyclic sulfate intermediate was used without further purification.

A 500-mL, three-necked, round-bottom flask equipped with a magnetic stirring bar and fitted with a nitrogen inlet adapter and two rubber septa was charged with LiBr (12.04 g, 138.60 mmol, 3 equiv.). The flask was placed under vacuum and heated to 120 °C in an oil bath for 1 hour to ensure LiBr was dry. The flask was then cooled to room temperature. The cyclic sulfate (12.39 g, 46.20 mmol, 1 equiv.) dissolved in 460 mL anhydrous THF was transferred to the flask with a capillary. (The reaction was run at ca. 0.1 M concentration of the cyclic sulfate.) The reaction mixture was stirred at 25 °C for 2 hours in a nitrogen atmosphere. The solution was concentrated

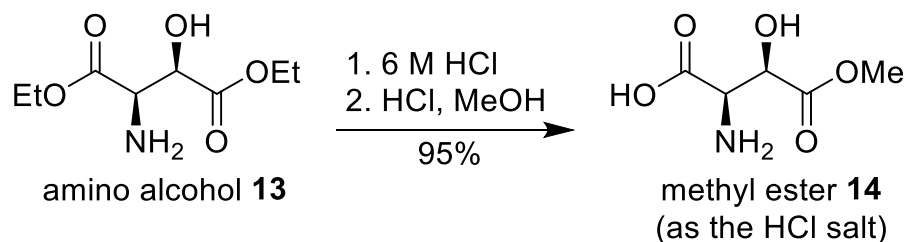
to dryness by rotary evaporation. The solution was dissolved in ca. 720 mL Et₂O and 480 mL aqueous 20% H₂SO₄. The solution was stirred for 18 hours at 25 °C. The organic and aqueous layers were separated, and the aqueous layer was extracted twice with 200 mL Et₂O and dried over Na₂SO₄. The solution was concentrated to dryness by rotary evaporation to afford bromo alcohol **12** as a yellow oil (12.43 g, 99 % yield of the unpurified product). Bromo alcohol **12** was generated as a mixture of diastereomers and used without further purification. ¹H NMR (500 MHz, CDCl₃): δ 4.81–4.65 (m, 2 H), 4.42–4.14 (m, 4 H), 1.40–1.23 (m, 6 H), 1.28 (q, *J* = 7.2 Hz, 1 H). [Note: Approximately 5 % (by integration) of an unknown impurity is present in this sample.] ¹³C{¹H} NMR (125.7 MHz, CDCl₃): δ 170.5, 166.8, 72.7, 71.4, 63.0, 59.9, 49.7, 47.9, 14.2. HRMS: *m/z*: [M + Na]⁺ calcd for C₈H₁₃BrO₅Na⁺ 290.9844, observed 290.9844.



Amino alcohol 13. A 250-mL, single-necked, round-bottom flask equipped with a magnetic stirring bar, a nitrogen inlet adapter, was charged with a solution of bromo alcohol **12** (12.43 g, 46.20 mmol, 1.0 equiv.) in 180 mL of anhydrous DMF. (The reaction was run at ca. 0.25 M concentration of the bromo alcohol **1**.) NaN₃ (9.01g, 138.60 mmol, 3 equiv.) was added to the solution, and the suspension was stirred for 21 h at 25 °C. The suspension was transferred to a separatory funnel and the round bottom flask was rinsed with 300 mL H₂O. The layers were separated, and the aqueous layer was extracted with EtOAc (3 x 200 mL). The combined organic layer was dried over Na₂SO₄, filtered, and dried using rotary evaporation to yield the azide

intermediate as a yellow oil (9.01 g, 84 % yield of the unpurified product). The azide intermediate was used without further purification.

A 500-mL, three-necked, round-bottom flask equipped with a magnetic stirring bar, a nitrogen inlet adapter, an inlet adapter fitted with a hydrogen balloon, and a rubber septum was charged with a solution of the crude azide intermediate (9.01 g, 38.97 mmol, 1.0 equiv.) in 100 mL of CH₃OH. (The reaction was run at 0.3 M concentration of the azide intermediate.) The flask was evacuated and back filled with nitrogen, and 10 % Pd/C (50% wet solid, 4.51 g, one half the mass of the azide intermediate) was added. A balloon containing H₂ gas was fitted to an inlet adapter and the system was evacuated and back filled with H₂ gas. The resulting suspension was stirred for 6 h, filtered through Celite, and washed with 200 mL of additional CH₃OH. The resulting solution was concentrated by rotary evaporation to and purified by column chromatography on silica gel (elution with 5:95 CH₃OH:CH₂Cl₂) to afford amino alcohol **13** as a yellow oil (2.69 g, 33 % yield). ¹H NMR (500 MHz, CDCl₃): δ 4.48 (d, *J* = 2.7 Hz, 1 H), 4.22–4.05 (m, 4 H), δ 3.75 (d, *J* = 2.8 Hz, 1 H) 2.53 (broad s, 3 H), 1.18 (q, *J* = 7.3 Hz, 6 H). [Note: Approximately 6 % (by integration) of an unknown impurity is present in this sample.] ¹³C {¹H} NMR (125.7 MHz, CDCl₃): δ 172.6, 172.4, 72.0, 61.8, 61.4, 56.7, 13.96, 13.94. HRMS: *m/z*: [M + Na]⁺ calcd for C₈H₁₅NO₅Na⁺ 228.0848, observed 228.0843.

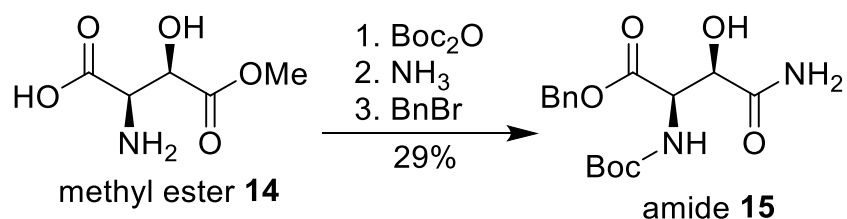


Methyl ester 14. A 250-mL, single-necked, round-bottom flask equipped with a magnetic stirring bar and a condenser fitted with a nitrogen inlet adapter was charged with a solution of amino alcohol **13** (2.69 g, 13.11 mmol, 1.0 equiv.) in 65 ml of 6 M HCl. (The reaction was run at ca. 0.2 M concentration of the amino alcohol **13**.) The mixture was heated in an oil bath and stirred for 16 h at 100 °C, cooled to room temperature, and concentrated to dryness by rotary evaporation to afford a beige solid (2.59 g, 99 % yield of the unpurified product). The crude carboxylic acid intermediate was used in the next step without purification.

A 250-mL, single-necked, round-bottom flask equipped with a magnetic stirring bar and a condenser fitted with a nitrogen inlet adapter was charged with a solution of the crude carboxylic acid intermediate (2.45 g, 13.11 mmol, 1.0 equiv.) in 65 mL of CH₃OH. (The reaction was run at ca. 0.2 M concentration of the crude intermediate.) The mixture was cooled to 0 °C using an ice bath. A solution of 12 M HCl (2.0 mL) was then added dropwise to the flask over a few minutes. The flask was then heated in a preheated water bath at 65 °C for 30 minutes. The mixture was let to cool to room temperature and concentrated to dryness by rotary evaporation to afford methyl ester **14** as a beige foam (2.59 g, 96 % yield of the unpurified product). Methyl ester **3** was used without further purification. ¹H NMR (500 MHz, CD₃OD): δ 4.65 (d, *J* = 3.0 Hz, 1 H), 4.16 (d, *J* = 3.2, 1 H), 3.71 (s, 3 H). ¹³C{¹H} NMR (125.7 MHz, CD₃OD) (major product, methyl ester **3**): δ 171.0, 168.8, 69.2, 55.2, 52.9; (minor impurity; diacid precursor impurity and dimethyl ester,

partial data): δ 170.6, 167.9, 69.1, 55.3, 52.9. HRMS: m/z : $[M + Na]^+$ calcd for $C_5H_9NO_5Na^+$ 164.0559, observed 164.0556.

NOTE: We have found that timing is essential to the selective formation of the monomethyl ester (methyl ester **14**) from the corresponding diacid precursor. When we ran this reaction for two hours at 65 °C we observed the predominant formation of the undesired the dimethyl ester product. When we ran this reaction for 15 minutes at 65 °C we observed ca. 50% conversion to the desired methyl ester **14**, with ca. 44% diacid precursor remaining, and ca. 6% of the dimethyl ester. When we ran this reaction for 30 minutes at 65 °C we observed mostly the desired methyl ester **14** (ca. 83%), with some remaining diacid precursor (ca. 12%), and some dimethyl ester (ca. 5%).



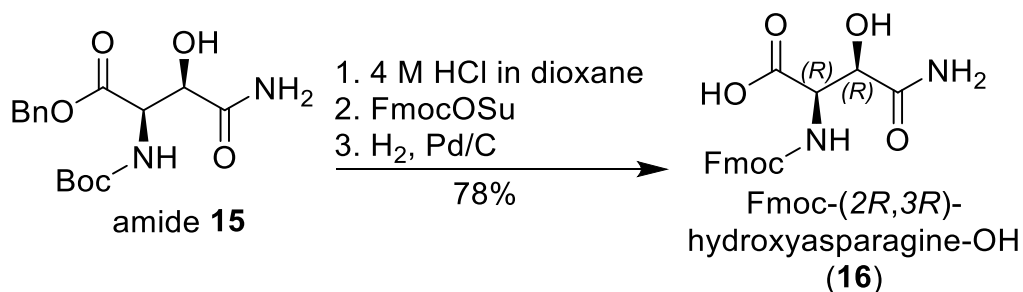
Amide 15. A 250-mL, single-necked, round-bottom flask equipped with a magnetic stirring bar and fitted with a nitrogen inlet adapter was charged with a solution of methyl ester **14** (containing the diacid precursor and dimethyl ester impurities) (2.59 g, 13.03 mmol, 1.0 equiv.) in 65 mL of 10 % w/v Na_2CO_3 . The solution was cooled to 0 °C using an ice bath. While on ice, a separate solution of Boc_2O (8.53 g, 39.09 mmol, 3.0 equiv.) dissolved in 65 mL dioxane was added dropwise over 2–3 minutes. (The reaction was run at ca. 0.15 M concentration of the methyl ester **14**.) The mixture was brought to room temperature, stirred for 20 h, and concentrated to dryness using rotary evaporation. The resulting residue was dissolved in 250 mL EtOAc and transferred to a separatory funnel. The mixture was washed with 1 M HCl (3 x 250 mL). The organic layer was dried over Na_2SO_4 and concentrated to a yellow oil. The crude product was purified by column

chromatography on silica gel (elution with 10:90 CH₃OH:CHCl₃) to afford the Boc-protected intermediate as an oil (1.43 g, 42% yield).

A 125-mL, single-necked, high-pressure flask equipped with a magnetic stirring bar was charged with a solution of the Boc-protected intermediate (1.43 g, 5.43 mmol, 1.0 equiv.) in ca. 18 mL CH₃OH. (The reaction was run at ca. 0.3 M concentration of the Boc-protected intermediate.) A flow of NH₃ gas was applied through a syringe directly into the solution and bubbled for 20–30 min to ensure saturation with NH₃. The vessel was then capped, and the solution was stirred for 72 h at 25 °C. The solution was concentrated to dryness using rotary evaporation to afford the amide intermediate as a beige solid (1.21 g, 94% yield of the unpurified product). The crude intermediate was used in the next step without further purification.

A 100-mL, single-necked, round-bottom flask equipped with a magnetic stirring bar and fitted with a nitrogen inlet adapter was charged with a solution of the amide intermediate (1.21 g, 11.9 mmol, 1.0 equiv.) in ca. 25 mL of anhydrous DMF. (The reaction was run at ca. 0.2 M concentration of the amide intermediate.) The solution was cooled to 0 °C using an ice bath, and NaHCO₃ (1.07 g, 12.70 mmol, 2.5 equiv.) followed by benzyl bromide (2.42 mL, 20.4 mmol, 4.0 equiv.) was added dropwise over 10 minutes. The mixture was stirred for 2 hours at 0 °C, warmed to room temperature, and stirred for an additional 24 hours under N₂. The resulting solution was cooled again to 0 °C using an ice bath, 75 mL of H₂O was added to quench the reaction. The solution was transferred to a separatory funnel and extracted with EtOAc (3 x 50 mL). The combined organic layer was washed with 50 mL saturated aqueous NaCl, dried with Na₂SO₄, and concentrated to using rotary evaporation. The crude product was then purified by column chromatography on silica gel (elution with 5:95 CH₃OH:CH₃Cl) to afford amide **15** as white solid

(1.27 g, 73% yield). ^1H NMR (500 MHz, CDCl_3): δ 7.31–7.36 (m, 5 H), 6.85 (br s, 1 H), 6.04 (br s, 1 H), 5.62 (d, $J = 9.1$ Hz, 1 H), 5.19 (s, 2 H), 5.17–5.30 (m, 2 H), 4.75 (br d, $J = 9.1$ Hz, 1 H), 4.61 (br s, 1 H), 1.39 (s, 9 H). [Note: Approximately 10 % (by integration) of an unknown impurity is present in this sample.] $^{13}\text{C}\{^1\text{H}\}$ NMR (125.7 MHz, CDCl_3): δ 173.7, 172.1, 170.2, 156.6, 135.1, 128.7, 128.5, 128.3, 81.6, 80.9, 74.8, 72.2, 68.1, 67.7, 56.4, 28.2. HRMS: m/z : $[\text{M} + \text{Na}]^+$ calcd for $\text{C}_{16}\text{H}_{22}\text{N}_2\text{O}_6\text{Na}^+$ 361.1375, observed 361.1371.



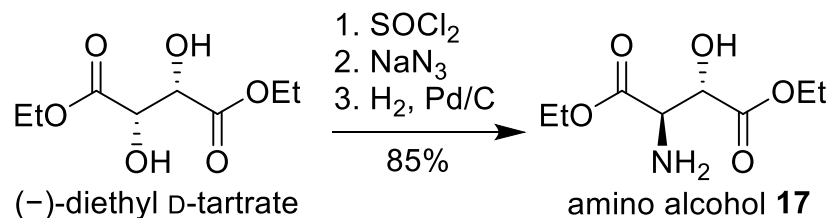
Fmoc-(2*R*,3*R*)-hydroxyasparagine-OH (16). A 250-mL, single-necked, round-bottom flask equipped with a magnetic stirring bar and fitted with a nitrogen inlet adapter was charged with a solution of amide **15** (1.27 g, 3.70 mmol, 1.0 equiv.) in ca. 40 mL of 4 N HCl in dioxane. (The reaction was run at ca. 0.1 M concentration of the amide **15**.) The solution was stirred for 2 hours at 25 °C and concentrated to dryness by rotary evaporation, to afford the amine intermediate as a pale-yellow solid (0.96 g, 95% yield of the unpurified product). The crude intermediate was used in the next step without further purification.

The crude amine intermediate (0.96 g, 3.50 mmol, 1.0 equiv.) was dissolved in 52 mL of 1:1 dioxane:water. (The reaction was run at ca. 0.06 M concentration of the crude amine intermediate.) The solution was cooled to 0 °C using an ice bath, and NaHCO_3 was added until the solution reached a pH of 6.8. Fmoc-OSu (1.42 g, 4.20 mmol, 1.2 equiv.) was then added, and the reaction mixture was stirred for 1 h on ice, warmed to room temperature, and stirred for an additional 20 hours under N_2 . The resulting suspension was diluted with 120 mL EtOAc and 180

mL of saturated NaHCO₃ and stirred for ca. 5 min at 25 °C. The solution was transferred to a separatory funnel and the organic layer was collected; the aqueous layer was then extracted with EtOAc (2 x 80 mL). The combined organic layer was then dried with Na₂SO₄ and concentrated to by rotary evaporation to a white solid (1.61 g, 99% yield). A sample of the crude product was then purified by column chromatography on silica gel (elution with 5:95 CH₃OH:CH₃Cl) to afford the Fmoc-protected intermediate as a white solid that was used in the subsequent reaction.

A 250-mL, three-necked, round-bottom flask equipped with a magnetic stirring bar, a nitrogen inlet adapter, an inlet adapter fitted with a hydrogen balloon, and a rubber septum was charged with a solution of the Fmoc-protected intermediate (0.21 g, 0.46 mmol, 1 equiv.) from the previous step in ca. 5 mL of CH₃OH. (The reaction was run at 0.05 M concentration of the Fmoc-protected intermediate.) The flask was evacuated and back filled with nitrogen, and 10 % Pd/C (50% wet solid, 0.07 g, one half the mass of Fmoc-protected intermediate) was added. A balloon containing H₂ gas was fitted to an inlet adapter and the system was evacuated and back filled with H₂ gas. The resulting suspension was stirred for 15 minutes, filtered through Celite, and washed with additional CH₃OH. The resulting solution was concentrated by rotary evaporation to afford Fmoc-(2*R*,3*R*)-hydroxyasparagine-OH as an off-white solid (0.14 g, 83% yield of the unpurified product). ¹H NMR (500 MHz, CD₃SOCD₃): δ 7.89 (d, *J* = 7.7 Hz, 2 H), 7.73 (t, *J* = 8.9 Hz, 2 H), 7.47–7.26 (m, 7 H), 6.97 (br s, 1 H), 4.43 (d, *J* = 8.9 Hz, 1 H), 4.37 (s, 1 H), 4.29–4.17 (m, 3 H); (minor rotamer, ca. 15%, partial data): δ 7.64 (d, *J* = 6.8 Hz, Fmoc aromatic CH), 6.39 (d, *J* = 8.1 Hz, carbamate NH), 4.59 (d, *J* = 8.3 Hz, hydroxyAsn CH), 4.41 (s, hydroxyAsn CH), 4.19–4.06 (m, hydroxyAsn CH). ¹³C{¹H} NMR (125.7 MHz, CD₃SOCD₃): δ 173.2, 171.9, 156.1, 143.8, 143.7, 140.7, 127.7, 127.2, 127.1, 125.4, 125.4, 120.1, 71.4, 65.9, 56.9, 46.5. HRMS: *m/z*: [M + Na]⁺ calcd for C₁₉H₁₈N₂O₆Na⁺ 393.1063, observed 393.1060.

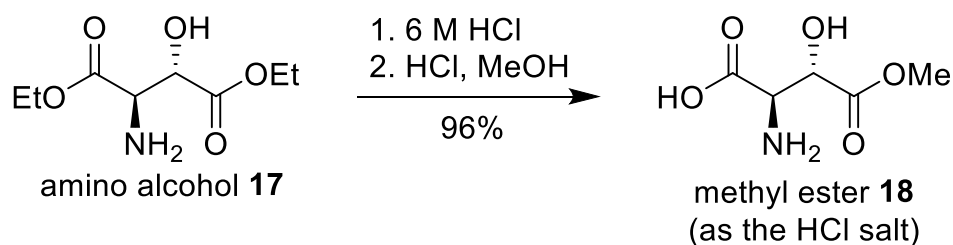
Chemical synthesis of Fmoc-(2*R*,3*S*)-hydroxyAsn.



Amino alcohol 17. A 500-mL, single-necked, round-bottom flask equipped with a magnetic stirring bar and a condenser fitted with a nitrogen inlet adapter was charged with a solution of (-)-diethyl-D-tartrate (8.56 mL, 50.00 mmol, 1.0 equiv.) in 250 mL of CH₂Cl₂ (the reaction was run at ca. 0.2 M concentration of the diethyl-D-tartrate). To the solution, SOCl₂ (7.25 mL, 100.00 mmol, 2.0 equiv.) was added dropwise, followed by 0.25 mL cat. anhydrous DMF. The reaction mixture was heated to 35 °C and stirred for 2 hours. Then, the solution was cooled to room temperature, and concentrated to dryness by rotary evaporation to afford a cyclic sulfite intermediate as a yellow oil (12.41 g, 98% yield of the unpurified product). The cyclic sulfite was used without further purification.

A 250-mL, single-necked, round-bottom flask equipped with a magnetic stirring bar, a nitrogen inlet adapter, was charged with a solution of the cyclic sulfite intermediate (12.41 g, 49.20 mmol, 1.0 equiv.) in 100 mL of anhydrous DMF (the reaction was run at 0.5 M concentration of the bromo alcohol **1**). NaN₃ (3.99 g, 61.50 mmol, 1.25 equiv.) was added to the solution, and the suspension was stirred for 21 h at 25 °C. The suspension was transferred to a separatory funnel and the round bottom flask was rinsed with 300 mL H₂O. The layers were separated and the aqueous layer was extracted with EtOAc (3 x 200 mL). The combined organic layer was dried over Na₂SO₄, filtered, and dried using rotary evaporation to yield the azide intermediate as a yellow oil (9.96 g, 88% yield of the unpurified product). The azide intermediate was used without further purification.

A 500-mL, three-necked, round-bottom flask equipped with a magnetic stirring bar, a nitrogen inlet adapter, an inlet adapter fitted with a hydrogen balloon, and a rubber septum was charged with a solution of the crude azide intermediate (9.96 g, 43.10 mmol, 1.0 equiv.) in 140 mL of CH₃OH (the reaction was run at 0.2 M concentration of the azide intermediate). The flask was evacuated and back filled with nitrogen, and 10 % Pd/C (50% wet solid, 4.98 g, one half the mass of the azide intermediate) was added. A balloon containing H₂ gas was fitted to an inlet adapter and the system was evacuated and back filled with H₂ gas. The resulting suspension was stirred for 6 h, filtered through Celite, and washed with 200 mL of additional CH₃OH. The resulting solution was concentrated by rotary evaporation to afford amino alcohol **17** as a yellow oil (8.84 g, 99% yield of the unpurified product). Amino alcohol **17** was used without further purification. An analytical sample was purified by column chromatography on silica gel (elution with 5:95 CH₃OH:CH₂Cl₂) for analysis. ¹H NMR (500 MHz, CDCl₃): δ 4.34 (d, *J* = 3.3 Hz, 1 H), 4.10–3.95 (m, 4 H), 3.75 (d, *J* = 3.3 Hz, 1 H) 3.75 (broad s, 3 H), 1.18 (m, 6 H). ¹³C {¹H} NMR (125.7 MHz, CDCl₃): δ 171.86, 171.82, 72.8, 61.5, 61.2, 57.5, 13.95, 13.94. HRMS: *m/z*: [M + Na]⁺ calcd for C₈H₁₅NO₅Na⁺ 228.0848, observed 228.0843.



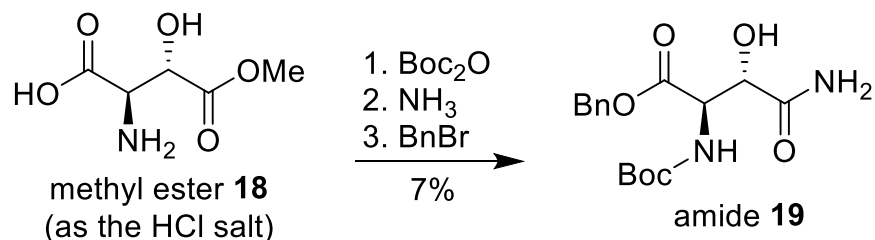
Methyl ester 18. A 250-mL, single-necked, round-bottom flask equipped with a magnetic stirring bar and a condenser fitted with a nitrogen inlet adapter was charged with a solution of amino alcohol **17** (8.84 g, 43.10 mmol, 1.0 equiv.) in 200 mL of 6 M HCl (the reaction was run at

ca. 0.2 M concentration of the amino alcohol **17**). The mixture was heated in an oil bath and stirred for 16 h at 100 °C, cooled to room temperature, and concentrated to dryness by rotary evaporation to afford a beige solid (7.99 g, 98% yield of the unpurified product). The crude carboxylic acid intermediate was used in the next step without purification.

A 250-mL, single-necked, round-bottom flask equipped with a magnetic stirring bar and a condenser fitted with a nitrogen inlet adapter was charged with a solution of the crude carboxylic acid intermediate (7.99, 43.10 mmol, 1.0 equiv.) in 240 mL of CH₃OH (the reaction was run at ca. 0.2 M concentration of the crude intermediate). The mixture was cooled to 0 °C using an ice bath. A solution of 12 M HCl (8 mL) was then added dropwise to the flask over 10 minutes. The flask was then heated in a preheated water bath at 65 °C for 15 minutes. The mixture was cooled to room temperature and concentrated to dryness by rotary evaporation to afford methyl ester **6** as a beige foam (8.60 g, 98% yield of the unpurified product). Methyl ester **6** was used without further purification. ¹H NMR (500 MHz, CD₃OD): (major product, methyl ester **18**, ca. 50% by integration): δ 8.65 (br s, 1 H), 4.67 (d, *J* = 2.6 Hz, 1 H), 4.46 (d, *J* = 2.6, 1 H), 3.80 (s, 3 H); (diacid precursor impurity, ca. 44% by integration): δ 4.61 (d, *J* = 2.5 Hz, 1 H), 4.45 (d, *J* = 2.5 Hz, 1 H). ¹³C{¹H} NMR (125.7 MHz, CD₃OD) (major product, methyl ester **18**): δ 170.5, 166.9, 69.9, 55.3, 51.8; (diacid precursor impurity): δ 171.5, 167.1, 68.8, 55.4. HRMS: *m/z*: [M + H]⁺ calcd for C₅H₉NO₅H⁺ 164.0559, observed 164.0558.

NOTE: Running the reaction for 15 minutes minimizes the formation of the dimethyl ester while still allowing a satisfactory yield of the desired monomethyl ester. Under these conditions, there is still a significant amount of the residual diacid precursor, which is observed in the ¹H NMR and ¹³C NMR spectra of the unpurified product. Based on our observation for the preparation

monomethyl ester **14** (above) we anticipate that 30 minutes of heating time would lead to a better yield of the desired methyl ester **18**.

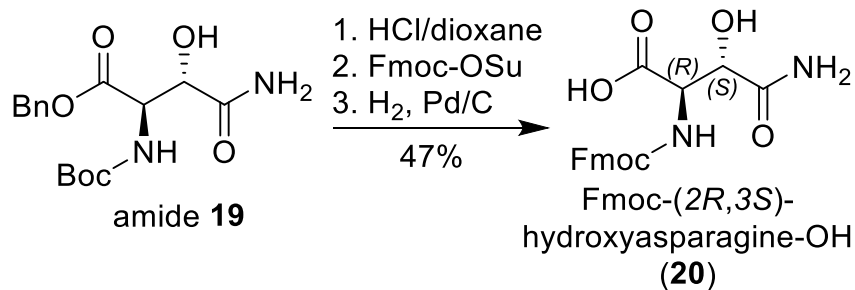


Amide 19. A 250-mL, single-necked, round-bottom flask equipped with a magnetic stirring bar and fitted with a nitrogen inlet adapter was charged with a solution of methyl ester **18** and the diacid precursor impurity (8.60 g, 43.10 mmol, 1.0 equiv.) in 140 mL of 10 % w/v Na_2CO_3 . The solution was cooled to 0 °C using an ice bath. While on ice, a separate solution of Boc_2O (7.51 g, 34.62 mmol, 3.0 equiv.) dissolved in 140 mL dioxane (to give a final concentration of 0.15 M for the methyl ester **18**) was slowly added over 2–3 minutes. The mixture was brought to room temperature, stirred for 19.5 h, and concentrated to dryness using rotary evaporation. The resulting residue was dissolved in 500 mL EtOAc and transferred to a separatory funnel. The mixture was washed with 1 M HCl (3 x 500 mL). The organic layer was dried over Na_2SO_4 and concentrated to a yellow oil. The crude product was purified by column chromatography on silica gel (elution with 10:90 $\text{CH}_3\text{OH}:\text{CHCl}_3$) to afford the Boc-protected intermediate as a yellow oil (1.65 g, 15% yield).

A 125-mL, single-necked, high-pressure flask equipped with a magnetic stirring bar was charged with a solution of the Boc-protected intermediate (1.65 g, 6.27 mmol, 1.0 equiv.) in ca. 20 mL CH_3OH (the reaction was run at ca. 0.3 M concentration of the Boc-protected intermediate). A flow of NH_3 gas was applied through a syringe directly into the solution and bubbled for 20–30 min to ensure saturation with NH_3 . The vessel was then capped, and the solution was stirred for 72 h at 25 °C. The solution was concentrated to dryness using rotary evaporation to afford the

amide intermediate as a beige solid (1.46 g, 98% yield of the unpurified product). The crude intermediate was used in the next step without further purification.

A 100-mL, single-necked, round-bottom flask equipped with a magnetic stirring bar and fitted with a nitrogen inlet adapter was charged with a solution of the amide intermediate (1.46 g, 3.64 mmol, 1.0 equiv.) in ca. 31 mL of anhydrous DMF (the reaction was run at ca. 0.2 M concentration of the amide intermediate). The solution was cooled to 0 °C using an ice bath, and NaHCO₃ (0.76 g, 9.10 mmol, 2.5 equiv.) followed by benzyl bromide (1.73 mL, 14.56 mmol, 4.0 equiv.) was added dropwise over 10 minutes. The mixture was stirred for 2 hours at 0 °C, warmed to room temperature, and stirred for an additional 24 hours under N₂. The resulting solution was cooled again to 0 °C using an ice bath, 75 mL of H₂O was added to quench the reaction. The solution was transferred to a separatory funnel and extracted with EtOAc (3 x 50 mL). The combined organic layer was washed with 50 mL saturated aqueous NaCl, dried with Na₂SO₄, and concentrated to using rotary evaporation. The crude product was then purified by column chromatography on silica gel (elution with 5:95 CH₃OH:CH₃Cl) to afford amide **19** as white solid (1.00 g, 47% yield). ¹H NMR (500 MHz, CDCl₃): δ 7.42–7.31 (m, 5 H), 6.79 (broad s, 1 H), 5.82 (broad d, *J* = 4.8 Hz, 1 H), 5.62 (broad s, 1 H), 5.54 (broad d, *J* = 6.6 Hz, 1 H), 5.31–5.18 (m, 2 H), 4.72 (broad d, *J* = 5.1 Hz, 1 H), 4.65 (broad d, *J* = 4.5 Hz, 1 H), 1.45 (s, 9 H). ¹³C{¹H} NMR (125.7 MHz, CDCl₃): δ 173.6, 168.1, 158.2, 135.1, 128.7, 128.7, 128.6, 81.7, 75.0, 68.2, 57.5, 28.3. HRMS: *m/z*: [M + Na]⁺ calcd for C₁₆H₂₂N₂O₆Na⁺ 361.1375, observed 361.1371.



Fmoc-(2*R*,3*S*)-hydroxyasparagine-OH (20). A 250-mL, single-necked, round-bottom flask equipped with a magnetic stirring bar and fitted with a nitrogen inlet adapter was charged with a solution of the amide **7** (1.00 g, 2.96 mmol, 1.0 equiv.) in ca. 30 mL of 4 N HCl in dioxane. (The reaction was run at ca. 0.1 M concentration of the amide **7**.) The solution was stirred for 2 h and concentrated to dryness by rotary evaporation to a white solid (0.71 g, 99% yield of the unpurified product).

The crude intermediate (0.71 g, 2.98 mmol, 1 equiv.) was dissolved in 52 mL of 1:1 dioxane:water. (The reaction was run at ca. 0.06 M concentration of the crude intermediate). The solution was cooled to 0 °C using an ice bath, and NaHCO₃ was added until the solution reached a pH of 6.8. Fmoc-OSu (1.20 g, 3.55 mmol, 1.2 equiv.) was then subsequently added, and mixture was stirred for 1 h on ice, brought to room temperature, and stirred for an additional 18–20 h under N₂. The resulting suspension was diluted with 120 mL EtOAc and 180 mL of saturated NaHCO₃ and stirred for ca. 5 min. The solution was transferred to a separatory funnel and the organic layer was collected; the aqueous layer was then extracted with EtOAc (2 x 80 mL). The combined organic layer was then dried with Na₂SO₄ and concentrated by rotary evaporation to a white solid. The crude product was then purified by column chromatography on silica gel (elution with 5:95 CH₃OH:CH₂Cl) to afford the Fmoc-protected intermediate as a white solid (1.07 g, 79% yield).

A 250-mL, three-necked, round-bottom flask equipped with a magnetic stirring bar, a nitrogen inlet adapter, an inlet adapter fitted with a hydrogen balloon, and a rubber septum was

charged with a solution of the Fmoc-protected intermediate (1.07 g, 2.32 mmol, 1 equiv.) from the previous step in ca. 55 mL of anhydrous CH₃OH. (The reaction was run at 0.05 M concentration of the Fmoc-protected intermediate assuming 100 % conversion). The flask was evacuated and back filled with nitrogen, and ca. 10 % Pd/C (50% wet solid, one half the mass of the Fmoc-protected intermediate, 0.5 g) was added. A balloon containing H₂ gas was fitted to an inlet adapter and the system was evacuated and back filled with H₂ gas. The resulting suspension was stirred for 24 h, filtered through Celite, and washed with additional CH₃OH. The resulting solution was concentrated by rotary evaporation to afford Fmoc-(2*R*,3*S*)-hydroxyasparagine-OH as an off-white solid (0.51 g, 60% yield of the unpurified product). ¹H NMR (500 MHz, CD₃SOCD₃): δ 7.89 (d, *J* = 7.5 Hz, 2 H), 7.77–7.69 (m, 2 H), 7.47–7.28 (m, 7 H), 7.03 (d, *J* = 9.5 Hz, 1 H), 4.47 (dd, *J* = 9.5, 2.1 Hz, 1 H), 4.37 (d, *J* = 2.0 Hz, 1 H), 4.26–4.19 (m, 3 H); (minor rotamer, ca. 16%, partial data): δ 7.63 (d, *J* = 7.2 Hz, Fmoc aromatic CH), 6.44 (d, *J* = 9.5 Hz, carbamate NH), 4.64 (d, *J* = 9.4 Hz, hydroxyAsn CH), 4.42 (s, hydroxyAsn CH), 4.14–4.04 (m, hydroxyAsn CH). ¹³C {¹H} NMR (125.7 MHz, CD₃SOCD₃): δ 173.2, 171.9, 156.1, 143.8, 143.7, 140.7, 127.7, 127.17, 127.13, 125.43, 125.36, 120.1, 71.4, 65.9, 56.9, 46.5. HRMS: *m/z*: [M + Na]⁺ calcd for C₁₉H₁₈N₂O₆Na⁺ 393.1063, observed 393.1073.

Synthesis of Novo29 and *epi*-Novo29 ⁶

Peptide synthesis procedure. Novo29 and *epi*-Novo29 were synthesized by manual solid-phase peptide synthesis of the corresponding linear peptide on 2-chlorotrityl resin, followed by on-resin esterification, solution-phase cyclization, deprotection, and purification. A step-by-step procedure is detailed below.

a. Loading the resin. 2-Chlorotrityl chloride resin (300 mg, 1.07 mmol/g) was added to a Bio-Rad Poly-Prep chromatography column (10 mL). Dry CH₂Cl₂ (8 mL) was used to suspend and swell the resin for 30 min with gentle rocking. After the solution was drained from the resin, a separate solution of Fmoc-Leu-OH (75 mg, 0.7 equiv., 0.21 mmol) in 6% (v/v) 2,4,6-collidine in dry CH₂Cl₂ (8 mL) was added and the suspension was gently rocked for 5–6 h. The solution was then drained, and a mixture of CH₂Cl₂/ CH₃OH /*N,N*-diisopropylethylamine (DIPEA) (17:2:1, 8 mL) was added immediately. The resin was gently rocked for 1 h, to cap the unreacted 2-chlorotrityl chloride resin sites. The resin was then washed three times with dry CH₂Cl₂ and dried by passing nitrogen through the vessel. This procedure typically yields 0.15–0.20 mmol of loaded resin, as assessed by spectrophotometric analysis.

b. Manual peptide coupling. The loaded resin was suspended in dry DMF and then transferred to a solid-phase peptide synthesis vessel. Residues 6 through 1 were manually coupled using Fmoc-protected amino acid building blocks. The coupling cycle consisted of *i.* Fmoc-deprotection with of 20% (v/v) piperidine in DMF (5 mL) for 5–10 min at room temperature, *ii.* washing with dry DMF (4 x 5 mL), *iii.* coupling of the amino acid (4 equiv.) with HCTU (4 equiv.) in 20% (v/v) 2,4,6-collidine in dry DMF (5 mL) for 20–30 min, and *iv.* washing with dry DMF (4 x 5 mL). The last amino acid coupling of the linear sequence is Boc-Phe-OH, which intentionally protects the *N*-terminus from being reactive during the esterification step and cyclization steps. The resin was then transferred to a clean Bio-Rad PolyPrep chromatography column.

c. Esterification. In a test tube, Fmoc-Leu-OH (10 equiv.) and diisopropylcarbodiimide (10 equiv.) were dissolved in dry CH₂Cl₂ (5 mL). The resulting solution was filtered through a 0.20- μ m nylon filter, and 4-dimethylaminopyridine (1 equiv.) was added to the filtrate. The resulting

solution was transferred to the resin and gently agitated for 1 h. The solution was then drained, and the resin was washed with dry CH₂Cl₂ (3 x 5 mL) and DMF (3 x 5 mL).

d. Fmoc deprotection of Leu₈. The Fmoc protecting group on Leu₈ was removed by adding 20% (v/v) piperidine in DMF for 30 min. The solution was drained, and the resin was washed with dry DMF (3 x 5 mL) and CH₂Cl₂ (3 x 5 mL).

e. Cleavage of the linear peptide from chlorotriyl resin. The linear peptide was cleaved from the resin by rocking the resin in a solution of 20% (v/v) 1,1,1,3,3,3-hexafluoroisopropanol (HFIP) in CH₂Cl₂ (8 mL) for 1 h. The suspension was filtered, and the filtrate was collected in a 250-mL round-bottomed flask. The resin was washed with additional cleavage solution (8 mL) for 30 min and filtered into the same 250 mL round bottom-bottomed flask. The combined filtrates were concentrated by rotary evaporation and further dried by vacuum pump to afford the crude protected linear peptide, which was cyclized without further purification.

d. Cyclization of the linear peptide. The crude protected linear peptide was dissolved in dry DMF (125 mL). HOAt (6 equiv.) and HATU (6 equiv.) were dissolved in 8 mL of dry DMF in a test tube to which 300 μL of diisopropylethylamine was added and the solution mixed until homogenous. The solution was then added to the round-bottom flask containing the dissolved peptide and the mixture was stirred under nitrogen at room temperature for 16–20 h. The reaction mixture was concentrated by rotary evaporation and further dried by vacuum pump to afford the crude protected cyclized peptide, which was immediately subjected to global deprotection.

e. Global deprotection of the cyclic peptide. The protected cyclic peptides were dissolved in TFA:triisopropylsilane (TIPS):H₂O (18:1:1, 10 mL) in a 1000-mL round-bottomed flask equipped with a stir bar. The solution was stirred for 1 h under nitrogen. During the 1 h deprotection, two 50-mL conical tubes containing 40 mL of dry Et₂O each were chilled on ice.

After the 1 h deprotection, the peptide solution was split between the two conical tubes of Et₂O. The tubes were then centrifuged at 600xg for 10 min, decanted, and washed with fresh Et₂O. This process of decanting and washing was repeated for two more times. The pelleted peptides were dried under nitrogen for 15–20 min. The deprotected cyclic peptide was then purified by reverse-phase HPLC (RP-HPLC).

f. Reverse-phase HPLC purification. The peptide was dissolved in 20% CH₃CN in H₂O (5 mL) and pre-purified on a Biotage Isolera One flash chromatography instrument equipped with a Biotage® Sfar Bio C18 D - Duo 300 Å 20 µm 25 g column. The solution of crude cyclic peptide was injected at 20% CH₃CN and eluted with a gradient of 20–50% CH₃CN. After this purification step Novo29 precipitated out of solution. The fractions containing the pure peptide were lyophilized. For *epi*-Novo29 the fractions containing the desired peptide were concentrated by rotary evaporation, diluted in 20% CH₃CN, injected on a Rainin Dynamax instrument, and eluted over a gradient of 20–40% CH₃CN over 90 min. The collected fractions were analyzed by analytical HPLC and MALDI-TOF, and the pure fractions were concentrated by rotary evaporation and lyophilized. These procedures typically yielded 5 mgs (~1 % yield) of synthetic peptides (Novo29 or *epi*-Novo29) as the TFA salts.

NMR spectroscopic studies of natural Novo29, synthetic Novo29, and *epi*-Novo29⁷

Sample Preparation. NMR spectroscopic studies of natural Novo29 and synthetic peptides were performed in DMSO-*d*₆. The solutions were prepared gravimetrically by dissolving a weighed portion of the peptide in the appropriate volume of solvent.

TOCSY and NOESY Data Collection. NMR spectra were recorded on a Bruker 600 MHz spectrometer with a Bruker CBBFO helium-cooled cryoprobe. TOCSY spectra were recorded with

2048 points in the f_2 dimension and either 512 increments in the f_1 dimension with NS = 8 and a 150-ms spin-lock mixing time. NOESY spectra were recorded with 2048 points in the f_2 dimension and 512 increments in the f_1 dimension with NS = 8 and a 200-ms mixing time.

TOCSY and NOESY Data Processing. NMR spectra were processed with Bruker TopSpin software. Automatic baseline correction was applied in both dimensions after phasing the spectra. 2D TOCSY and NOESY spectra were Fourier transformed to a final matrix size of 1024 x 1024 real points using a Qsine weighting function and forward linear prediction in the f_1 dimension.

MIC assays⁸

Preparing the peptide stocks. Solutions of natural Novo29, synthetic Novo29, and *epi*-Novo29 were prepared gravimetrically by dissolving an appropriate amount of peptide in an appropriate volume of sterile DMSO to make 1 mg/mL stock solutions. The stock solutions were stored at -20 °C for subsequent experiments.

Preparation and tray setup. *Bacillus subtilis* (ATCC 6051), *Staphylococcus epidermidis* (ATCC 14990), and *Escherichia coli* (ATCC 10798) were cultured from glycerol stocks in Mueller-Hinton broth overnight in a shaking incubator at 37 °C. An aliquot of the 1 mg/mL antibiotic stock solutions were diluted to make a 64 µg/mL solution with Mueller-Hinton broth. A 200-µL aliquot of the 64 µg/mL solution was transferred to a 96-well plate. Two-fold serial dilutions were made with media across a 96-well plate to achieve a final volume of 100 µL in each well. These solutions had the following concentrations: 64, 32, 16, 8, 4, 2, 1, 0.5, 0.25, 0.125, and 0.0625 µg/mL. The overnight cultures of each bacterium were diluted with Mueller-Hinton broth to an OD₆₀₀ of 0.075 as measured for 200 µL in a 96-well plate. The diluted mixture was further diluted to 1×10^6 CFU/mL with the appropriate media. A 100-µL aliquot of the 1×10^6 CFU/mL

bacterial solution was added to each well in 96-well plates, resulting in final bacteria concentrations of 5×10^5 CFU/mL in each well. As 100 μ L of bacteria were added to each well, natural Novo29, synthetic Novo29 and *epi*-Novo29 were also diluted to the following concentrations: 32, 16, 8, 4, 2, 1, 0.5, 0.25, 0.125, 0.0625, and 0.03125 μ g/mL. The plate was covered with a lid and incubated at 37 °C for 16 h. The optical density measurements were recorded at 600 nm and were measured using a 96-well UV/vis plate reader (MultiSkan GO, Thermo Scientific). The MIC values were taken as the lowest concentration that had no bacteria growth. Each MIC assay was run in triplicate in three independent runs to ensure reproducibility.

X-ray crystallography of *epi*-Novo29⁹

Crystallization of epi-Novo29. The hanging-drop vapor-diffusion method was used to determine initial crystallization conditions for *epi*-Novo29. Each peptide was screened in 96-well plate format using three crystallization kits (Crystal Screen, Index, and PEG/ION) from Hampton Research. A TTP LabTech Mosquito nanondisperse was used to make three 150 nL hanging drops for each well condition. The three hanging drops differed in the ratio of peptide to well solution for each condition in the 96-well plate. A 10 mg/mL solution of *epi*-Novo29 peptide in deionized water was combined with a well solution in ratios of 1:1, 1:2, and 2:1 peptide:well solution at appropriate volumes to create the three 150 nL hanging drops. Crystals of *epi*-Novo29 grew in well conditions of 2.8 M sodium acetate at pH 7.0.

Crystallization conditions for *epi*-Novo29 were optimized using a 4 x 6 matrix Hampton 24-well plate. For the *epi*-Novo29, the pH of the buffer was varied in each row (6.5, 6.6, 6.8, and 7.0). The concentration of sodium acetate in each column was varied in increments of 0.2 M (2.2, 2.4, 2.6, 2.8, 3.0, 3.2). Three hanging-drops were prepared on borosilicate glass slides by combining a 10 mg/mL solution of *epi*-Novo29 in deionized water with the well solution in the following

amounts: 1 μL :1 μL , 2 μL :1 μL , and 1 μL :2 μL . Slides were inverted and pressed firmly against the silicone grease surrounding each well. Crystals were harvested with a nylon loop attached to a copper or steel pin, and flash frozen in liquid nitrogen prior to data collection. A single crystal was soaked in a mixture of potassium iodide (KI) and well solution to incorporate iodide heavy atoms into the lattice. A higher resolution data set was subsequently collected from crystals grown in similar conditions and collected on a synchrotron X-ray source. The final optimized crystallization condition for *epi*-Novo29 is summarized in Tables S2 and S3.

Data collection, data processing, and structure determination. X-ray diffraction data from a single *epi*-Novo29 crystal soaked in a mixture of well solution and potassium iodide were collected using a Rigaku Micromax-007HF X-ray diffractometer with a rotating copper anode and a HyPix-6000HE Hybrid Photon Counting (HPC) X-ray detector. X-ray diffraction data were also collected from a single *epi*-Novo29 crystal using a synchrotron X-ray source (Advanced Light Source beamline 5.0.2) and a Pilatus3 6M 25 Hz detector. The dataset was indexed and integrated with XDS and scaled and merged with pointless and aimless. The crystallographic phase determination was done with Phaser. The structure was refined using phenix.refine, with manipulation of the model performed using Coot. Data collection and refinement statistics are shown Tables S2 and S3.

References

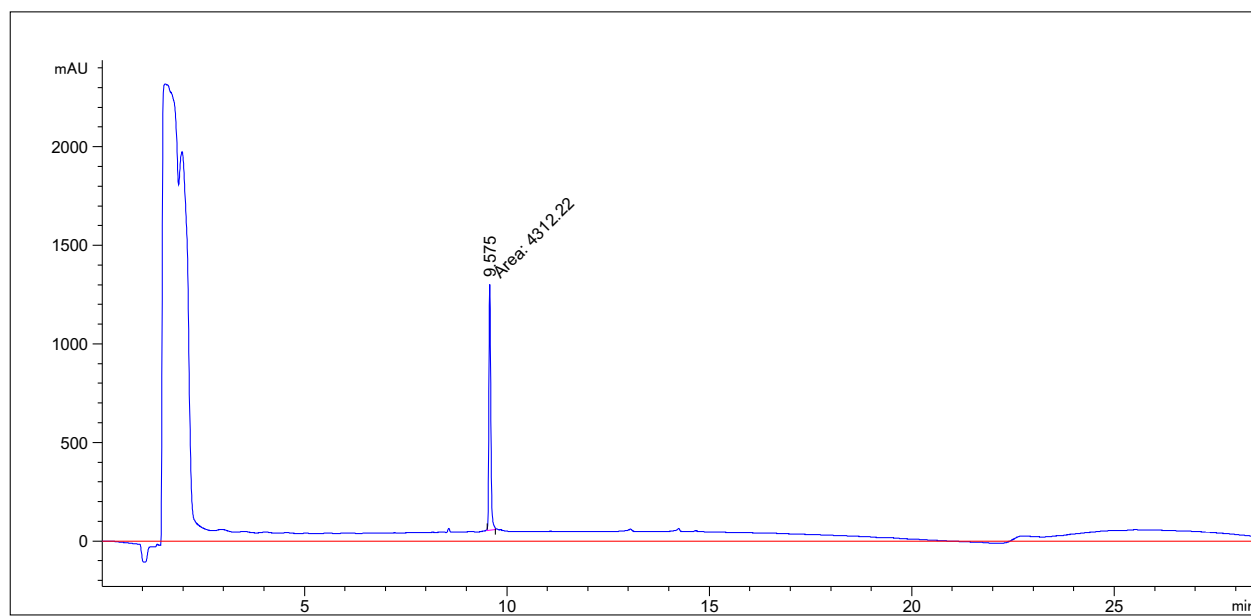
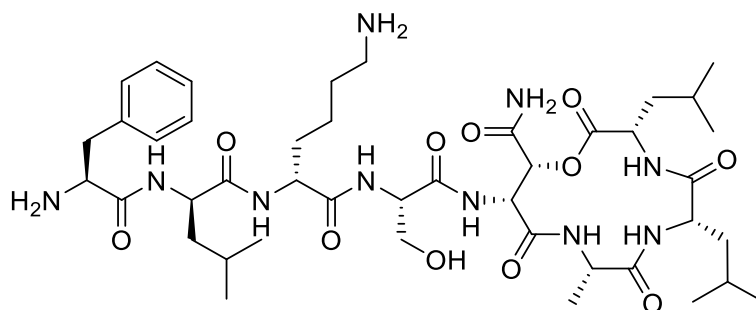
1. Gao, B.; Sharpless, K. B. Vicinal diol cyclic sulfates. Like epoxides only more reactive. *J. Am. Chem. Soc.* **1988**, *110*, 7538–7539.
2. He, L.; Byun, H.S.; Bittman, R. Efficient synthesis of chiral α,β -epoxyesters via a cyclic sulfate intermediate. *Tetrahedron Lett.* **1998**, *39*, 2071–2074.
3. France, B.; Bruno, V.; Nicolas, I. Synthesis of a protected derivative of (2R,3R)- β -hydroxyaspartic acid suitable for Fmoc-based solid phase synthesis. *Tetrahedron Lett.* **2013**, *54*, 158–161.
4. Guzmán-Martinez; A.; Vannieuwenhze, M. S. An Operationally Simple and Efficient Synthesis of Orthogonally Protected L-threo-beta-Hydroxyasparagine. *Synlett* **2007**, *10*, 1513–1516.
5. Liu, L.; Wang, B.; Bi, C.; He, G.; Chen, G. Efficient preparation of β -hydroxy aspartic acid and its derivatives. *Chin. Chem. Lett.* **2018**, *29*, 1113–1115.
6. The procedure for peptide synthesis follow closely to those that our laboratory has previously published. The procedures in this section were either adapted from or taken verbatim from: Yang, H.; Du Bois, D. R.; Ziller, J. W.; Nowick, J. S. X-ray crystallographic structure of a teixobactin analogue reveals key interactions of the teixobactin pharmacophore. *Chem. Commun.* **2017**, *53*, 2772–2775.
7. General procedures for NMR spectroscopy were either adapted from or taken verbatim from: Li, X.; Rios, S. E.; Nowick, J. S. Enantiomeric β -sheet peptides from A β form homochiral pleated β -sheets rather than heterochiral rippled β -sheets. *Chem. Sci.* **2022**, *13*, 7739–7746.
8. General procedures for minimum inhibitory concentration assays were either adapted from or taken verbatim from: Morris, M. A.; Malek, M.; Hashemian, M. H.; Nguyen, B. T.; Manuse, S.; Lewis, K. L.; Nowick, J. S. A Fluorescent Teixobactin Analogue. *ACS Chem. Biol.* **2020**, *15*,

1222–1231.

9. General procedures for X-ray crystallography were either adapted from or taken verbatim from: Li, X.; Sabol, A. L.; Wierzbicki, M.; Salveson, P. J.; Nowick, J. S. An improved turn structure for inducing β -hairpin formation in peptides. *Angew. Chem. Int. Ed.* **2021**, *60*, 22776–22782 and Samdin, T. D.; Wierzbicki, M.; Kreutzer, A. G.; Howitz, W. J.; Valenzuela, M.; Smith, A.; Sahrai, V.; Truex, N. L.; Klun, M.; Nowick, J. S. Effects of N-terminal residues on the assembly of constrained β -hairpin peptides derived from A β . *J. Am. Chem. Soc.* **2020**, *142*, 11593–11601.

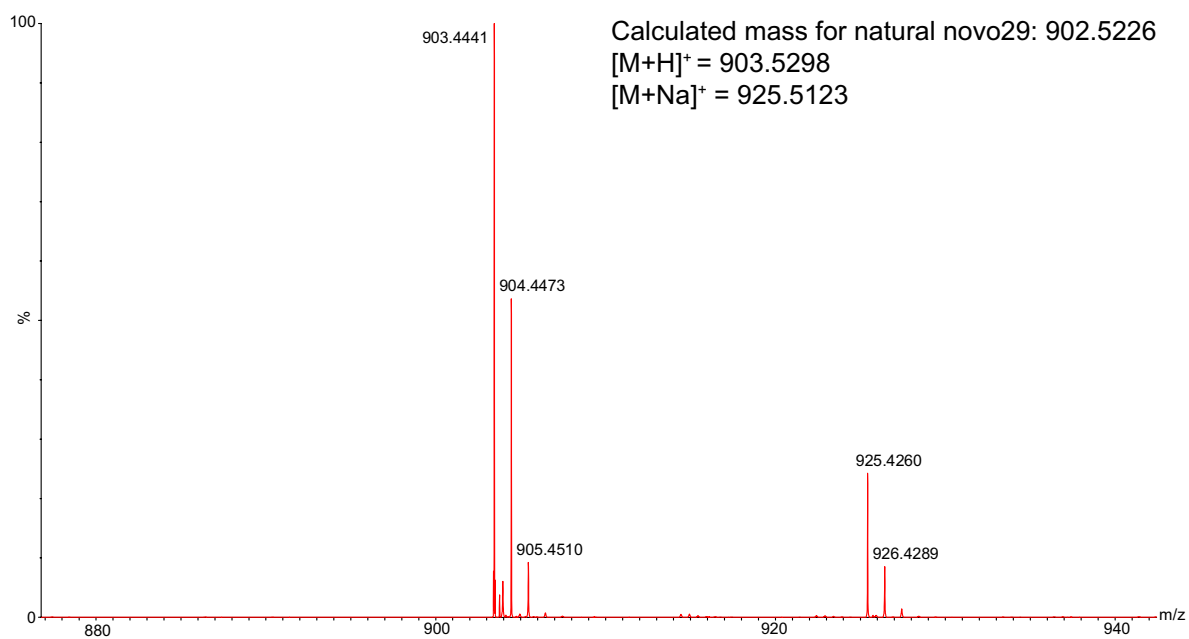
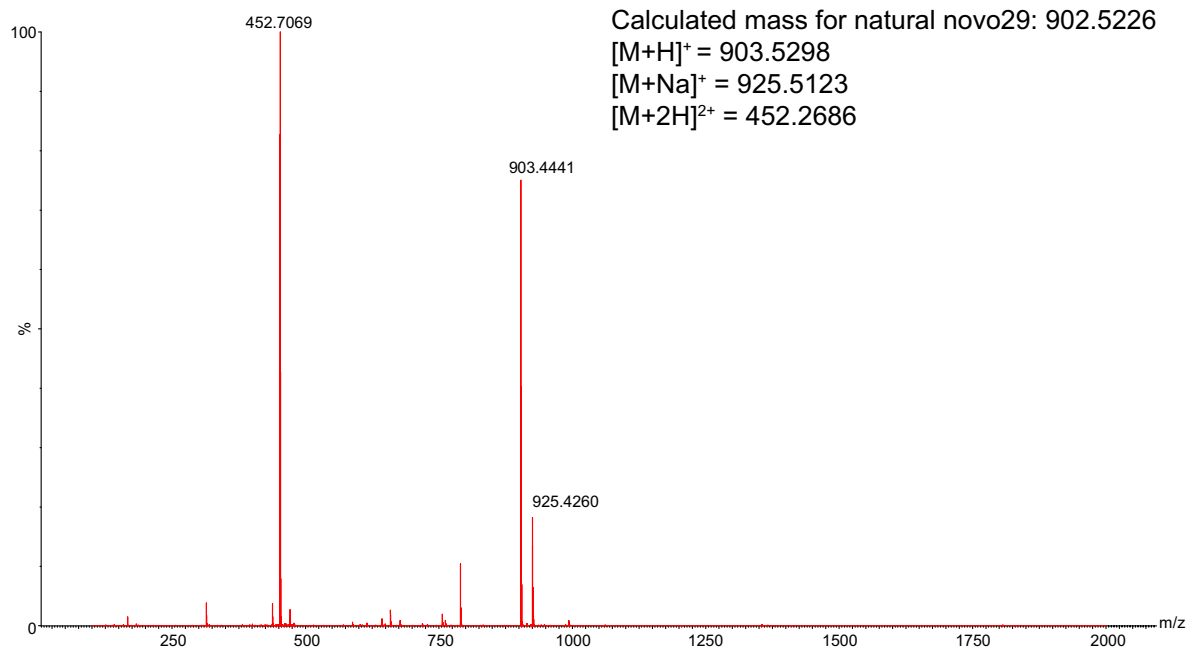
Characterization Data

Characterization of natural Novo29

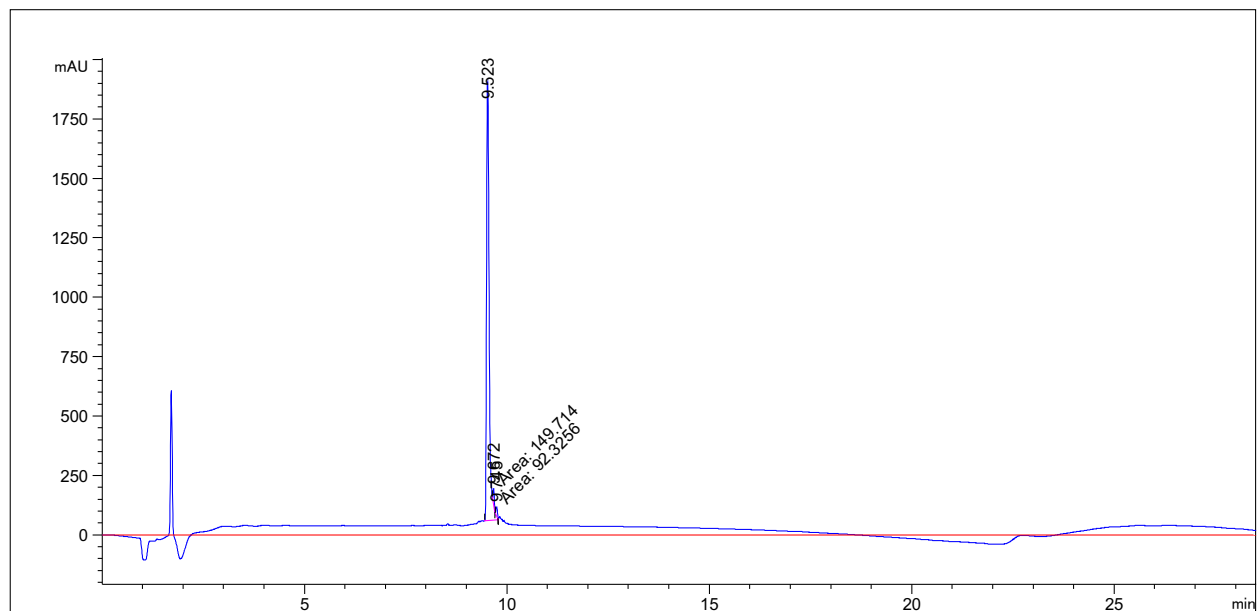
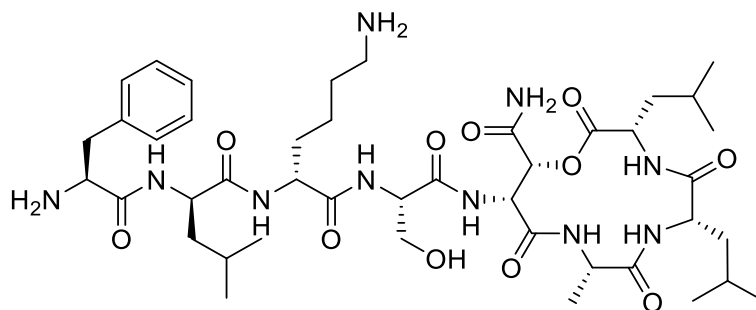


Signal 1: MWD1 A, Sig=214,4 Ref=off

Peak #	RetTime [min]	Type	Width [min]	Area [mAU*s]	Height [mAU]	Area %
1	9.575	MM	0.0569	4312.21582	1262.37280	100.0000

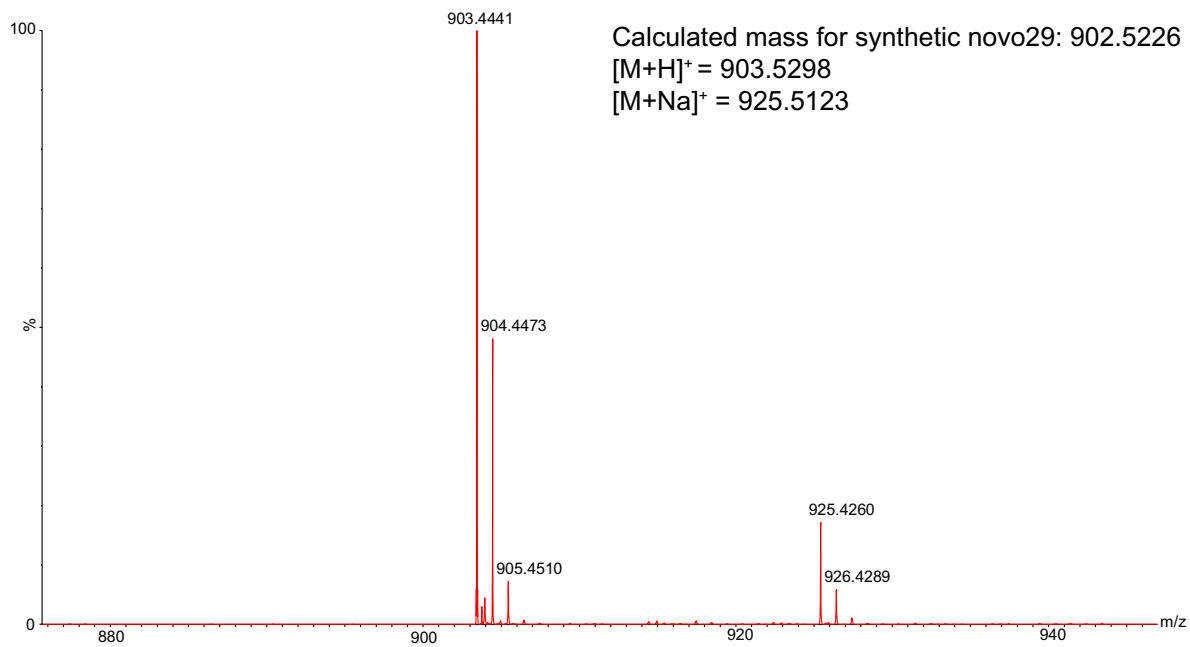
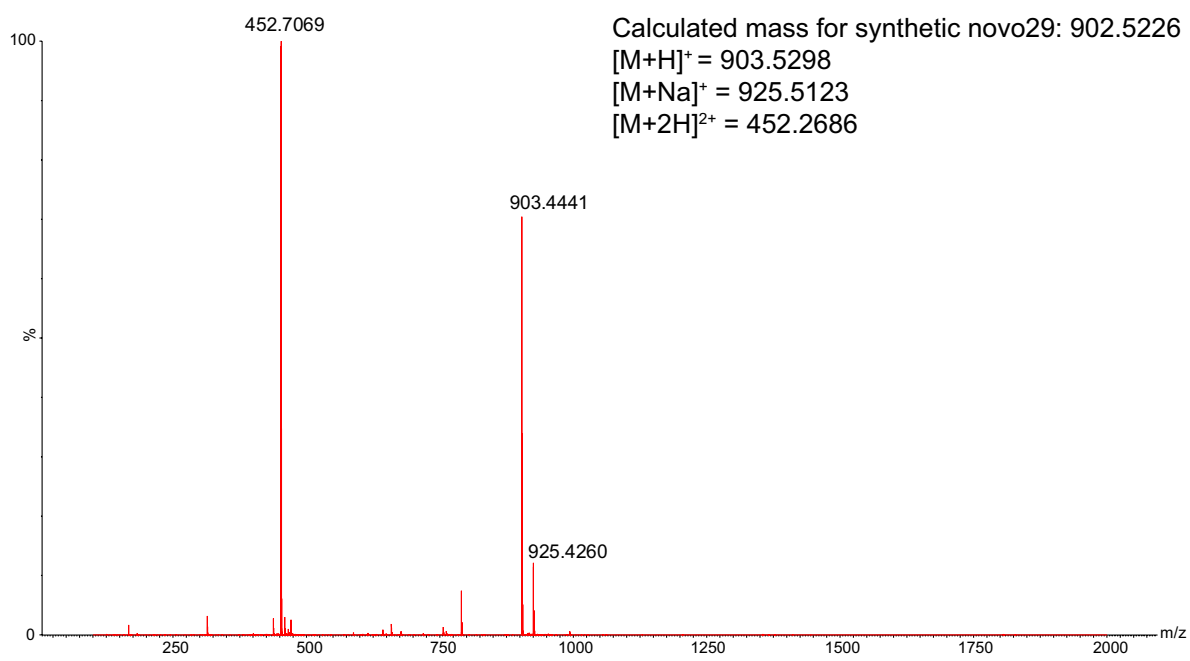


Characterization of synthetic Novo29

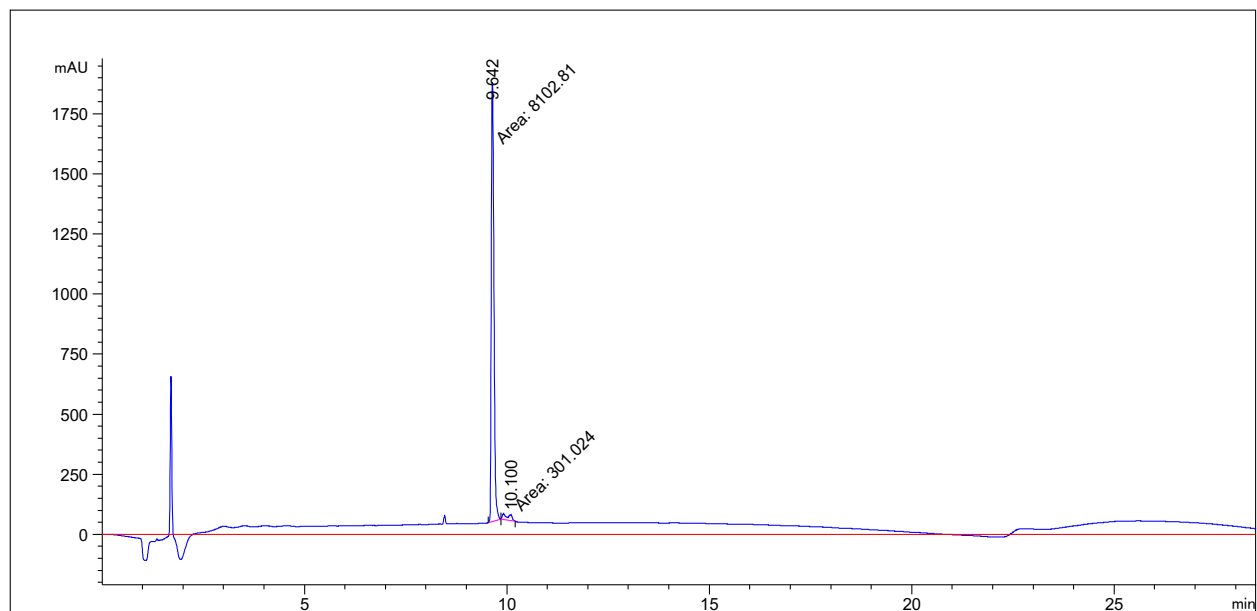
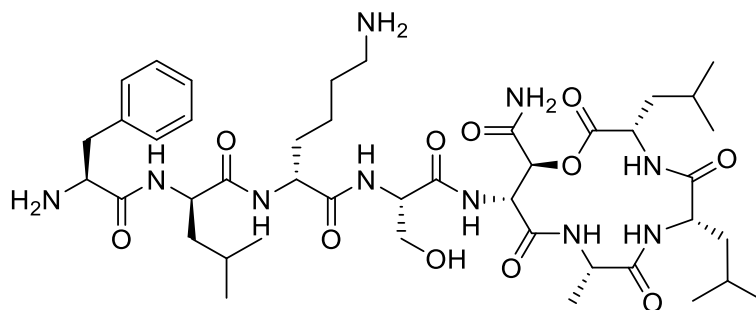


Signal 1: MWD1 A, Sig=214,4 Ref=off

Peak #	RetTime [min]	Type	Width [min]	Area [mAU*s]	Height [mAU]	Area %
1	9.523	MM R	0.0728	8129.04150	1861.80823	97.1086
2	9.672	MM T	0.0363	149.71405	68.68908	1.7885
3	9.745	MM T	0.0403	92.32558	38.15857	1.1029

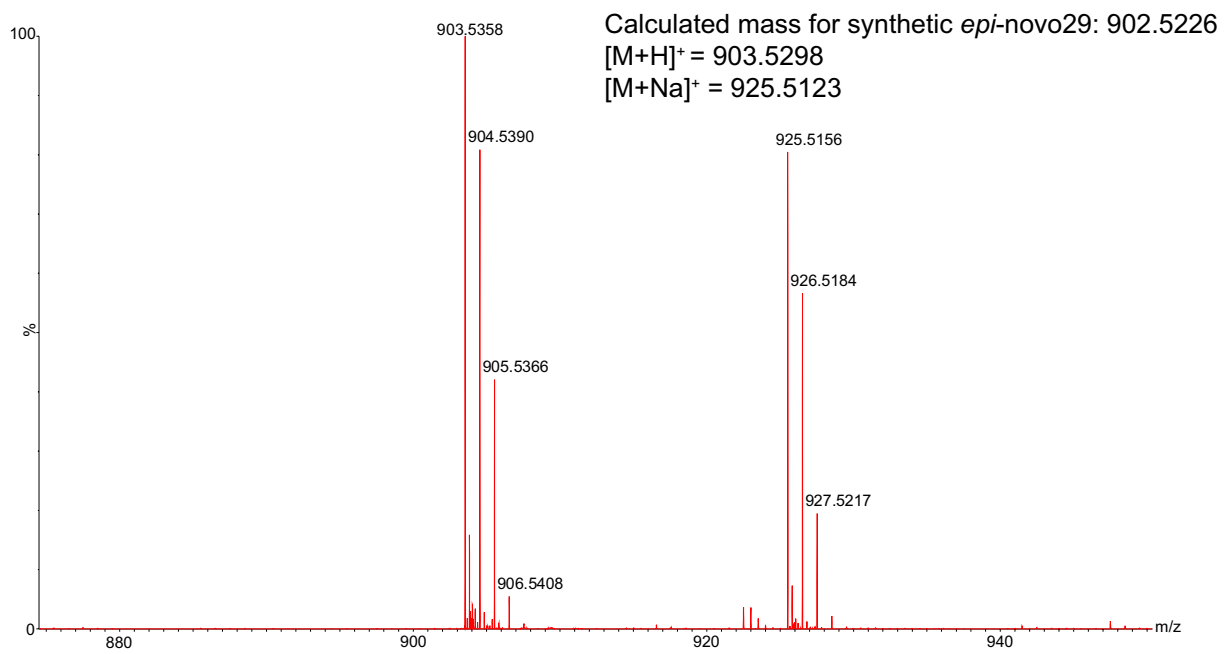
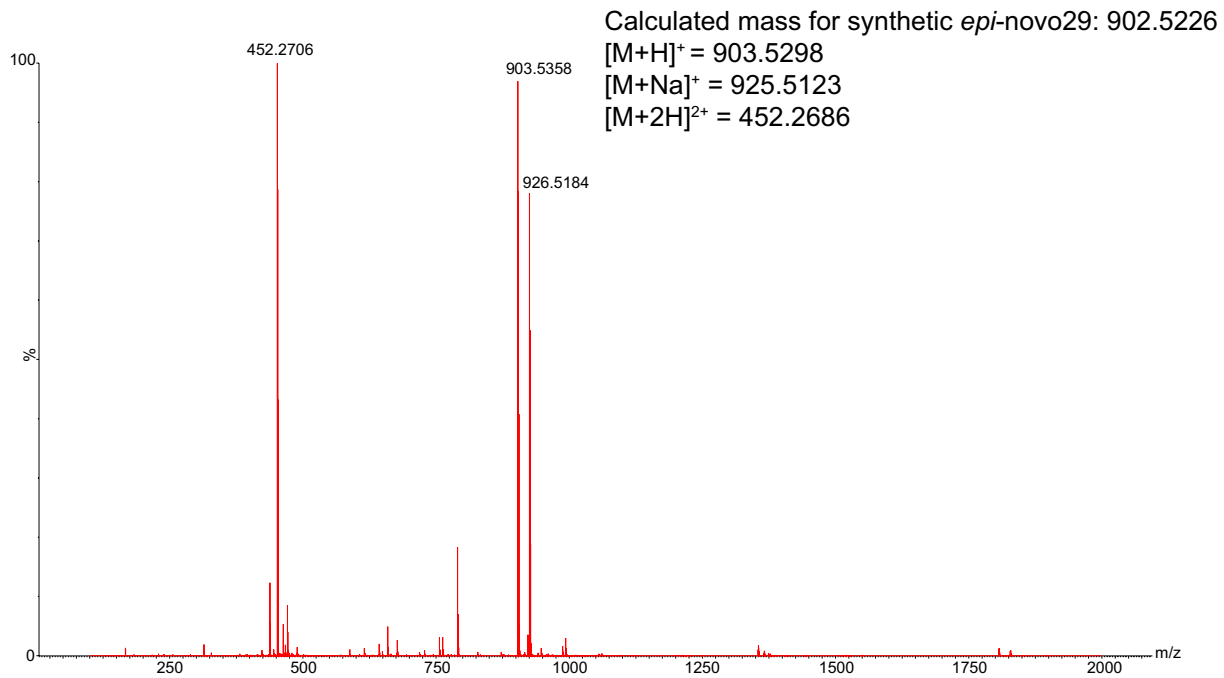


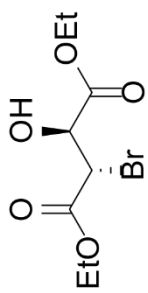
Characterization of synthetic epi-Novo29



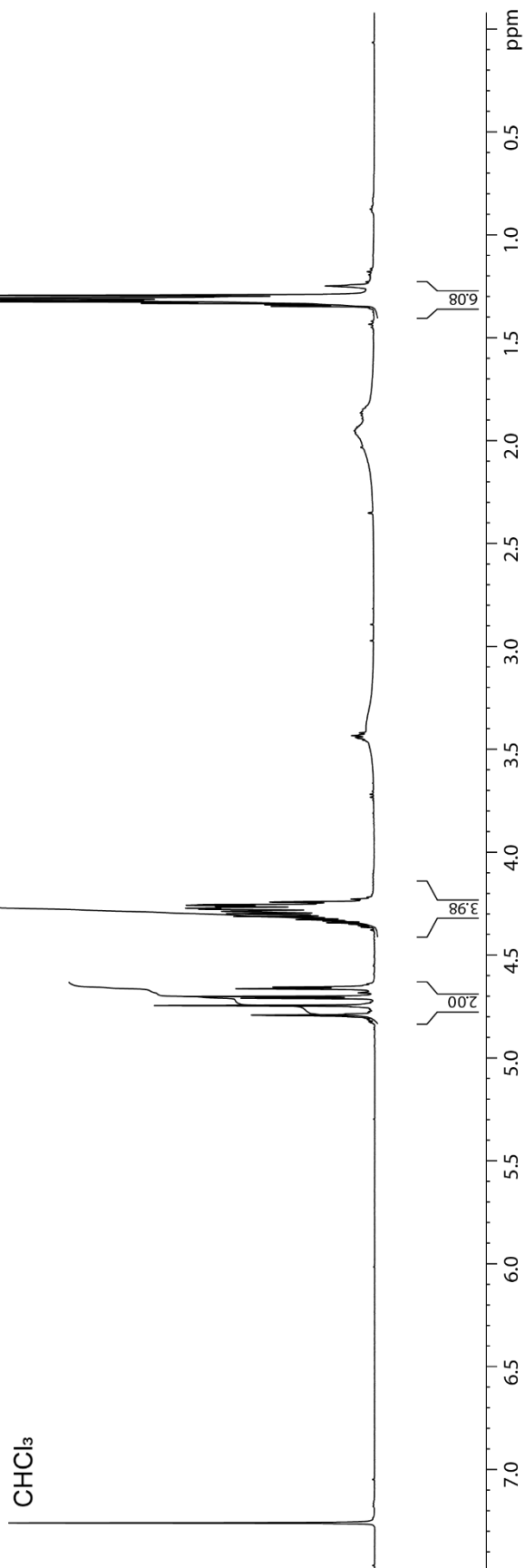
Signal 1: MWD1 A, Sig=214,4 Ref=off

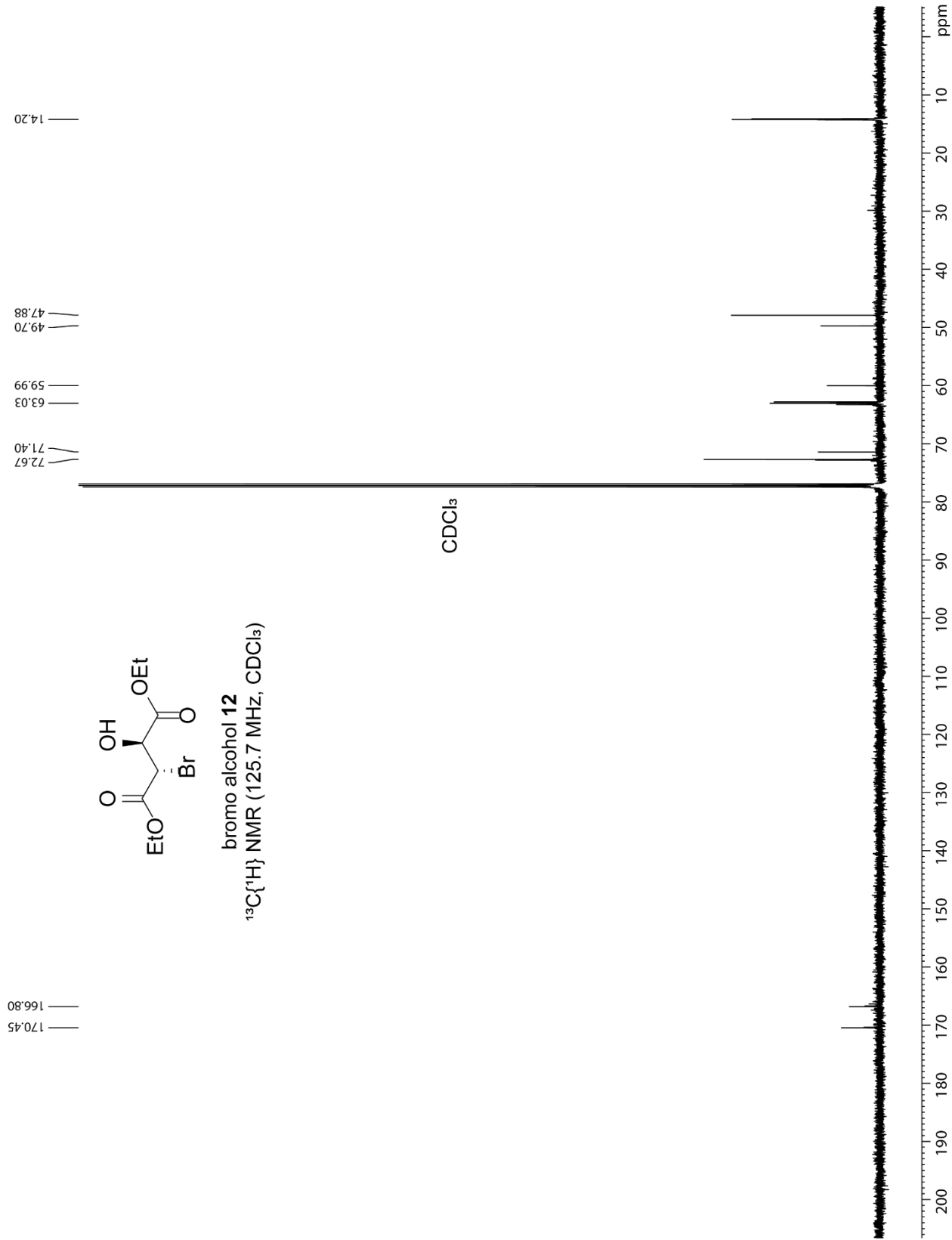
Peak #	RetTime [min]	Type	Width [min]	Area [mAU*s]	Height [mAU]	Area %
1	9.642	MM	0.0735	8102.80859	1836.76953	96.4180
2	10.100	MM	0.2067	301.02429	24.26878	3.5820

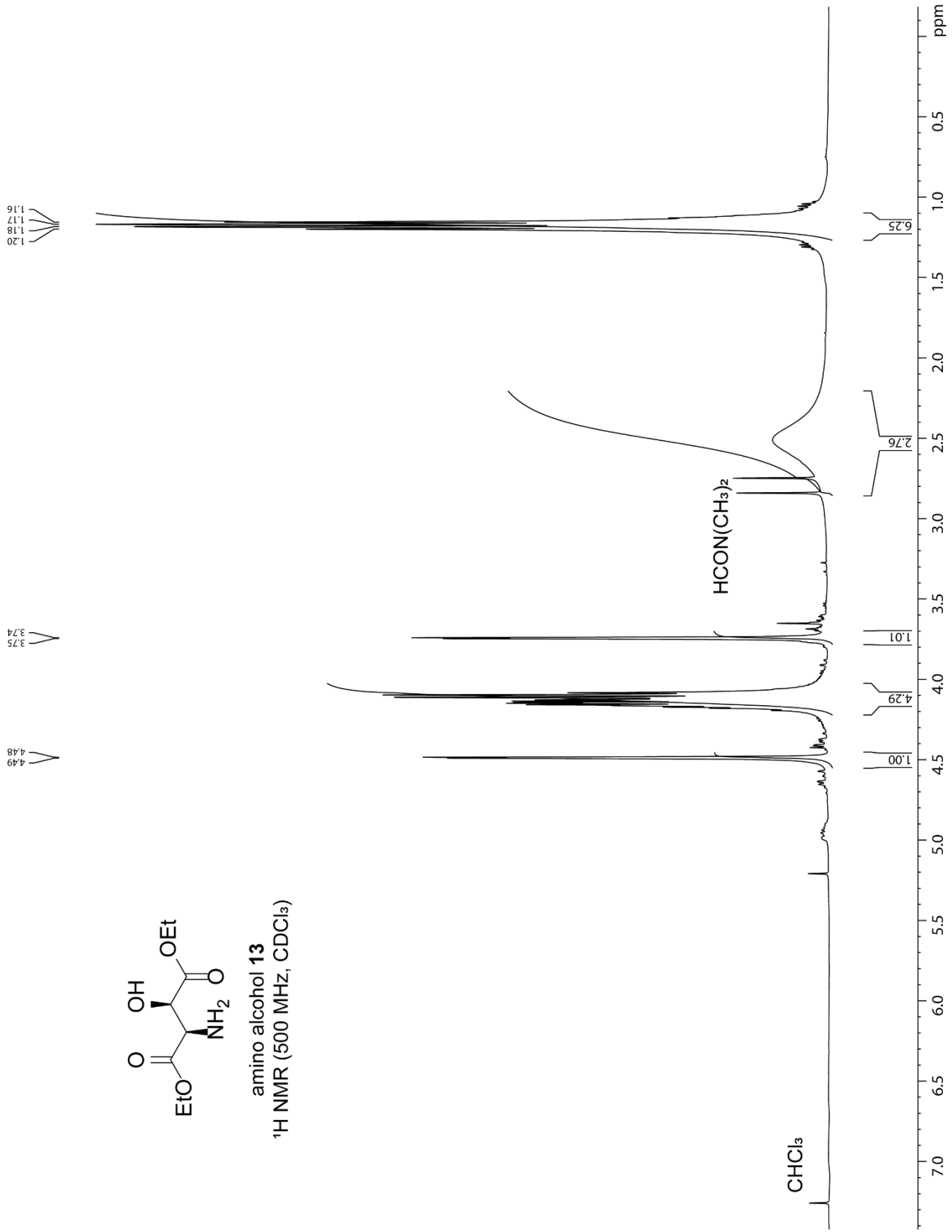
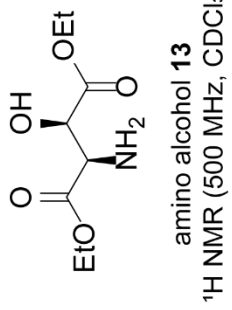




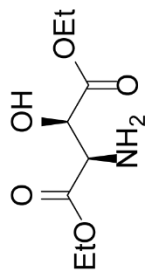
bromo alcohol **12**
 ^1H NMR (500 MHz, CDCl_3)







172.62
172.36



amino alcohol **13**
¹³C{¹H} NMR (125.7 MHz, CDCl₃)

13.96
13.96

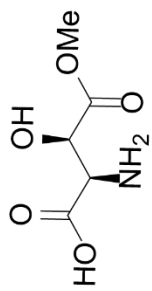
56.70
61.81
61.81

72.01

CDCl₃

200 190 180 170 160 150 140 130 120 110 100 90 80 70 60 50 40 30 20 10 ppm

4.81
4.78
4.69
4.68
4.62
4.62
4.41
4.41



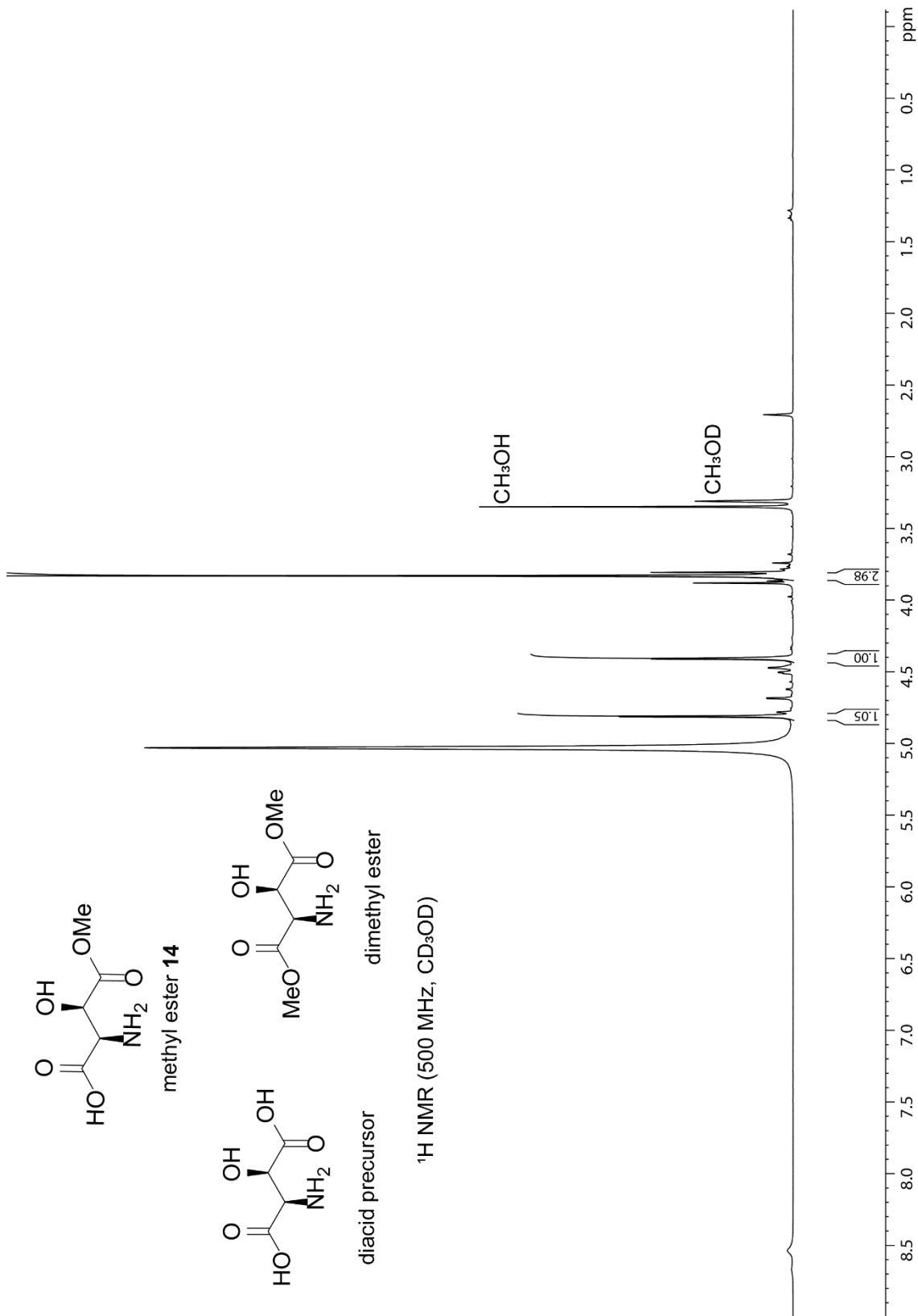
methyl ester **14**



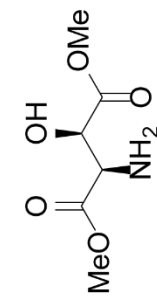
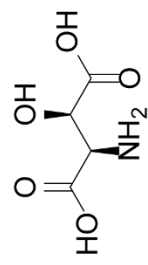
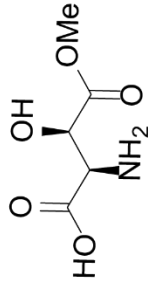
diacid precursor

dimethyl ester

^1H NMR (500 MHz, CD_3OD)



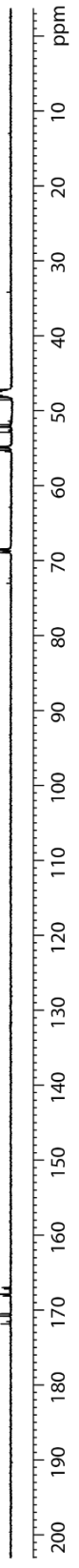
171.82
170.80
170.51
168.10
167.87
166.99



68.91
68.57
68.41
55.27
54.77
52.85
52.12
51.84

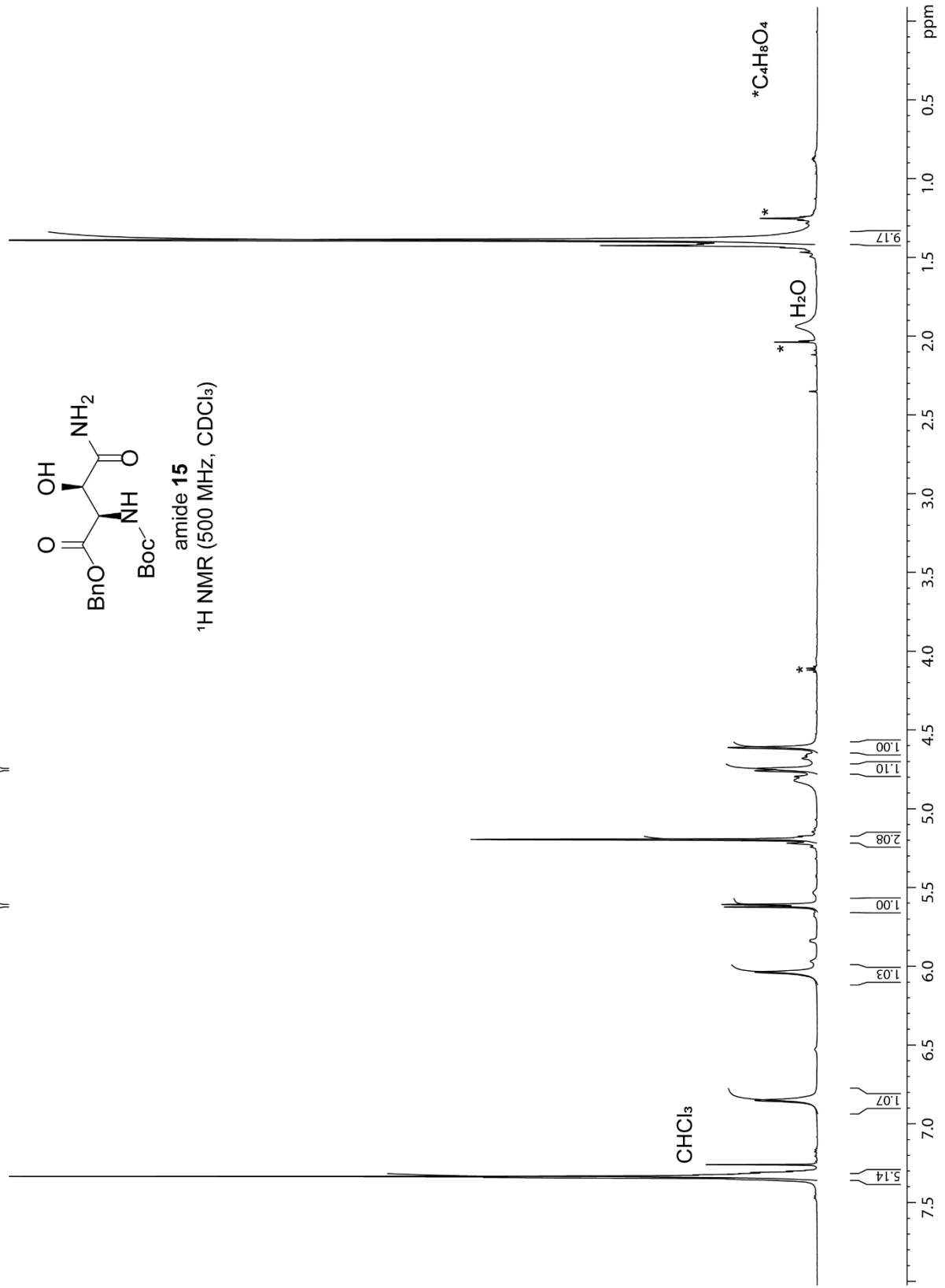
CD₃OD

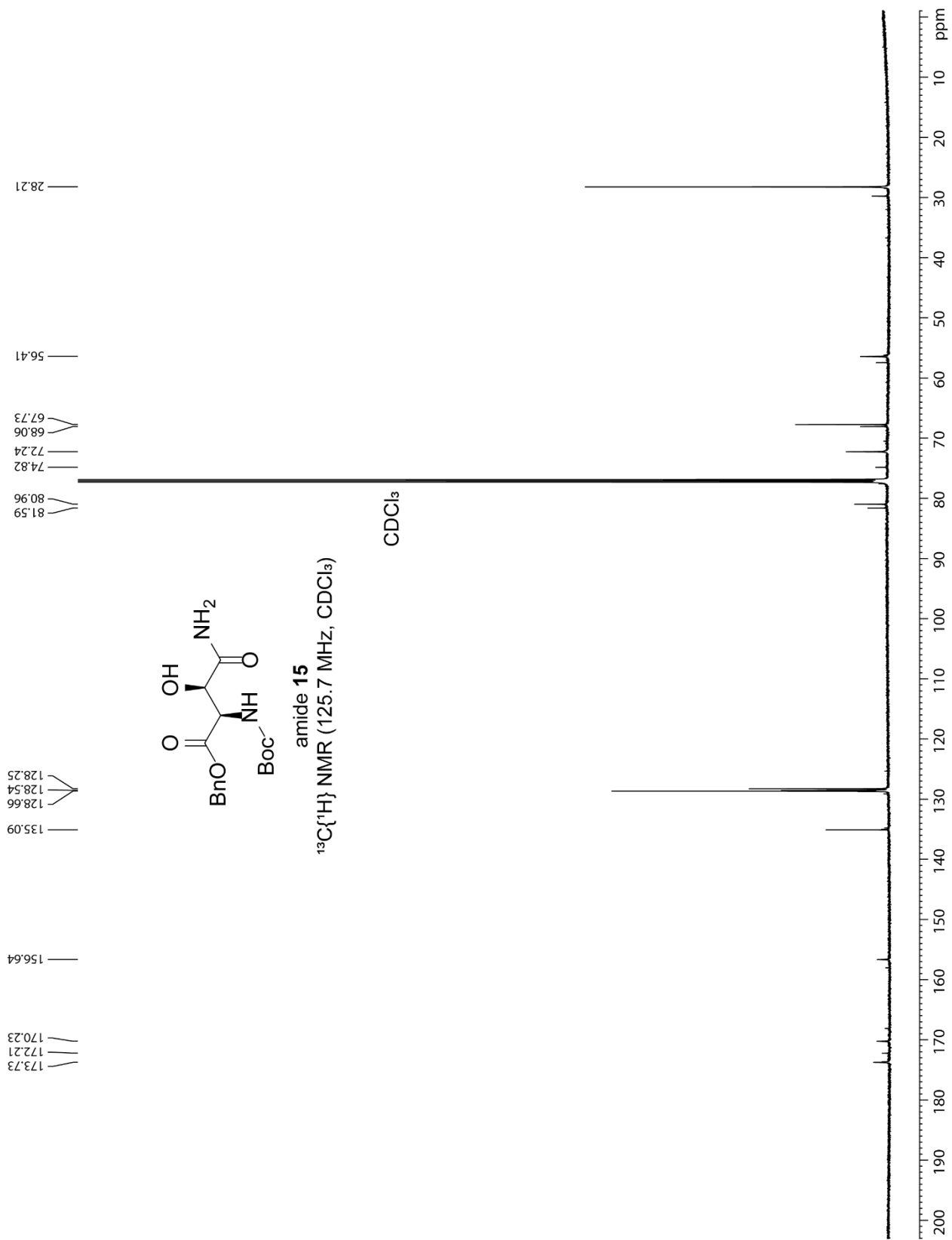
¹³C{¹H} NMR (125.7 MHz, CD₃OD)



4.76
4.74

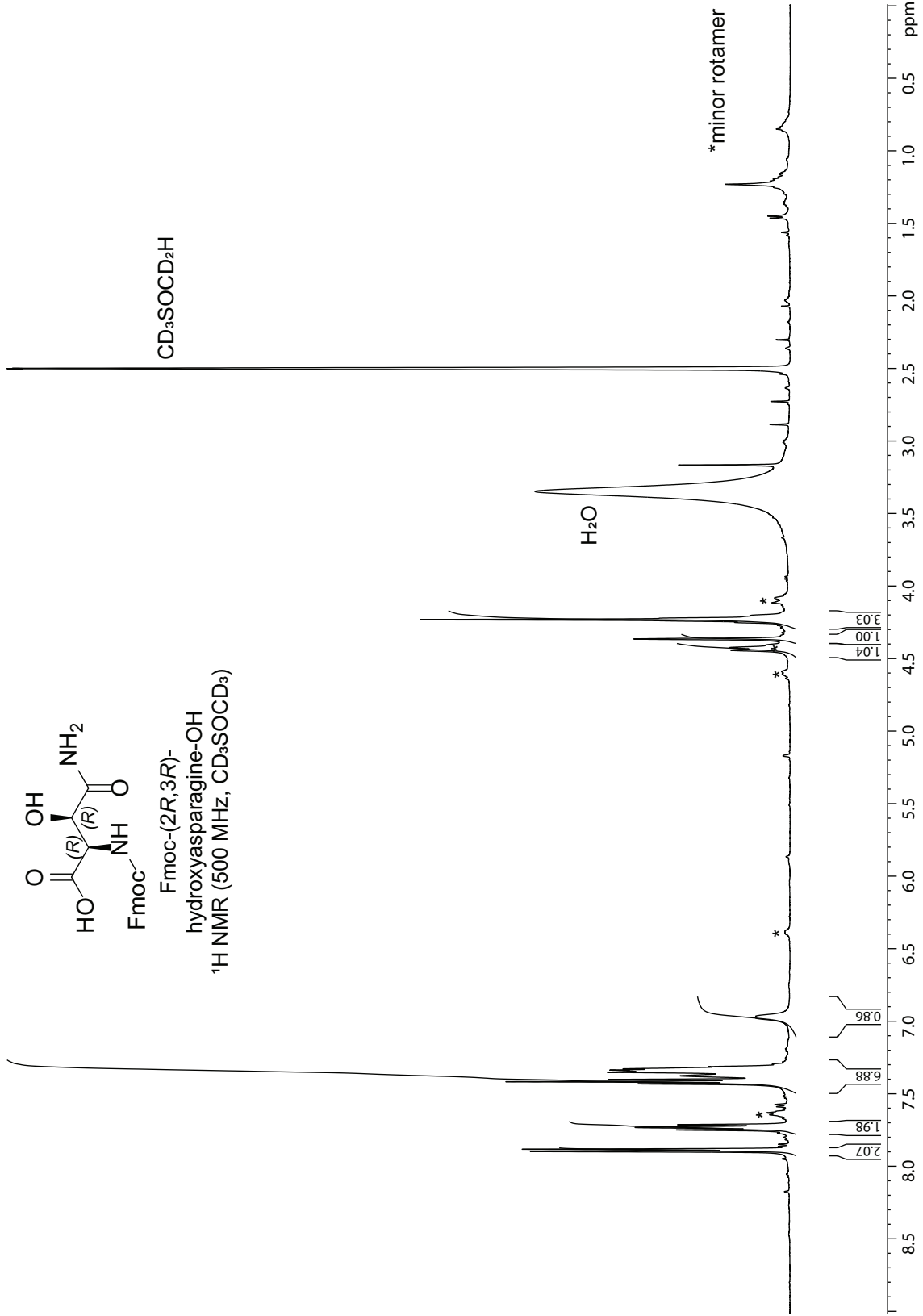
5.62
5.61

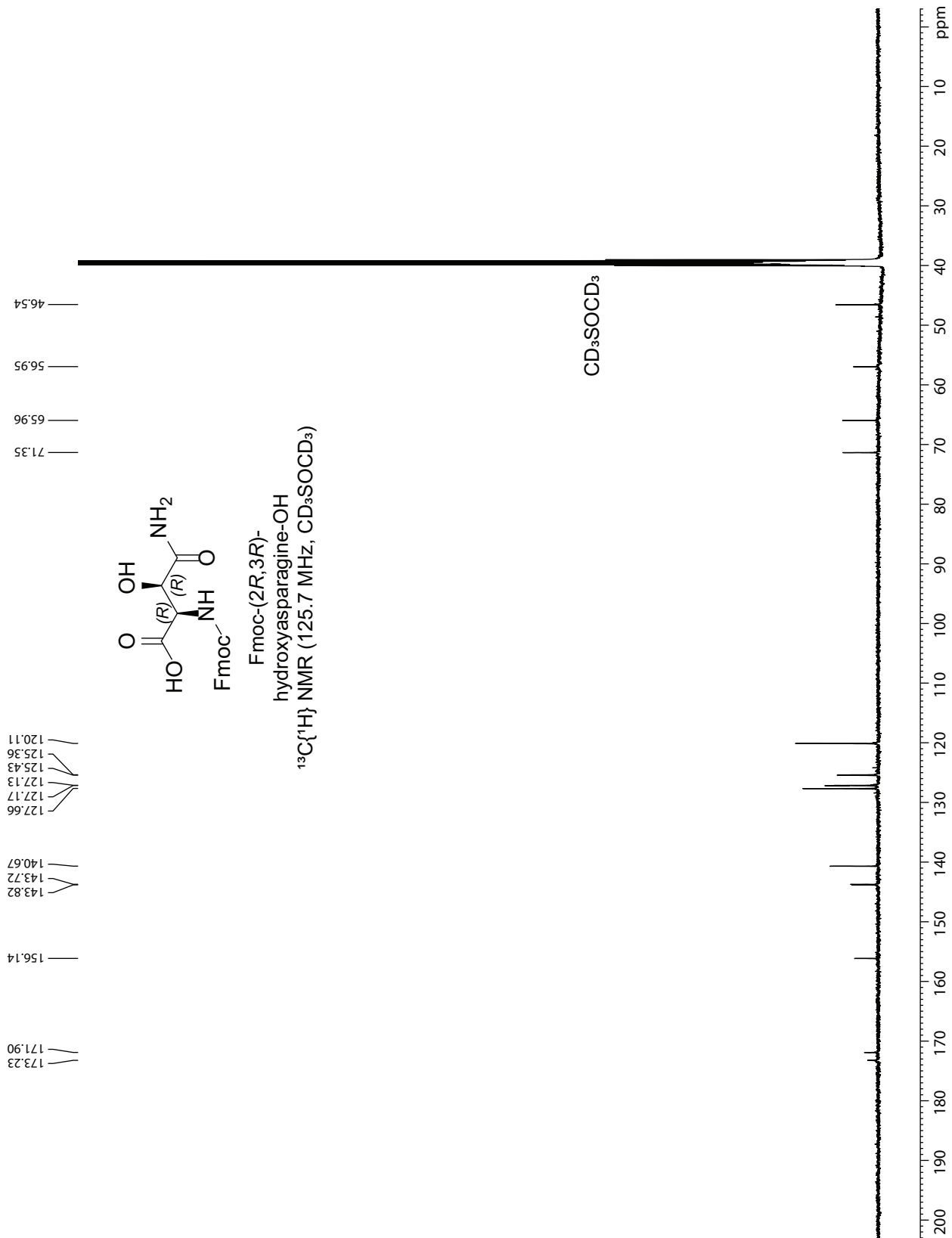


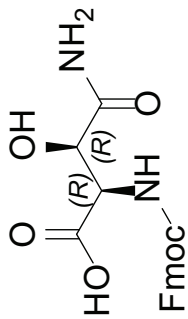


7.90
7.88
7.75
7.73
7.71

4.42
4.44







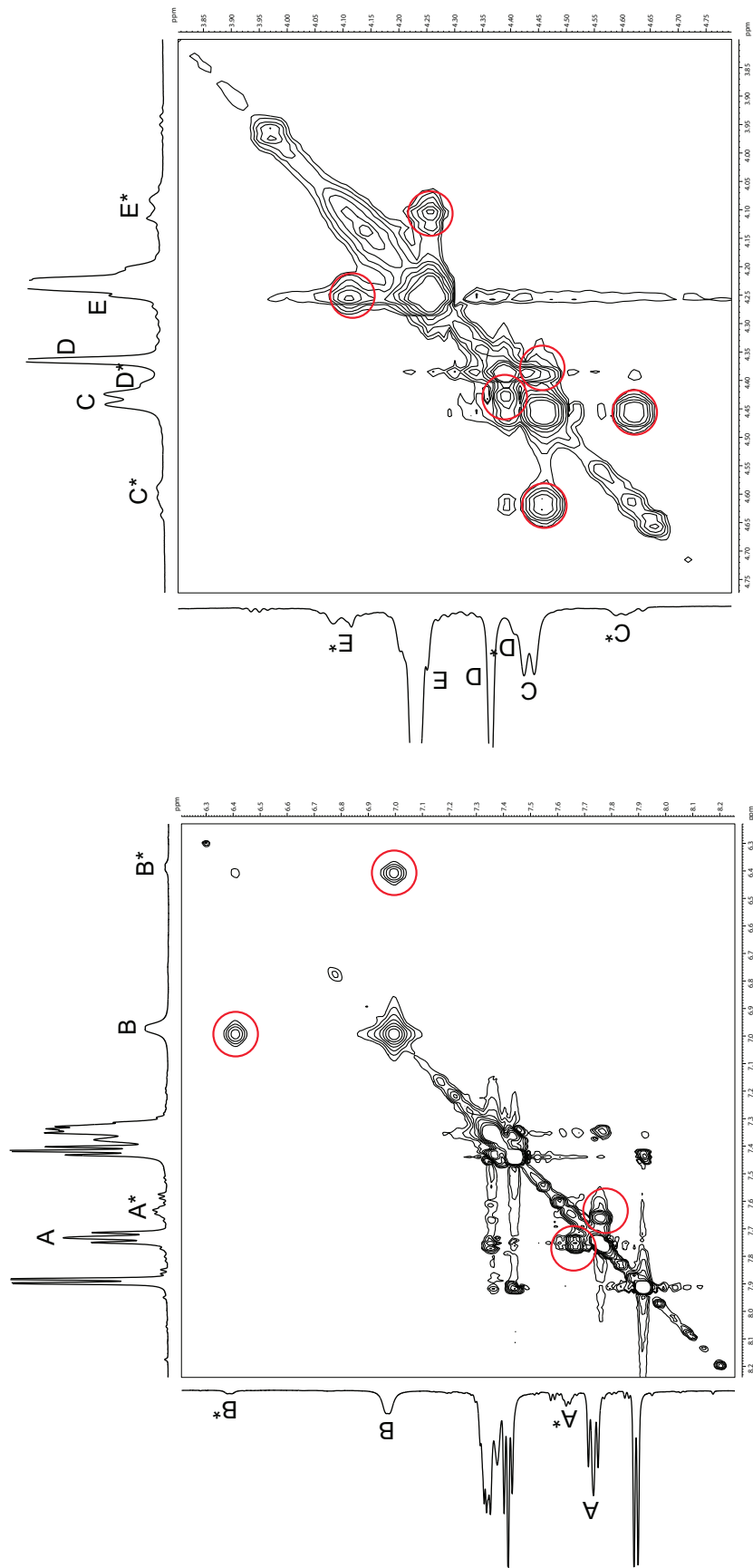
Fmoc-(2*R*,3*R*)-hydroxyAsn-OH

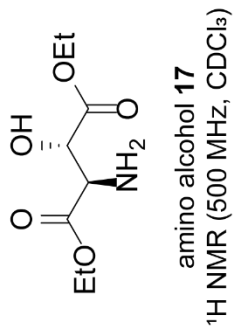
500 MHz EXSY (NOESY) spectrum of Fmoc-(2*R*,3*R*)-hydroxyAsn illustrating the exchange between rotamers.

800-ms mixing time in DMSO-*d*₆, 298 K.

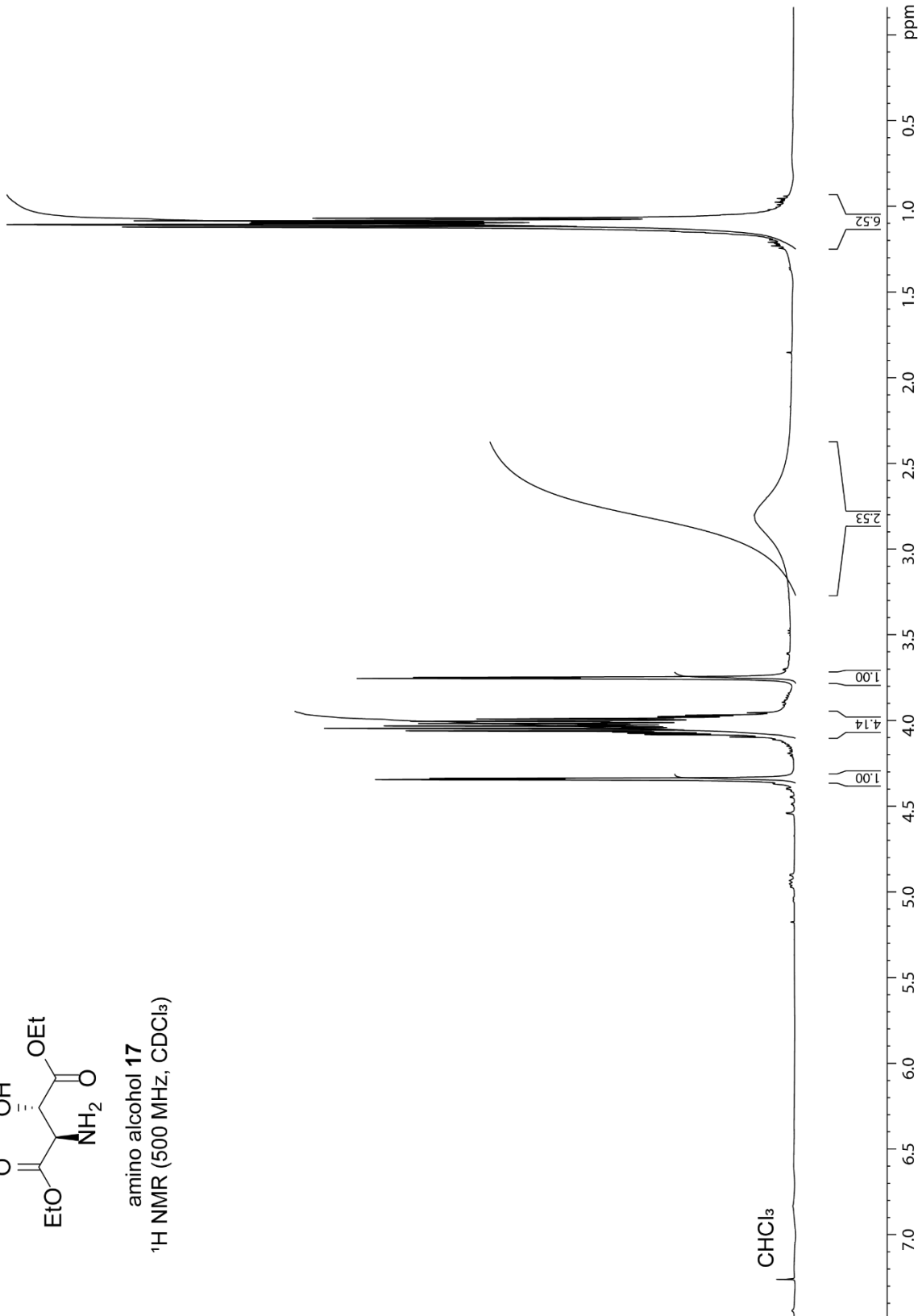
Cross peaks demonstrating exchange of protons from rotamers are circled in red.

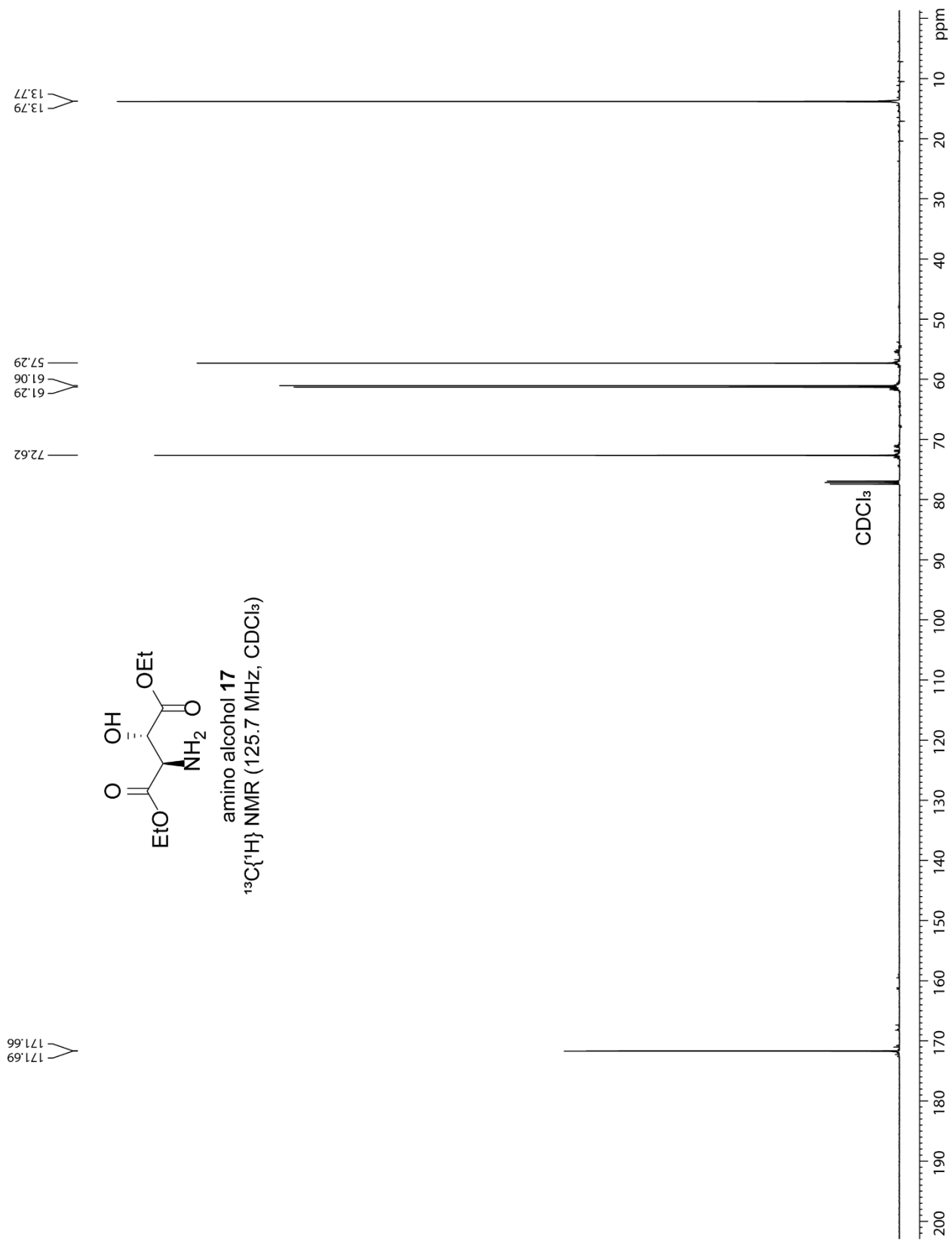
Pairs of resonances associated with major and minor rotamers are designated A and A*, B and B*, etc.



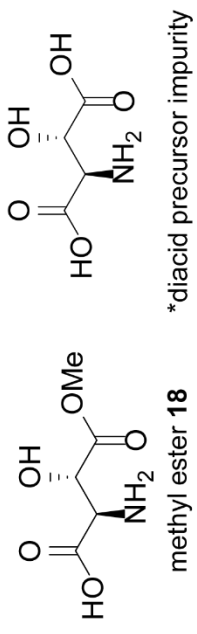


4.34
 3.75

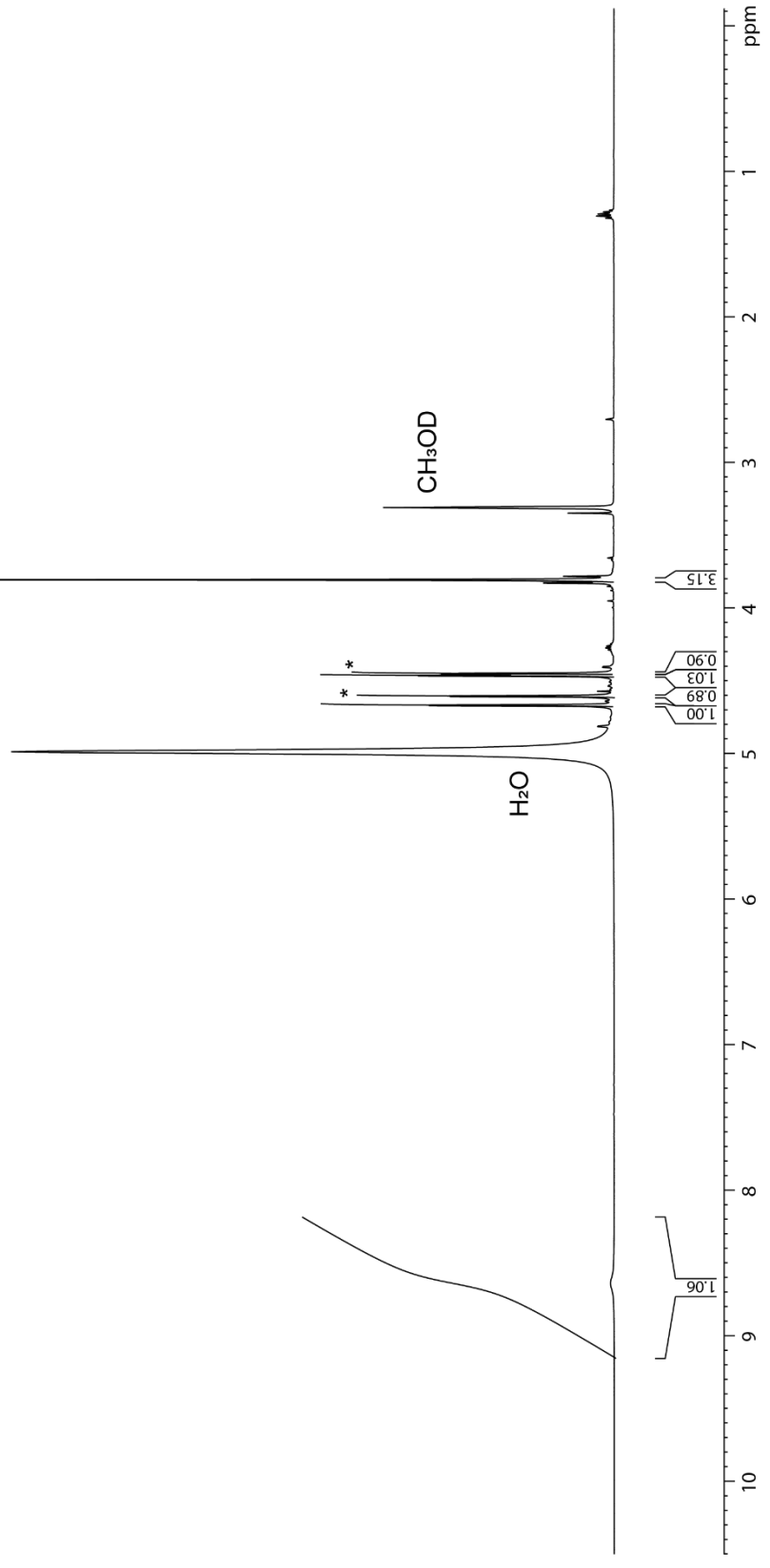




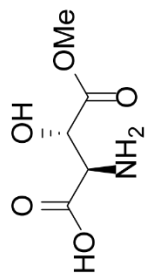
4.67
4.61
4.60
4.47
4.46
4.45
4.45



¹H NMR (500 MHz, CD₃OD)



172.86*
171.84
168.49*
168.35

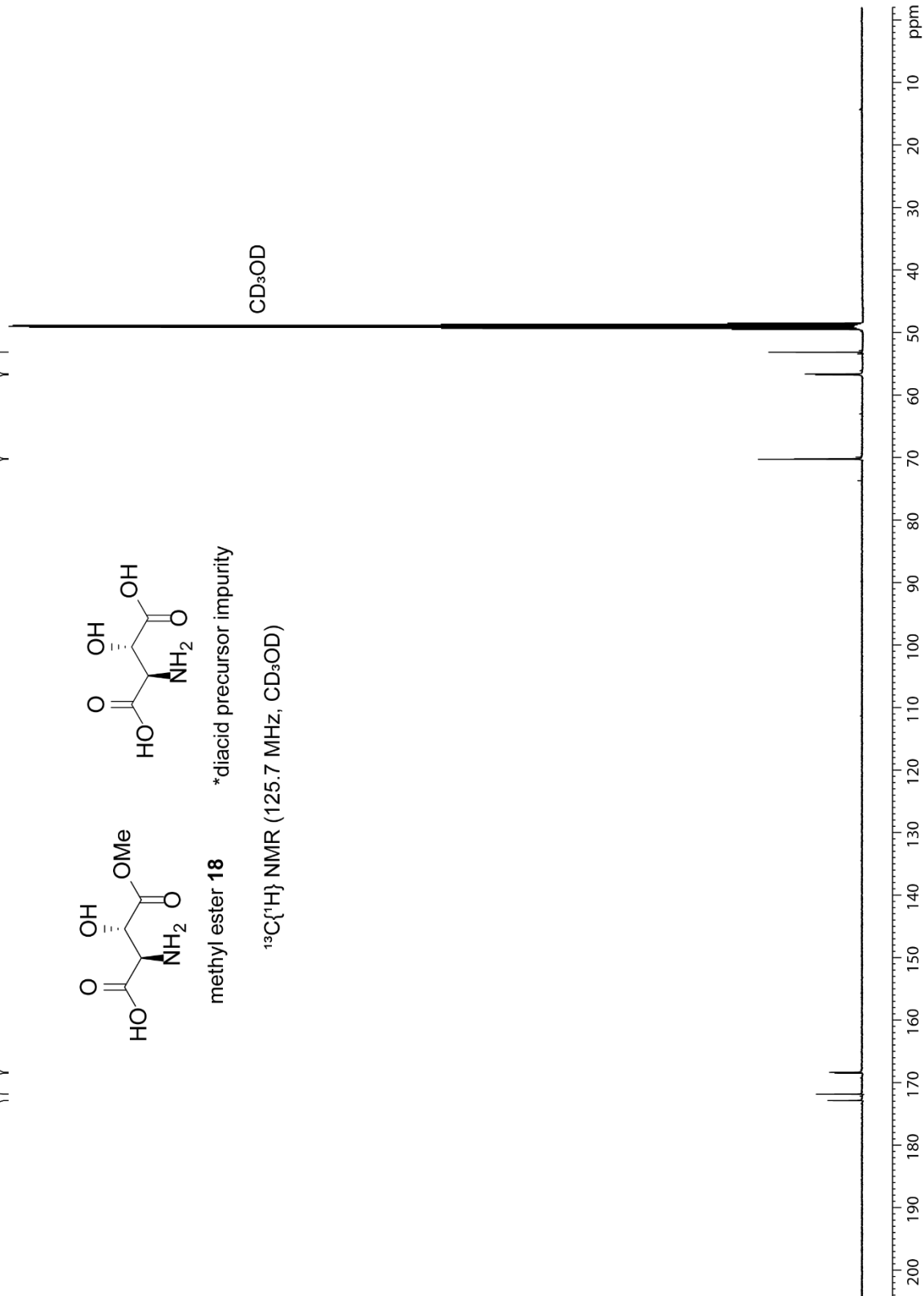


methyl ester **18**

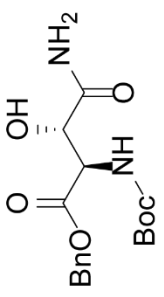
* diacid precursor impurity

¹³C{¹H} NMR (125.7 MHz, CD₃OD)

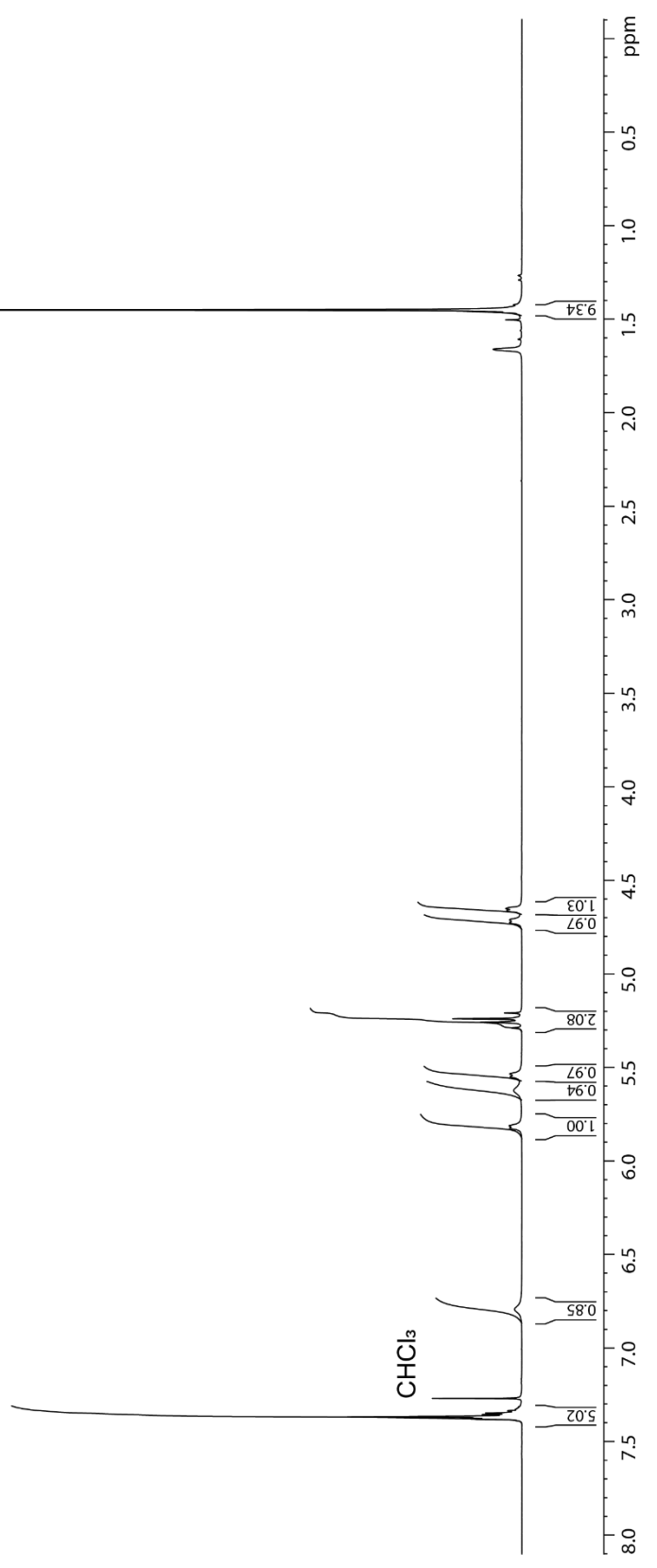
70.27
70.18*
56.78*
56.62
53.15

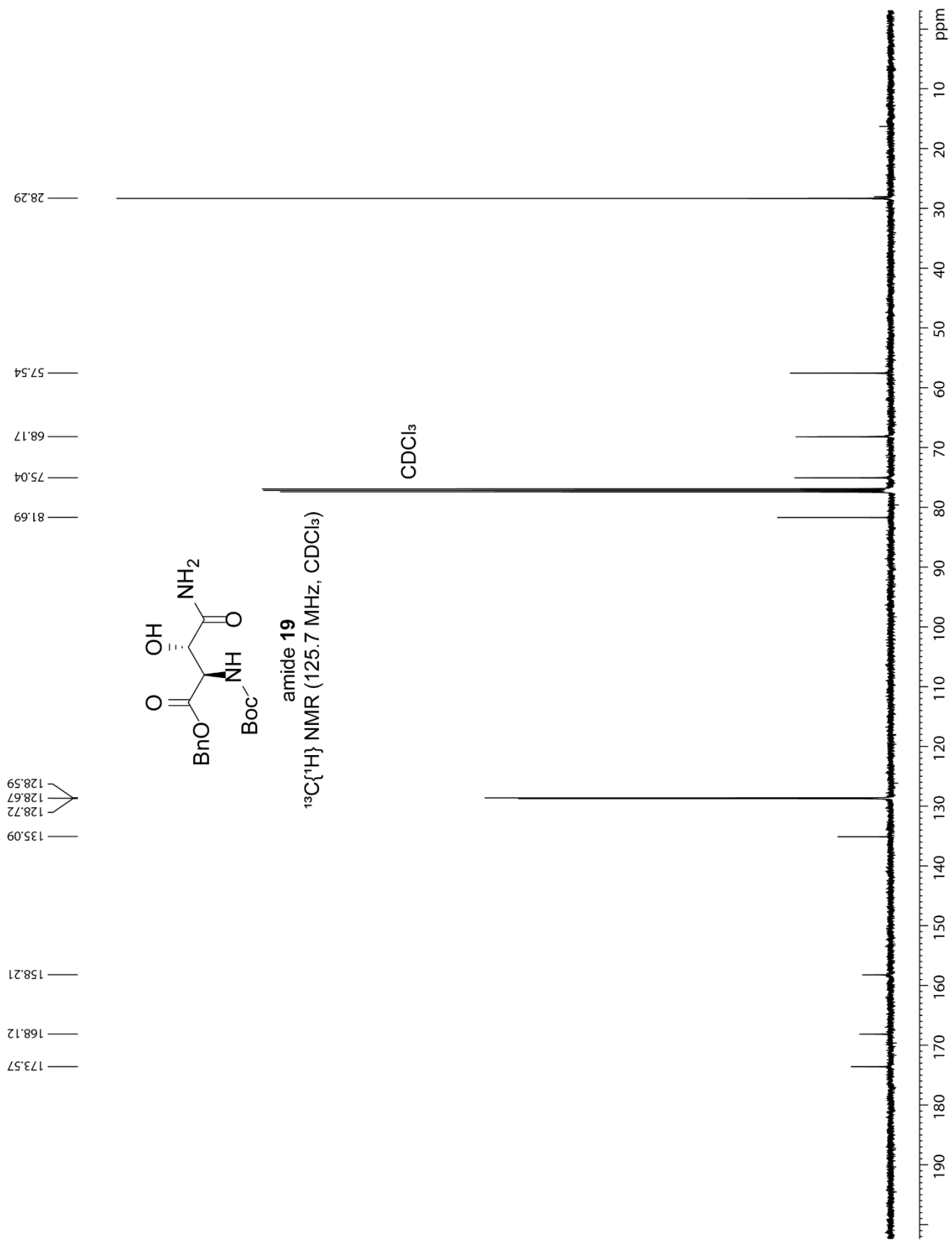


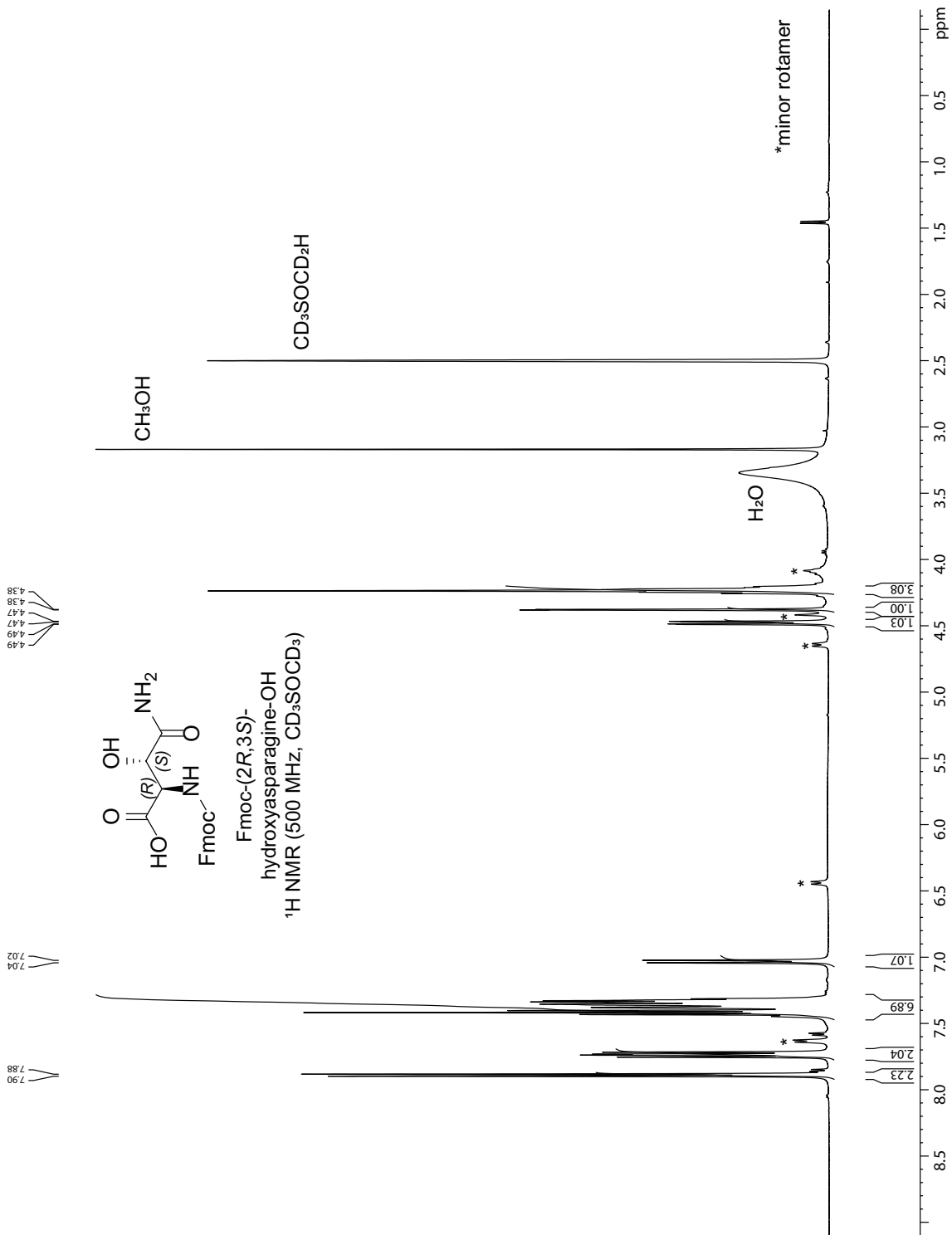
5.82
5.81
5.55
5.53
4.72
4.71
4.66
4.65

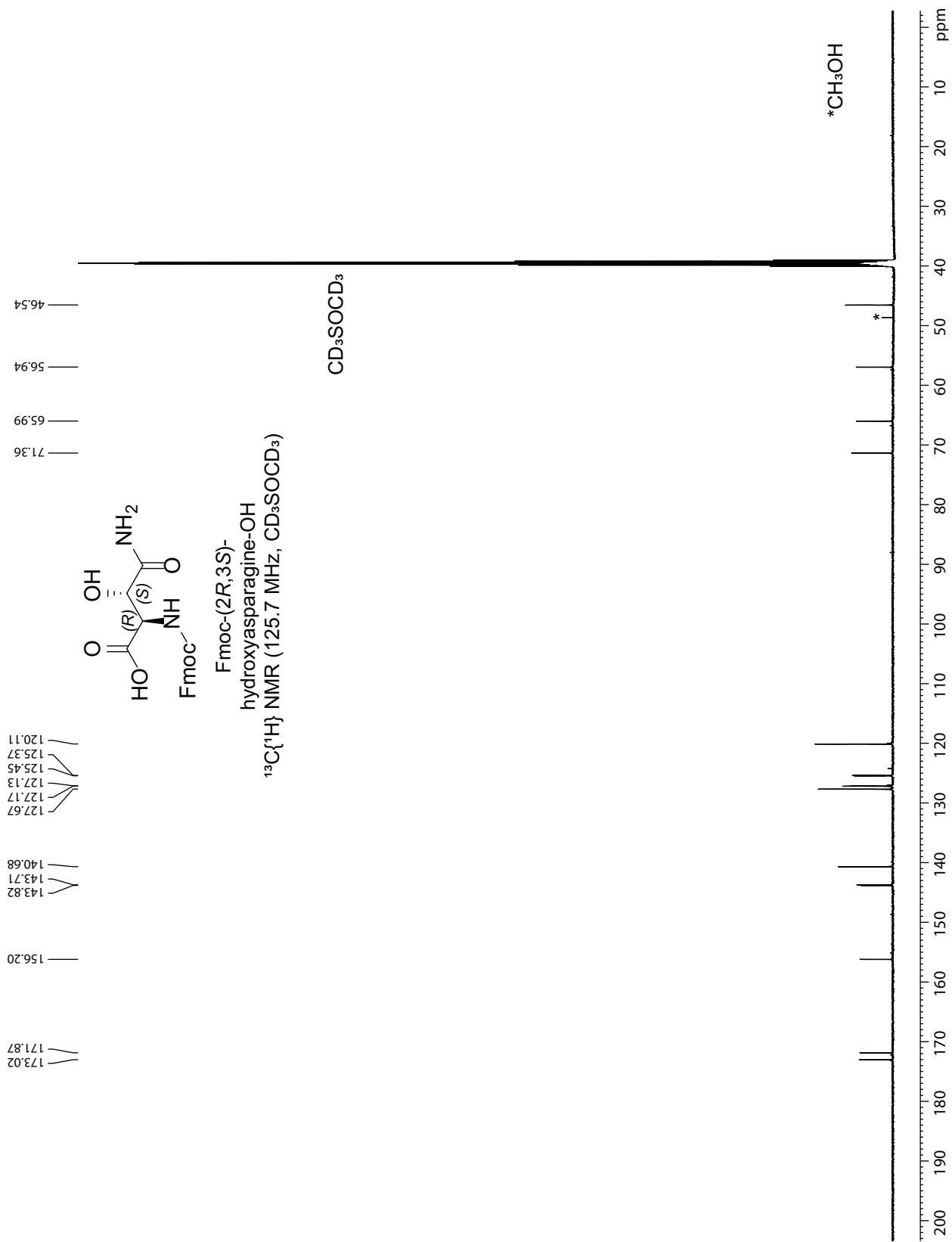


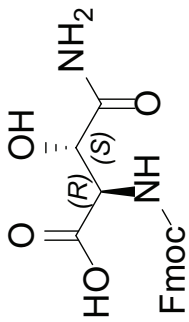
amide 19
¹H NMR (500 MHz, CDCl₃)





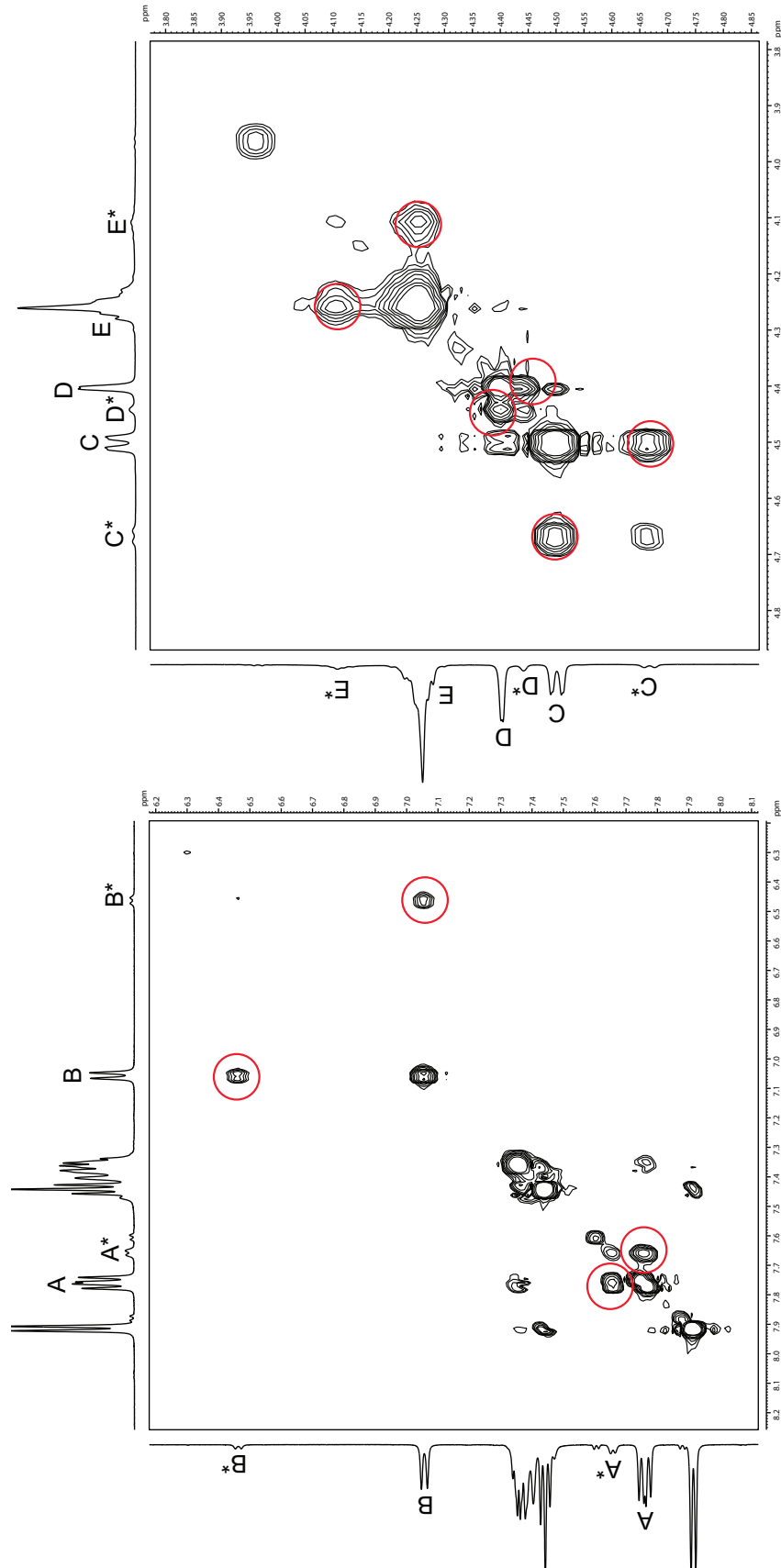




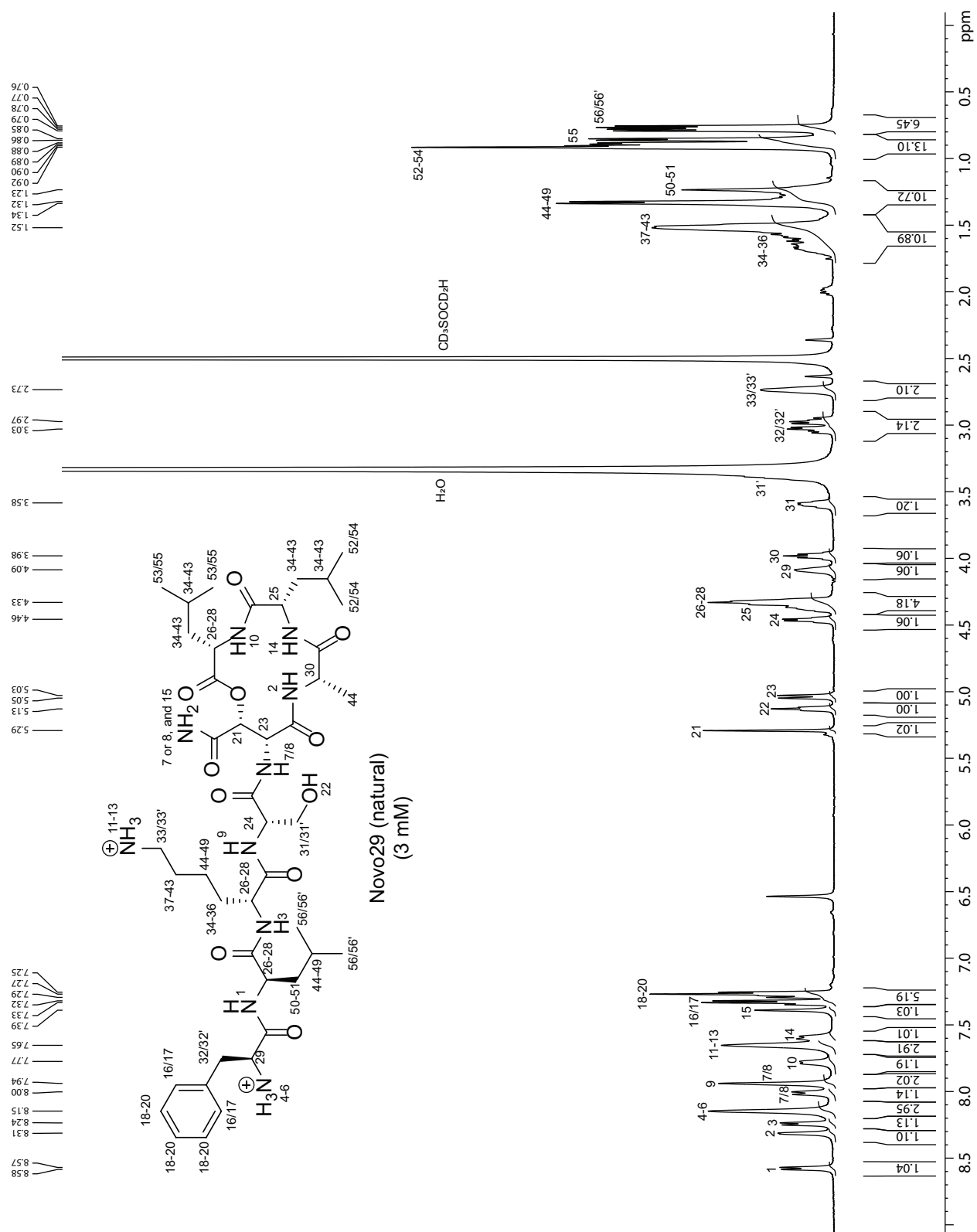


Fmoc-(2*R*,3*S*)-hydroxyAsn-OH

500 MHz EXSY (NOESY) spectrum of Fmoc-(2*R*,3*S*)-hydroxyAsn illustrating the exchange between rotamers.
 1000-ms mixing time in DMSO-*d*₆, 298 K.
 Cross peaks demonstrating exchange of protons from rotamers are circled in red.
 Pairs of resonances associated with major and minor rotamers are designated A and A*, B and B*, etc.



^1H NMR of 3 mM natural Novo29 in $\text{DMSO-}d_6$ at 500 MHz and 298 K



2.0 mM natural Novo29
in DMSO-*d*₆, 200-ms mixing time, 298 K
600 MHz NOESY spectrum

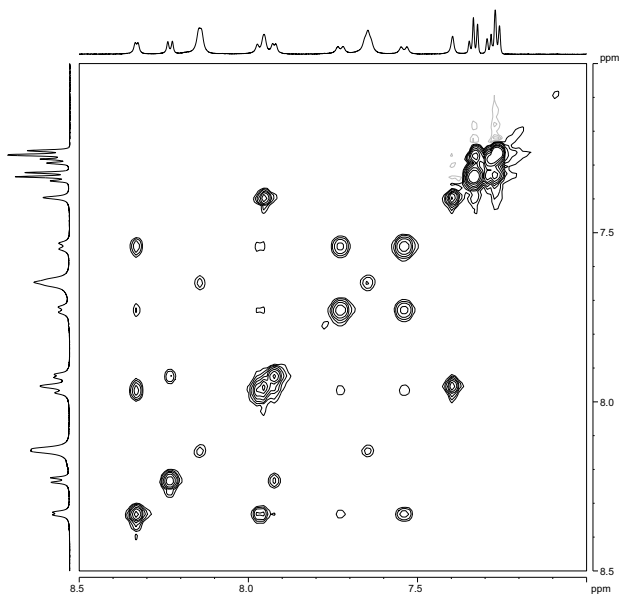
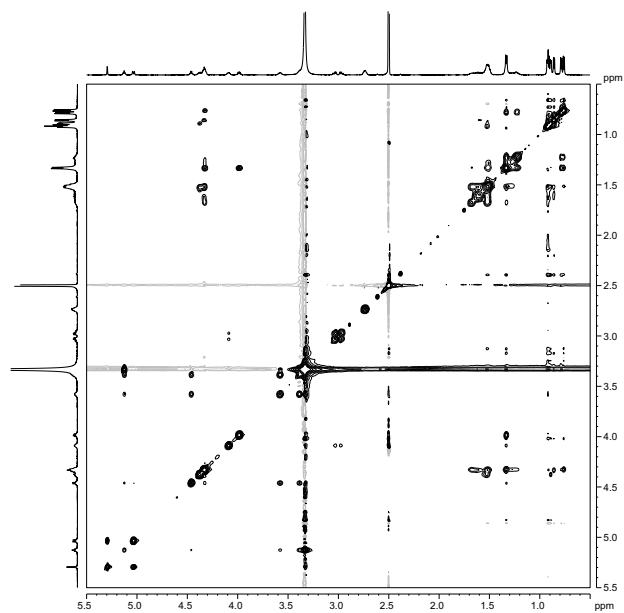
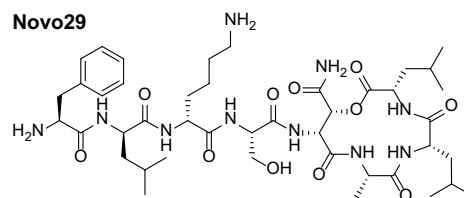
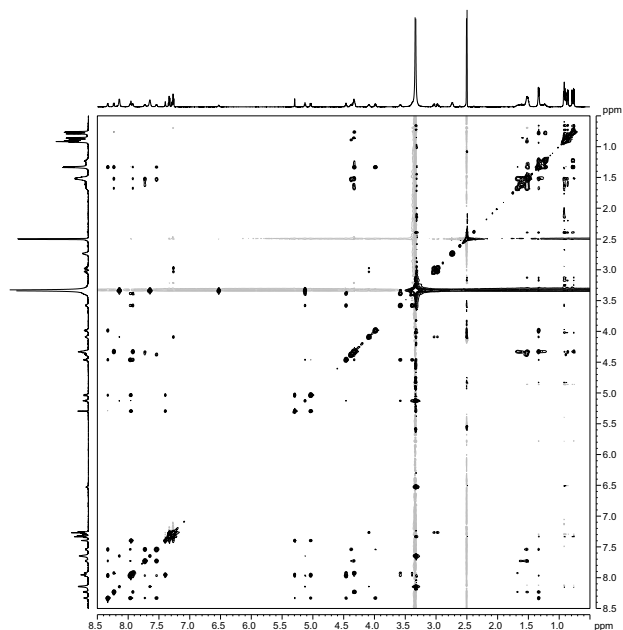
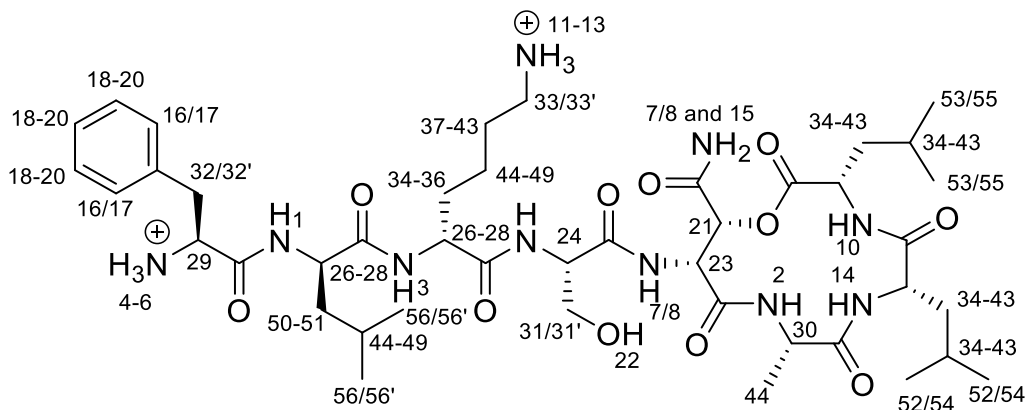


Table S3.3. Chemical shift assignments for natural Novo29.



#	Natural Novo29 3 mM (nominal)	#	Natural Novo29 3 mM (nominal)
1	8.57	25	4.38
2	8.31	26-28	4.33
3	8.24	29	4.09
4-6	8.15	30	3.98
7/8	8.01	31/31'	3.59
	and		and
	7.95		3.91
9	7.94	32/32'	3.00
10	7.78	33/33'	2.74
11-13	7.65	34-36	1.63
14	7.60	37-43	1.52
15	7.39	44-49	1.33
16/17	7.33	50-51	1.23
18-20	7.27	52-54	0.92
21	5.29	55	0.86
22	5.13	56/56'	0.77
23	5.04		
24	4.46		

^1H NMR of 2 mM synthetic Novo29 in DMSO-d_6 at 500 MHz and 298 K

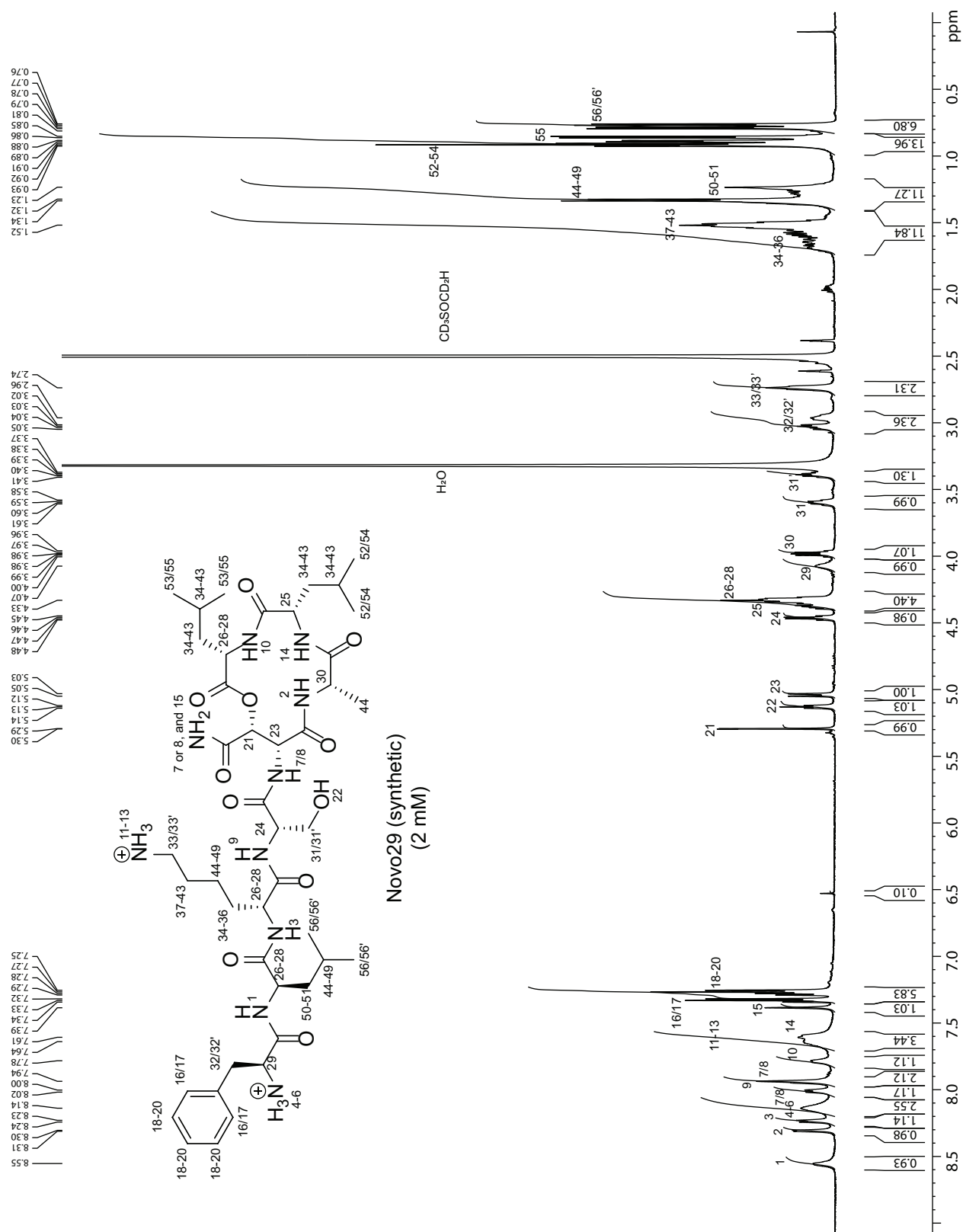
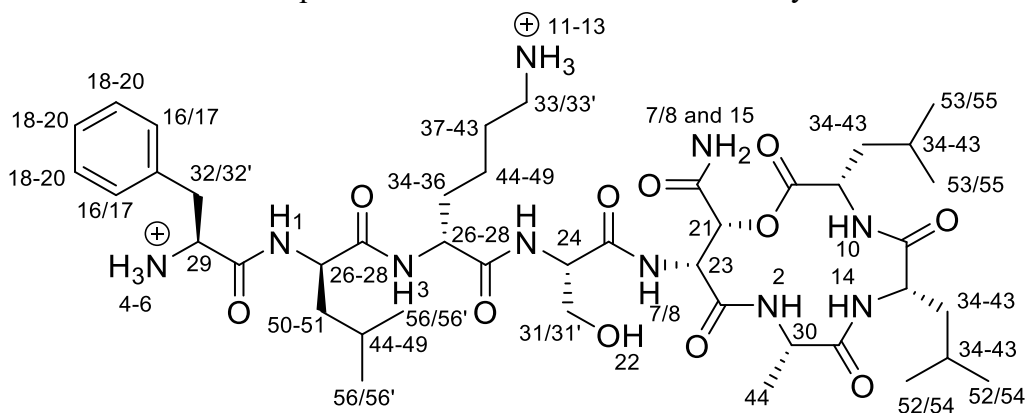
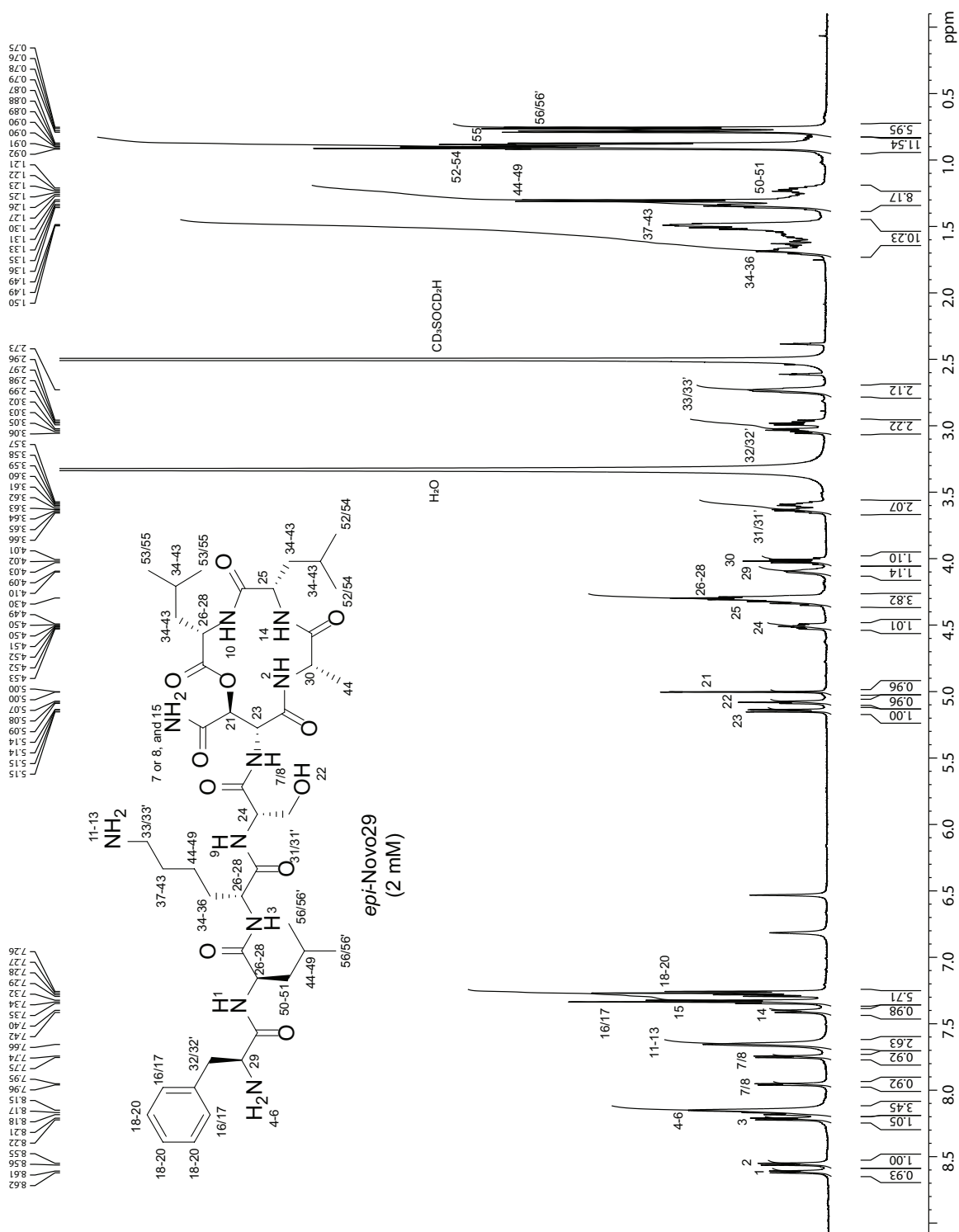


Table S3.4. Chemical shift comparison between natural Novo29 and synthetic Novo29.



#	natural Novo29 3 mM (nominal)	synthetic Novo29 2 mM (nominal)	$\Delta\delta$ ppm	#	natural Novo29 3 mM (nominal)	synthetic Novo29 2 mM (nominal)	$\Delta\delta$ ppm
1	8.57	8.56	-0.01	25	4.38	4.38	0
2	8.31	8.30	+0.01	26-28	4.33	4.33	0
3	8.24	8.24	0	29	4.09	4.08	-0.01
4-6	8.15	8.14	-0.01	30	3.98	3.98	0
7/8	8.01	8.01	0	31/31'	3.59	3.59	0
	and	and	and		and	and	and
	7.95	7.94	-0.01		3.91	3.91	0
9	7.94	7.94	0	32/32'	3.00	3.00	0
10	7.78	7.78	0	33/33'	2.74	2.74	0
11-13	7.65	7.65	0	34-36	1.63	1.63	0
14	7.60	7.60	0	37-43	1.52	1.52	0
15	7.39	7.39	0	44-49	1.33	1.33	0
16/17	7.33	7.33	0	50-51	1.23	1.23	0
18-20	7.27	7.27	0	52-54	0.92	0.92	0
21	5.29	5.29	0	55	0.86	0.86	0
22	5.13	5.13	0	56/56'	0.77	0.77	0
23	5.04	5.04	0				
24	4.46	4.46	0				

¹H NMR of 2 mM epi-Novo29 in DMSO-d₆ at 500 MHz and 298 K



Chapter IV

Efforts Toward the Synthesis of aza-Novo29 (aza-Clovibactin), a Macrolactam Analogue of Novo29 (Clovibactin) with an Improved Hydrolytic Stability

Certain aspects of this chapter were completed collaboratively between myself and a past Nowick Group member Dr. Xingyue Li. A current graduate student in the Nowick Group – Jackson Edward Hart Brunicardi is currently continuing and expanding on this work.

ABSTRACT

A recently reported peptide natural Novo29 (clovibactin) suffers from hydrolytic instability in conditions that would be required for clinical development as an antibiotic. In this chapter, I build on the work described in Chapter III and expand on the studies toward the synthesis of aza-Novo29, a macrolactam variant of Novo29 that would not suffer from the same hydrolytic instability. Novo29 hydrolyzes in slightly basic or neutral pH conditions at the ester linkage of the macrolactone. To prevent the hydrolysis, I propose synthesizing aza-Novo29 which contains a novel noncanonical amino acid – (2*R*,3*R*)-aminoasparagine in the five position, replacing the hydrolytically labile ester with a more stable amide bond. Numerous synthetic approaches unfortunately did not yield the desired product, but this work establishes an important foundation for future research into the synthesis of aminoasparagine and aza-Novo29.

INTRODUCTION

Novo29 (clovibactin) is a recently reported eight-residue depsipeptide that contains a noncanonical amino acid hydroxyasparagine that forms the ester bond in the macrolactone ring of Novo29.¹ Novo29 was isolated from a soil bacterium closely related to *Eleftheria terrae*, and it is active against Gram-positive bacteria, including drug-resistant human pathogens such as MRSA and VRE. This potent peptide antibiotic kills bacteria without detectable resistance by inhibiting cell-wall synthesis. In the previous chapter and in a recent publication, I was able to determine the stereochemistry in Novo29 through chemical synthesis and structural elucidation, resulting in the first total synthesis and full structural elucidation of this natural product.

Novo29 is not a promising drug candidate, however, due to its hydrolytic instability in neutral and mildly basic pH conditions in both buffer and serum. After one hour in PBS (pH 7.2) at 37 °C, LC-MS analysis shows that 60% of Novo29 is hydrolyzed to an inactive linear form. I hypothesized that the electron-withdrawing amide side chain of hydroxyAsn₅ activates the macrolactone ester linkage to Leu₈ for hydrolysis (Figure 4.1). LC-MS results show that the new peak that appears in the trace following treatment in neutral or basic pH results in an addition of +18, indicating that the hydrolysis is likely occurring at the labile ester linkage (Figure S4.1).

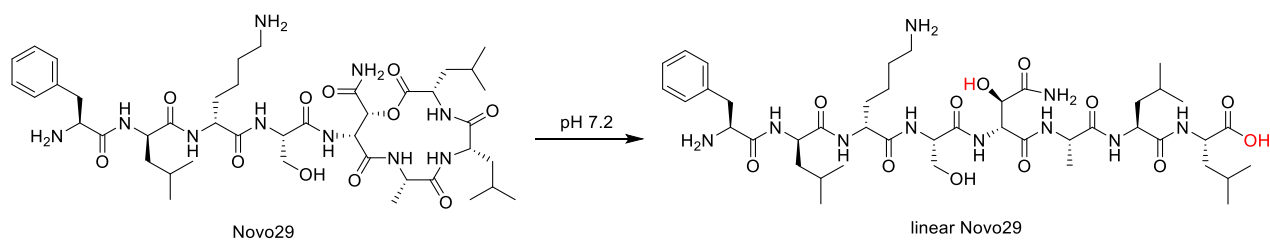


Figure 4.1. Hypothesized hydrolysis of Novo29. The newly formed hydroxy group on hydroxyAsn₅ and the carboxylic acid on Leu₈ are shown in red.

To prevent or minimize the hydrolysis of Novo29 while maintaining its activity I hypothesized that I can synthesis aza-Novo29 (aza-clovibactin) (Figure 4.2). In aza-Novo29 the hydrolytically unstable ester bond is replaced with an amide bond. I hypothesize that the electron-withdrawing effect of the side-chain amide on hydroxyAsn₅ would not occur in an aza-analogue of this peptide due to the increased electron-donating effect of nitrogen, as compared to oxygen. Previously, our lab has published a synthesis of aza-teixobactin analogues, an aza-analogue of a similar peptide antibiotic which showed improved activity compared to its native form with an ester linkage in the macrolactone ring.² Aza-Novo29 could not only have improved hydrolytic stability when compared to Novo29 but could also have improved activity due to the presence of another hydrogen-bond donor which could result in better binding with its target – a phosphate group.

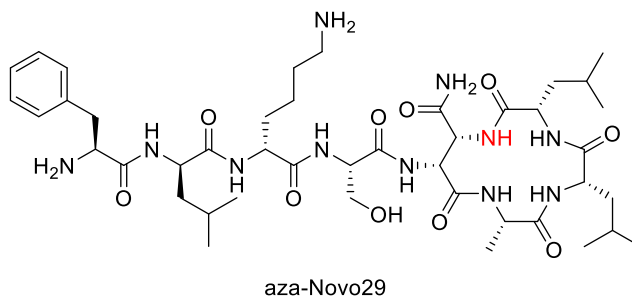


Figure 4.2. Structure of the proposed aza-Novo29, the newly formed amide bond in the five position is shown in red.

RESULTS AND DISCUSSION

Novo29 hydrolyzes in water at 37 °C in 24 hours to ~22 % hydrolyzed product (Table 4.1 and Figure S4.1). Previous studies conducted by NovoBiotic Pharmaceuticals revealed that the hydrolyzed product is inactive against bacteria, and hence improving the hydrolytic stability of Novo29 is crucial to maintaining its activity. To corroborate the hydrolysis studies a 100 μ L

solution of a 1 mg/mL Novo29 was prepared in water from a 10 mg/mL DMSO stock and incubated at 37 °C for a period of 24 hours. LC-MS analysis reveals that some Novo29 is already hydrolyzed at the zero-hour timepoint, most likely due to the fact that Novo29 was stored in DMSO and the sample likely slowly hydrolyzed in these conditions. A gradual increase in hydrolyzed product proceeded to form over the next 24 hours (Table 4.1).

Table 4.1. Table representing the % of hydrolyzed Novo29 based on integration measurement from an LC-MS TIC trace.

time (h)	% hydrolyzed Novo29
0	5
2	8
4	10
6	11
8	12
24	22

Previous studies from our laboratory have shown that teixobactin analogues bind an anion at the macrolactone ring in its X-ray crystallographic structure through hydrogen bonding between the anion as a hydrogen-bond acceptor and the amide groups as hydrogen-bond donors.³ It has been postulated that this binding is critical to the activity of teixobactin as it likely serves as the binding site for a phosphate group when interacting with the outer cell wall of Gram-positive bacteria.^{4,5} Mutating the ester linkage in teixobactin to an amide resulted in one more hydrogen-bond donor being present in this binding site which could result in stronger binding of the anionic phosphate group. Aza-teixobactin analogues have better activity than ester-containing teixobactin analogues against all tested Gram-positive bacteria.³

Synthesis of aza-Novo29 can be achieved via two potential routes — through an off-resin or through an on-resin approach. Off-resin synthesis would require the synthesis of an orthogonally protected Fmoc-(2R,3R)-amino-Alloc-asparagine-OH, followed by regular SPPS coupling, a

deprotection of the Alloc protecting group, and an on-resin amide coupling (Figure 4.3). On-resin synthesis could mimic the approach that was previously outlined for aza-teixobactin analogues and would require an on-resin mesylation, azidation, reduction of the azide, and side-chain amide coupling (Figure 4.3).

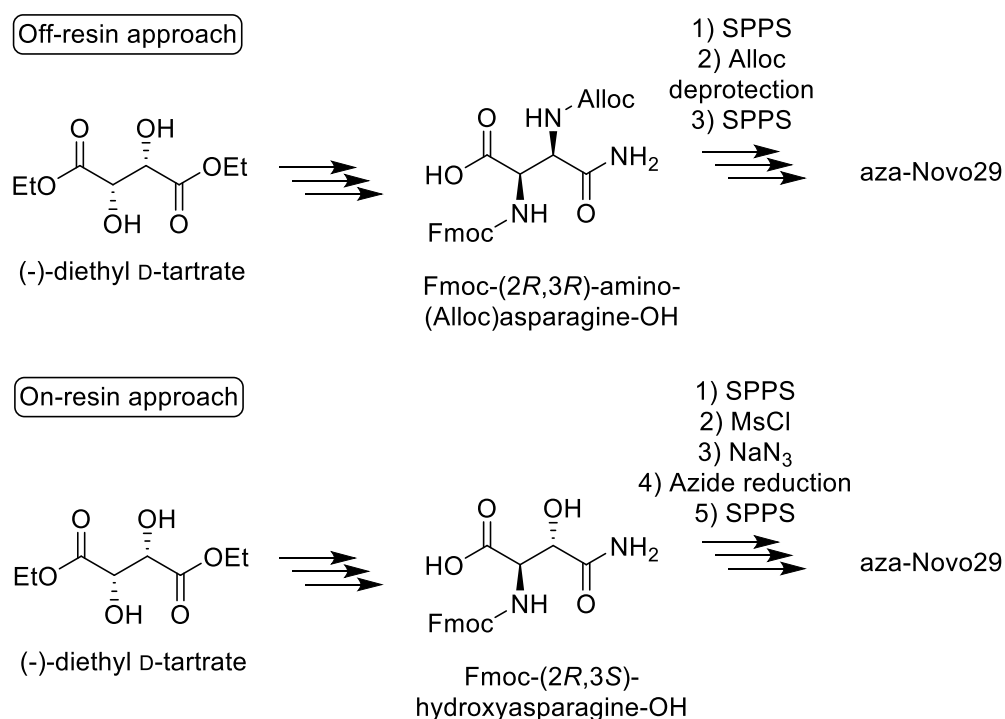


Figure 4.3. Different potential synthetic approaches to aza-Novo29.

The advantage of the off-resin approach was that it afforded a novel noncanonical amino acid which could potentially be useful in more applications than just the synthesis of aza-Novo29, hence that was the approach that I decided to take. Additionally, during the studies of Novo29 (Chapter III) I was able to obtain a critical intermediate (amide **19**) that was used as an intermediate for the synthesis of Fmoc-(2*R*,3*S*)-hydroxyasparagine-OH, which is also an intermediate on the route toward Fmoc-(2*R*,3*R*)-amino-(Alloc)asparagine-OH (Figure 4.4).

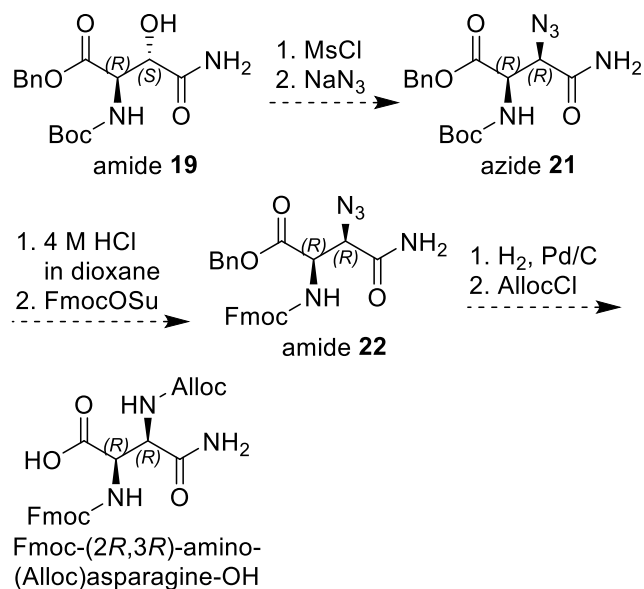
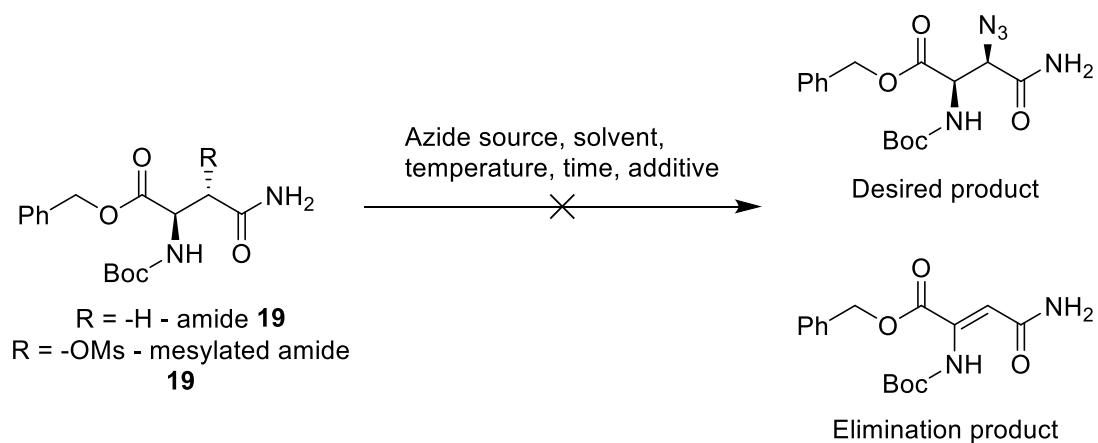


Figure 4.4. Proposed synthetic route toward Fmoc-(2*R*,3*R*)-amino-(Alloc)asparagine-OH.

All attempted S_N2 displacements of the mesylated amide **19** resulted in either elimination or no reaction. Generally, the stereochemistry of the 3-position mesylate or hydroxy group was to be inverted through an S_N2 or an S_N2-like mechanism with a nucleophilic nitrogen source. S_N2 displacement with NaN₃ of mesylated amide **19** in DMF-*d*₇ resulted in elimination of the hydrogen in the 1-position (Table 4.2, entry 1). This was further confirmed with the use of the polar protic solvent methanol which also resulted in elimination (Table 4.2, entry 2). I hypothesized that the elimination is occurring due to the slight basicity of the reaction due to the presence of NaN₃, to try and control the pH of the reaction I opted to increase the acidity of the reaction mixture with either one equivalent of H₂SO₄ or two equivalents of NaHSO₄ (Table 4.2, entries 3 and 4). While neither of these conditions resulted in the undesired elimination, neither produced any product, most likely because the nucleophilicity of NaN₃ was attenuated in acidic conditions. Two different sources of azide – tetramethylguanidinium azide (TMGN₃) and LiN₃ – also both resulted in elimination (Table 4.2, entries 5 and 6).



entry	R	azide source	solvent	temperature (°C)	time (h)	additive	outcome
1	-OMs	NaN ₃	DMF- <i>d</i> ₇	25	24	N/A	elimination
2	-OMs	NaN ₃	CD ₃ OD	25	24	N/A	elimination
3	-OMs	NaN ₃	CD ₃ OD/D ₂ O	25	48	H ₂ SO ₄	no reaction
4	-OMs	NaN ₃	CD ₃ OD	25	48	NaHSO ₄	no reaction
5	-OMs	TMGHN ₃	CDCl ₃	0 – 25	48	N/A	elimination
6	-OMs	LiN ₃	CD ₃ OD/H ₂ O	25	>24	N/A	elimination
7	-OH	DPPA	THF- <i>d</i> ₈	0 – 25, then 50	24	PPh ₃ , DIAD	no reaction
8	-OH	DPPA	THF- <i>d</i> ₈	0 – 25, then 50	24	PPh ₃ , DEAD	no reaction
9	-OH	DPPA, then NaN ₃	THF- <i>d</i> ₈	0 – 25	48	DBU	elimination

Figure 4.5 and **Table 4.2.** Overview of the reaction conditions that were attempted to azidate amide **19** or mesylated amide **19**.

The proton in the 2-position appeared to suffer from increased acidity and the reaction was hence unlikely to proceed favorably when reacted through the mesylate intermediate. The Mitsunobu reaction is a dehydrative coupling of an alcohol to a pronucleophile completed through an activation of the alcohol between DEAD or DIAD and PPh₃, using diphenylphosphoryl azide (DPPA) as the source of the nucleophilic azide. Unfortunately, these reactions did not produce any product, and when additional azide was added in the source of NaN₃ the reaction only produced the undesired elimination product (Table 4.2, entries 7, 8, and 9).

CONCLUSION

Novo29 is a promising peptide antibiotic that can act against Gram-positive bacteria without inducing bacterial resistance. However, Novo29 is hydrolytically unstable which precludes it from being an effective preclinical candidate. The ester bond in the macrolactone ring of Novo29 hydrolyzes in neutral or slightly basic pH, to try and prevent this from happening I propose to synthesize aza-Novo29 where the ester bond is replaced with a more hydrolytically stable amide bond. Two different approaches can be taken to try and synthesize aza-Novo29, either an on-resin or an off-resin approach. In this chapter I explored my attempts of the off-resin synthesis of Fmoc-(2R,3R)-amino-(Alloc)asparagine-OH that can then be incorporated into the peptide through standard SPPS. Unfortunately, none of the approaches in this synthesis have worked, but a current graduate student in the Nowick group is further pursuing routes toward the synthesis of aza-Novo29.

NOTES AND REFERENCES

1. Krumberger, M.; Li, X.; Kreutzer, A. G.; Peoples, A. J.; Nitti, A. G.; Cunningham, A. M.; Jones, C. R.; Achorn, C.; Ling, L. L.; Hughes, D. E.; Nowick, J. S. Synthesis and Stereochemical Determination of the Peptide Antibiotic Novo29. *J. Org. Chem.* **2023**, *88*, 2214–2220.
2. Yang, H.; Pishenko, A. V.; Li, X.; Nowick, J. S. Design, Synthesis, and Study of Lactam and Ring-Expanded Analogues of Teixobactin. *J. Org. Chem.* **2020**, *85*, 1331–1339.
3. Yang, H.; Bois, D. R. D.; Ziller, J. W.; Nowick, J. S. X-Ray Crystallographic Structure of a Teixobactin Analogue Reveals Key Interactions of the Teixobactin Pharmacophore. *Chem. Commun.* **2017**, *53*, 2772–2775.

4. Shukla, R.; Medeiros-Silva, J.; Parmar, A.; Vermeulen, B. J. A.; Das, S.; Paioni, A. L.; Jekhmane, S.; Lorent, J.; Bonvin, A. M. J. J.; Baldus, M.; Lelli, M.; Veldhuizen, E. J. A.; Breukink, E.; Singh, I.; Weingarth, M. Mode of Action of Teixobactins in Cellular Membranes. *Nat. Commun.* **2020**, *11*, 2848.
5. Shukla, R.; Lavore, F.; Maity, S.; Derks, M. G. N.; Jones, C. R.; Vermeulen, B. J. A.; Melcrová, A.; Morris, M. A.; Becker, L. M.; Wang, X.; Kumar, R.; Medeiros-Silva, J.; van Beekveld, R. A. M.; Bonvin, A. M. J. J.; Lorent, J. H.; Lelli, M.; Nowick, J. S.; MacGillavry, H. D.; Peoples, A. J.; Spoering, A. L.; Ling, L. L.; Hughes, D. E.; Roos, W. H.; Breukink, E.; Lewis, K.; Weingarth, M. Teixobactin Kills Bacteria by a Two-Pronged Attack on the Cell Envelope. *Nature* **2022**, *608*, 390–396.

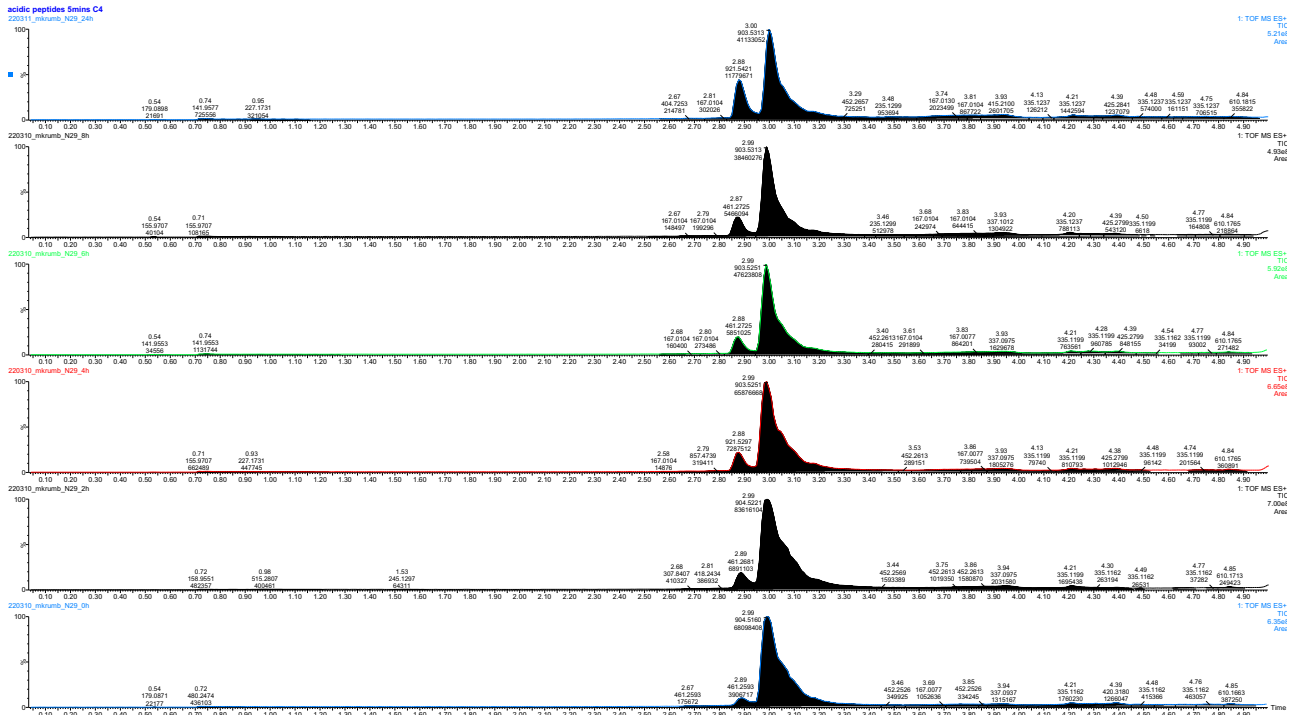
Supporting information for Chapter IV:

**Efforts Toward the Synthesis of aza-Novo29 (aza-Clovibactin), a Macrolactam Analogue of
Novo29 (Clovibactin) with an Improved Hydrolytic Stability**

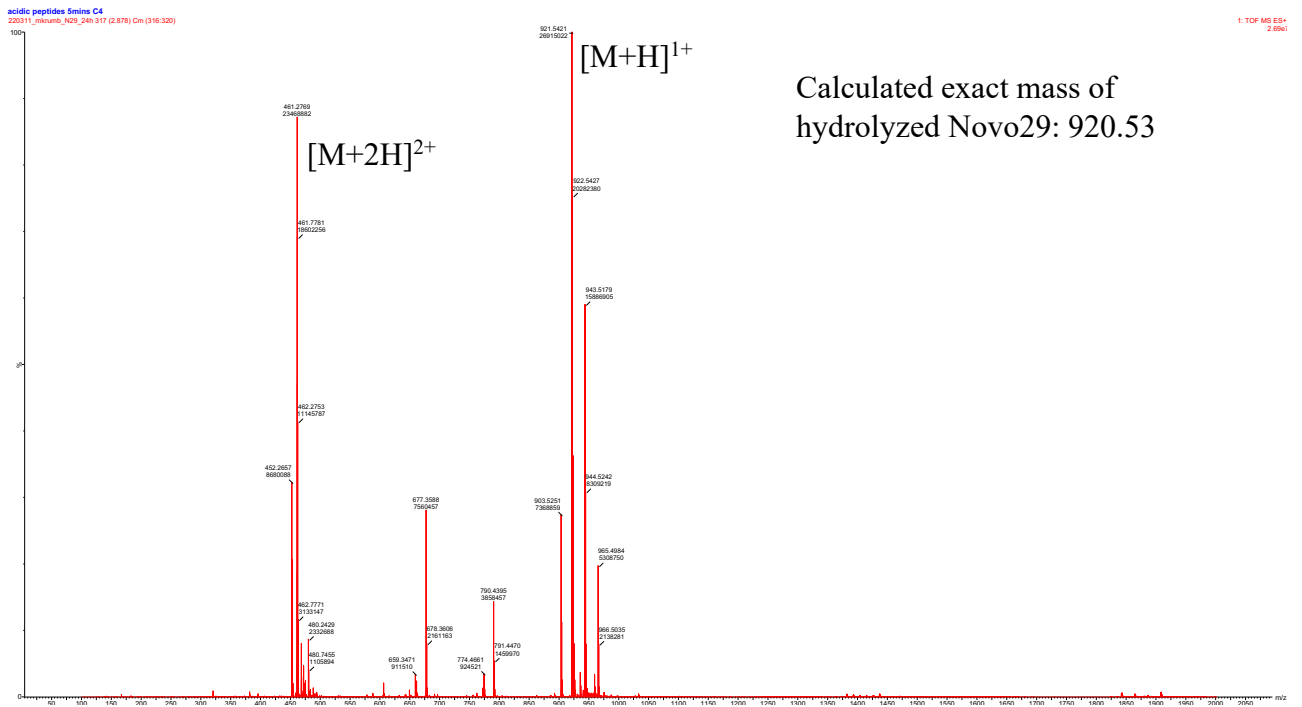
Table of Contents

Figure S4.1.....	183
General synthetic procedures	183

A



B



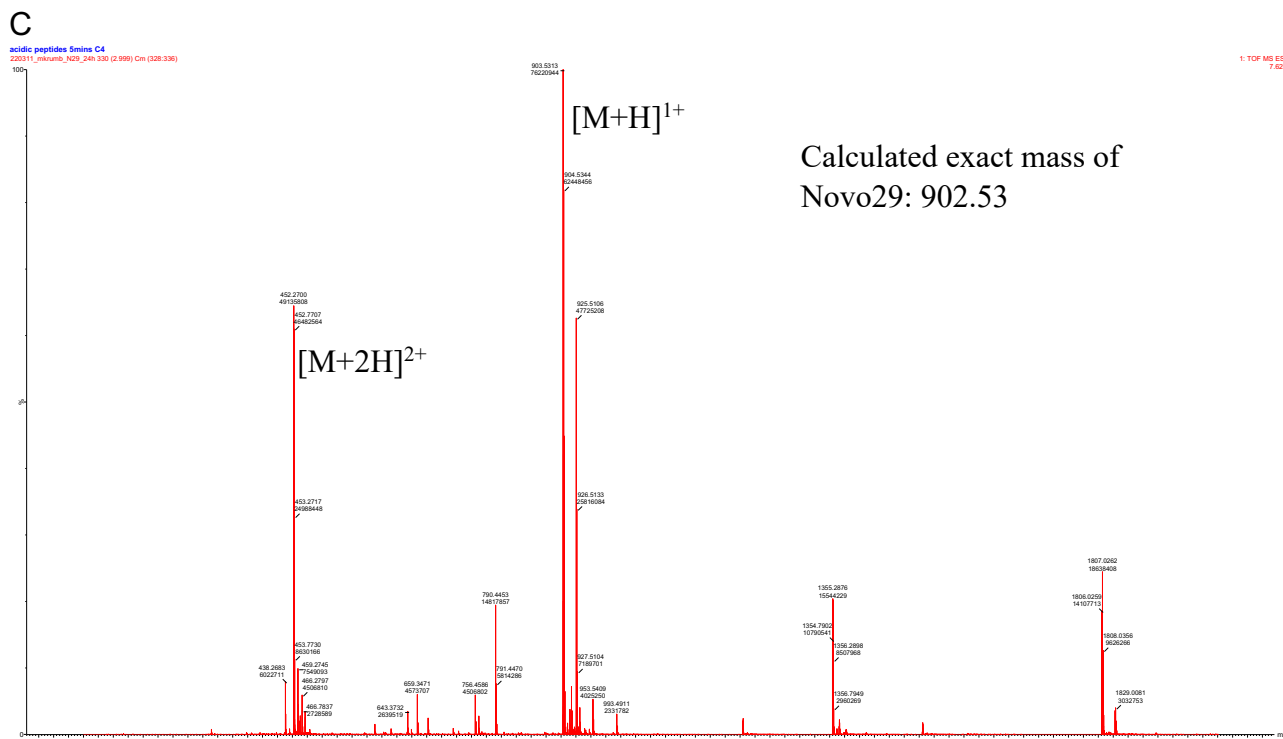


Figure S4.1. Mass spectrometric studies of hydrolysis of natural Novo29. Novo29 was dissolved in a 1 mg/mL solution in H₂O and incubated at 37 °C for 24 hours. (A) TIC trace of the hydrolysis experiment of Novo29 at 0, 2, 4, 6, 8, and 24 hours (bottom to top) with the integrated areas under the curve. (B) ESI-MS spectrum of the left peak which shows the hydrolyzed mass of Novo29. (C) ESI-MS spectrum of the right peak which shows Novo29.

General synthetic procedures

General synthetic procedure for entries 1–6 in Table 4.2:

Mesylated amide **9** (0.02 g, 0.029 mmol, 1 equiv.) was dissolved in a scintillation vial in 0.5 mL of the corresponding deuterated solvent (DMF-*d*₇, CD₃OD, D₂O, or CDCl₃) and the azide source (NaN₃, TMGHN₃, or LiN₃) was added (1.5 equiv.) and transferred to an NMR tube. The products were not isolated, but the reaction mixtures were tracked through NMR and LC-MS. The appearance of an alkene peak in the NMR and the mass corresponding to the elimination product was observed in entries 1, 2, 5, and 6, and no change was observed in entries 3 and 4 (Table 4.2). Products were not further purified, isolated, and analyzed.

General synthetic procedure for entries 7–9 in Table 4.2:

Amide **9** (0.02 g, 0.029 mmol, 1 equiv.) was dissolved in a scintillation vial in 0.5 mL THF-*d*₈. The PPh₃ (4 equiv.) and DIAD/DEAD (6 equiv.), and DBU (1.5 equiv.) were added followed by the addition of the Mitsunobu azide source DPPA (1.3 equiv.) was added and transferred to an NMR tube. The products were not isolated, but the reaction mixtures were tracked through NMR and LC-MS. The appearance of an alkene peak in the NMR and the mass corresponding to the elimination product was observed in entry 9 and no change was observed in entries 7 and 8 (Table 4.2). Products were not further purified, isolated, and analyzed.